Multi-target tracking by non-linear set-membership methods

Julius Ibenthal

université PARIS-SACLAY

Multi-target tracking by non-linear set-membership methods

Pistage multi-cibles par méthodes ensemblistes non-linéaires

Thèse de doctorat de l'université Paris-Saclay

École doctorale n° 580, Sciences et Technologies de l'Information et de la Communication (STIC)
Spécialité de doctorat : Automatique
Graduate School : Sciences de l'ingénierie et des systèmes
Référent : Faculté des sciences d'Orsay

Thèse préparée dans l'unité de recherche **Traitement de l'information et systèmes – DTIS** (Université Paris-Saclay, ONERA), sous la direction d'**Hélène PIET-LAHANIER**, Directrice de recherche, la co-direction de **Michel KIEFFER**, Professeur des universités, et le co-encadrement de **Luc MEYER**, Ingénieur de recherche.

Thèse soutenue à Paris-Saclay, le 19 octobre 2022, par

Julius IBENTHAL

Composition du Jury

Cristina STOICA MANIU Professeure des universités, Université Paris-Saclay	Présidente
Matthias GERDTS Professeur des universités, Universität der Bundeswehr München	Rapporteur & Examinateur
Isaac KAMINER Professeur des universités, Naval Postgraduate School	Rapporteur & Examinateur
Eric GOUBAULT Professeur des universités, École Polytechnique	Examinateur
Erik-Jan van KAMPEN Professeur associé, Delft University of Technology	Examinateur
Hélène PIET-LAHANIER Directrice de recherche, ONERA, Université Paris-Saclay	Directrice de thèse

THESE DE DOCTORAT

NNT : 2022UPAST124

université PARIS-SACLAY

ÉCOLE DOCTORALE
Sciences et technologies de l'information et de la communication (STIC)

Titre : Pistage multi-cibles par méthodes ensemblistes non-linéaires

Mots clés : Système multi-agents ; Estimation ensembliste ; Commande coopérative distribuée ; Pistage multi-cibles

Résumé : La recherche et le suivi de cibles mobiles constituent une tâche d'intérêt mais notablement difficile parmi les diverses applications des robots. Cette thèse considère la recherche et le suivi d'un nombre inconnu de cibles mobiles se déplaçant dans une zone délimitée par une flotte coopérative de véhicules aériens sans pilote (UAV). Des schémas d'estimation et de contrôle distribués sont présentés. Les schémas d'estimation reposent sur l'hypothèse que les perturbations d'état et les bruits de mesure sont bornés. Des estimateurs distribués robustes ensemblistes sont utilisés pour caractériser l'ensemble garanti de contenir les cibles. Les estimations ensemblistes sont mises à jour par chaque drone à l'aide des informations recueillies par ses propres capteurs et par les drones voisins. Les trajectoires des UAVs sont calculées en utilisant des approches de contrôle prédictif de modèle. Les lois de commande sont conçues afin de diminuer l'incertitude d'estimation des cibles inconnues, non encore détectées, et des cibles déjà connues et faisant l'objet d'un suivi.

Les schémas d'estimation et de contrôle développés reposent sur de nouveaux modèles détaillés de conditions déterministes d'identification et de détection des cibles. Ces conditions tiennent compte des états du drone et de la cible, des contraintes des capteurs et des obstacles environnementaux. Les estimateurs développés utilisent des mesures de cibles identifiées et non identifiées et sont robustes à la présence de leurres potentiels, qui peuvent être confondus avec les cibles. En outre, le nouveau modèle de détection déterministe permet d'évaluer des estimations ensemblistes garanties de l'emplacement des cibles dans des environnements structurés inconnus, où il est difficile de démontrer l'absence d'une cible à une localisation donnée. Pour effectuer cette estimation, il n'est pas nécessaire de disposer d'une carte de l'environnement ou de la construire.

Diverses simulations illustrent la capacité des approches proposées à rechercher et à suivre efficacement un nombre inconnu de cibles mobiles dans une zone de recherche délimitée. De plus, les résultats obtenus par de premières expérimentations sont présentés.

université PARIS-SACLAY

ÉCOLE DOCTORALE
Sciences et technologies de l'information et de la communication (STIC)

Title : Multi-target tracking by non-linear set-membership methods

Keywords : Multi-agent systems; Set-membership state estimation; Cooperative distributed control; Multi-target tracking

Abstract : Searching and tracking mobile targets remains a challenging task among the various applications for robots. This thesis considers the search and track of an unknown number of targets moving in a bounded area by a cooperative Unmanned Aerial Vehicle (UAV) fleet. Distributed estimation and control schemes are presented. The estimation schemes rely on the assumption that state perturbations and measurement noises are bounded. Robust distributed set-membership estimators are used to evaluate set estimates that are guaranteed to contain the target states. The set estimates are updated by each UAV using information collected from its sensors and from the neighboring UAVs. The trajectories of the UAVs are designed using model predictive control approaches. The control is designed to decrease the estimation uncertainty of the unknown, not yet detected targets and known, tracked targets.

The developed estimation and control schemes rely on new detailed models of deterministic identification and detection conditions of the targets. These conditions account for UAV and target states, sensor constraints, and environmental obstacles. The developed estimators utilize measurements of identified and unidentified targets and are robust to the presence of potential decoys, which may be confused with the targets. Furthermore, the new deterministic detection model allows the evaluation of guaranteed set estimates of target locations in unknown structured environments, where it is challenging to demonstrate the absence of a target at a given location. To estimate the target locations, neither having nor building a map of the environment is necessary.

Various simulations illustrate the ability of the proposed approaches to efficiently search and track an unknown number of moving targets within some delimited search area. Additionally, preliminary experimental studies are carried out.

Für meine Mutter, für meinen Vater, und für Charline,

Erwachsen – Was heißt das schon?
Vernünftig – Wer ist das schon?
Ich bin ich,
Und du bist du.
Das ist alles,
Was ich weiß.

(Peter Maffay, Rolf Zuckowski)

Acknowledgments

I want to express my great gratitude to all the people who have supported me during the last few years. Your help in various forms led to the great success of my Ph.D.

My special thanks go to my supervisors. I'm grateful to Hélène for her guidance and all our time discussing possible research directions and handling administrative matters. She gave me advice that always led to a solution to every problem I encountered. I want to address a special thanks to Michel for his keen sense of detail, his high standards, and his constructive criticism. We polished the equations until they became diamonds. An equally special thanks to Luc for the joint exploration of new ideas and his good humor, which was a steady source of motivation. It was always a pleasure to work with you all.

I want to thank the reviewers and the entire defense jury for agreeing to evaluate my work. I want to express my gratitude to Professor Kaminer and Professor Gerdts for their detailed reports and discussions during the defense, which helped me to improve the manuscript further. I'm equally grateful to Professor van Kampen, Professor Stoica Maniu, and Professor Giboult for the critical discussions and their valuable comments during the defense. Thanks to Christophe Guilmart for representing the AID at my defense.

I want to also thank ONERA and AID for the financial support and for providing good research facilities. This allowed me to focus on my Ph.D. Regarding the experimental studies, I thank the Copernic Lab, Martial Sanfourche, and Julien Marzat for providing all the equipment and know-how. Also, I would like to thank Emile Siboulet for preparing the simulations with AirSim and the experiments in the flight arena.

Furthermore, thanks to all the Ph.D. students and interns I have spent the last three years with for the nice evenings and many discussions. Thanks to Étienne, Antonello, Clément, Hanae (merci spécialement pour ma portion quotidienne d'eau chaude), Clara, Mathieu (l'aubergine : le meilleur des légumes), Juliette, Paul, Baptiste, Jorge (best swim buddy), Renato, Romain (the final squash boss), Thomas, Pelin, Jules, Périclès, and Mathieu. Thanks to the "stagiaire éternel" Thomas for checking all the fake news. Finally, thanks to Jonas, the Ph.D. student I met first and who was surprisingly another German (the only other). We had some great tennis matches weekly in the morning on top of the Gare Montparnasse.

Ich möchte mich auch bei meiner Familie und meinen Freunden für ihre unermüdliche Unterstützung und Ermutigungen bedanken. Meiner Mutter Bommi und meinem

Vater Stefan danke ich für die Ermöglichung meiner langjährigen Ausbildung und die Unterstützung jeder meiner Entscheidungen. Schließlich möchte ich meiner großen Liebe Charline danken, dass sie immer für mich da war und dass sie mich mit ihrer unermüdlichen positiven Energie aus jedem Tief geholt hat.

Abstract

Searching and tracking mobile targets remains a challenging task among the various applications for robots. This thesis considers the search and track of an unknown number of targets moving in a bounded area by a cooperative Unmanned Aerial Vehicle (UAV) fleet. Distributed estimation and control schemes are presented. The estimation schemes rely on the assumption that state perturbations and measurement noises are bounded. Robust distributed set-membership estimators are used to evaluate set estimates that are guaranteed to contain the target states. The set estimates are updated by each UAV using information collected from its sensors and from the neighboring UAVs. The trajectories of the UAVs are designed using model predictive control approaches. The control is designed to decrease the estimation uncertainty of the unknown, not yet detected targets and known, tracked targets.

The developed estimation and control schemes rely on new detailed models of deterministic identification and detection conditions of the targets. These conditions account for UAV and target states, sensor constraints, and environmental obstacles. The developed estimators utilize measurements of identified and unidentified targets and are robust to the presence of potential decoys, which may be confused with the targets. Furthermore, the new deterministic detection model allows the evaluation of guaranteed set estimates of target locations in unknown structured environments, where it is challenging to demonstrate the absence of a target at a given location. To estimate the target locations, neither having nor building a map of the environment is necessary.

Various simulations illustrate the ability of the proposed approaches to efficiently search and track an unknown number of moving targets within some delimited search area. Additionally, preliminary experimental studies are carried out.

Résumé

La recherche et le suivi de cibles mobiles constituent une tâche d'intérêt mais notablement difficile parmi les diverses applications des robots. Cette thèse considère la recherche et le suivi d'un nombre inconnu de cibles mobiles se déplaçant dans une zone délimitée par une flotte coopérative de véhicules aériens sans pilote (UAV). Des schémas d'estimation et de contrôle distribués sont présentés. Les schémas d'estimation reposent sur l'hypothèse que les perturbations d'état et les bruits de mesure sont bornés. Des estimateurs distribués robustes ensemblistes sont utilisés pour caractériser l'ensemble garanti de contenir les cibles. Les estimations ensemblistes sont mises à jour par chaque drone à l'aide des informations recueillies par ses propres capteurs et par les drones voisins. Les trajectoires des UAVs sont calculées en utilisant des approches de contrôle prédictif de modèle. Les lois de commande sont conçues afin de diminuer l'incertitude d'estimation des cibles inconnues, non encore détectées, et des cibles déjà connues et faisant l'objet d'un suivi.

Les schémas d'estimation et de contrôle développés reposent sur de nouveaux modèles détaillés de conditions déterministes d'identification et de détection des cibles. Ces conditions tiennent compte des états du drone et de la cible, des contraintes des capteurs et des obstacles environnementaux. Les estimateurs développés utilisent des mesures de cibles identifiées et non identifiées et sont robustes à la présence de leurres, qui peuvent être confondus avec les cibles. En outre, le nouveau modèle de détection déterministe permet d'évaluer des estimations ensemblistes garanties de l'emplacement des cibles dans des environnements structurés inconnus, où il est difficile de démontrer l'absence d'une cible à une localisation donnée. Pour effectuer cette estimation, il n'est pas nécessaire de disposer d'une carte de l'environnement ou de la construire.

Diverses simulations illustrent la capacité des approches proposées à rechercher et à suivre efficacement un nombre inconnu de cibles mobiles dans une zone de recherche délimitée. De plus, les résultats obtenus par de premières expérimentations sont présentés.

Contents

List of Figures

List of Tables

List of Acronyms

CMOMMT	Cooperative Multirobot Observation of Multiple Moving Targets
CSAT	Cooperative Search, Acquisition, and Tracking
CT	Cooperative Tracking
FoV	Field of View
MPC	Model Predictive Control
MPE	Multirobot Pursuit Evasion
RoI	Region of Interest
SAT	Search, Acquisition, and Tracking
SME	Set-Membership Estimator
UAV	Unmanned Aerial Vehicle

1. Introduction

1.1. Context

This thesis takes part in the context of Search, Acquisition, and Tracking (SAT) of targets. The objective of SAT is to search persistently for new and to keep track of already known targets, where a target may be any object of interest. The SAT problem encompasses many considerations, such as, *e.g.,* the confidence and guaranties for the target presence, the accuracy of the estimated target locations, optimal placement of the sensors, energy consumption of the deployed robots, available search time, and environmental hazards. Consequently, SAT of targets is a very challenging task that is still an active research field after more than 60 years of development (Koopman, 1956). In the last decades, the field has received increased interest due to the recent advances in the development of mobile robots. Robot deployment considerably facilitates the collection of observations when the task is solved in an automated and autonomous fashion.

SAT problems and other observation tasks such as, *e.g.,* target localization, tracking, awareness, rescue, guarding, capture, and hunting, have all in common the necessity of collecting observations of targets. These observations may be used for target detection, state estimation, or visual feedback. Additionally, the robots use the collected information on the targets and environment to derive deployment strategies to complete their missions.

SAT is a challenging observation problem since the deployment strategy of the robots has to incorporate two almost opponent objectives. The search objective requires an efficient displacement and distribution of the robots over the region of interest to increase the likelihood of detecting new targets. On the other hand, the tracking objective requires that the robots remain close to known targets and collect observations of the targets persistently. Both objectives have to be balanced for a successful mission accomplishment. The deployment strategy and control design become even more complex considering Cooperative SAT (CSAT), where a fleet of cooperating and interacting robots performs the SAT. Each robot deploys a strategy such that the whole fleet benefits from its actions. The deployment strategies can be designed in a centralized, decentralized, or distributed framework, where most of the state-of-the-art techniques rely on a cooperative distributed strategy design, which increases each robot's autonomy and the fleet's robustness against the failure of individual robots. This thesis focuses on CSAT of targets by a fleet of Unmanned Aerial Vehicles (UAVs).

There is a large number of potential applications for CSAT missions. One important application is, *e.g.*, the search and tracking of humans in disaster areas for rescue operations. A UAV fleet is excellently suited to carry out this mission. The cooperating fleet can monitor a large region of interest, and its deployment does not rely on existing infrastructure that may be corrupted. They allow a persistent localization and search for humans in the area and a more efficient task allocation of the rescue services. The advantages are that the locations of the humans are registered, and their potential movements are estimated over the complete mission duration. The deployment of a fleet becomes increasingly beneficial the more autonomous the UAVs act, and the less human resources are necessary.

Though CSAT is desirable in some scenarios, there are still very few real-world applications. This comes from the high complexity of CSAT missions since they encompass several disciplines, such as signal processing, navigation, estimation, and control. Many approaches focus on a given discipline/sub-problem and simplify assumptions regarding the others. Robin and Lacroix (2016) synthesized the most critical areas and directions researchers should pursue to improve target detection and tracking approaches. The most important directions comprise improving the models, developing decentralized algorithms, and strengthening the validation process.

Substantial deficits concern modeling the measurement process, the targets, and the environment. The measurement process models the availability, quality, and reliability of the information collected by the robots. The availability represents the possibility of collecting a measurement of the target state. The quality models the accuracy of the collected measurements. The reliability expresses that measurements may not be caused by detecting a target. The availability, quality, and reliability of measurements are often assumed to follow the realization of random events. The measurement perturbations are treated as additive noises, which are assumed to be Gaussian processes. The variance translates the quality of the measurement, *e.g.*, measurements are of low quality when the variance of the process is considerable. Nevertheless, *a priori* probability density functions describing the process and measurement noises may not always be available. The resulting performance may prove sensitive to these *a priori* assumptions, as pointed out in Gu et al. (2015).

A weakness concerning the modeling of the measurement reliability is that most approaches assume that targets are either always or never identified. Nevertheless, the identification process may be subject to uncertainties, leading to false identification or confusion of targets and other objects in the search area. This process should be linked to more refined observation conditions depending on the robot, target, and environment.

Another weakness concerning the modeling of the measurement availability is that the limited detection abilities of the sensors are usually modeled with probabilities of false alarm and detection. Both might be chosen as constant, dependent on the detection range, the measurement signal-to-noise ratio, or the target state. Their

choice significantly impacts the search performance, but choosing appropriate values *a priori* is again difficult. Furthermore, for a probabilistic description, it proves difficult to integrate the influence of the environment on the detection abilities of the robot. Nevertheless, the detection model should account for the local environment since it has a considerable impact as, *e.g.*, a target hidden behind an obstacle can never be detected.

Regarding the environment model, additional weaknesses are noticeable. Most approaches assume a 2D representation of the environment and that knowledge of its structure is *a priori* available or can be evaluated by the robots. Very few approaches assume unknown 3D environments. Nevertheless, evaluating the structure of an unknown environment is a time and computation-demanding task which introduces the additional problem of simultaneous localization and mapping. Alternative assumptions could be made where the robots have only partial knowledge of the environment, and the search strategy accounts for these limitations.

Finally, search approaches often rely on discretized probability maps representing the potential locations of targets. For these discretized probability maps, it proves difficult to account for real target dynamics in the update process of the map. Instead, the target motion models are often probabilistic and follow random walks, Bayesian, or Markovian models. It would be beneficial if the robots could account for the target dynamics in their search scheme.

1.2. Thesis outline and contributions

This thesis focuses on the problem of CSAT using a fleet of UAVs equipped with sensors to detect and localize targets within some observation subset of the search area. It proposes detailed modeling of target detection and identification condition, which are target and environment dependent, as an alternative to the widely used probabilistic description. Moreover, alternative noise and uncertainty assumptions are considered. Instead of assuming some probability density function characterizing the noise distribution, it is assumed that noise and uncertainties remain within *a priori* known bounds. Set-membership estimation techniques are then used to evaluate target state *set estimates*. These estimates consist of sets instead of points. The set estimates are guaranteed to contain the true state of the targets as long as the errors are absolutely bounded. The structure and contributions of the thesis are detailed hereafter.

Chapter 2 provides background information for the studies carried out in this thesis. This includes the definition and characterization of the general problem and a review of existing approaches. Furthermore, target state estimation and robot control techniques for target search and tracking are discussed.

Chapter 3 formulates the considered general problem. Deterministic geometric target detectability, recognition (distinguishability between true and false targets), and

identification conditions are introduced in place of the widely-used probability of detection/non-detection. The new conditions account for obstacles in the environment and target and UAV states. For each detected target, it is assumed that some noisy measurement of its state is available. The noise corrupting the state observation is assumed to be bounded with known bounds, which may depend on the observation conditions.

Chapter 4 presents a new cooperative target search and tracking scheme. When a target is detected, it is assumed that its identity is revealed only if some observation conditions are satisfied. This situation is typically encountered with cameras: the identity of a target is available only when it is observed from a satisfying point of view. Additionally, false targets, such as environmental clutter or decoys, are assumed to be present. These false targets may be erroneously identified as true targets, yet they are distinguished from them when observed under specific conditions. For each detected (true and false) target, it is assumed that some noisy measurement of its state is available. The noise corrupting the state observation is assumed to be bounded with known bounds, which may depend on the observation conditions. A robust distributed set-membership estimator run by each UAV is proposed, which enables to determine

- set estimates containing the state of each *identified* target,
- a set estimate containing the states of *detected* but *not yet identified* (true and false) targets,
- and a set possibly containing targets remaining to be detected (the part of the search area still to be explored).

The estimator is able to process measurements associated with detected but unidentified targets prior to their identification at later time instants. The set estimator alternates predictions and corrections using measurements from the sensor of each UAV and measurements received during communications with its neighbors. The control inputs for each UAV are designed using a Model Predictive Control (MPC) approach adapted to the set-membership estimation context, which aims at minimizing the volume of the set estimates. The MPC approach accounts for the impact of future measurements on the set estimates and infers future information communicated by neighbors. A limited communication range is also considered. In summary, the set-membership estimator proposed in Chapter 4 enables the detection and tracking of moving targets in the presence of moving false targets. Issues related to false detection and misidentification of false targets, and potential non-identification of true targets are considered. The distinction between true and false targets relies on some deterministic observation conditions. The distributed MPC approach accounts for the evolution of the set estimates, information from neighbors, and limited communications between UAVs. Simulations of scenarios, including the presence of false targets, illustrate the ability of the proposed approach to efficiently search and track an unknown number of moving targets within some delimited search area. Additionally, preliminary experimental studies are carried out.

Chapter 5 contributes to cooperative target search and tracking in uncharted environments when the targets are moving and may be partially hidden. Previous approaches try to build a map of the environment during the search mission, and partial occlusions of targets are usually modeled via probabilities of non-detection. An alternative approach modeling partial occlusions and addressing the search and tracking problem is proposed. UAVs do not try to build any map of the possibly evolving environment to avoid frequent and resource-consuming map updates. This avoids assuming that UAVs are able to perceive the obstacles and exploit this information, which is particularly relevant for night observations when the contrast of the environment diminishes when using RGB (red, green, and blue color model) or infrared cameras. Moreover, the ability of a UAV to detect targets depends on the target location and on the point of view of the UAV.

For each possible target location in the Region of Interest (RoI), one introduces its *detectability set* as the set of all UAV locations from where the target is visible, such that it is in line of sight of the UAV. Due to the uncharted time-varying environment, the detectability sets are unknown to the UAVs and evolve with time. It is assumed that at each time instant, each detectability set contains at least one non-zero volume half-cone. This means that targets are never fully occluded by the environment. The absence of a map of the environment and the unknown detectability sets makes it particularly challenging for UAVs to conclude the absence of a moving target when they observe a part of the RoI.

A solution to this problem is derived by assuming that the targets and obstacles in the environment are static. To address this problem, the notion of *conic observation subsets* of observation locations is introduced. It is then assumed that one of these conic subsets is included in the detectability set associated with each location in the RoI. Under this assumption, it is possible to guarantee that a location is free from a target when observed from different points of view, each belonging to a different observation subset. Consequently, the UAVs can gradually explore the search area from different points of view and prove the absence of the targets.

This solution is then extended to the general case where targets and obstacles may move. Then, to state that a location in the RoI is clear from any target, one has to observe this location simultaneously with sufficient diversity of points of view. To reach this diversity, the fleet of UAVs is partitioned into groups, where each UAV is in charge of observing the RoI from a given point of view. Once a target is detected, it is assumed again that its location is obtained with some bounded uncertainty. The distributed set-membership state estimator is adapted to evaluate sets guaranteed to contain target locations within the RoI and a set that is proven to be clear from any target. Contrary to Chapter 4, the proposed approach is able to guarantee the detection of partly hidden *moving* targets in an unknown *changing* environment. The trajectory of each group of UAVs is again designed in a distributed way minimizing a measure of the target state estimation uncertainty via an MPC approach.

Chapter 6 compares the proposed set-membership target state estimator with a classical stochastic estimation scheme and highlights the differences between the approaches. Both approaches are compared in simulations with static ground targets. Advantages and drawbacks are discussed.

Chapter 7 concludes the thesis and outlines important research directions and perspectives.

1.3. Publications

Peer-Reviewed International Journal article:

1) J. Ibenthal, M. Kieffer, L. Meyer, H. Piet-Lahanier and S. Reynaud. "Bounded-Error Target localization and tracking using a Fleet of UAVs". Automatica 132 (2021), p. 109809.

Peer-Reviewed International Conference papers:

2) J. Ibenthal, L. Meyer, M. Kieffer and H. Piet-Lahanier. "Bounded-Error Target Localization and Tracking in Presence of Decoys Using a Fleet of UAVs". In: IFAC-PapersOnLine. Vol. 53. 2020, pp. 9521–9528.

3) J. Ibenthal, L. Meyer, H. Piet-Lahanier and M. Kieffer. "Target Search and Tracking Using a Fleet of UAVs in Presence of Decoys and Obstacles". In: Proc. IEEE CDC. 2020, pp. 188–194.

4) J. Ibenthal, L. Meyer, H. Piet-Lahanier and M. Kieffer. "Localization of Partially Hidden Targets Using a Fleet of UAVs via Robust Bounded-Error Estimation". In: Proc. IEEE CDC. 2021, pp. 1224-1231.

Submitted Peer-Reviewed International Journal articles:

5) J. Ibenthal, H. Piet-Lahanier, L. Meyer and M. Kieffer. "Localization of Partially Hidden Moving Targets Using a Fleet of UAVs via Robust Bounded-Error Estimation". Submitted to IEEE Transactions on Robotics.

2. State of the art

This chapter provides background information for the studies carried out in this thesis. Section 2.1–2.6 encompass the definition and characterization of the general problem and a review of existing approaches. Section 2.7 introduces the set-membership and stochastic Bayesian estimation frameworks that are used for target state estimation for searching and tracking. Finally, Section 2.8 takes a look at the control design for searching and tracking and details the model predictive control approach.

2.1. Mobile robots observing mobile targets

Observing mobile targets evolving in some geographical area is a demanding task that groups of robots can efficiently address. The simultaneous and partly unpredictable evolution of the robots and targets makes this problem particularly challenging. Observing targets encompasses tasks such as search, surveillance, area coverage, tracking, pursuit-evasion, and others. Robin and Lacroix (2016) provide a survey of existing approaches. The common objectives of these tasks are that the states or locations of single or multiple targets need to be estimated, and the search trajectories or observation locations of the robots are usually designed to optimize the target state estimation accuracy.

In this thesis, the search mission is assumed to be carried out by a fleet of UAVs, which may be, *e.g.*, small fixed-wing aircrafts or quadcopters. The vehicles are equipped with sensors for collecting measurements of the target states. Their sensors have limited a range and opening angles. The limitations of the senor define the Field of View (FoV) which is a volume of the search space where a measurement can be collected for a given sensor.

Different tasks and missions can be classified into several observation problems. A selection of four important observation problems is presented in Table 2.1, which is based on the classification of Khan et al., 2016. This thesis focuses on the problem of cooperative search, acquisition, and tracking of multiple mobile targets, which will be detailed in Section 2.2. Other observation problem are briefly presented in the Sections 2.1.1–2.1.3.

Observation problem	Task
Cooperative search, acquisition, and tracking	situational awareness, search, rescue
Cooperative tracking	surveillance
Cooperative multirobot observation of multiple moving targets	patrolling, monitoring
Multirobot pursuit evasion	guarding, hunting, rescue, games

Table 2.1.: Four observing problems and relevant tasks; classification from Khan et al. (2016).

2.1.1. Cooperative tracking

The aim of Cooperative Tracking (CT) is to minimize the time duration between consecutive sensor observations of the target. The increased observation frequency of the target state and the resulting update of the estimate lead to a reduction of the estimation uncertainty. In a CT mission, the estimated locations of the targets are often known, and the robots do not search for new targets. CT is commonly applied for surveillance missions when the number of targets is of the same magnitude as the number of robots. The robots have to switch between the observation of different targets when there are more targets than robots. The robots may be partitioned into flocks or teams that observe a single target cooperatively when there are fewer targets than robots (La and Sheng, 2012). For example, Briñón-Arranz et al. (2019) address the problem of encircling a moving target with a fleet of unicycle-like vehicles. The motivation to observe a target from different observation locations may be to decrease its state estimation uncertainty as in, *e.g.,* Guerra et al. (2018). In Morbidi and Mariottini (2012), robots relocate themselves in the 3-D space to maximize the accuracy of their own position estimate and that of multiple moving targets. A control scheme for optimal UAV locations and camera gimbal poses to track the maximum number of targets is proposed in Farmani et al. (2015). Another motivation is to observe a target with some given formation (Ma and Hovakimyan, 2013).

2.1.2. Cooperative multirobot observation of multiple moving targets

Cooperative Multirobot Observation of Multiple Moving Targets (CMOMMT) aims to maximize the coverage of all tracked targets. The positioning of the robots has to be dynamically adapted to keep all targets under observation. CMOMMT was first presented in Parker and Emmons (1997); Parker (1999, 2002). The target locations

are uncertain and may be initially unknown. The robots often possess a search and a track mode. A robot searches until it detects a target. Then the robot switches to the track mode and persistently tracks the targets. CMOMMT is suited for patrolling and monitoring missions when the number of targets is smaller than the number of robots. The control design is derived from, *e.g.*, virtual forces (Parker, 2002; Kolling and Carpin, 2006), total target coverage (Pan et al., 2017; Tokekar et al., 2014), and model predictive control (Kuhn et al., 2011). The cooperation between the robots is quite limited since the robots often do not share their local target state estimate or their perception of the environment. In Kolling and Carpin (2006), some cooperation is achieved by allowing the robots to exchange help requests.

2.1.3. Multirobot pursuit evasion

The problem considered in Multirobot Pursuit Evasion (MPE) differs from the previous problems since the targets may exhibit an evasive behavior and move faster than the robots (Vidal et al., 2002; Durham et al., 2012; Alexopoulos et al., 2015; Lhommeau et al., 2007). The objective of the robots is to capture the targets, *i.e.*, to approach the target up to some threshold. Typical tasks are guarding, hunting, rescue, and games. The targets may be intelligent and can anticipate the intent of the robots. Consequently, the motion of the targets and the robots are interdependent, and motion planning is related to a game theoretical framework, economic-based negotiation, or auction mechanisms. The objectives of the control design are either minimizing the time of capture or maximizing the probability of capture.

2.2. Cooperative search, acquisition, and tracking

The CSAT problem has received increased interest in the last decades due to the wide range of applications that it concerns. Most state-of-the-art CSAT techniques rely on cooperative control strategies and on distributed state estimation. The objective of CSAT is to continuously search for new unknown targets and to track the location of already detected targets. CSAT has to deal with the trade-off between estimating accurately the states of known targets and the exploration of the search zone to find new unknown targets. Control strategies vary according to the different modes, *e.g.*, a search mode to find not yet detected targets and a track mode to refine the estimate of already identified targets, see How et al. (2009) and Khan et al. (2016) and references therein. The transition between these two modes depends typically on some probabilistic measure of the likelihood of potential target locations. A robot tracks and observes a target until the estimation uncertainty becomes reasonably small. Then the robot switches to the search mode, leaves the target, and heads to zones where the detection of a new target may be likely. When the uncertainty of known targets becomes larger than some threshold, the robot switches back to the track mode and tries to observe known targets to reduce their state estimation

uncertainty. This control strategy has some drawbacks since the transitions between different modes need to be balanced to achieve target search and tracking with equal importance. Nevertheless, even in a well-balanced control design, robots may still remain close to the targets since the estimation uncertainty may grow too fast if the targets are not observed.

In this thesis, the considered observation problems are closely related to CSAT. The objectives are to search for unknown and to track already known targets simultaneously. The developed control scheme is not mode-based. Instead, the objective/cost function naturally combines the need for searching or tracking. However, the searching and tracking still need to be balanced within the cost.

CSAT approaches can often be divided into separate search and tracking schemes. Therefore searching and tracking approaches are presented independently hereafter.

2.3. Target search

Target search is related to area exploration problems. The general objectives are to find all targets in the Region of Interest (RoI) as fast as possible and to increase the probability of detection of new targets. Many approaches consider a grid-based probability map of the search zone representing the confidence for potential target locations (Furukawa et al., 2006; Yang et al., 2004, 2007; Bertuccelli and How, 2006b; Khan et al., 2015; Vidal et al., 2001; Hespanha et al., 1999). The probability of the presence of a target in each cell can be either modeled as a single value (Yang et al., 2007) or as a stochastic variable with a probability density distribution (Bertuccelli and How, 2005, 2006a). The evolution and update of the map are performed by recursive Bayesian filtering. The correction step after measurement accounts for probabilities of true positive and false positive detection but does not explicitly integrate measurement uncertainties (Hu et al., 2017, 2012). Nevertheless, limited Fields of View (FoV) of the embedded sensors and communication constraints can be taken into account as in Khodayi-mehr et al. (2019) and Zhang et al. (2017). The correction step after communication for multi-agent probability map fusion can be performed as a consensus-like map update as proposed in Hu et al. (2014). The prediction step often relies on simplified target dynamics. Target motion models are usually probabilistic such as random walks or Markovian models. Introducing a more precise description of the target dynamics requires disposing of a level of *a priori* knowledge that is seldom available.

A weakness of classical search strategies lies in the need to describe the sensor detection and discrimination abilities, which are usually modeled with probabilities of true positive and false positive detection. Both might be chosen constant over the RoI (Li and Duan, 2017), dependent on the detection range or measurement signal-to-noise ratio as in (Hu et al., 2014), or dependent on the target state (Song et al., 2010). Choosing appropriate values might prove difficult *a priori*, although,

as pointed out in Gu et al. (2015), their choices considerably impact the search performance. Furthermore, a probabilistic description proves difficult to integrate the influence of the environment on the ability to detect the targets. In the overview Bucci and Varshney (2019), only Ulmke and Koch (2006) are mentioned to account for obstacles and environmental obstruction in modeling the detection probability. A deterministic geometric description seems more appropriate to characterize a target occlusion by a part of the environment. For example, the ability of a UAV to detect a target partially hidden by an obstacle is severely decreased. This is more easily translated in terms of geometrical considerations than in some probability of non-detection. In this sense, Yao et al. (2016); Klodt et al. (2015, 2014) present approaches to model visible areas by *visibility sets/regions*. In Pan et al. (2017), a model of the quality of observation depending on the target heading is introduced. Nevertheless, these approaches are designed for surveillance or area coverage and not search problems.

Another interesting search-related problem is the characterization of the explored area that does not contain any target. Set-membership techniques are well suited to characterize such areas with either deterministic boundaries, as in Desrochers and Jaulin (2016); Drevelle et al. (2013), or with uncertain boundaries, as in Boukezzoula et al. (2021).

2.4. Target tracking

Target tracking aims to obtain consecutive observations of a known target to determine its trajectory and estimate its state while predicting more accurately its next position. The estimation starts with an *a priori* estimate of the target state usually obtained during the search process. The target dynamics and measurements are then used in a stochastic Bayesian filtering framework for state estimation, such as classical Kalman filtering and its variants. A variety of models can describe the target dynamics. Classical models include zero-velocity, constant velocity, linear, or nonlinear dynamics (Allik, 2019; He et al., 2017). The estimation scheme typically accounts for detection probabilities and measurement uncertainties, which are assumed to be Bernoulli and Gaussian distributions, respectively. Tracking with state-dependent probability of detection is, *e.g.*, considered in Song et al. (2010). Various types of measurements can be integrated, *e.g.*, noisy heterogeneous ranging and direction of arrival measurements are considered in Guerra et al. (2019). Incorporating a covariance matrix of the target state perturbation allows to account for the uncertain movement of mobile targets and increases the estimation uncertainty when targets are not tracked (Frew and Elston, 2008). Few tracking schemes account for the absence of information. However, in Allik (2019), negative information is used to refine the target state estimate.

When measurements can not be associated with a specific target, the correction step from measurements becomes a data association problem. Joint probabilistic data

association, multiple hypothesis tracking or random finite set methods can then be used to estimate the target state (Blackman, 2004; Bar-Shalom et al., 2011).

There are few approaches considering set-membership estimation techniques for target tracking. In Bai et al. (2021), a single target is tracked in a centralized wireless network. Xia et al. (2018) evaluate local and global ellipsoidal set estimates for target tracking in a distributed network set-membership filter. Ellipsoidal set estimates are also used in Hou et al. (2021) to persistently track a single UAV using static ground robots equipped with optical seekers. Nevertheless, these approaches consider static sensor networks and do not propose any control scheme for the evolution of the robots. In the context of target search and tracking, initial works were suggested in Reynaud et al. (2018) and Reboul et al. (2019), although they did not address several major issues such as identification and detection conditions of targets, the potential presence of decoys, and limited communication range.

Low visibility, high clutter, and target density impact target tracking in a structured environment. Exploiting as much *a priori* information as possible is desirable to improve the target state estimation accuracy. Important information encompasses realistic models of the measurements, sensors, target dynamics, possible target locations, clutter/obstacles, and *a priori* knowledge about the target locations. In Yu et al. (2014), moving ground targets in an urban environment are tracked. The approach accounts for the occlusion by obstacles. However, the environment is assumed to be perfectly known.

2.5. Target observation – Detection, Recognition, Identification

An essential process for target search and tracking is the observation process, which is the only moment when new information about the target is acquired. When an observation is taken, the sensing system (*e.g.,* image processing system) of the robot has to carry out an interpretation process. The quality of the observation limits the amount of information that can be obtained. Important information is, *e.g.*, whether a target is present, where it is located, and what kind of target is detected. In Johnson (1958), in the context of target observations with image forming systems, the available information and the decision response of the image processing system is quantized into six distinct levels:

1. no detection,
2. detection,
3. orientation,
4. shape recognition,
5. detail recognition,

6. and identification.

The more information is extracted, the more precise the decision response. In this thesis, a simplified model for the decision response is considered, and classification into no detection, detection, recognition, and identification is assumed. *No detection* means that no target is detected by the sensing system. *No detection* can appear if no target is within the FoV or the collected observation is of very low quality. When a target is within the FoV, and the observation quality is sufficiently high, the sensing system response may be the *detection* of a target. Detection does not allow to conclude that the detected object is a target; it only means that "something" is detected. Nevertheless, detection always leads to the collection of a measurement. The measurement allows estimating the state of the detected object (*e.g.*, location, orientation, velocity, and others). Depending on the type and quality of the observation, not all properties of the detected object may be measurable. When the observation quality further increases, the system response will be a *recognition*. The detected object is classified by some characteristics and is now treated as a target. The classification may be rudimentary (*e.g.*, static or moving object) or more detailed (*e.g.*, animal, human, vehicle, and others). Recognition does not allow the differentiation between two targets belonging to the same class. If targets are only recognized, it is difficult to estimate the number of different targets that have been detected. Finally, the most precise system response is the *identification* of a target. An identified target is characterized by a unique feature that allows differentiating the target from other targets of the same class. The unique feature may be, *e.g.*, the license plate of a car or the face of a human.

The decision response of the image processing system may be erroneous when a noisy sensor is considered. A classification of correct and incorrect decision responses is shown in Table 2.2.

True positive detection means that a target is correctly detected, and the collected measurement is generated by a real target. Most tracking approaches rely on measurements that are obtained from true positive detections to refine the target state estimates. False positive detection may appear when the decision response of the sensing system is erroneous due to low observation quality, clutter, or decoys. The collected measurement is not generated by a real target. Depending on the estimation scheme, the erroneous measurement may increase the estimation uncertainty, lead to an inconsistent target state estimate, or the loss of the tracked targets. In Bar-Shalom et al. (2011); Li and Duan (2017); Dames (2020), a probability of false detection/alarm is introduced to account for the imperfect processing of the information acquired by the sensors. Another possibility consists of considering the presence of clutter, decoys, or false targets, *i.e.*, objects that are assumed to be a true target when seen from a specific point of view. For example, Flint et al. (2004) introduces a Bayesian filter for cooperative search to determine whether a detected target or object is real or not. In He et al. (2017), the random finite set probability density is used to model both target-generated observations and false alarms. An interactive multi-model filter is then used to estimate the modes of the detected

Used term	Other terms	Interpretation
True positive detection	True detection; detection	Target within the FoV **and** target detected
False positive detection	False detection; false alarm; spurious detection, decoy; ghosting	Target not within the FoV **and** target detected
True negative detection	No detection, absent measurement;	Target not within the FoV **and** target not detected
False negative detection	Missed detection; non-detection; non-observation	Target within the FoV **and** target not detected
Recognition	-	Detected target recognized as target (assumed to belong to target class)
False recognition	-	Detected decoy recognized as target (assumed to belong to target class)
Identification	-	Detected target identified as target and its unique identifier is obtained
Misidentification	Misidentification; false identification	Incorrect target identity obtained
Confusion	Confusion; misidentification; false identification	Incorrect target identity obtained **but** identity belongs to the list of considered target identities

Table 2.2.: Classification of decision responses

objects. Detection can also be linked to some additional observation conditions not only depending on the field of view but also on the relative orientation of the robot and target.

True negative detection corresponds to the case when no target is within the FoV and nothing is detected. The sensing system does not collect a measurement when true negative detection occurs. Nevertheless, this negative information can still be used for target state estimation. Most target search schemes rely on this negative information to prove the absence of targets in an observed zone. Only a few tracking schemes actually make use of this negative sensor information (Allik, 2019; Blanding et al., 2006). When the sensing system is erroneous or due to environmental conditions, false negative detection may occur, *i.e.*, a target is in sensing range, but it is not detected. This situation may occur due to low signal-to-noise ratio of the sensing system or because the target is partially hidden due to, *e.g.*, obstacles, clouds, shadows, and others factors. False negative detection is often modeled by some probability of detection which may be constant (Allik, 2019), or depends on state (Song et al., 2010), time (Hu et al., 2014), or space (Ulmke and Koch, 2006). Detection may also be linked to some additional observation conditions depending

on the sensor and the relative orientation of the robot and target. A target monitoring problem is considered in Pan et al. (2017), where the detection of a target depends on the target heading angle.

Recognition and identification conditions are rarely considered or even distinguished in approaches considering mobile robots observing mobile targets. Common approaches assume that the targets are either always (distinguishable targets) (How et al., 2009) or never (indistinguishable targets) identified (Hu et al., 2017). Some approaches consider that the target identity is revealed when some additional observation conditions are satisfied. Results have been obtained in Blasch and Kahler (2005), where simultaneous target tracking and identification from electro-optical and infrared sensors are considered.

In this thesis, in Chapter 4, a search and tracking approach is developed that accounts for the different levels of information obtained from the decision response of the sensor, *i.e.*, the approach accounts for false negative detection, detection, recognition, and identification of targets and false targets. The term *false target* will be used for clutter or decoys. Additionally, misidentification and confusion are also considered. Confusion means that a false target is detected and misidentified as a true target.

Possible decision responses of the sensing system are strongly linked to the sensor types that are used. The classification introduced above is well adapted for image forming systems, such as RGB-Cameras or IR-Cameras. Nevertheless, different sensors allow measuring different properties such as, *e.g.*, the presence or absence of a target, its type, identity, location, velocity, and others. Recent approaches consider robots with heterogeneous sensors, where the collected information is fused to estimate the target state (Guerra et al., 2019, 2018).

The detection capabilities of a sensor depend on its performance (*e.g.*, noise and detection errors) and the environmental conditions. The detection capabilities of the sensor can be modeled using deterministic (How et al., 2009; Vencatasamy et al., 2018) or stochastic detection models. Both models can account for measurement noise, while the latter also allows accounting for stochastic detection errors. The detection errors are often modeled with some probabilities of true positive detection and false positive detection (Allik, 2019; Zhong et al., 2017; Dames, 2020; Li and Duan, 2017).

In this thesis, UAVs are equipped with vision-based sensors such as RGB-Cameras. The FoV of the Camera may be reduced in some scenarios due to the presence of obstacles. For the estimation scheme, a new deterministic detection model is introduced that accounts for false negative detection of the targets when they are located within the FoV of the UAVs but hidden behind obstacles.

2.6. Characteristic of the search and tracking problem

Among the various elements that impact the search and tracking performances, the most important elements, according to Khan et al., 2016, are the characteristics of the targets, robots, environment, sensors, and coordination methods. The characteristics and models of sensors and the obtained information have been discussed in Section 2.5. Consequently, this section focuses on the remaining four elements and presents the common assumptions that are made regarding their modeling.

2.6.1. Modeling of the targets

The type and behavior of targets vary between different observation applications and significantly impact the difficulty of estimating the target location. Cooperative targets facilitate the observation task drastically since they may transmit their locations and trajectories to the robots (Pack et al., 2009). More common is the assumption that the targets are non-cooperative, *i.e.*, they exhibit a passive behavior, do not actively transmit information to the robots, and completely ignore the robots (Parker, 2002; Kuhn et al., 2011). Consequently, they do not try to hide. More challenging becomes the observation of evasive targets which can sense the robots and avoid being observed (Hu et al., 2017).

A second important characteristic of the targets is their mobility. Most studies assume that the targets do not cooperate with other targets and that their movements are independent. Their trajectories are often unknown (Dames, 2020) and follow either random walks (Tokekar et al., 2014; Kolling and Carpin, 2006), parameterized linear (Schweppe, 1968; Gu et al., 2015; Liu and Zhao, 2014; Bai et al., 2021), or non-linear dynamic models (Baek and York, 2020), with partially or totally unknown parameters. The mobility of the targets is often inferior to that of the robots, such that, *e.g.*, the maximum speed of the targets is smaller than that of the robots. Regarding the degree of freedom, many studies consider ground targets that evolve on a plane (Ma and Hovakimyan, 2013; Kolling and Carpin, 2006). Much fewer studies consider targets moving in 3D space (Morbidi and Mariottini, 2012).

Assumptions considering the number of targets vary among approaches. Some studies assume a constant and known number of targets. Other approaches consider an unknown but constant (How et al., 2009; Tokekar et al., 2014; Kolling and Carpin, 2006; Li and Duan, 2017) or changing number of targets (Dames, 2020). When the number is changing, some enter and exit zones are defined, which may be available (Dames et al., 2017) or unavailable (Dames, 2020) to the robots.

This thesis presents an observation and estimation scheme that allows estimating the target state vector (potentially evolving in a higher dimension than $\mathbb{R}^3$) of targets whose location may evolve in the 3D space. However, in the simulation part, the estimator is only validated for targets moving on a plane. In every approach, it is assumed that the number of targets is unknown and constant. A changing number

of targets could be integrated by introducing enter and exit zones. The entering zones need to be known.

2.6.2. Modeling of the robots

Most approaches assume that every robot has a sensor to observe the targets and the environment. The fleet can be either homogeneous (Kuhn et al., 2011; Parker, 2002) or heterogeneous (Guerra et al., 2019), *i.e.*, the robots and their sensing capabilities may be identical or differ among the group. Some applications require heterogeneity of the fleet, *e.g.*, the search and track of targets moving inside or outside buildings needs the cooperation of ground and aerial vehicles since their accessible areas are very different (Klodt et al., 2015; Tanner and Christodoulakis, 2006).

Each robot collects a measurement locally and may transmit the collected information to the rest of the group. Using this information, the estimation of the target state may be evaluated in a centralized (Pitre et al., 2012), decentralized (Tanner and Christodoulakis, 2006), or distributed (Dames, 2020; Kolling and Carpin, 2006) fashion, where the processing scheme depends mostly on the processing capabilities of each robot and the properties of the communication network. Some approaches consider silent surveillance missions where communication is forbidden (Vencatasamy et al., 2018). For cooperative missions between different classes of robots, the robots may transmit target state estimates, their own locations, control inputs, or other intended actions (Pan et al., 2017; Tanner and Christodoulakis, 2006; Klodt et al., 2015). The objective of their control design may be, *e.g.*, the search for new targets (Tang et al., 2020; Hu et al., 2017), the localization of known targets (La and Sheng, 2012), or taking observations from different points of view (Cichella et al., 2015).

Regarding different classes of robots, the application of aerial robotic swarms is very favorable for distributed sensing. The swarms can simultaneously gather observations from disjoint locations that may not be accessible to ground robots. They are consequently very well suited for target search, monitoring, and area mapping, as pointed out by (Chung et al., 2018).

This thesis considers deploying a fleet of UAVs to observe moving ground targets. The UAVs are able to detect the targets when they are in sensing range. The collected information, either obtained by measurements or communication, is processed locally by each UAV independently. Consequently, each UAV evaluates a target state estimate in a distributed fashion.

2.6.3. Modeling of the environments

The characteristics of the environment containing the targets and the robots are quite diverse. The considered deployment of the robots may be, *e.g.*, on the ground

(Kuhn et al., 2011; Kolling and Carpin, 2006; Parker, 2002), in the air (Pitre et al., 2012; Tokekar et al., 2014; Li and Duan, 2017) or in/on the water (Cao et al., 2018; Drevelle et al., 2013). The selected environment has a major impact on the dynamics of the robots and the target, the types of sensors that can be used, and the information available to the robots (*e.g.*, operating in GPS-denied environments makes self-localization difficult). The considered RoI can be a 2D plane (Ma and Hovakimyan, 2013; Allik, 2019; Dames et al., 2017; Vencatasamy et al., 2018; Pitre et al., 2012), commonly used for ground robots, or a 3D space (Guerra et al., 2019; Morbidi and Mariottini, 2012), commonly used for aerial vehicles. Furthermore, the environment may restrict the FoV of the sensor and limit the sensing range with which a target can be detected (Li and Duan, 2017). These limitations come mainly from the structure of the environment and obstacles therein. In a known environment, the complete structure of the terrain, the locations of obstacles, and the allowed or forbidden zones for the targets are available to the robots and can be used to refine the target state estimate (Ulmke and Koch, 2006; Drevelle and Bonnifait, 2013; Li and Duan, 2017; Yu et al., 2014). The observation task becomes much more challenging if no information about the environment is available. The allowed zones for the targets are then unknown, and the targets may be partially hidden behind unknown obstacles (Cao et al., 2018; Xu et al., 2019). Furthermore, not only is the observation of the targets more difficult but also the navigation of the robots becomes challenging (La and Sheng, 2012) or even dangerous (Pitre et al., 2012). In an unknown environment, the robots may also need to perform self-localization and area mapping (Kim et al., 2018; Lyu et al., 2019). Finally, an additional level of complexity is added by dynamically evolving environments where the evolution may be known or unknown. The target observation becomes then very challenging since the robots have to adapt their observation strategies dynamically.

In this thesis, Chapter 4 deals with target search and tracking in a known structured or unstructured environment. Then, Chapter 5 extends the developed approach to unknown static environments (see Section 5.3) and unknown evolving environments (see Section 5.4).

2.6.4. Coordination methods of the robots

The possible coordination methods of the robots depend strongly on their communication capabilities, *i.e.*, the connectivity of the communication graph and the characteristics of the communication network, *e.g.,* the bandwidth, and delays. Similar to the target estimation scheme, the coordination method can be centralized (Yao et al., 2016), decentralized (Tanner and Christodoulakis, 2006), or distributed (Guerra et al., 2019; Li and Duan, 2017).

In a centralized coordination network, the robots transmit the collected information to a central node which processes all the data and evaluates for every robot the next action to be taken. The evaluated actions are then broadcast, and each robot applies

its allocated action. The advantage is that the central node can use all available information to solve the estimation and optimization problem. The disadvantages are bad scaling regarding the number of robots, sensibility to the loss of robots, and the requirement of a completely connected network.

The robots are partitioned into groups with leaders in a decentralized coordination network. The leader often has stronger processing capabilities and serves as a central node to process the collected information. The leader then allocates actions to its followers. Decentralized coordination allows to gain more robustness against the loss of robots and allows intermittent communication between different groups. The disadvantage is that the leaders do not have all the information, and the elaborated strategies become suboptimal.

The robots can autonomously evaluate their control design in a distributed coordination network. This requires that every robot has sufficient processing power and that the estimation and control scheme can be evaluated in a distributed fashion. The advantage of a distributed coordination network is that each robot operates only with partially available information. Consequently, the performance of the group is less affected by communication problems or the loss of robots in the group. The disadvantage is again that each robot does not have all the group information, which also makes the resulting strategies suboptimal.

In this thesis, the developed estimation and control schemes are fully distributed, allowing the UAVs to operate even when communication is limited.

2.7. State estimation for target search and tracking

The aim of state estimation in the context of target search and tracking is to characterize variables of interest of a target system, such as, *e.g.* its location, orientation, velocity, and acceleration. These variables of interest are collected in the target *state vector,* which is usually associated with a simplified system representation. The process of state estimation consists of determining state vector components as close as possible to the true state value for a chosen metric. The estimation process incorporates information about the model, measurements of the state vector, and the various errors that impact the state estimation.

Three error types appear when measuring a real system (*e.g.*, a target) and estimating its state (Walter and Pronzato, 1994). First, *measurement errors* are caused by imperfect sensing devices. Second, *structural errors* reflect the fact that the model used to describe the system and its evolution is always an approximation and simplification of reality. Finally, *perturbations* reflect that uncertain external inputs (also called disturbance) affect the system.

A class of frequently used estimation techniques is based on statistical means, where one assumes that the noises and uncertainties affecting the estimation can be modeled by random variables with known probability density function. The estimates

are obtained using maximum likelihood determination – when only hypotheses on the probability density function describing the measurement noise are available – or using Bayesian optimal filtering – when *a priori* information about the estimated variable is available –. From a Bayesian perspective, maximum likelihood estimation evaluates the maximum *a posteriori* estimation assuming a uniform prior distribution of the estimated variable. A limitation of statistical estimation techniques is that they are weakly adapted for systematic errors, *i.e.*, when the measurement error has a constant component that does not follow the realization of a random variable. Systematic errors appear, *e.g.*, due to discretization in numerical processing systems or as bias on the measurement such as, *e.g.*, those collected by an inertial measurement unit. Another limitation arises when the knowledge of the errors is sparse and does not allow assessing a probability density function. Most often, it is still possible to gather some information on the variations of the errors by providing the bounds within which they must vary.

Assuming that the probability density function of the measurement error is unknown but bounded leads to another class of estimation techniques, *i.e.*, set-membership estimation or bounded error estimation. The objective of set-membership estimation is to evaluate set estimates that are guaranteed to contain the actual state of a system. The set estimate is derived from the collected measurements assuming that noises and perturbations remain within *a priori* known bounds. Every point within the set estimate is a potential candidate for the actual system state. Nothing can be said about the likelihood of a point (in the set estimate) compared to another. Contrary, maximum likelihood and Bayesian estimation techniques usually provide point estimates for most of the classically used density functions.

The approaches in this thesis focus on set-membership estimation techniques. However, the developed set-membership approach is compared with existing classical statistic estimation techniques in Chapter 6. Consequently, both types of estimators are presented hereafter. Section 2.7.1 formalizes the estimation problem. A general scheme for set-membership estimation is presented in Section 2.7.2. A brief presentation of optimal Bayesian filtering is given in Section 2.7.3.

2.7.1. Estimation problem

Let N^{t} targets evolve independently in a given Region of Interest. The initial locations, number, and trajectories of the targets may be *a priori* unknown. Assuming that time is sampled with a constant period T, the state vector of target j at time $t_k = kT$ is

$$\mathbf{x}_{j,k}^{\mathrm{t}} = \left(x_{j,k,1}^{\mathrm{t}}, x_{j,k,2}^{\mathrm{t}}, \ldots, x_{j,k,n^{\mathrm{t}}}^{\mathrm{t}}\right)^{\top} \tag{2.1}$$

where n^{t} is the dimension of the target state vector, *i.e.*, $\mathbf{x}_{j,k}^{\mathrm{t}} \in \mathbb{R}^{n^{\mathrm{t}}}$. The elements $x_{j,k,1}^{\mathrm{t}}$, $x_{j,k,2}^{\mathrm{t}}$, $\ldots$, and $x_{j,k,n^{\mathrm{t}}}^{\mathrm{t}}$ may represent, *e.g.*, the location, orientation, velocity,

and acceleration of the target in some frame of reference. The evolution of the state vector is modeled as

$$\mathbf{x}^{\mathrm{t}}_{j,k+1} = \mathbf{f}^{\mathrm{t}}_k \left(\mathbf{x}^{\mathrm{t}}_{j,k}, \mathbf{v}_{j,k} \right), \tag{2.2}$$

where $\mathbf{f}^{\mathrm{t}}_k$ is the known dynamic model of the target and $\mathbf{v}_{j,k}$ is the state perturbation of target j at time t_k.

In order to observe the N^{t} targets, a set of N^{u} UAVs is deployed. The state of UAV i at time t_k is

$$\mathbf{x}^{\mathrm{u}}_{i,k} = \left(x^{\mathrm{u}}_{i,k,1}, x^{\mathrm{u}}_{i,k,2}, \ldots, x^{\mathrm{u}}_{i,k,n^{\mathrm{u}}} \right)^\top \tag{2.3}$$

where n^{u} is the dimension of the state vector, *i.e.*, $\mathbf{x}^{\mathrm{u}}_{j,k} \in \mathbb{R}^{n^{\mathrm{u}}}$. Similar to (2.1), the elements $x^{\mathrm{u}}_{i,k,1}$, $x^{\mathrm{u}}_{i,k,2}$, …, and $x^{\mathrm{u}}_{i,k,n^{\mathrm{u}}}$ may represent, *e.g.*, the location, orientation, velocity, and acceleration of the UAV. Additionally, $\mathbf{x}^{\mathrm{u}}_{i,k}$ may also contain information about the state of the sensor of UAV i. The evolution with time of the state of UAVs is modeled as

$$\mathbf{x}^{\mathrm{u}}_{i,k+1} = \mathbf{f}^{\mathrm{u}}_k \left(\mathbf{x}^{\mathrm{u}}_{i,k}, \mathbf{u}_{i,k} \right), \tag{2.4}$$

where $\mathbf{f}^{\mathrm{u}}_k$ is the known dynamic model and $\mathbf{u}_{i,k}$ the control input of the UAVs.

The UAV are equipped with a sensor able to observe the targets. When a target is observed and detected, a noisy measurement

$$\mathbf{y}_{j,k} = \mathbf{h} \left(\mathbf{x}^{\mathrm{t}}_{j,k} \right) + \mathbf{w}_{j,k}, \tag{2.5}$$

is obtained, where $\mathbf{h}$ is the observation equation (also called measurement equation) and $\mathbf{w}_{j,k}$ the measurement noise associated to target j at time t_k. The measurement vector $\mathbf{y}_{j,k} = \left(y^{\mathrm{t}}_{j,k,1}, y^{\mathrm{t}}_{j,k,2}, \ldots, y^{\mathrm{t}}_{j,k,n^{\mathrm{m}}} \right)^\top$ of dimension n^{m} contains all measured values, such as, *e.g.* relative distances, angles, and velocities between the robot and the target.

The collected measurement allow the robot to estimate some state elements $x^{\mathrm{t}}_{j,k,n}$, $n = 1, \ldots, n^{\mathrm{u}}$, and to derive a target state estimate. Set-membership state estimation is detailed hereafter.

2.7.2. Set-membership estimation

Set-membership estimation techniques assume that noises and uncertainties affecting the measurements and the dynamic system remain within bounded sets. No assumptions are made about the probability density functions of the noises and uncertainties. The evaluated state estimate consists of sets instead of points. The set estimate is guaranteed to contain the actual state of the system as long as the errors

are absolutely bounded. A set estimate consists of all the state values that are consistent with the measurements and dynamic model, given the bounds on the errors and perturbations. Every point within the set estimate is a potential candidate for the actual system state.

Set-membership estimation was first proposed in Schweppe (1968), where a recursive state estimator is used to evaluate an ellipsoidal set to bound the feasible state of a linear dynamic system. The dynamic system and the measurements are corrupted by perturbations and noise, respectively. Schweppe (1968) assumes that both errors remain within bounded sets, which are approximated by ellipsoids.

For the set-membership estimation, it is assumed that the target state perturbation in (2.2) belongs to the known and bounded set $\{\mathbf{v}\}$ and that the measurement noise in (2.5) belongs to the known and bounded set $\{\mathbf{w}\}$.

At time t_k, let $\mathbb{X}_k$ be the initialized set estimate of the target state $\mathbf{x}_k^{\mathrm{t}}$. The initial set estimate satisfies $\mathbf{x}_k^{\mathrm{t}} \in \mathbb{X}_k$. Target index j is omitted for simplification. The aim of the estimator is to evaluate the set estimate $\mathbb{X}_{k+1}$ at time t_{k+1} accounting for the dynamics and the measurements of the target. The estimation scheme starts with the prediction of the evolution of the system state. For the prediction step, the estimator can only account for information that is available at time t_k. The *a priori* (predicted) estimate

$$\mathbb{X}_{k+1|k} = \left\{ \mathbf{f}_k^t \left(\mathbf{x}, \mathbf{v} \right) \mid \mathbf{x} \in \mathbb{X}_k, \mathbf{v} \in \{\mathbf{v}\} \right\} \tag{2.6}$$

contains all possible states that can be reached from a state $\mathbf{x} \in \mathbb{X}_k$ considering the dynamics $\mathbf{f}_k^{\mathrm{t}} \left(\mathbf{x}, \mathbf{v} \right)$ and all possible perturbations $\mathbf{v} \in \{\mathbf{v}\}$.

At time t_{k+1}, a measurement $\mathbf{y}_k$ of $\mathbf{x}_k^{\mathrm{t}}$, using (2.5), is collected and the set estimate $\mathbb{X}_{k+1|k}$ can be corrected. The *a posteriori* estimate

$$\mathbb{X}_{k+1} = \left\{ \mathbf{x} \in \mathbb{X}_{k+1|k} \mid \mathbf{x} \in \mathbf{h}^{-1} \left(\mathbf{y}_k - \mathbf{w} \right), \mathbf{w} \in \{\mathbf{w}\} \right\} \tag{2.7}$$

is the subset of $\mathbb{X}_{k+1|k}$ that is consistent with the measurement $\mathbf{y}_k$ the inverse observation equation $\mathbf{h}^{-1} \left(. \right)$ and the measurement noise set $\{\mathbf{w}\}$. An alternative to (2.7) is to compute $\mathbb{X}_{k+1} = \mathbb{X}_{k+1|k} \cap \mathbb{X}_{k+1}^{\mathrm{o}}$ where

$$\mathbb{X}_{k+1}^{\mathrm{o}} = \left\{ \mathbf{x} \in \mathbb{R}^{n^{\mathrm{t}}} \mid \mathbf{x} \in \mathbf{h}^{-1} \left(\mathbf{y}_k - \mathbf{w} \right), \mathbf{w} \in \{\mathbf{w}\} \right\} \tag{2.8}$$

is the observation set, which is the set of states that are only consistent with measurement $\mathbf{y}_k$ and the bounded noise $\{\mathbf{w}\}$. Consequently, the *a posteriori* estimate is the intersection of the *a priori* estimate with the observation set. The evaluation of $\mathbb{X}_{k+1}$ in (2.7) or (2.7) requires the inverse observation equation $\mathbf{h}^{-1} \left(. \right)$. Obtaining $\mathbf{h}^{-1} \left(. \right)$ may not be trivial considering the general case of a nonlinear observation function. When it is not possible to evaluate $\mathbf{h}^{-1} \left(. \right)$, the correction step in (2.7)

becomes a set inversion problem and can be rewritten as

$$\mathbb{X}_{k+1} = \left\{ \mathbf{x} \in \mathbb{X}_{k+1|k} \mid \mathbf{h}(\mathbf{x}) \in \{\mathbf{y}_k - \mathbf{w}\}, \mathbf{w} \in \{\mathbf{w}\} \right\}. \tag{2.9}$$

The solution of (2.9) can be numerically approximated by, *e.g.*, set inversion via interval analysis (Jaulin and Walter, 1993; Moore, 1992).

The evaluated sets in the estimation scheme can be represented by, *e.g.*, ellipsoids, intervals, polytopes, and others. Techniques to find appropriate sets for $\{\mathbf{v}\}$ and $\{\mathbf{w}\}$ can be found in Piet-Lahanier and Walter (1994); Han et al. (2018). In practice, the assumption of bounded measurement noise and state perturbation may not always be verifiable. However, if these bounds are not satisfied, then the confidence of the estimate decreases monotonically towards zero as the time approaches infinity (Jaulin, 2011b). Noisy measurements outside the assumed noise bounds are treated as outliers, which lead directly to incorrect estimates. To overcome this issue, one may assume that the noise is bounded with a known probability (Jaulin, 2011b), or that the number of outliers within some time interval is limited (Jaulin, 2009; Drevelle and Bonnifait, 2013).

Set-membership estimation has many applications and is attractive due to its guaranteed properties and limited assumptions. Langerwisch and Wagner (2012) use set-membership estimation techniques for self-localization of a mobile robot. A secured zone that does not contain targets is evaluated in Vencatasamy et al. (2018). Simultaneous localization and tracking are performed in (Jaulin, 2011a). (Lhommeau et al., 2007) evaluate a guaranteed capture basin of a target which corresponds to initial robot states that can reach the target. (Drevelle and Bonnifait, 2010) presents a car localization approach that is robust to a given maximum ration of measurement outliers.

In the context of mobile robots observing mobile targets, set-membership estimation has been applied since 2015 in Gu et al. (2015). Xia et al. (2018) evaluate local and global ellipsoidal set estimates for target tracking in a distributed network set-membership filter. In Bai et al. (2021), a single target is tracked in a centralized wireless network. Hou et al. (2021) evaluate ellipsoidal set estimates to persistently track a single UAV using static ground robots equipped with optical seekers.

2.7.3. Stochastic Bayesian estimation

The state of a system can be estimated by stochastic estimation techniques when noises and uncertainties are assumed to be random variables with known probability density function. Bayesian optimal filtering allows the evaluation of conditional probability densities based on *a priori* information, state transition densities, and measurement densities. An estimate of the state may then be evaluated based on maximum likelihood. The framework of Bayesian optimal filtering is presented hereafter.

Bayesian optimal filtering aims at evaluating the conditional probability density $p\left(\mathbf{x}_{k+1}^{\mathrm{t}} \mid \mathcal{Y}_{k+1}\right)$ of the state $\mathbf{x}_{k+1}^{\mathrm{t}}$ given all the past measurements $\mathcal{Y}_{k+1} = \{\mathbf{y}_1, \mathbf{y}_2, \ldots, \mathbf{y}_{k+1}\}$. It is assumed that a *a posteriori* probability density function (pdf) $p\left(\mathbf{x}_k^{\mathrm{t}} \mid \mathcal{Y}_k\right)$ is given, which quantifies the density of $\mathbf{x}_k^{\mathrm{t}}$ given all measurements up to time t_k. Additionally, to predict the evaluation of the state it is assumed that the state transition conditional density $p\left(\mathbf{x}_{k+1}^{\mathrm{t}} \mid \mathbf{x}_k^{\mathrm{t}}\right)$ is known. The density $p\left(\mathbf{x}_{k+1}^{\mathrm{t}} \mid \mathbf{x}_k^{\mathrm{t}}\right)$ models the probability of reaching some state $\mathbf{x}_{k+1}^{\mathrm{t}}$ at time t_{k+1} given the state $\mathbf{x}_k^{\mathrm{t}}$ at time t_k. The transition conditional density accounts for the dynamics and uncertain evolution of the system which depends – in our case – on $\mathbf{f}_k^{\mathrm{t}}\left(\mathbf{x}_k^{\mathrm{t}}, \mathbf{v}_k\right)$ and the assumed density distribution of $\mathbf{v}_k$. For the transition conditional density it is assumed that the future state $\mathbf{x}_{k+1}^{\mathrm{t}}$ is independent of the past states $\mathbf{x}_{1:k}^{\mathrm{t}} = \{\mathbf{x}_1^{\mathrm{t}}, \mathbf{x}_2^{\mathrm{t}}, \ldots, \mathbf{x}_k^{\mathrm{t}}\}$ given the present state $\mathbf{x}_k^{\mathrm{t}}$, *i.e.*,

$$p\left(\mathbf{x}_{k+1}^{\mathrm{t}} \mid \mathbf{x}_{1:k}^{\mathrm{t}}, \mathcal{Y}_k\right) = p\left(\mathbf{x}_{k+1}^{\mathrm{t}} \mid \mathbf{x}_k^{\mathrm{t}}\right), \tag{2.10}$$

and also *vice versa*, the past is independent of the future given the present state. Finally, it is assumed that the conditional density $p\left(\mathbf{y}_{k+1} \mid \mathbf{x}_{k+1}^{\mathrm{t}}\right)$ is available and that the measurements $\mathbf{y}_{1:k}$ are conditionally independent given $\mathbf{x}_{k+1}^{\mathrm{t}}$, *i.e.*,

$$p\left(\mathbf{y}_{k+1} \mid \mathbf{x}_{1:k+1}^{\mathrm{t}}, \mathcal{Y}_{1:k}\right) = p\left(\mathbf{y}_{k+1} \mid \mathbf{x}_{k+1}^{\mathrm{t}}\right). \tag{2.11}$$

The Bayesian optimal filter evaluates $p\left(\mathbf{x}_{k+1}^{\mathrm{t}} \mid \mathcal{Y}_{k+1}\right)$ from $p\left(\mathbf{x}_k^{\mathrm{t}} \mid \mathcal{Y}_k\right)$ by applying a prediction and correction step.

At time t_k, the probability density $p\left(\mathbf{x}_k^{\mathrm{t}} \mid \mathcal{Y}_k\right)$ is available and convoluted with the transition conditional density $p\left(\mathbf{x}_{k+1}^{\mathrm{t}} \mid \mathbf{x}_k^{\mathrm{t}}\right)$ to evaluate the *a priori* density

$$p\left(\mathbf{x}_{k+1}^{\mathrm{t}} \mid \mathcal{Y}_k\right) = \int_{\mathbb{R}^{n^{\mathrm{t}}}} p\left(\mathbf{x}_{k+1}^{\mathrm{t}} \mid \mathbf{x}_k^{\mathrm{t}}\right) p\left(\mathbf{x}_k^{\mathrm{t}} \mid \mathcal{Y}_k\right) \mathrm{d}\mathbf{x}_k^{\mathrm{t}}, \tag{2.12}$$

which accounts for the time evolution of the conditional probability following the Chapman-Kolmogorov equation. At time t_{k+1}, measurement $\mathbf{y}_{k+1}$ is collected and $p\left(\mathbf{y}_{k+1} \mid \mathbf{x}_{k+1}^{\mathrm{t}}\right)$ is available. The *a posteriori* density

$$p\left(\mathbf{x}_{k+1}^{t} \mid \mathcal{Y}_{k+1}\right) = \frac{p\left(\mathbf{y}_{k+1} \mid \mathbf{x}_{k+1}^{t}\right) p\left(\mathbf{x}_{k+1}^{t} \mid \mathcal{Y}_k\right)}{\int_{\mathbb{R}^{n^t}} p\left(\mathbf{y}_{k+1} \mid \mathbf{x}_{k+1}^{t}\right) p\left(\mathbf{x}_{k+1}^{t} \mid \mathcal{Y}_k\right) \mathrm{d}\mathbf{x}_k^{t}} \tag{2.13}$$

is obtained by Bayes' law, which corrects the predicted density $p\left(\mathbf{x}_{k+1}^{\mathrm{t}} \mid \mathcal{Y}_k\right)$ by accounting for the measurement density $p\left(\mathbf{y}_{k+1} \mid \mathbf{x}_{k+1}^{\mathrm{t}}\right)$. One can evaluate an point estimate $\widehat{\mathbf{x}}_{k+1}^{\mathrm{t}}$ from $p\left(\mathbf{x}_{k+1}^{\mathrm{t}} \mid \mathcal{Y}_{k+1}\right)$ using, *e.g.*, a maximum *a posteriori* estimator,

i.e.,

$$\widehat{\mathbf{x}}_{k+1}^{\mathrm{t}} = \underset{\mathbf{x}_{k+1}^{\mathrm{t}}}{\arg\max} \left(p\left(\mathbf{x}_{k+1}^{\mathrm{t}} \mid \mathcal{Y}_{k+1} \right) \right). \tag{2.14}$$

The estimate $\widehat{\mathbf{x}}_{k+1}^{\mathrm{t}}$ is considered optimal when the density $p\left(\mathbf{x}_{k+1}^{\mathrm{t}} \mid \mathcal{Y}_{k+1} \right)$ is unimodal, *i.e.*, a probability distribution which has a single peak.

The Bayesian optimal filter is an exact formulation to evaluate conditional densities. In order to obtain more practical estimation techniques, several assumptions can be made, leading to a variety of estimation techniques, such as the Kalman filter, extended Kalman filter, particle filter, and others. The Kalman filter is one of the most famous state estimation methods within the Bayesian framework (Meinhold and Singpurwalla, 1983). It is optimal in the sense of mean squared errors when the uncertainty is Gaussian distributed, and the system model is linear. For nonlinear systems, the extended Kalman filter linearizes the nonlinear system model via a Taylor series expansion such that the classical filter can be applied.

In the context of mobile robots observing mobile targets, the Bayesian estimation framework has been used for target search (Bertuccelli and How, 2006a; Flint et al., 2004; Yang et al., 2007) and tracking (Allik, 2019; Shorinwa et al., 2020). These two objectives are often treated separately due to the type of estimate that is needed. Target search requires, in general, a probability density distribution that covers the complete RoI and the state estimation of potentially multiple targets. As opposed to this, target tracking requires estimating the state of a single target, and an explicit probability density distribution often models the state, such as, *e.g.*, a Gaussian distribution.

2.8. Control design for target search and tracking strategies

Cooperative target search and tracking generally consist of the four following tasks:

1. A robot collects observations, and new information on the target state is obtained.
2. The locally collected information is transmitted over the network.
3. The available information is fused to obtain refined target state estimates.
4. Control laws are designed to derive search trajectories or drive the robots to observation locations improving the target state estimation accuracy.

This section focus on the evaluation of control laws. The design of these laws should account for the following requirements. The cooperation of the fleet is addressed in a distributed way in the latter proposed approaches. Consequently, the control input has to be designed such that it can be computed by each robot locally using

only information collected in its neighborhood. The control laws are derived from an optimality criterion that depends on the utilities or costs of different control choices. It is important that these utilities or costs can be easily evaluated and that they discriminate efficiently between the potential solutions. The evaluated utility should reflect the objectives of searching and tracking such that both objectives can be jointly optimized. Moreover, a well-designed control scheme should be general and self-adaptable to various types of targets, robots, sensors, and environments. The evaluation of the utility and the control inputs should be simple to allow their online computation by robots with limited processing capabilities.

During target tracking, the main objective is to drive or distribute the robots such that additional observations are collected to refine the target state estimate. Regarding the control design for target search, trajectories of the robots are evaluated to extract the maximum amount of information on the potential target locations either by detecting the target and estimating their positions or ruling out zones where the targets can be positioned.

Determination of these trajectories can be obtained offline using explicit planning methods, which determine predicted environmental states, estimated target movements, and potential sensor observations (see Raap et al. (2019) for a review of path-constrained approaches). Online determination is commonly performed using optimal control methods (Foraker et al., 2016a,b; Walton et al., 2014) or, if accounting for adversary decision making, obtained with cooperative game approaches (Li and Duan, 2017). The criterion used for UAV displacement strategies can be designed, *e.g.*, to increase the probability of detection of a new target as in Sun et al., 2014 or to emphasize consensus decision-making (Baek and York, 2020) and information seeking (Meyer et al., 2015). Furthermore, Pitre et al. (2012) presents an objective function that integrates the conflicting objectives of simultaneous searching and tracking. However, the relative importance of these objectives still needs to be balanced.

Finding the general solution to an optimal control problem proves especially difficult when the problem is constrained and its evolution model and the optimality criterion are nonlinear. Model predictive control is a well-adapted framework for determining efficient solutions to the optimization problem using an explicit and numerical approach for designing controls optimizing a criterion while satisfying potential constraints. This makes it a good candidate for defining search and tracking strategies as in Farmani et al., 2015 or Tokekar et al., 2014. In Bertrand et al. (2014), an MPC strategy is proposed that allows area exploration via a cooperative grid allocation and task assignment. The need to optimize a more complex criterion (the target state estimation uncertainty) while satisfying control input constraints led to the choice of an MPC-based control scheme for the developed approaches in this thesis. The control input for each UAV is derived by predicting the impact of future measurements on the estimation uncertainty.

Assuming that time is discretized, a predictive controller uses, at each sampling

instant, the system current inputs and outputs, the state, and the assumed system model to calculate, over a finite horizon, a future sequence of control inputs that optimize a given criterion and fulfills constraints on the control values. The controller applies only the first control input of the optimal sequence of control inputs. This procedure is repeated every time instant.

More formally speaking, assume that the dynamic model of the UAVs evolves as in (2.4). At time t_k, for a given control input $\mathbf{u}_{i,k}$ and state $\mathbf{x}^{\mathrm{u}}_{i,k}$ of UAV i, one can evaluate the predicted state $\mathbf{x}^{\mathrm{u,P}}_{i,k+1}$ of $\mathbf{x}^{\mathrm{u}}_{i,k+1}$ at time t_{k+1} using (2.4). This procedure can be repeated recursively to use a given control input sequence $\mathbf{u}_{i,k:k+h-1}$ to evaluate the predicted state sequence $\mathbf{x}^{\mathrm{u,P}}_{i,k+1:k+h}$ at the time instants $\{t_{k+1}, t_{k+2}, \ldots, t_{k+h-1}\}$, where h is the prediction and control horizon. A control input is consequently applied in each prediction step of the system state.

Let $J_i\left(\mathbf{x}^{\mathrm{u,P}}_{i,k+1:k+h}, \mathbf{u}_{i,k:k+h-1}\right)$ be a criterion – a cost function to minimize – that represents the objective of the control, which depends on the control input sequence $\mathbf{u}_{i,k:k+h-1}$ and the predicted state sequence $\mathbf{x}^{\mathrm{u,P}}_{i,k+1:k+h}$. Classically, the cost function accounts for the tracking error between set-points and the predicted target states and the costs for control actions. In the context of target search and tracking the cost $J_i\left(\mathbf{x}^{\mathrm{u,P}}_{i,k+1:k+h}, \mathbf{u}_{i,k:k+h-1}\right)$ will account for the estimation uncertainty of the target states $\mathbf{x}^{\mathrm{t}}_{j,k}$, $j = 1, \ldots, N^{\mathrm{t}}$, which depends on the actions and observations taken by UAV i. The optimization problem

$$\widehat{\mathbf{u}}_{i,k:k+h-1} = \arg \min_{\mathbf{u}_{i,k:k+h-1}} J_i\left(\mathbf{x}^{\mathrm{u,P}}_{i,k+1:k+h}, \mathbf{u}_{i,k:k+h-1}\right) \tag{2.15}$$

searches for the optimal control input sequence $\widehat{\mathbf{u}}_{i,k:k+h-1}$ that minimizes the cost $J_i\left(\mathbf{x}^{\mathrm{u,P}}_{i,k+1:k+h}, \mathbf{u}_{i,k:k+h-1}\right)$ for a control input sequence. At time t_k, only the first element $\widehat{\mathbf{u}}_{i,k}$ of the optimal control input sequence is applied to control UAV i. This procedure is repeated at time t_{k+1} to evaluate the optimal control input $\widehat{\mathbf{u}}_{i,k+1}$.

For cooperative control, the optimization problem (2.15) needs to be adapted such that the UAVs account for the control inputs of the other UAVs with which they communicate. The problem could be formalized as the joint optimization

$$\{\widehat{\mathbf{u}}_{i,k:k+h-1}\}_{i\in\mathcal{N}_g} = \arg \min_{\{\mathbf{u}_{i,k:k+h-1}\}_{i\in\mathcal{N}_g}} \sum_{i\in\mathcal{N}_g} J_i\left(\mathbf{x}^{\mathrm{u,P}}_{i,k+1:k+h}, \mathbf{u}_{i,k:k+h-1}\right) \tag{2.16}$$

of a group of UAVs with index in $\mathcal{N}_g$, which has a much larger complexity than (2.15).

Explicit closed-form solutions of (2.15) and (2.16) may not be available or too complex to evaluate. Nevertheless, numerical optimization methods are available to approximate the solution. The selection of a suitable numerical optimization algorithm depends on the structure of the problem, such as, *e.g.,* the type cost function and if the function is linear, differentiable, convex, or constrained. A nice overview of available methods and a discussion of their advantages and drawbacks are presented

in Walter (2014). Additionally, the NEOS Guide website and Optimization Guide (Czyzyk et al., 1998) provide information about the taxonomy of optimization and many of its sub-disciplines. The website also presents optimization case studies.

Several considerations have to be taken into account when solving an optimization problem numerically. It might prove difficult to find a global solution to the problem due to potential local extrema. Furthermore, the computational time strongly depends on the parameterization of the optimization methods and the initialization of the optimization procedure. An alternative to iterative optimization methods consists of introducing finite sets of predefined feasible control sequences as in Rochefort et al. (2014). A suboptimal solution is searched within finite sets of control input sequences. The advantages are that the computational time is constant and that the systematic search might be less sensitive to local extrema. Furthermore, no initialization procedure is required. An optimization method similar to that in Rochefort et al. (2014) is deployed in this thesis to solve the optimization problems for the control input design.

3. Assumptions and problem formulation

This chapter formalizes the general target search and tracking problem considered in the remainder of the thesis. The problem is introduced in a general fashion. The following chapters may consider special cases of the general problem. Each section starts with an illustrative *Scene* describing a situation that is going to be formalized.

3.1. Introduction

Scene 1:

Consider a fleet of autonomous UAVs equipped with RGB cameras flying, e.g., at an altitude between 60 and 100 m for a surveillance mission within an urban environment. The mission of the fleet is to search for a group of specific cars within some delimited region and to track the location of every already detected car that is of interest. The difficulty one encounters is that the cars may sometimes be hidden behind the buildings and are not detected by the UAVs. Furthermore, even when a car is located within the FoV of a UAV, identification may not be possible because the license plate is not visible due to an inadequate point of view of the UAV. Another problem arises if the features for identification are not unique or can be easily confused. This may appear if the cars are identified by their colors or the license plates are soiled and difficult to read.
Considering the fleet displacement, the UAVs have to adapt in real-time their search and tracking strategies to account for new collected information during the flight. Their strategies should enhance cooperation to benefit from the abilities of the complete fleet.

The following aim is to formalize the search and tracking problem described in Scene 1. More precisely, the introduced formalization has to account for the fact that the environment may partly hide targets, that their identity may not always be available, and that they may be confused with other objects, *e.g.*, clutter or decoys.

Consider a fleet of N^{u} UAVs searching and tracking an unknown number N^{t} of targets within some delimited Region of Interest (RoI) $\mathbb{X}_0$. The RoI may be a part of a plane for the localization of ground targets. Higher dimension may be

considered when estimating heading angles and velocities, or the location of flying targets. The targets may be static or moving. Each target is associated to an identifier belonging to the list $\mathcal{N}^{\mathrm{t}} = \{1, \ldots, N^{\mathrm{t}}\}$. Considering Scene 1, the identifier may be related to the license plate number of a car. The identifier of a target may not be always accessible. When available, it can be used to distinguish targets from each other. The RoI may also contain N^{o} obstacles which may partially hide the targets. Each UAV possesses a sensing system capable of detecting targets within its Field of View (FoV). The detection may depend additionally on some deterministic observation conditions. When a target is detected a measurement of its state is obtained. Furthermore, it is assumed that the sensing system may collect erroneous measurements that are not generated by a detected target but, *e.g.*, by some features of the environment (clutter) or decoys, called *false* targets hereafter. Figure 3.1 illustrates an example of the RoI containing UAVs, targets (black dots), false targets (circles), and obstacles (gray boxes).

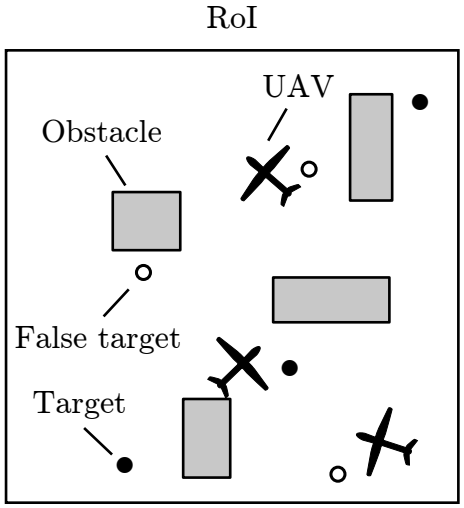

Figure 3.1.: Region of Interest containing UAVs, targets, false targets and obstacles.

The general objective is to obtain an estimate as precise as possible of the state of all targets in the RoI. This state estimate should be consistent with the measurements collected by the complete fleet of UAVs. Additionally, if false targets are present, then the state of these false targets should not belong to the target state estimates when the search is completed. Considering the control design, the UAVs should be guided in a distributed way – due to communication limitations – such that the sensing system collects beneficial information that allows refining the target state estimates. Furthermore, the control strategy should enhance cooperation between every member of the fleet.

Table 3.1 summarizes the major notations introduced in this chapter.

Variable	Definition
$\mathcal{D}^{\mathrm{I}}_{i,k}$	List of detected and *identified* targets by UAV i at time t_k
$\mathcal{D}^{\mathrm{U}}_{i,k}$	List of detected and *unidentified* targets by UAV i at time t_k
$\mathbb{D}_k(\boldsymbol{x}) \subset \mathbb{R}^3$	Detectability set of point $\boldsymbol{x}$ at time t_k
$\mathbf{f}^{\mathrm{u}}_k$, $\mathbf{f}^{\mathrm{t}}_k$	Dynamical model of UAVs, and targets
$\mathbb{F}_i(\mathbf{x}^{\mathrm{u}}_{i,k}) \subset \mathbb{R}^{n^{\mathrm{t}}}$	Field of View (FoV) of UAV i at t_k
$g^{\mathrm{t}}_j\left(\mathbf{x}^{\mathrm{u}}_{i,k}, \mathbf{x}^{\mathrm{t}}_{j,k}\right) \geqslant 0$	Identifiability condition of true targets j
$g^{\mathrm{f}}_\ell\left(\mathbf{x}^{\mathrm{u}}_{i,k}, \mathbf{x}^{\mathrm{f}}_{\ell,k}\right) \geqslant 0$	Identifiability condition of false targets ℓ
$\mathbf{h}_i\left(\mathbf{x}^{\mathrm{u}}_{i,k}, \mathbf{x}^{\mathrm{t}}_{j,k}\right)$	Observation equation of UAV i at time t_k
$\mathcal{J}^{\mathrm{t}}$	List of *a priori* known target identifiers
$\mathcal{J}^{\mathrm{f}}$	List of *a priori* known false target identifiers
$\mathbb{I}_{i,k}$	Information available to UAV i at time t_k
$\mathcal{L}_{i,k}$	List of indices of tracked targets of UAV i at time t_k
n^{u}, n^{t}	State vector size for UAVs and true targets
N^{u}, N^{t}, N^{f}	Number of UAVs, true, and false targets
$\mathcal{N}^{\mathrm{u}}$, $\mathcal{N}^{\mathrm{t}}$, $\mathcal{N}^{\mathrm{f}}$	List of indices of UAVs, true, and false targets
$\mathcal{N}_{i,k}$	List of indices of UAVs connected with UAV i at time t_k
$\mathcal{O}_{m,k} \subset \mathbb{R}^3$	Solids obstacle m at time t_k
$p^{\mathrm{u}}(\mathbf{x}) \in \mathbb{R}^3$	Vectors representing the location of $\mathbf{x} \in \mathbb{R}^{n^{\mathrm{u}}}$
$p^{\mathrm{t}}(\mathbf{x}) \in \mathbb{R}^3$	Vectors representing the location of $\mathbf{x} \in \mathbb{R}^{n^{\mathrm{t}}}$
$q^{\mathrm{f}}_\ell\left(\mathbf{x}^{\mathrm{u}}_{i,k}, \mathbf{x}^{\mathrm{f}}_{\ell,k}\right) \geqslant 0$	Confusion condition of false target ℓ
$\mathbf{u}_{i,k} \in \mathbb{U}$	UAV i control input at time t_k
$\mathbf{v}_{j,k} \in [\mathbf{v}_k]$	Unknown state perturbation of target j at time t_k
$\mathbf{w}_{i,j,k} \in [\mathbf{w}_{i,k}]$	Observation noise
$\mathbf{x}^{\mathrm{u}}_{i,k}$, $\boldsymbol{x}^{\mathrm{u}}_{i,k}$	State vector and location of UAV i at time t_k
$\mathbf{x}^{\mathrm{t}}_{j,k}$, $\boldsymbol{x}^{\mathrm{t}}_{j,k}$	State vector and location of target j at time t_k
$\mathbf{x}^{\mathrm{f}}_{\ell,k}$, $\boldsymbol{x}^{\mathrm{f}}_{\ell,k}$	State vector and location of false target ℓ at time t_k
$\mathbf{x}^{\mathrm{t}}_{j,k} \in \mathbb{F}_i\left(\mathbf{x}^{\mathrm{u}}_{i,k}\right)$	Detection condition for true targets
$\mathbf{x}^{\mathrm{f}}_{\ell,k} \in \mathbb{F}_i\left(\mathbf{x}^{\mathrm{u}}_{i,k}\right)$	Detection condition for false targets
$\mathbb{X}_0 \subset \mathbb{R}^{n^{\mathrm{t}}}$	Initial set of target states; RoI
$\mathbb{X}^{\mathrm{T}}_k \subseteq \mathbb{X}_0$	Set of possible target locations
$\mathbb{X}_{i,j,k}$	Set estimate for target j by UAV i at time t_k
$\mathbb{X}^{\mathrm{U}}_{i,k}$	Set estimate for unidentified targets by UAV i at time t_k
$\mathcal{X}_{i,k}=\{\mathbb{X}_{i,j,k}\}_{j\in\mathcal{L}_{i,k}}$	List of set estimates by UAV i at time t_k
$\overline{\mathbb{X}}_{i,k}$	Set still to be explored
$\mathbf{y}^{\mathrm{I}}_{i,j,k}$	Measurement of the identified target $j \in \mathcal{D}^{\mathrm{I}}_{i,k}$
$\mathbf{y}^{\mathrm{U}}_{i,m,k}$	Measurement of the unidentified target $m \in \mathcal{D}^{\mathrm{U}}_{i,k}$
$\phi(\mathbb{A})$	Measure of set $\mathbb{A}$
$\overline{\Phi}_k$	Average estimation uncertainty at time t_k
$\pi_{i,k}(j), \pi_{i,k}(\ell)$	Unknown mapping from $\mathcal{J}^{\mathrm{t}} \cup \mathcal{J}^{\mathrm{f}}$ to $\mathbb{N}$

Table 3.1.: Used notation and their definitions

3.2. UAV and target states

Scene 2:

The UAVs search for cars. Consequently, the class of targets is a priori *known, and additional information is available,* e.g.*, the size of the cars, their dynamics, maximal speed, maximal turn radius, and others. The UAVs also have access to a list of license plates for cars that must be searched. Nevertheless, it is not guaranteed that all the cars from the list are present in the considered RoI. Consequently, the number of cars to search for is unknown. The RoI also contains some other cars whose license plates do not belong to the list of license plates of interest.*

To model this situation, one introduces the dynamic modeling of the UAVs, targets, and false targets. The fleet of N^{u} UAVs searches and tracks an unknown number $N^{\mathrm{t}} \leqslant |\mathcal{J}^{\mathrm{t}}|$ of targets moving within a limited RoI. One assumes that a unique identifier may be associated to each target and that the set $\mathcal{J}^{\mathrm{t}}$ of target identifiers is known *a priori*. Furthermore, the RoI may also contain *false* targets. The set $\mathcal{J}^{\mathrm{f}}$ of false target identifiers is unknown but assumed to be such that $\mathcal{J}^{\mathrm{t}} \cap \mathcal{J}^{\mathrm{f}} = \emptyset$. The RoI $\mathbb{X}_0 \subset \mathbb{R}^{n^{\mathrm{t}}}$ is assumed to be bounded. A reference frame $(\mathbf{O}, \mathcal{F})$ is attached to $\mathbb{X}_0$ with $\mathbf{O}$ the origin and $\mathcal{F}$ the set of axis.

Time is sampled with a constant period T. At time $t_k = kT$, let $\mathbf{x}^{\mathrm{u}}_{i,k} \in \mathbb{R}^{n^{\mathrm{u}}}$ be the state vector of UAV $i \in \mathcal{N}^{\mathrm{u}} = \{1, \ldots, N^{\mathrm{u}}\}$, $\mathbf{x}^{\mathrm{t}}_{j,k} \in \mathbb{R}^{n^{\mathrm{t}}}$ the state vector of target $j \in \mathcal{J}^{\mathrm{t}}$, and $\mathbf{x}^{\mathrm{f}}_{\ell,k} \in \mathbb{R}^{n^{\mathrm{t}}}$ the state vector of false target $\ell \in \mathcal{J}^{\mathrm{f}}$. The evolution with time of the state of UAVs and targets is modeled as

$$\mathbf{x}^{\mathrm{u}}_{i,k+1} = \mathbf{f}^{\mathrm{u}}_k \left(\mathbf{x}^{\mathrm{u}}_{i,k}, \mathbf{u}_{i,k} \right), \tag{3.1}$$

and

$$\mathbf{x}^{\mathrm{t}}_{j,k+1} = \mathbf{f}^{\mathrm{t}}_k \left(\mathbf{x}^{\mathrm{t}}_{j,k}, \mathbf{v}_{j,k} \right), \tag{3.2}$$

where $\mathbf{f}^{\mathrm{u}}_k$ and $\mathbf{f}^{\mathrm{t}}_k$ are known functions. The control input $\mathbf{u}_{i,k}$ of UAV i is constrained in a set $\mathbb{U}$ of admissible control inputs. The unknown state perturbation $\mathbf{v}_{j,k}$ of target j at time t_k belongs to the known box $[\mathbf{v}]$. The coordinates of UAV i and target j expressed in $(\mathbf{O}, \mathcal{F})$ are denoted as $\boldsymbol{x}^{\mathrm{u}}_{i,k} = p^{\mathrm{u}}(\mathbf{x}^{\mathrm{u}}_{i,k})$ and $\boldsymbol{x}^{\mathrm{t}}_{j,k} = p^{\mathrm{t}}(\mathbf{x}^{\mathrm{t}}_{j,k})$, where $p^{\mathrm{u}}(\mathbf{x}) \in \mathbb{R}^3$ and $p^{\mathrm{t}}(\mathbf{x}) \in \mathbb{R}^3$ are vectors representing the coordinates of $\mathbf{x} \in \mathbb{R}^{n^{\mathrm{u}}}$ and $\mathbf{x} \in \mathbb{R}^{n^{\mathrm{t}}}$, respectively. No particular assumption is considered about the evolution of $\mathbf{x}^{\mathrm{f}}_{\ell,k}$: false targets may be static or moving. The UAVs search and track targets only within the RoI $\mathbb{X}_0$. Figure 3.2 illustrates the evolution of the different states.

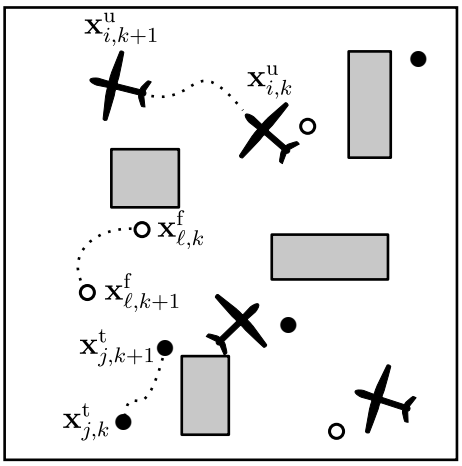

Figure 3.2.: Evolution of the UAV, target, and false target states.

3.3. Obstacle representation

Scene 3:

The considered urban environment may contain static obstacles such as buildings, bridges, and walls, which may hide the cars. Furthermore, the environment may also contain dynamic obstacles such as large trucks, other cars, or even fog/clouds (at low altitude), which may reduce the visible area of the UAVs. The locations of the obstacles may be available to the UAVs if they have a map of the environment. However, the locations of some obstacles may be unknown which makes it much harder to search for all the cars in the RoI because the hidden areas are unknown.
Furthermore, the obstacles may have also an impact on the communication between UAVs the radio waves may be reflected, scattered, and absorbed.

Considering Scene 3, a modeling of obstacles in the environment is proposed. The RoI may contain N^{o} obstacles. It is assumed that the obstacles can be described as solids $\mathcal{O}_{m,k} \subset \mathbb{R}^3$ with $m \in \{1, \ldots, N^{\mathrm{o}}\}$, for all $k \geqslant 0$. An obstacle m may be static, *i.e.*, $\mathcal{O}_{m,k} = \mathcal{O}_{m,0}$ for all $k \geqslant 0$, or moving. No assumptions are made about the motion of the obstacles. Obstacle m is modeled as $\mathcal{P}^{\mathrm{u}}_{m,k} = \mathcal{O}_{m,k} \times \mathbb{R}^{n^{\mathrm{u}}-3}$ to be consistent with the UAV state space and as $\mathcal{P}^{\mathrm{t}}_{m,k} = \mathcal{O}_{m,k} \times \mathbb{R}^{n^{\mathrm{t}}-3}$ to be consistent with the target state space.

It is assumed that the targets do not enter the obstacles. Consequently, they may only be located in a subset

$$\mathbb{X}^{\mathrm{T}}_k = \mathbb{X}_0 \setminus \bigcup_{m=1}^{N^{\mathrm{o}}} \mathcal{P}^{\mathrm{t}}_{m,k}, \tag{3.3}$$

where $\mathbb{A} \setminus \mathbb{B}$ the set difference of $\mathbb{A}$ and $\mathbb{B}$. The set $\mathbb{X}_k^{\mathrm{T}}$ may not be available to the UAVs if the obstacles are considered unknown as in Chapter 5.

3.4. Field of view

Scene 4:

The UAVs are equipped with RGB cameras to search for the cars. The region that can be observed (the FoV) is well defined by the specifications of the camera and the current location and orientation of the UAV. Considering a surveillance mission, it is common that the observable region is much smaller than the RoI, so the UAVs have to collect several observations at different time instants to explore the complete RoI entirely. The sensor allows the UAVs to collect information about the targets. This information could only indicate that a car is present or absent at a given location, but it may also indicate, e.g.*, the speed or heading of a car.*

To formalize the characteristics of the observable region, it is assumed that the sensor of each UAV i, with state $\mathbf{x}_{i,k}^{\mathrm{u}}$, is able to observe a subset $\mathbb{F}_i(\mathbf{x}_{i,k}^{\mathrm{u}}) \subset \mathbb{X}_0$ of the RoI $\mathbb{X}_0$. The FoV $\mathbb{F}_i(\mathbf{x}_{i,k}^{\mathrm{u}})$ is characterized by a set of n_i unit vectors $v_{i,m}^{\mathrm{F}}(\mathbf{x}_{i,k}^{\mathrm{u}})$, $m = 1, \ldots, n_i$, depending on $\mathbf{x}_{i,k}^{\mathrm{u}}$, and spanning a non-zero volume half-cone. One has

$$\mathbb{F}_i\left(\mathbf{x}_{i,k}^{\mathrm{u}}\right) = \left\{\boldsymbol{x}_{i,k}^{\mathrm{u}} + a_1 \boldsymbol{v}_{i,1}^{\mathrm{F}}\left(\mathbf{x}_{i,k}^{\mathrm{u}}\right) + \cdots + a_{n_i} \boldsymbol{v}_{i,n_i}^{\mathrm{F}}\left(\mathbf{x}_{i,k}^{\mathrm{u}}\right) \mid a_m \in \mathbb{R}^+, m = 1, \ldots, n_i\right\} \cap \mathbb{X}_0. \quad (3.4)$$

The mean

$$\overline{\boldsymbol{v}}_i^{\mathrm{F}}\left(\mathbf{x}_{i,k}^{\mathrm{u}}\right) = \left(\sum_{m=1,\ldots,n_i} \boldsymbol{v}_{i,m}^{\mathrm{F}}\left(\mathbf{x}_{i,k}^{\mathrm{u}}\right)\right) / \left\|\sum_{m=1,\ldots,n_i} \boldsymbol{v}_{i,m}^{\mathrm{F}}\left(\mathbf{x}_{i,k}^{\mathrm{u}}\right)\right\| \quad (3.5)$$

of the vectors $\boldsymbol{v}_{i,1}^{\mathrm{F}}\left(\mathbf{x}_{i,k}^{\mathrm{u}}\right), \ldots, \boldsymbol{v}_{i,n_i}^{\mathrm{F}}\left(\mathbf{x}_{i,k}^{\mathrm{u}}\right)$ represents the orientation of the FoV of UAV i with state $\mathbf{x}_{i,k}^{\mathrm{u}}$.

The shape of the FoV depends on the type of sensor used. The representation as a half cone seems reasonable for camera-based sensors. However, other sensors and models can be easily integrated into the estimation and control scheme. When using, e.g., an omnidirectional Radar, the FoV could be modeled as a sphere or torus. In general, the sensor should be able to observe the target state components that need to be estimated. The more information is obtained about the target state, the more efficient are the UAVs in tracking the targets.

A possible shape of the FoV is illustrated in Figure 3.3. The FoV is spanned by the black vertices. Its intersection with the ground plane is illustrated by pink lines.

Additionally, the obscured subset which is hidden behind an obstacle is highlighted in dark gray. The obscured subset of the FoV can only be evaluated by the UAV if the obstacle is known or if the shape of the obstacle can be obtained from the collected measurements. Different assumptions are made on the obstacles in Chapter 4 (obstacles are known) and 5 (obstacles are unknown) which determines if the obscured subset is accessible or not.

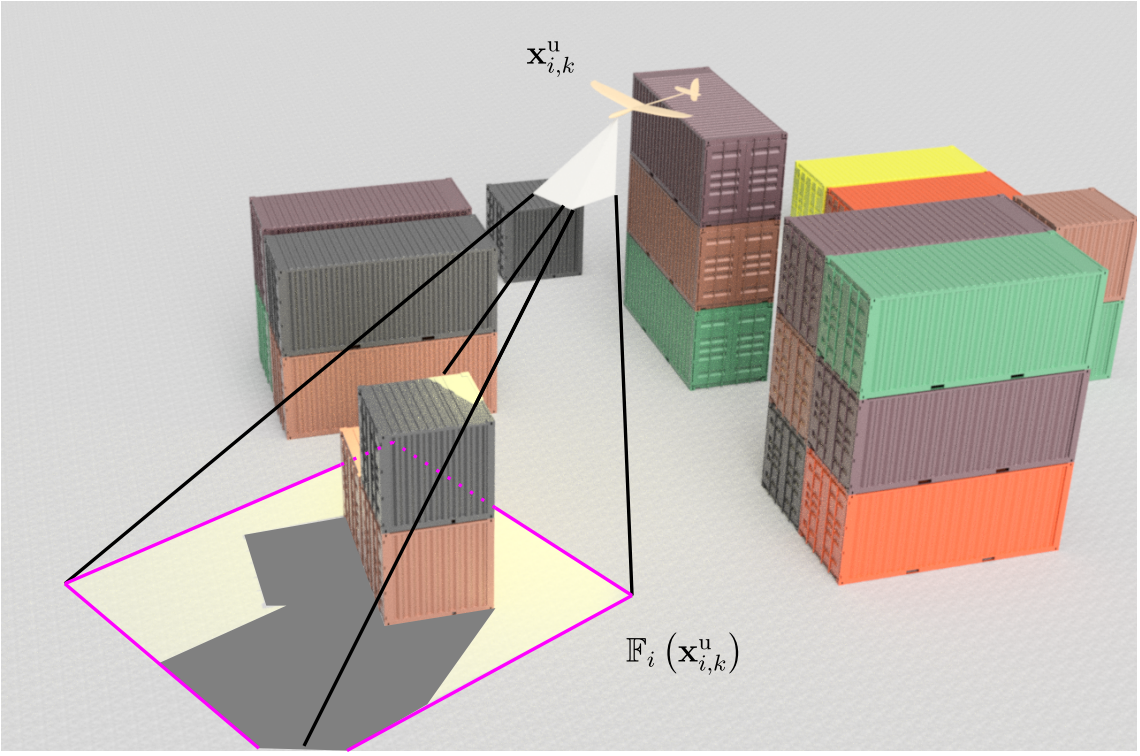

Figure 3.3.: Field of View $\mathbb{F}_i\left(\mathbf{x}^{\mathrm{u}}_{i,k}\right)$ characterized by its vertices (in black and pink) of UAV i: The FoV may sometimes be reduced due to the presence of obstacles. If the obstacles are unknown the UAVs may not be able to evaluate the obscured area (in gray).

3.5. Detectability conditions

Scene 5:

A UAV may take an observation and not detect any car. Assuming that the observations are perfectly processed, and false negative detection does not appear, one can conclude that the observed region is free from any car. This conclusion can not be made if the area contains buildings or other obstacles since the FoV may contain some obscured areas, as illustrated in Figure 3.3. The obscured areas can only be evaluated if the location and shape of the buildings are known or if the UAVs possess a powerful image processing system that can reconstruct a 3D map of the environment or evaluate the obscured areas of its FoV. This becomes even more difficult when the cars are hidden behind some moving trucks or buses. Updating the evolving map of obstacles becomes then very costly. Instead of changing the effective size of the FoV or mapping the area, an additional detectability condition is introduced.
Another example illustrating the difficulty of mapping the environment is a surveillance mission at night where the UAVs search for luminous targets (headlights of the cars). The contrast of the environment may be very low, which makes it hard or even impossible to map the location of obstacles. The UAV can then only detect the headlights of the cars if they are in a direct line of sight without intersecting any obstacle.

As illustrated in Scene 5, due to obstacles, some points $\mathbf{x} \in \mathbb{X}_k^{\mathrm{T}}$ may be partly hidden and not visible from all locations. For all $\mathbf{x} \in \mathbb{X}_k^{\mathrm{T}}$, with location $\boldsymbol{x} = p^{\mathrm{t}}(\mathbf{x})$, one introduces the *detectability* set $\mathbb{D}_k(\boldsymbol{x}) \subset \mathbb{R}^3$ of $\boldsymbol{x}$ as the set of all UAV locations $\boldsymbol{x}^{\mathrm{u}} \in \mathbb{D}_k(\boldsymbol{x})$ from where a target located at $\boldsymbol{x}$ can be detected when observed at time t_k. $\mathbb{D}_k(\boldsymbol{x})$ depends only on the shape of obstacles and is time-dependent if the environment is dynamically changing. It is assumed that $\mathbb{D}_k(\boldsymbol{x})$ does not depend on the type and characteristics of the sensing device. This is realistic for camera-based sensing. Depending on the processing capability of the sensing devices, UAVs may be able to characterize $\mathbb{D}_k(\boldsymbol{x})$. The detectability set $\mathbb{D}_k(\boldsymbol{x})$ can be evaluated *a priori* if the obstacles are known. UAVs can determine whether target occlusions may occur from the knowledge of $\mathbb{D}_k(\boldsymbol{x})$.

Following this reasoning, the two conditions are necessary to detect a target. The target must be located in the FoV of the UAV and the UAV must be located in the detectability set of the target, *i.e.*,

$$\mathbf{x}_{j,k}^{\mathrm{t}} \in \mathbb{F}_i\left(\mathbf{x}_{i,k}^{\mathrm{u}}\right) \text{ and } \boldsymbol{x}_{i,k}^{\mathrm{u}} \in \mathbb{D}_k\left(\boldsymbol{x}_{j,k}^{\mathrm{t}}\right). \tag{3.6}$$

When $\mathbb{D}_k(\boldsymbol{x})$ is available, the UAVs my directly evaluate

$$\mathbb{F}_i^{\mathrm{D}}\left(\mathbf{x}_{i,k}^{\mathrm{u}}\right) = \left\{\mathbf{x} \in \mathbb{X}_0 \mid \mathbf{x} \in \mathbb{F}_i\left(\mathbf{x}_{i,k}^{\mathrm{u}}\right), \boldsymbol{x}_{i,k}^{\mathrm{u}} \in \mathbb{D}_k\left(p^{\mathrm{t}}(\mathbf{x})\right)\right\}. \tag{3.7}$$

The set $\mathbb{F}_i^{\mathrm{D}}\left(\mathbf{x}_{i,k}^{\mathrm{u}}\right)$ contains only points in the FoV $\mathbb{F}_i\left(\mathbf{x}_{i,k}^{\mathrm{u}}\right)$ that are visible and not hidden behind an obstacle. Consequently, every target in $\mathbb{F}_i^{\mathrm{D}}\left(\mathbf{x}_{i,k}^{\mathrm{u}}\right)$ is guaranteed to be detected. The subset $\mathbb{F}_i^{\mathrm{D}}\left(\mathbf{x}_{i,k}^{\mathrm{u}}\right)$ for a given value $\mathbf{x}_{i,k}^{\mathrm{u}}$, can be also defined as the intersection between the FoV and the visible region of the UAV. The visible region is then defined as the set of points from which a line segment connecting the UAV location $p\left(\mathbf{x}_{i,k}^{\mathrm{u}}\right)$ to this point does not intersect any obstacle. This region can be computed for polyhedral obstacles using the algorithm proposed in Blinn (1988).

In Chapter 4, it is assumed that $\mathbb{D}_k\left(\boldsymbol{x}\right)$ is always available to the UAVs. As opposed to this, $\mathbb{D}_k\left(\boldsymbol{x}\right)$ is not available to the UAVs in Chapter 5.

Figure 3.4 shows a simple box-shaped obstacle. The resulting detectability set $\mathbb{D}_k\left(\boldsymbol{x}\right) \subset \mathbb{R}^3$ (in red and gray) is illustrated for a point $\boldsymbol{x} \in \mathbb{X}_k^{\mathrm{T}}$ (in blue).

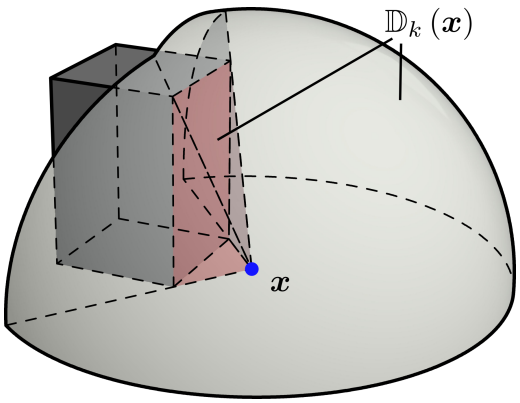

Figure 3.4.: Detectability set $\mathbb{D}_k\left(\boldsymbol{x}\right) \subset \mathbb{R}^3$ (red and gray) for a point $\boldsymbol{x} \in \mathbb{X}_k^{\mathrm{T}}$ (blue) located close to a box-shaped.

Figure 3.5 and 3.6 show the detection conditions and the different outcomes for true and false targets, respectively.

3.6. Identification conditions

Scene 6:

A detected car inside the FoV of a UAV can only be identified if the license plate is also visible. This is only the case if the car is observed with a satisfying point of view from the front or rear. The identification becomes even more complicated if the identification process is not faultless. In this case, some cars may be misidentified and confused with others. The misidentification may depend on lighting conditions, the point of view of the UAV, the position of the license plate, and other factors.

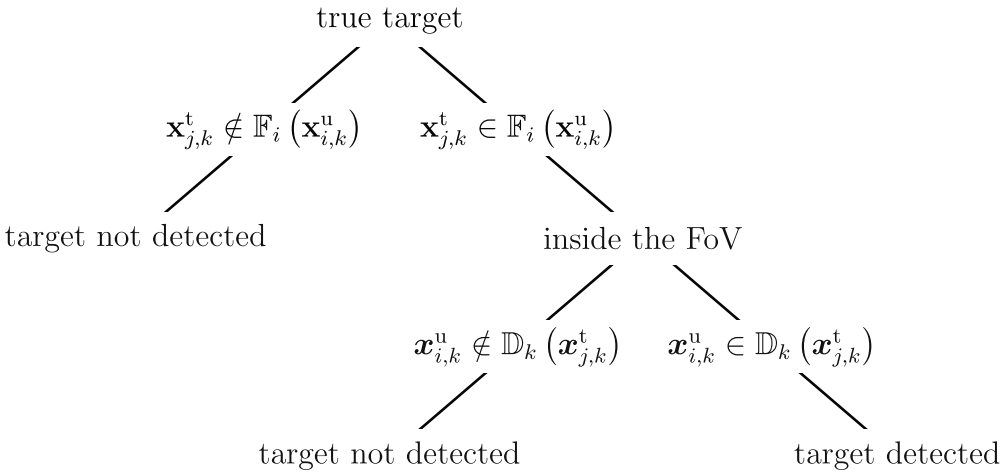

Figure 3.5.: Detection conditions for true targets.

To model different decision responses, as introduced in Section 2.5, and situations described in Scene 6, a new modeling for recognition and identification conditions of targets is proposed.

When a target is detected, two cases may occur depending on an additional *identification* condition g^{t}. If condition g^{t} is satisfied, then the target is identified as a true target and its unique identifier $j \in \mathcal{J}^{\mathrm{t}}$ is obtained. If the condition g^{t} is not satisfied, then no information on the target identity is available and the target is only recognized as potential target: the UAV does not know if the detected object is a true or a false target. It is assumed that misidentification does not occur for true targets.

When a false target $\ell \in \mathcal{J}^{\mathrm{f}}$ is detected and an identification condition g^{f} holds, an

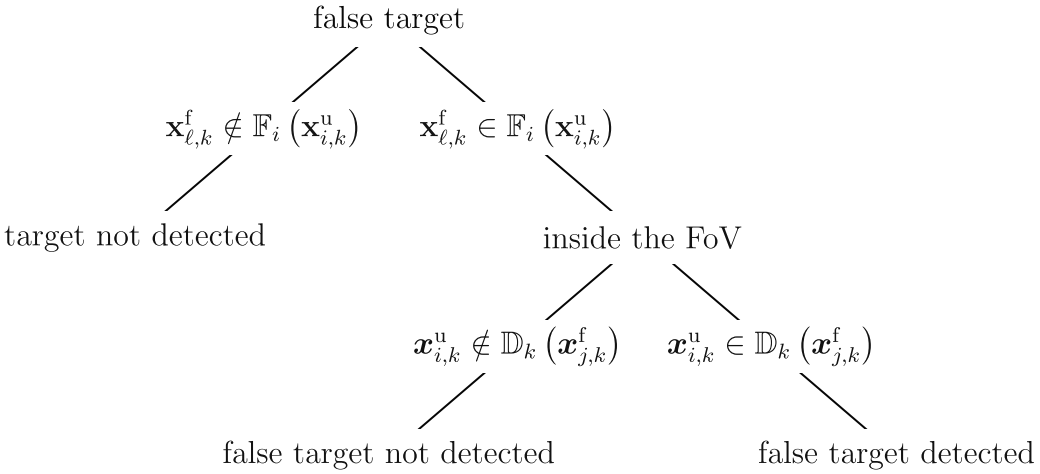

Figure 3.6.: Detection conditions for false targets.

identifier j is obtained, which may not necessarily be equal to ℓ. A misidentification may occur depending on an additional condition q^{f}. If q^{f} is satisfied, the obtained identifier is $J(\ell) \in \mathcal{J}^{\mathrm{t}}$, where J is some deterministic *confusion* function, *i.e.*, a false target is always confused with the same true target. If q^{f} is not satisfied, then the obtained identifier is $\ell \in \mathcal{J}^{\mathrm{f}}$, which allows the UAV to determine that a false target is detected. When g^{f} is not satisfied, the UAV does not know if the detected target is a true or a false target and does not have access to its identifier.

More formally, at time t_k, UAV i obtains two lists $\mathcal{D}^{\mathrm{I}}_{i,k}$, and $\mathcal{D}^{\mathrm{U}}_{i,k}$ from the information gathered in $\mathbb{F}_i(\mathbf{x}^{\mathrm{u}}_{i,k})$. $\mathcal{D}^{\mathrm{I}}_{i,k} \subset \mathcal{J}^{\mathrm{t}}$ contains the identifiers of all true targets that are detected and identified at time t_k, *i.e.*,

$$\underbrace{\mathbf{x}^{\mathrm{t}}_{j,k} \in \mathbb{F}_i\left(\mathbf{x}^{\mathrm{u}}_{i,k}\right) \text{ and } \boldsymbol{x}^{\mathrm{u}}_{i,k} \in \mathbb{D}_k\left(\boldsymbol{x}^{\mathrm{t}}_{j,k}\right)}_{\text{Detection conditions}} \text{ and } \underbrace{g^{\mathrm{t}}_j\left(\mathbf{x}^{\mathrm{u}}_{i,k}, \mathbf{x}^{\mathrm{t}}_{j,k}\right) \geqslant 0}_{\text{Identifiation condition}} \Rightarrow\ j \in \mathcal{D}^{\mathrm{I}}_{i,k}, \quad (3.8)$$

where g^{t}_j is the identification condition for the true target j. The condition g^{t}_j may be modeled, *e.g.*, by a half circular cone in $\mathbb{R}^3$, such that

$$g^{\mathrm{t}}_j\left(\mathbf{x}^{\mathrm{u}}_{i,k}, \mathbf{x}^{\mathrm{t}}_{j,k}\right) = \left(\mathbf{x}^{\mathrm{u}}_{i,k} - \mathbf{x}^{\mathrm{t}}_{j,k}\right)^{\top} \mathbf{a}^{\mathrm{t}}_{j,k} - \left\|\mathbf{x}^{\mathrm{u}}_{i,k} - \mathbf{x}^{\mathrm{t}}_{j,k}\right\| \left\|\mathbf{a}^{\mathrm{t}}_{j,k}\right\| \left(\cos \lambda^{\mathrm{t}}_j\right), \quad (3.9)$$

where, at time t_k, $\mathbf{a}^{\mathrm{t}}_{j,k}$ is the axis of this cone and $2\lambda^{\mathrm{t}}_j$ its aperture. Figure 3.7 illustrates the case where the condition g^{t}_j is modeled by a half circular cone. The target is only detected and identified if the target is located inside the FoV of the UAV and if the UAV is located inside the green region.

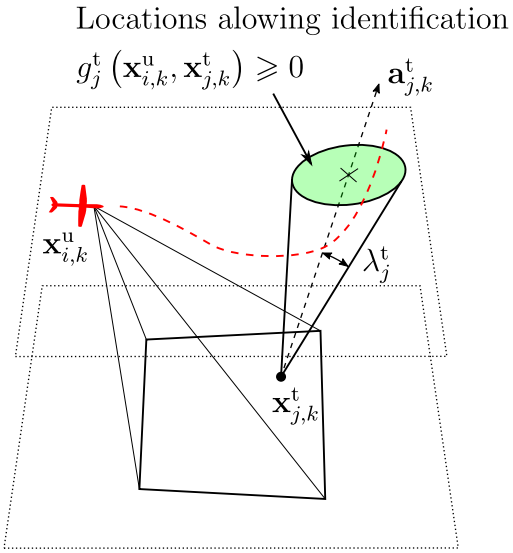

Figure 3.7.: Illustration of a possible identification condition for target j. The target can be only identified if the UAV is located in the green region.

The list$\mathcal{D}^{\mathrm{I}}_{i,k}$ also contains the identifiers of all false targets with state $\mathbf{x}^{\mathrm{f}}_{\ell,k}$ that were

detected and misidentified, and so confused with a target $j \in \mathcal{J}^{\mathrm{t}}$ at time t_k, *i.e.*,

$$\underbrace{\mathbf{x}^{\mathrm{f}}_{\ell,k} \in \mathbb{F}_i\left(\mathbf{x}^{\mathrm{u}}_{i,k}\right) \text{ and } \boldsymbol{x}^{\mathrm{u}}_{i,k} \in \mathbb{D}_k\left(\mathbf{x}^{\mathrm{f}}_{\ell,k}\right)}_{\text{Detection conditions}} \text{ and } \underbrace{g^{\mathrm{f}}_{\ell}\left(\mathbf{x}^{\mathrm{u}}_{i,k}, \mathbf{x}^{\mathrm{f}}_{\ell,k}\right) \geqslant 0}_{\text{Identifiation condition}} \text{ and } \underbrace{q^{\mathrm{f}}_{\ell}\left(\mathbf{x}^{\mathrm{u}}_{i,k}, \mathbf{x}^{\mathrm{f}}_{\ell,k}\right) \geqslant 0}_{\text{Misidentification condition}} \Rightarrow J(\ell) \in \mathcal{D}^{\mathrm{I}}_{i,k}, \quad (3.10)$$

where g^{f}_{ℓ} and q^{f}_{ℓ} are the identification and misidentification conditions for the false target ℓ. The functions g^{f}_{ℓ} and q^{f}_{ℓ} may have similar shape as in (3.9). An identifier j may appear multiple times in $\mathcal{D}^{\mathrm{I}}_{i,k}$ due to the potential presence of a true target and one or more false targets confused with that true target in the FoV of the UAV.

Furthermore, $\mathcal{D}^{\mathrm{U}}_{i,k}$ is a list of integers referring to true and false targets that are detected but not identified (conditions g^{t} and g^{f} are not satisfied). For a true target $j \in \mathcal{J}^{\mathrm{t}}$, one has

$$\underbrace{\mathbf{x}^{\mathrm{t}}_{j,k} \in \mathbb{F}_i\left(\mathbf{x}^{\mathrm{u}}_{i,k}\right) \text{ and } \boldsymbol{x}^{\mathrm{u}}_{i,k} \in \mathbb{D}_k\left(\boldsymbol{x}^{\mathrm{t}}_{j,k}\right)}_{\text{Detection conditions}} \text{ and } \underbrace{g^{\mathrm{t}}_{j}\left(\mathbf{x}^{\mathrm{u}}_{i,k}, \mathbf{x}^{\mathrm{t}}_{j,k}\right) < 0}_{\text{Non-Identifiation condition}} \Rightarrow \pi_{i,k}(j) \in \mathcal{D}^{\mathrm{U}}_{i,k}, \quad (3.11)$$

where $\pi_{i,k}$ maps $\mathcal{J}^{\mathrm{t}} \cup \mathcal{J}^{\mathrm{f}}$ to $\mathbb{N}$. For a false target $\ell \in \mathcal{J}^{\mathrm{f}}$, one has

$$\underbrace{\mathbf{x}^{\mathrm{f}}_{\ell,k} \in \mathbb{F}_i\left(\mathbf{x}^{\mathrm{u}}_{i,k}\right) \text{ and } \boldsymbol{x}^{\mathrm{u}}_{i,k} \in \mathbb{D}_k\left(\mathbf{x}^{\mathrm{f}}_{\ell,k}\right)}_{\text{Detection conditions}} \text{ and } \underbrace{g^{\mathrm{f}}_{\ell}\left(\mathbf{x}^{\mathrm{u}}_{i,k}, \mathbf{x}^{\mathrm{f}}_{\ell,k}\right) < 0}_{\text{Non-Identifiation condition}} \Rightarrow \pi_{i,k}(\ell) \in \mathcal{D}^{\mathrm{U}}_{i,k}. \quad (3.12)$$

The function $\pi_{i,k}$ is used to assign an integer to the index of unidentified targets in the order they are processed $\mathcal{D}^{\mathrm{U}}_{i,k} = \{1, 2, 3, ...\}$. For example $\mathcal{D}^{\mathrm{U}}_{i,k} = \{1, 2, 3\}$ indicates that three unidentified targets are detected at time t_k by UAV i. The mapping $\pi_{i,k}$ is not available to the UAVs.

When false target is detected, identified and $q^{\mathrm{f}}_{\ell}\left(\mathbf{x}^{\mathrm{u}}_{i,k}, \mathbf{x}^{\mathrm{f}}_{\ell,k}\right) \geqslant 0$ holds, then it is revealed as false target, *i.e.*,

$$\underbrace{\mathbf{x}^{\mathrm{f}}_{\ell,k} \in \mathbb{F}_i\left(\mathbf{x}^{\mathrm{u}}_{i,k}\right) \text{ and } \boldsymbol{x}^{\mathrm{u}}_{i,k} \in \mathbb{D}_k\left(\mathbf{x}^{\mathrm{f}}_{\ell,k}\right)}_{\text{Detection conditions}} \text{ and } \underbrace{g^{\mathrm{f}}_{\ell}\left(\mathbf{x}^{\mathrm{u}}_{i,k}, \mathbf{x}^{\mathrm{f}}_{\ell,k}\right) \geqslant 0}_{\text{Identifiation condition}} \text{ and } \underbrace{q^{\mathrm{f}}_{\ell}\left(\mathbf{x}^{\mathrm{u}}_{i,k}, \mathbf{x}^{\mathrm{f}}_{\ell,k}\right) < 0}_{\text{Reveal condition}} \Rightarrow \ell \in \mathcal{D}^{\mathrm{F}}_{i,k}. \quad (3.13)$$

False targets in $\mathcal{D}^{\mathrm{F}}_{i,k}$ are not tracked and the measurements can be discarded.

The UAVs are not aware of the structure of g^{t}_{j}, g^{f}_{ℓ}, and q^{f}_{ℓ}, *i.e.*, the UAVs from Scene 6 may not know where the license plats are located, or if they are soiled. The condition $g^{\mathrm{t}}_{j}(\mathbf{x}^{\mathrm{u}}_{i,k}, \mathbf{x}^{\mathrm{t}}_{j,k}) \geqslant 0$ may represent a situation where the UAV i identifies the true target since it is observed from some specific point of view belonging, *e.g.*, to some polyhedral cone whose apex is $\mathbf{x}^{\mathrm{t}}_{j,k}$. A similar structure is assumed

for the identification condition g_ℓ^{f} for false targets. The misidentification condition $q_\ell^{\mathrm{f}}(\mathbf{x}_{i,k}^{\mathrm{u}}, \mathbf{x}_{\ell,k}^{\mathrm{f}}) \geqslant 0$ is satisfied if, *e.g.*, UAV i is *not* located within some polyhedral cone whose apex is $\mathbf{x}_{\ell,k}^{\mathrm{f}}$. The design of the observation conditions is inspired by the approach in Pan et al. (2017), where UAVs monitor multiple moving ground targets. In this approach, targets are detected and considered as covered if the targets are facing the UAVs, *i.e.*, if their heading angel satisfies some constraints. In Pan et al. (2017), the additional observation condition is assumed to be known by the UAVs.

Figure 3.8 and 3.9 show the measurement process and the information obtained depending on the identification and misidentification conditions.

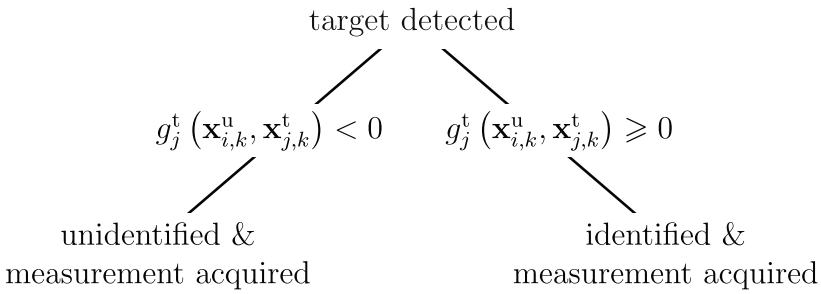

Figure 3.8.: Identification of true targets depending on the identification condition g_j^{t}.

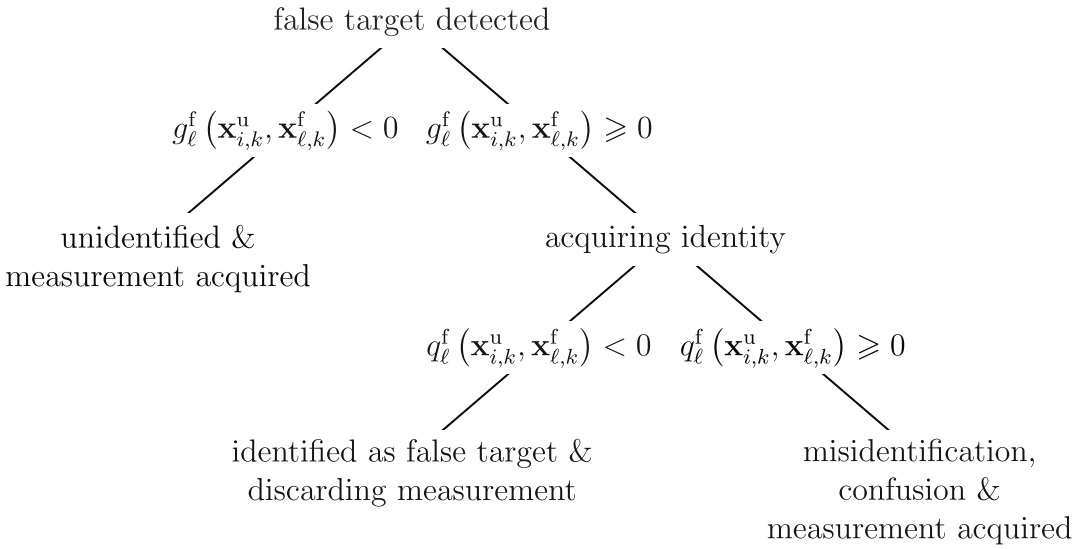

Figure 3.9.: Identification and misidentification condition for false targets: obtained information depends on the identification condition g_ℓ^{f} and the misidentification condition q_ℓ^{f}.

Figure 3.10 illustrates different scenarios when a target is detected. It is assumed that $\boldsymbol{x}_{i,k}^{\mathrm{u}} \in \mathbb{D}_k\left(\boldsymbol{x}_{j,k}^{\mathrm{t}}\right)$ is always satisfied. The red UAV detects and identifies the

false target ℓ_1 as $\mathbf{x}^{\mathrm{f}}_{\ell_1,k} \in \mathbb{F}_i(\mathbf{x}^{\mathrm{u}}_{i,k})$ and $g^{\mathrm{f}}_{\ell_1}(\mathbf{x}^{\mathrm{u}}_{i,k}, \mathbf{x}^{\mathrm{f}}_{\ell_1,k}) \geqslant 0$. Moreover, target ℓ_1 is correctly identified as a false target as $q^{\mathrm{f}}_{\ell_1}(\mathbf{x}^{\mathrm{u}}_{i,k}, \mathbf{x}^{\mathrm{f}}_{\ell_1,k}) < 0$. The green UAV detects and identifies correctly the true target j_1 as $\mathbf{x}^{\mathrm{t}}_{j_1,k} \in \mathbb{F}_i(\mathbf{x}^{\mathrm{u}}_{i,k})$ and $g^{\mathrm{t}}_{j_1}(\mathbf{x}^{\mathrm{u}}_{i,k}, \mathbf{x}^{\mathrm{t}}_{j_1,k}) \geqslant 0$. The blue UAV detects the true target j_2 as $\mathbf{x}^{\mathrm{t}}_{j_2,k} \in \mathbb{F}_i(\mathbf{x}^{\mathrm{u}}_{i,k})$ but it is not identified since $g^{\mathrm{t}}_{j_2}(\mathbf{x}^{\mathrm{u}}_{i,k}, \mathbf{x}^{\mathrm{t}}_{j_2,k}) < 0$. Finally, the blue UAV detects and identifies the false target ℓ_2 as $\mathbf{x}^{\mathrm{f}}_{\ell_2,k} \in \mathbb{F}_i(\mathbf{x}^{\mathrm{u}}_{i,k})$ and $g^{\mathrm{f}}_{\ell_2}(\mathbf{x}^{\mathrm{u}}_{i,k}, \mathbf{x}^{\mathrm{f}}_{\ell_2,k}) \geqslant 0$, but it is confused with a true target since $q^{\mathrm{f}}_{\ell_2}(\mathbf{x}^{\mathrm{u}}_{i,k}, \mathbf{x}^{\mathrm{f}}_{\ell_2,k}) \geqslant 0$.

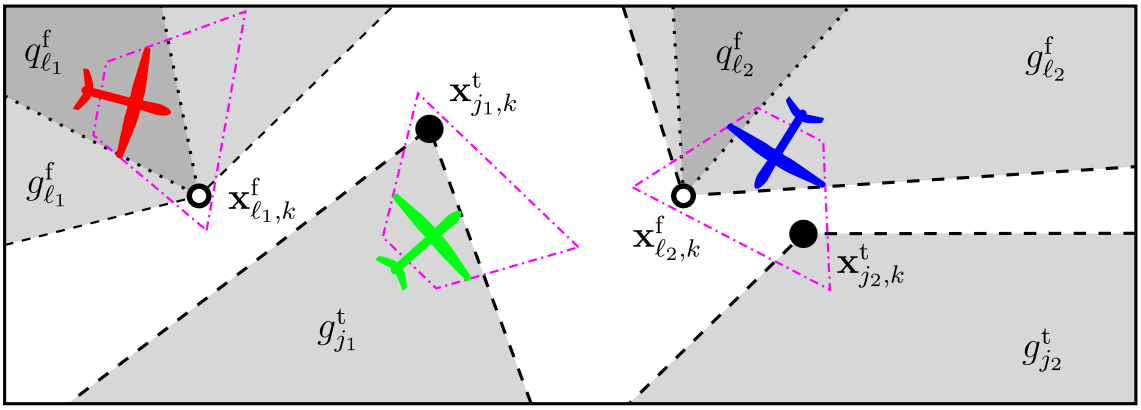

Figure 3.10.: Projection of the 2D plane (x_1, x_2) of the RoI as well as of the state of true targets $\mathbf{x}^{\mathrm{t}}_{i,k}$ (filled circles) and false targets $\mathbf{x}^{\mathrm{f}}_{\ell,k}$ (empty circles). The boundary of each FoV is in dashed-dotted magenta. The subsets defined by $g^{\mathrm{t}}_{j}(\mathbf{x}^{\mathrm{u}}_{i,k}, \mathbf{x}^{\mathrm{t}}_{j,k}) \geqslant 0$ and $g^{\mathrm{f}}_{\ell}(\mathbf{x}^{\mathrm{u}}_{i,k}, \mathbf{x}^{\mathrm{f}}_{\ell,k}) \geqslant 0$ where targets can be identified are illustrated by the projection of the conic subspace in light gray. The subset defined by $q^{\mathrm{f}}_{\ell}(\mathbf{x}^{\mathrm{u}}_{i,k}, \mathbf{x}^{\mathrm{f}}_{\ell,k}) < 0$ where false targets are correctly identified as false targets is represented by the projection of the conic subspace in dark gray.

3.7. Measurements

Scene 7:

A UAV that has detected a car collects a measurement. This measurement consists of one or several images that are taken by the RGB camera. The images are processed by object-detection software that outputs the location of the car in the image frame. The software may process not only the location but also the orientation, speed, acceleration, and other state components of the car within the image frame. The extracted information needs to be transformed from the image frame into the target state space. That is the actual location of the car on the road. A nonlinear measurement function may describe this transformation.

The measurement process is affected by noise and uncertainties that will degrade the quality of the measurement. Uncertainty sources in the considered example may be an uncertain UAV location, uncertain relative camera orientation, discretization error due to, e.g., the resolution of the collected images, uncertain camera specifications, and motion blur (due to UAV and car motion).

This section models the measurement process to account for the noises and uncertainties of the collected measurements when a target is detected.

A noisy observation of the state $\mathbf{x}^{\mathrm{t}}_{j,k}$ is obtained for each identified true target $j \in \mathcal{D}^{\mathrm{I}}_{i,k}$ as

$$\mathbf{y}^{\mathrm{I}}_{i,j,k} = \mathbf{h}_i\left(\mathbf{x}^{\mathrm{u}}_{i,k}, \mathbf{x}^{\mathrm{t}}_{j,k}\right) + \mathbf{w}_{i,j,k}, \tag{3.14}$$

and for each unidentified true target $m \in \mathcal{D}^{\mathrm{U}}_{i,k}$, such that $j = \pi^{-1}_{i,k}(m) \in \mathcal{J}^{\mathrm{t}}$, as

$$\mathbf{y}^{\mathrm{U}}_{i,m,k} = \mathbf{h}_i\left(\mathbf{x}^{\mathrm{u}}_{i,k}, \mathbf{x}^{\mathrm{t}}_{j,k}\right) + \mathbf{w}_{i,j,k}, \tag{3.15}$$

where $\mathbf{h}_i$ is the observation equation of UAV i and $\mathbf{w}_{i,j,k}$ represents some measurement noise. It is assumed that measurement noise $\mathbf{w}_{i,j,k}$ is bounded in some box $[\mathbf{w}_{i,j,k}]$. Usually the size of this box varies according to environmental and measurement conditions and is unknown, see *e.g.* the approaches in Cortes et al. (2004); Li and Duan (2017). One assumes, however, that a known box $[\mathbf{w}_{i,k}]$ such that $[\mathbf{w}_{i,j,k}] \subset [\mathbf{w}_{i,k}]$ can be obtained, considering, *e.g.*, worst-case measurement conditions.

Furthermore, a noisy observation of the state $\mathbf{x}^{\mathrm{f}}_{\ell,k}$ of false target ℓ, which is misidentified, *i.e.*, $J(\ell) \in \mathcal{D}^{\mathrm{I}}_{i,k}$, is obtained as

$$\mathbf{y}^{\mathrm{I}}_{i,J(\ell),k} = \mathbf{h}_i\left(\mathbf{x}^{\mathrm{u}}_{i,k}, \mathbf{x}^{\mathrm{f}}_{\ell,k}\right) + \mathbf{w}_{i,\ell,k}, \tag{3.16}$$

and of unidentified false target $m \in \mathcal{D}^{\mathrm{U}}_{i,k}$, such that $\ell = \pi^{-1}_{i,k}(m) \in \mathcal{J}^{\mathrm{f}}$, as

$$\mathbf{y}^{\mathrm{U}}_{i,m,k} = \mathbf{h}_i\left(\mathbf{x}^{\mathrm{u}}_{i,k}, \mathbf{x}^{\mathrm{f}}_{\ell,k}\right) + \mathbf{w}_{i,\ell,k}, \tag{3.17}$$

where $\mathbf{w}_{i,\ell,k}$ belongs to some box $[\mathbf{w}_{i,\ell,k}]$. One assumes again that the same box $[\mathbf{w}_{i,k}]$ is such that $[\mathbf{w}_{i,\ell,k}] \subset [\mathbf{w}_{i,k}]$.

As presented in the following chapters, measurements and noise bounds are used to get set estimates of the target locations. When the noise bounds $[\mathbf{w}_{i,k}]$ depend, *e.g.*, on the distance to the target, a first estimate can be obtained from conservative noise bounds. It may then be possible to obtain more accurate noise bounds using the estimated target location. This way, the noise bound could be updated iteratively.

Figure 3.11 shows the detection of a target and the collected measurement $\mathbf{y}^{\mathrm{I}}_{i,j,k}$

(green dot) projected on to the ground plan.

The shape of the measurement function $\mathbf{h}_i$ depends on the type of sensor that is used. In the case of a pinhole camera model, the measurements might be obtained in angles. Consequently, the noise $\mathbf{w}_{i,j,k}$ and its bounds $[\mathbf{w}_{i,k}]$ would be in angles also. Nevertheless, in the simulations in Chapter 4 and 5 a simplified measurement model is considered. It is assumed that the measurement function is the identity function, and that only the location of the target is measured. Therefore, the target location is directly available to the UAV and the noise is added to the measured location.

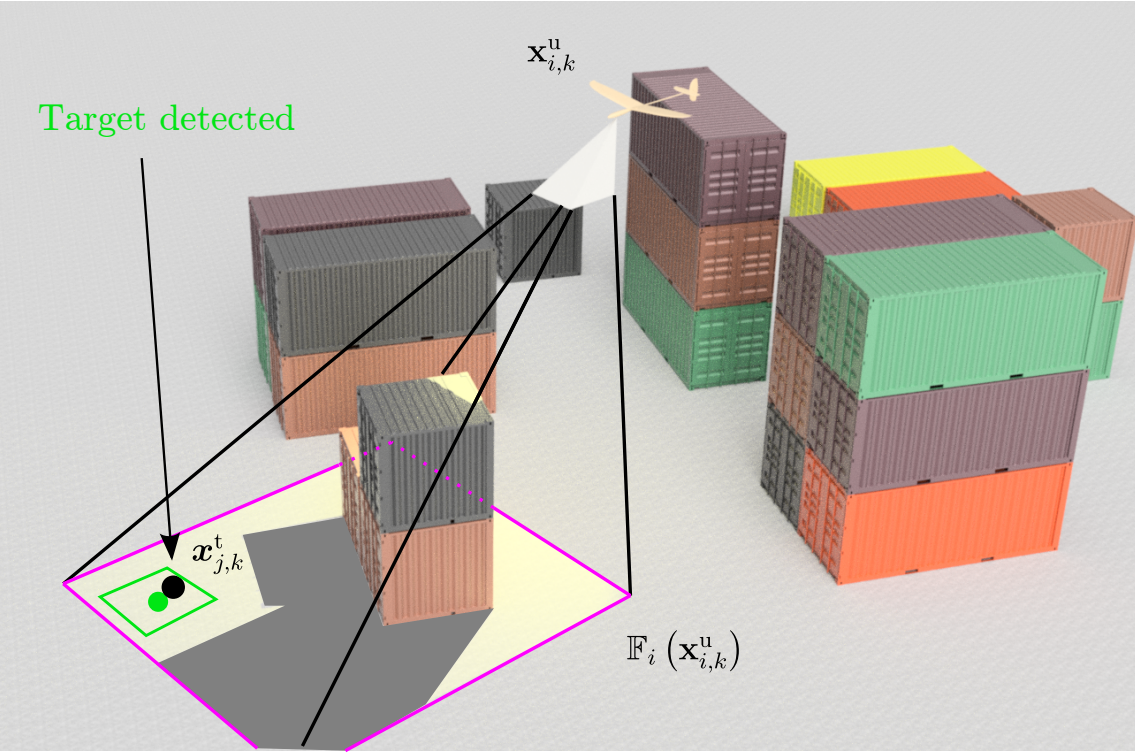

Figure 3.11.: Field of View $\mathbb{F}_i\left(\mathbf{x}^{\mathrm{u}}_{i,k}\right)$ characterized by its vertices (black and pink) of UAV i: Detection of target j and collection of a measurement $\mathbf{y}^{\mathrm{I}}_{i,j,k}$ (green dot). The noise bound $[\mathbf{w}_{i,k}]$ is illustrated as a green square surrounding the measurement of the target location.

3.8. Communication

Scene 8:

The UAVs can communicate and transmit information using, e.g., a wireless network protocol such as the IEEE 802.11 local area network standard. The communication is intermittent due to the range of the transmitter and receiver and also due to the buildings within the search area. The buildings may reflect, scatter, and absorb the radio waves.

The search is carried out by cooperating UAVs that exchange information. To model the communicate, it is assumed that two UAVs exchange information only when they are in vicinity. The UAV network is represented by a set of nodes $\mathcal{N}^{\mathrm{u}} = \{1, 2, ..., N^{\mathrm{u}}\}$. The set of edges of the network $\mathcal{E}_k \subset \mathcal{N}^{\mathrm{u}} \times \mathcal{N}^{\mathrm{u}}$ describes the connectivity at time t_k. An undirected graph $\mathcal{G}_k = (\mathcal{N}^{\mathrm{u}}, \mathcal{E}_k)$ summarizes the communication topology of the fleet at time t_k. $\mathcal{N}_{i,k} = \{i' \in \mathcal{N}^{\mathrm{u}} | \, (i, i') \in \mathcal{E}_k, \; i \neq i'\}$ is the set of neighbors connected to UAV i at time t_k. UAVs i and i' exchange information without error and delay when $(i, i') \in \mathcal{E}_k$, and they are unable to communicate when $(i, i') \notin \mathcal{E}_k$. The edges of the network at time t_k depend on some communication condition c. One has

$$c\left(\mathbf{x}^{\mathrm{u}}_{i,k}, \mathbf{x}^{\mathrm{u}}_{i',k}\right) \geqslant 0 \Rightarrow (i, i') \in \mathcal{E}_k, \tag{3.18}$$

where c may depend, *e.g.*, on the distance between two UAVs or on the environment (absorption, reflection, scattering due to the presence of obstacles).

Some simplifications are made regarding the communication. It is assumed that the UAVs possess perfectly synchronized clocks and that the communication events are perfectly timed. The UAVs have instantaneous access to the transmitted information of direct neighbors in the communication graph. The amount of transmitted data is not limited. Furthermore, the communication takes place without delay, and the transmitted information is not corrupted. A review of communication protocols for teams of UAVs considering inspection tasks is, *e.g.*, presented in Shi et al. (2021).

UAV i has now access to different sources of information to estimate the state of the targets. The next section introduces set estimates derived from the collected information to estimate the targets states.

3.9. Set estimates of the target state

Scene 9:

A UAV has detected some cars, collected measurements, and estimated their locations in the environment. This knowledge is used to evaluate regions that are guaranteed to contain the location of the tracked cars. The shape of these regions evolves when new observations are collected and as time passes since the cars may drive and change their locations.

The UAVs have to process the collected information to obtain the target state estimates. The information sources that the UAVs can account for are:

- the observed regions,
- the collected measurements of the detected targets,
- the obtained identities of tracked targets,
- the dynamics of the targets,
- the assumptions on the noise and uncertainties,
- and information obtained from another UAV of the fleet.

Regarding different estimation techniques, many target search and tracking approaches consider a probabilistic estimation of the zone representing the target locations. The prediction and update of the estimates are performed by recursive Bayesian filtering in a stochastic context, *e.g.,* as in Tian et al. (2017). This thesis considers set-membership estimation techniques for target tracking, where the aim is to define bounded sets that are guaranteed to contain the state or location of every target within the RoI. Set-membership estimation techniques are well suited when the probabilistic distributions of noises and uncertainties are unknown but bounded.

One introduces the set $\mathbb{I}_{i,k}$ to gather the information available to UAV i up to time t_k. From $\mathbb{I}_{i,k}$, UAV i is able to evaluate $\mathcal{L}_{i,k}$, the *list* of indices of targets already detected and identified, or which presence has been signaled by another UAV of the fleet to UAV i. Targets in $\mathcal{L}_{i,k}$ are tracked. Furthermore, $\mathbb{I}_{i,k}$ is used to evaluate a *list* of *target set estimates* $\mathcal{X}_{i,k} = \{\mathbb{X}_{i,j,k}\}_{j\in\mathcal{L}_{i,k}}$ and the *set estimate* $\mathbb{X}^{\mathrm{U}}_{i,k}$. $\mathbb{X}_{i,j,k}$ contains all possible values of the state of the identified target j that are consistent with the information available to UAV i at time t_k. It is possible that $\mathbb{X}_{i,j,k}$ does not contain the actual values of $\mathbf{x}^{\mathrm{t}}_{j,k}$ due to misidentification of false targets. $\mathbb{X}^{\mathrm{U}}_{i,k}$ contains the union of all possible values of $\mathbf{x}^{\mathrm{t}}_{j,k}$ and $\mathbf{x}^{\mathrm{f}}_{\ell,k}$ for all detected targets still to be identified. UAV i also maintains a set $\overline{\mathbb{X}}_{i,k}$ containing the possible state values of targets not yet detected. UAV i searches for new targets in the set $\overline{\mathbb{X}}_{i,k}$. Finally, the set $\widetilde{\mathbb{X}}_{i,k}$ is explored and does not contain any true targets state. Figure 3.12 illustrates the different set estimates. The same color code will be used throughout the manuscript.

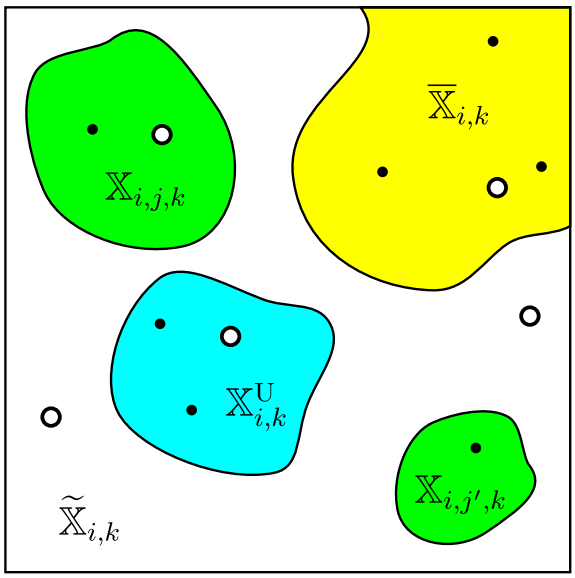

Figure 3.12.: Introduction of the set set estimates: target set estimates $\mathbb{X}_{i,j,k}$ and $\mathbb{X}_{i,j',k}$ of target j and j' (in green); set estimate of unidentified targets $\mathbb{X}^{\mathrm{U}}_{i,k}$ (in cyan), unexplored set/set of states of unknown targets $\overline{\mathbb{X}}_{i,k}$ (in yellow), and explored set $\widetilde{\mathbb{X}}_{i,k}$ (in white).

3.10. Problem formulation

Section 3.9 introduced the set estimates that are evaluated by each UAV. The aim of the approaches presented in Chapters 4 and 5 is to evaluate set estimates that are as precise as possible. For this, it is necessary to define a measure of the uncertainty with which the target state is estimated. This section introduces the target state estimation uncertainty for a single UAV and for the complete fleet. The aim is to drive each UAV so that the estimation uncertainty for the complete fleet decreases. This is a quite challenging problem since each UAV has only local knowledge of its own set estimates due to communication constraints. The estimation of the target states and the design of the UAV control inputs have to be distributed. Consequently, a cost function is needed that can be evaluated by each UAV and represent the global performance of the complete fleet. This cost function has to incorporate the objectives of searching for new targets and tracking already identified ones.

Consider UAV i and assume that at time t_k, $\mathbb{X}^{\mathrm{U}}_{i,k}$ and $\overline{\mathbb{X}}_{i,k}$ are empty and that set estimates $\mathbb{X}_{i,j,k}$ are available for all $j \in \mathcal{J}^{\mathrm{t}}$. Then, $\mathbf{x}^{\mathrm{t}}_{j,k} \in \mathbb{X}_{i,j,k}$ and the estimation uncertainty for the state of target j may be defined as $\phi(\mathbb{X}_{i,j,k})$, where $\phi(\mathbb{X})$ represents some measure of the set $\mathbb{X}$. The measure $\phi(.)$ can be, *e.g.*, the area of $\mathbb{X}$ when $\mathbb{X} \subset \mathbb{R}^2$ or the volume of $\mathbb{X}$ when $\mathbb{X} \subset \mathbb{R}^3$ or of higher dimension.

When $\mathbb{X}^{\mathrm{U}}_{i,k}$ or $\overline{\mathbb{X}}_{i,k}$ are not empty, due to the presence of a false target, one has not necessarily $\mathbf{x}^{\mathrm{t}}_{j,k} \in \mathbb{X}_{i,j,k}$ and the estimation uncertainty for the state of target j has to

account for $\mathbb{X}^{\mathrm{U}}_{i,k}$ and $\overline{\mathbb{X}}_{i,k}$ (which both may contain $\mathbf{x}^{\mathrm{t}}_{j,k}$). The estimation uncertainty may be defined as $\Phi_j(\mathcal{X}_{i,k}, \mathbb{X}^{\mathrm{U}}_{i,k}, \overline{\mathbb{X}}_{i,k}) = \phi(\mathbb{X}_{i,j,k} \cup \mathbb{X}^{\mathrm{U}}_{i,k} \cup \overline{\mathbb{X}}_{i,k})$ then. The estimation uncertainty for target j is then the measure of the union of the sets to which the state of target j may belong.

The target state estimation uncertainty at time t_k for UAV i accounts for all sets and every target and is defined as

$$\Phi\left(\mathcal{X}_{i,k}, \mathbb{X}^{\mathrm{U}}_{i,k}, \overline{\mathbb{X}}_{i,k}\right) = \phi\left(\left(\bigcup_{\mathbb{X}_{i,j,k} \in \mathcal{X}_{i,k}} \mathbb{X}_{i,j,k}\right) \cup \mathbb{X}^{\mathrm{U}}_{i,k} \cup \overline{\mathbb{X}}_{i,k}\right). \tag{3.19}$$

When $\mathcal{X}_{i,k} = \emptyset$, (3.19) boils down to $\Phi(\mathcal{X}_{i,k}, \mathbb{X}^{\mathrm{U}}_{i,k}, \overline{\mathbb{X}}_{i,k}) = \phi(\mathbb{X}^{\mathrm{U}}_{i,k} \cup \overline{\mathbb{X}}_{i,k})$, which gives more importance to the exploration of the area and the identification of new targets. Finally, the average estimation uncertainty among all UAVs at time t_k is

$$\overline{\Phi}_k = \frac{1}{N^{\mathrm{u}}} \sum_{i=1}^{N^{\mathrm{u}}} \Phi\left(\mathcal{X}_{i,k}, \mathbb{X}^{\mathrm{U}}_{i,k}, \overline{\mathbb{X}}_{i,k}\right). \tag{3.20}$$

The aim of the approaches presented in the remainder of the manuscript is to evaluate a sequence of control inputs for each UAV so as to minimize the estimation uncertainty $\overline{\Phi}_k$ as much as possible. This requires first determining the evolution of the various set estimates managed by the UAVs. A distributed control design strategy can then be derived.

Chapter 4 presents a distributed estimation scheme that allows processing measurements of identified and unidentified targets for identification conditions as described in Section 3.6. A distributed control design based on model predictive control is then used to derive the control input of each UAV, reducing the size of the different set estimates. Chapter 5 studies the detection condition presented in Section 3.5 and proposes two target search approaches in unknown cluttered environments. The first approach considers the special case of static targets. The second one is more general and considers moving targets in a changing environment. The adapted control schemes account for the points of view of each UAV when taking a measurement.

4. Tracking of targets in presence of decoys

In this chapter, a distributed set-membership estimation and control scheme is presented. This scheme relies on the description of uncertainties and noises as bounded processes. Constraints on the FoV, as well as the presence of false targets, are taken into account. The target states are estimated by set estimates . Each UAV maintains several set estimates: one for each detected and identified true target, one for detected but not yet identified targets, and one for not yet detected targets, which is also the subset of the state space still to be explored. These sets are updated by each UAV using the information coming from its sensors as well as received from its neighbors.

A distributed set-membership model predictive control approach is considered to compute the trajectories of the UAVs. The control input minimizing a measure of the set-membership estimates predicted h-step ahead is then evaluated. Simulations of scenarios including the presence of false targets illustrate the ability of the proposed approach to efficiently search and track an unknown number of moving targets within some delimited Region of Interest (RoI). Additionally, preliminary experimental studies are carried out.

4.1. Introduction

This chapter considers a fleet of UAVs searching for an unknown number of targets located in an *a priori* given zone. Each UAV is equipped with a sensing device able to detect and localize targets. It is assumed that the targets are always detected if they are located in the observed subset of the sensing device which simplifies the detection conditions modeled in Section 3.5. When a target is detected, its identity is revealed only if some observation conditions are satisfied. This situation is typically encountered with cameras: the identity of a target is available only when it is observed from a specific point-of-view. The approach also accounts for the presence of moving false targets. These false targets may be erroneously identified as true targets and can be distinguished from true targets only when observed under specific conditions. The identification conditions were formally introduced in Section 3.6. For each detected (true and false) target, it is assumed that some noisy measurement of its state is available. The noise corrupting the state observation is assumed to be bounded with known bounds, which may depend on the observation conditions.

This chapter presents a robust distributed set-membership estimator run by each UAV. This estimator determines

- *i*) set estimates containing the state of each *identified* target,
- *ii*) a set estimate containing the states of *detected* but *not yet identified* (true and false) targets,
- and *iii*) a set possibly containing targets remaining to be detected (the part of the RoI still to be explored).

The estimator is able to process measurements associated to detected but unidentified targets, prior to their identification at later time instants. The set estimator alternates predictions and corrections using measurements from the sensor of each UAV and measurements received during communications with its neighbors. The control inputs for each UAV are designed using a MPC approach adapted to the set-membership estimation context, which aims at minimizing a measure of the set estimates (*e.g.*, area or volume of the sets). The MPC approach accounts for the impact of future measurements on the set estimates and infers future information communicated by neighbors. A limited communication range is also considered.

In summary, issues related to false detection and misidentification of false targets, as well as potential non-identification of true targets are considered. The distinction between true and false targets relies on some deterministic observation conditions formally introduced in Section 3.6 and generalizing that introduced in Ibenthal et al. (2020a,b). The distributed MPC approach introduced here accounts for limited and possibly delayed communications between UAVs, extending previous results in Reboul et al. (2019); Ibenthal et al. (2020a). Finally, a better management of set estimates leads to a more efficient and computationally less demanding control law design compared to that of Ibenthal et al. (2020a). The work presented in this chapter is published in Ibenthal et al. (2021a).

Section 4.2, recapitulates the addressed CSAT problem. The evolution of set estimates for a given UAV and the way measurements are taken into account is described in Section 4.3. Section 4.4 introduces the considered distributed MPC approach, focusing on the various simplifications required to get a manageable complexity. Simulations and experiments are presented in Section 4.5 and 4.6, respectively. Some conclusions are drawn in Section 4.7.

4.2. Problem formulation

This chapter addresses the problem of searching and tracking targets which can be identified based on some of their features, *e.g.*, license plates for cars, face characteristics for humans. It is assumed that a unique identifier may be associated with each target and that the set $\mathcal{J}^{\mathrm{t}}$ of target identifiers is known *a priori*. A fleet of N^{u} UAVs searches and tracks an unknown number $N^{\mathrm{t}} \leqslant |\mathcal{J}^{\mathrm{t}}|$ of targets moving within

a limited RoI. Furthermore, this RoI also contains clutter or possibly moving decoys that can be confused with the targets, called *false* targets. The set $\mathcal{J}^{\mathrm{f}}$ of false target identifiers is unknown but assumed to be such that $\mathcal{J}^{\mathrm{t}} \cap \mathcal{J}^{\mathrm{f}} = \emptyset$.

The general problem presented in Chapter 3 is simplified as it is assumed that no obstacles are present in the RoI. Furthermore, $p^{\mathrm{u}}(\mathbf{x}^{\mathrm{u}}_{i,k}) \in \mathbb{D}_k \left(\boldsymbol{x}^{\mathrm{t}}_{j,k}\right)$, where $\mathbf{x}^{\mathrm{u}}_{i,k} \in \mathbb{R}^{n^{\mathrm{u}}}$, is always satisfied for every target which leads to $\mathbb{F}^{\mathrm{D}}_i \left(\mathbf{x}^{\mathrm{u}}_{i,k}\right) = \mathbb{F}_i \left(\mathbf{x}^{\mathrm{u}}_{i,k}\right)$. However, the presented approach may still be applied when the search area contains only *known* obstacles and when the subset $\mathbb{F}^{\mathrm{D}}_i \left(\mathbf{x}^{\mathrm{u}}_{i,k}\right)$ of the FoV can be evaluated by the UAVs. The set $\mathbb{F}_i \left(\mathbf{x}^{\mathrm{u}}_{i,k}\right)$ has then to be replaced by $\mathbb{F}^{\mathrm{D}}_i \left(\mathbf{x}^{\mathrm{u}}_{i,k}\right)$ in the estimation scheme.

To estimate the location of the targets each UAV i maintains the set estimates $\mathcal{X}_{i,k} = \{\mathbb{X}_{i,j,k}\}_{j \in \mathcal{L}_{i,k}}$, $\mathbb{X}^{\mathrm{U}}_{i,k}$, and $\overline{\mathbb{X}}_{i,k}$. The aim of the approach presented in this chapter is to evaluate a sequence of control inputs for each UAV so as to minimize the estimation uncertainty $\overline{\Phi}_k$ as much as possible. This requires first to be able to determine the evolution of the various set estimates managed by UAVs, as detailed in Section 4.3. A distributed control design strategy is then presented in Section 4.4.

4.3. Evolution of set estimates for a given UAV

This section describes the evolution with time of the list $\mathcal{L}_{i,k}$ and the sets $\mathcal{X}_{i,k}$, $\mathbb{X}^{\mathrm{U}}_{i,k}$, and $\overline{\mathbb{X}}_{i,k}$ managed by a given UAV i. The UAVs evaluate the set estimates considering a generalization of a nonlinear recursive set-membership state estimator. Similar to the classical Kalman filter, it alternates prediction and correction steps, the latter being based on measurements but also on exchanged information via communication with the neighbors.

At time $t_{k=0}$, only the set of unexplored states $\overline{\mathbb{X}}_{i,0}$ is non empty and initialized with the considered RoI since all targets are assumed to stay in $\mathbb{X}_0$. Thus, the initial set values are $\mathcal{L}_{i,0} = \emptyset$, $\mathcal{X}_{i,0} = \emptyset$, $\mathbb{X}^{\mathrm{U}}_{i,0} = \emptyset$ and $\overline{\mathbb{X}}_{i,0} = \mathbb{X}_0$ for $i = 1, \ldots, N^{\mathrm{u}}$.

4.3.1. Prediction step

Scene 10:

Continuing with Scene 9, assume that a UAV tracks two identified cars. Two regions represent the current locations of these cars, each containing a single car. The value of $\mathbb{X}_{i,j,k}$ and $\mathcal{L}_{i,k}$ translate this knowledge. Another regions is still to be explored and may contain unknown cars. This regions is modeled by $\overline{\mathbb{X}}_{i,k}$. Time passes, and the UAV has to update the two regions since the cars may have changed their locations. The UAV can predict the possible future locations of a car by, e.g., inflating the estimated zones, where the magnitude of the inflation depends on the maximal distance the cars could travel during the passed period. This prediction can be more accurate if more information is available, such as the previous speed of the car, maximal acceleration, the previous heading angle, and maximal turn rate.

Following Scene 10, the prediction of the evolution of the set estimates is presented in this section.

UAV i has access to $\mathcal{L}_{i,k}$, $\mathcal{X}_{i,k}$, $\mathbb{X}^{\mathrm{U}}_{i,k}$, and $\overline{\mathbb{X}}_{i,k}$ at time t_k. One is unable to predict whether UAV i will detect new targets at time t_{k+1}, thus the predicted list of tracked targets is

$$\mathcal{L}_{i,k+1|k} = \mathcal{L}_{i,k}. \tag{4.1}$$

For each target in $\mathcal{L}_{i,k+1|k}$, one is able to predict the set of possible future state values at time t_{k+1}, *i.e*, the set of all target state values that are consistent with $\mathbb{X}_{i,j,k}$, with the dynamics (3.2), and the bounded state perturbation, *i.e.*,

$$\begin{aligned}\mathbb{X}_{i,j,k+1|k} &= \left\{\mathbf{f}^{\mathrm{t}}_k(\mathbf{x},\mathbf{v}) \mid \mathbf{x} \in \mathbb{X}_{i,j,k}, \mathbf{v} \in [\mathbf{v}_k]\right\} \cap \mathbb{X}_0 \\ &= \mathbf{f}^{\mathrm{t}}_k\left(\mathbb{X}_{i,j,k}, [\mathbf{v}_k]\right) \cap \mathbb{X}_0. \end{aligned} \tag{4.2}$$

The intersection with $\mathbb{X}_0$ is computed since targets are assumed not to leave the RoI. The predicted sets $\mathbb{X}^{\mathrm{U}}_{i,k+1|k}$ and $\overline{\mathbb{X}}_{i,k+1|k}$ are obtained in the same manner since all true targets evolve according to the same dynamics (3.2) and have the same bounds for the state perturbation. The value of $\mathbb{X}^{\mathrm{U}}_{i,k+1|k}$ is evaluated as

$$\begin{aligned}\mathbb{X}^{\mathrm{U}}_{i,k+1|k} &= \left\{\mathbf{f}^{\mathrm{t}}_k(\mathbf{x},\mathbf{v}) \mid \mathbf{x} \in \mathbb{X}^{\mathrm{U}}_{i,k}, \mathbf{v} \in [\mathbf{v}_k]\right\} \cap \mathbb{X}_0 \\ &= \mathbf{f}^{\mathrm{t}}_k\left(\mathbb{X}^{\mathrm{U}}_{i,k}, [\mathbf{v}_k]\right) \cap \mathbb{X}_0, \end{aligned} \tag{4.3}$$

and $\overline{\mathbb{X}}_{i,k+1|k}$ as

$$\begin{aligned}\overline{\mathbb{X}}_{i,k+1|k} &= \left\{\mathbf{f}_k^{\mathrm{t}}\left(\mathbf{x},\mathbf{v}\right) \mid \mathbf{x} \in \overline{\mathbb{X}}_{i,k}, \mathbf{v} \in [\mathbf{v}_k]\right\} \cap \mathbb{X}_0 \\ &= \left\{\mathbf{f}_k^{\mathrm{t}}\left(\overline{\mathbb{X}}_{i,k}, [\mathbf{v}_k]\right)\right\} \cap \mathbb{X}_0. \end{aligned} \tag{4.4}$$

Figure 4.1 illustrates the prediction step of the sets in $\mathbb{R}^2$. UAV i can only account for information available at time t_k.

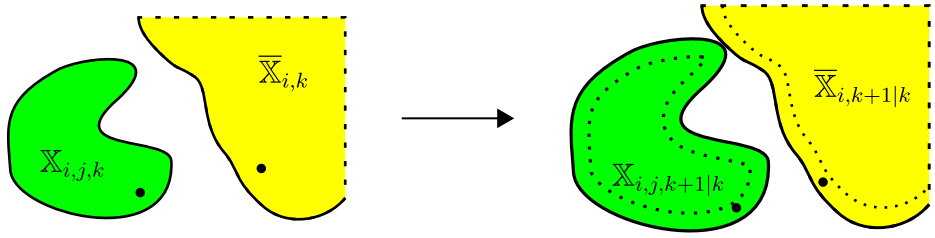

Figure 4.1.: Prediction of the set estimates: set estimates $\mathbb{X}_{i,j,k}$ and $\overline{\mathbb{X}}_{i,k}$ at time t_k (left side) and set estimates $\mathbb{X}_{i,j,k+1|k}$ and $\overline{\mathbb{X}}_{i,k+1|k}$ the after the prediction step (right side). The evolution is determined by the dynamics of the targets and the bounded state perturbation.

4.3.2. Correction step from measurements

Scene 11:

Assume a UAV takes a picture with its RGB camera. In the collected image, the UAV detects two cars. The license plate of the first car is visible. The license plate of the second car is not visible. Consequently, only the first car can be identified. If it has not been identified before, a new target set estimate can be created representing the estimated location of this car. Otherwise, the previous set estimate of the car can be updated.
The second car is unidentified but it is located in a region of a previously detected car (target set estimate $\mathbb{X}_{i,j,k}$). Consequently, it may correspond to an already identified car that is detected again.

Scene 11 illustrates just three possible outcomes when an observation is taken but there are several other possibilities. The following description starts by updating and correcting the target set estimate $\mathbb{X}_{i,j,k+1|k}$.

UAV i obtains a measurement $\mathbf{y}^{\mathrm{I}}_{i,j,k+1}$ for identified targets $j \in \mathcal{D}^{\mathrm{I}}_{i,k+1}$ and a measurement $\mathbf{y}^{\mathrm{U}}_{i,m,k+1}$ for unidentified targets $m \in \mathcal{D}^{\mathrm{U}}_{i,k+1}$ after processing the information in

$\mathbb{F}_i\left(\mathbf{x}^{\mathrm{u}}_{i,k+1}\right)$ at time t_{k+1}. Consequently, the total collected information is

$$\mathbb{I}_{i,k+1|k+1} = \mathbb{I}_{i,k} \cup \left\{ \mathcal{D}^{\mathrm{I}}_{i,k+1}, \left\{\mathbf{y}^{\mathrm{I}}_{i,j,k+1}\right\}_{j\in\mathcal{D}^{\mathrm{I}}_{i,k+1}}, \mathcal{D}^{\mathrm{U}}_{i,k+1}, \left\{\mathbf{y}^{\mathrm{U}}_{i,m,k+1}\right\}_{m\in\mathcal{D}^{\mathrm{U}}_{i,k+1}} \right\}. \quad (4.5)$$

4.3.2.1. Updating the set of identified targets

One has to consider different cases to determine the updated set $\mathbb{X}_{i,j,k+1|k+1}$ from $\mathbb{X}_{i,j,k+1|k}$ for an identified target $j \in \mathcal{L}_{i,k+1|k} \cup \mathcal{D}^{\mathrm{I}}_{i,k+1}$, where the list $\mathcal{L}_{i,k+1|k}$ contains the identifier of tracked targets and the list $\mathcal{D}^{\mathrm{I}}_{i,k+1}$ contains the identifier of detected and identified targets at time t_k. When evaluating $\mathbb{X}_{i,j,k+1|k+1}$ one has to account for identified measurements $\mathbf{y}^{\mathrm{I}}_{i,j,k+1}$, $j \in \mathcal{D}^{\mathrm{I}}_{i,k+1}$, and unidentified measurements $\mathbf{y}^{\mathrm{U}}_{i,m,k+1}$, $m \in \mathcal{D}^{\mathrm{U}}_{i,k+1}$. The next paragraph presents the processing of identified measurements $\mathbf{y}^{\mathrm{I}}_{i,j,k+1}$, $j \in \mathcal{D}^{\mathrm{I}}_{i,k+1}$.

Accounting for measurements of identified targets

When $j \in \mathcal{D}^{\mathrm{I}}_{i,k+1}$, a measurement $\mathbf{y}^{\mathrm{I}}_{i,j,k+1}$ of an identified target is available and three cases have to be considered.

If $\mathbb{X}_{i,j,k+1|k} \cap \mathbb{F}_i(\mathbf{x}^{\mathrm{u}}_{i,k+1}) \neq \emptyset$, then $\mathbf{y}^{\mathrm{I}}_{i,j,k+1}$ may correspond to a previously detected and identified target j that is observed again. Under that hypothesis, the set of all state values $\mathbf{x}$ consistent with $\mathbb{X}_{i,j,k+1|k}$, $\mathbf{y}^{\mathrm{I}}_{i,j,k+1}$, the measurement equations (3.14), and the measurement noise bound $[\mathbf{w}_{i,k+1}]$ is

$$\mathbb{S}_1 = \left\{ \mathbf{x} \in \mathbb{X}_{i,j,k+1|k} \,|\, \mathbf{h}_i\left(\mathbf{x}^{\mathrm{u}}_{i,k+1}, \mathbf{x}\right) \in \mathbf{y}^{\mathrm{I}}_{i,j,k+1} - [\mathbf{w}_{i,k+1}] \right\}. \quad (4.6)$$

Figure 4.2 (a) illustrates the case where the set $\mathbb{S}_1 \neq \emptyset$.

If $\mathbb{X}^{\mathrm{U}}_{i,k+1|k} \cap \mathbb{F}_i(\mathbf{x}^{\mathrm{u}}_{i,k+1}) \neq \emptyset$, then $\mathbf{y}^{\mathrm{I}}_{i,j,k+1}$ may correspond to the true target j or to a false target ℓ, such that $J(\ell) = j$, which was only detected at t_k and (mis-) identified at time t_{k+1}. Under this hypothesis, the set of all state values $\mathbf{x}$ consistent with $\mathbb{X}^{\mathrm{U}}_{i,k+1|k}$, $\mathbf{y}^{\mathrm{I}}_{i,j,k+1}$, the measurement equations (3.14), and the measurement noise bound $[\mathbf{w}_{i,k+1}]$ is

$$\mathbb{S}_2 = \left\{ \mathbf{x} \in \mathbb{X}^{\mathrm{U}}_{i,k+1|k} \,|\, \mathbf{h}_i\left(\mathbf{x}^{\mathrm{u}}_{i,k+1}, \mathbf{x}\right) \in \mathbf{y}^{\mathrm{I}}_{i,j,k+1} - [\mathbf{w}_{i,k+1}] \right\} \quad (4.7)$$

Figure 4.3 (a) illustrates the case where $\mathbb{S}_2 \neq \emptyset$.

If $\overline{\mathbb{X}}_{i,k+1|k} \cap \mathbb{F}_i(\mathbf{x}^{\mathrm{u}}_{i,k+1}) \neq \emptyset$, then $\mathbf{y}^{\mathrm{I}}_{i,j,k+1}$ may correspond to a new target in $\overline{\mathbb{X}}_{i,k+1|k} \cap \mathbb{F}_i(\mathbf{x}^{\mathrm{u}}_{i,k+1})$. This target may either be the true target j or a misidentified false target ℓ such that $J(\ell) = j$. The set of all state values $\mathbf{x}$ consistent with $\overline{\mathbb{X}}_{i,k+1|k}$, $\mathbf{y}^{\mathrm{I}}_{i,j,k+1}$, the measurement equations (3.14), and the measurement noise bound $[\mathbf{w}_{i,k+1}]$ is

$$\mathbb{S}_3 = \left\{ \mathbf{x} \in \overline{\mathbb{X}}_{i,k+1|k} \,|\, \mathbf{h}_i\left(\mathbf{x}^{\mathrm{u}}_{i,k+1}, \mathbf{x}\right) \in \mathbf{y}^{\mathrm{I}}_{i,j,k+1} - [\mathbf{w}_{i,k+1}] \right\}. \quad (4.8)$$

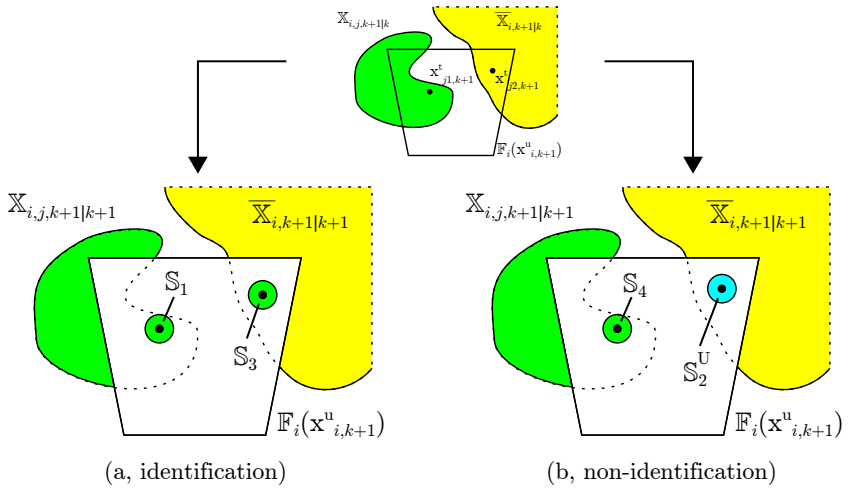

(a, identification) (b, non-identification)

Figure 4.2.: Correction from measurement I: set estimates of $\mathbb{X}_{i,j,k+1|k}$ (in green) and $\overline{\mathbb{X}}_{i,k+1|k}$ (in yellow) before correction from measurement (top); (bottom-a), where targets were detected and identified, the set estimates (in green) inside $\mathbb{F}_i\left(\mathbf{x}^{\mathrm{u}}_{i,k+1}\right)$ are $\mathbb{S}_1$ and $\mathbb{S}_3$. In (b), the targets were detected but not identified. The set estimate (in green) inside $\mathbb{F}_i\left(\mathbf{x}^{\mathrm{u}}_{i,k+1}\right)$ is $\mathbb{S}_4$. The set estimate (in cyan) inside $\mathbb{F}_i\left(\mathbf{x}^{\mathrm{u}}_{i,k+1}\right)$ is $\mathbb{S}^{\mathrm{U}}_2$.

Figure 4.2 (a) illustrates the case where the set $\mathbb{S}_3 \neq \emptyset$.

Finally, if

$$\left(\mathbb{X}_{i,j,k+1|k} \cup \mathbb{X}^{\mathrm{U}}_{i,k+1|k} \cup \overline{\mathbb{X}}_{i,k+1|k}\right) \cap \mathbb{F}_i\left(\mathbf{x}^{\mathrm{u}}_{i,k+1}\right) = \emptyset, \tag{4.9}$$

then the measurement $\mathbf{y}^{\mathrm{I}}_{i,j,k+1}$ is necessarily due to a false target misidentified and confused with target j, since $\mathbf{x}^{\mathrm{t}}_{j,k+1}$ is necessarily in $\mathbb{X}_{i,j,k+1|k} \cup \mathbb{X}^{\mathrm{U}}_{i,k+1|k} \cup \overline{\mathbb{X}}_{i,k+1|k}$.

Accounting for measurements of unidentified targets

When $j \in \mathcal{L}_{i,k+1|k}$ and $\mathcal{D}^{\mathrm{U}}_{i,k+1} \neq \emptyset$, some targets with $j \in \mathcal{L}_{i,k+1|k}$ are tracked and new measurements are available which can not be associated to a specific target in $\mathcal{L}_{i,k+1|k}$. Consequently, the measurements $\mathbf{y}^{\mathrm{U}}_{i,m,k+1}$, $m \in \mathcal{D}^{\mathrm{U}}_{i,k+1}$, may be due to the detection of true target j, $j \in \mathcal{L}_{i,k+1|k}$. Under this hypothesis, the set of all state values $\mathbf{x}$ consistent with $\mathbb{X}_{i,j,k+1|k}$, $\mathbf{y}^{\mathrm{U}}_{i,m,k+1}$, $m \in \mathcal{D}^{\mathrm{U}}_{i,k+1}$, the measurement equations (3.15), and the measurement noise bound $[\mathbf{w}_{i,k+1}]$ is

$$\mathbb{S}_4 = \bigcup_{m \in \mathcal{D}^{\mathrm{U}}_{i,k+1}} \left\{\mathbf{x} \in \mathbb{X}_{i,j,k+1|k} \,|\, \mathbf{h}_i\left(\mathbf{x}^{\mathrm{u}}_{i,k+1}, \mathbf{x}\right) \in \mathbf{y}^{\mathrm{U}}_{i,m,k+1} - [\mathbf{w}_{i,k+1}]\right\}. \tag{4.10}$$

The union for all $m \in \mathcal{D}^{\mathrm{U}}_{i,k+1}$ is evaluated due to the data association problem, *i.e.*, any of the collected measurement may be caused by target j.

Figure 4.2 (b) shows a case where $\mathbb{S}_4$ is not empty. $\mathbb{S}_4$ leads to situations where the

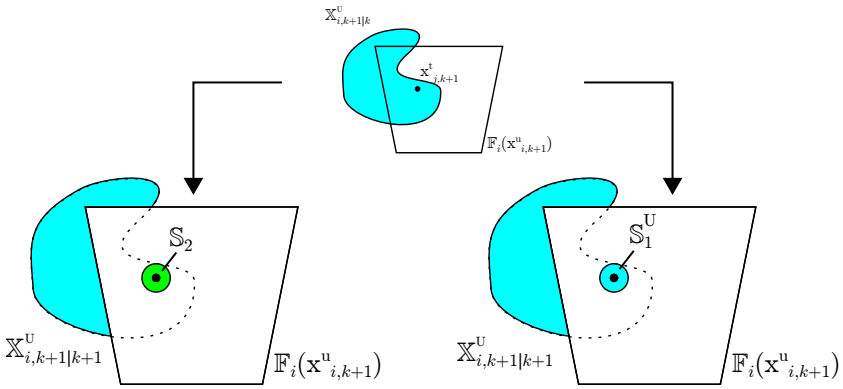

(a; identification) (b; non-identification)

Figure 4.3.: Correction from measurement II: detection of a target inside $\mathbb{X}^{\mathrm{U}}_{i,k+1|k}$ (in cyan in the top subfigure): (a) a target is detected and identified as target j (possible mis-identification for a false target), the set estimate (in green) inside $\mathbb{F}_i\left(\mathbf{x}^{\mathrm{u}}_{i,k+1}\right)$ is $\mathbb{S}_2$; (b) the target is detected but not identified, the set estimate (in cyan) inside $\mathbb{F}_i\left(\mathbf{x}^{\mathrm{u}}_{i,k+1}\right)$ is $\mathbb{S}^{\mathrm{U}}_1$.

measurements might be used several times for the set estimates of different targets. In Figure 4.4, the observed target lays inside the intersection of two set estimates. Due to the data association problem, the measurement $\mathbf{y}^{\mathrm{U}}_{i,m,k+1}$ is used to update the set estimate $\mathbb{X}_{i,j_1,k+1|k}$ and $\mathbb{X}_{i,j_2,k+1|k}$ (Figure 4.4, b).

The sets $\mathbb{S}_1$ to $\mathbb{S}_4$ account for various hypotheses related to the obtained measurements which may be due to the true target j or to a false target misidentified with j. Additionally, one has to account for the fact that all targets or decoys located in the FOV are assumed to be detected and that all information in $\mathbb{F}_i(\mathbf{x}^{\mathrm{u}}_{i,k})$ has been processed. Therefore, $\mathbf{x}^{\mathrm{t}}_{j,k+1} \notin \mathbb{F}_i(\mathbf{x}^{\mathrm{u}}_{i,k+1}) \setminus (\mathbb{S}_1 \cup \mathbb{S}_2 \cup \mathbb{S}_3 \cup \mathbb{S}_4)$. Introducing,

$$\mathbb{S}_5 = \mathbb{X}_{i,j,k+1|k} \setminus \mathbb{F}_i\left(\mathbf{x}^{\mathrm{u}}_{i,k+1}\right), \tag{4.11}$$

which accounts for the fact that the target may be located in $\mathbb{X}_{i,j,k+1|k}$ and outside the FoV of the UAV. The updated set estimate accounting for all hypotheses, is then

$$\mathbb{X}_{i,j,k+1|k+1} = \mathbb{S}_1 \cup \mathbb{S}_2 \cup \mathbb{S}_3 \cup \mathbb{S}_4 \cup \mathbb{S}_5. \tag{4.12}$$

Some of the sets $\mathbb{S}_1, \ldots, \mathbb{S}_5$ may be empty.

When $j \notin \mathcal{L}_{i,k+1|k}$ and $j \in \mathcal{D}^{\mathrm{I}}_{i,k+1}$, the true target j or a false target misidentified with j is detected and identified for the first time. In that case, the set estimate (4.12) down to

$$\mathbb{X}_{i,j,k+1|k+1} = \mathbb{S}_2 \cup \mathbb{S}_3. \tag{4.13}$$

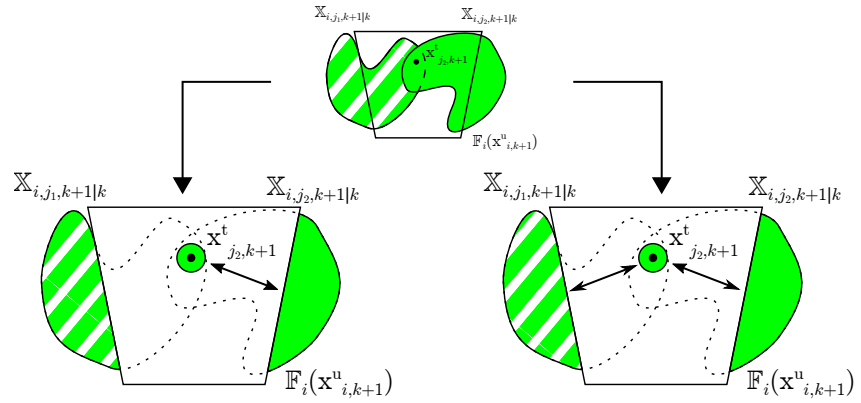

Figure 4.4.: Correction from measurement III: detection of a target inside the intersection of different target set estimates. In (a), where the target was detected and identified, the set estimate (in green) inside $\mathbb{F}_i\left(\mathbf{x}^{\mathrm{u}}_{i,k+1}\right)$ is $\mathbb{S}_1$. The measurement can be linked to target j_2. In (b), where the target was detected but not identified, the set estimate (in green) inside $\mathbb{F}_i\left(\mathbf{x}^{\mathrm{u}}_{i,k+1}\right)$ is $\mathbb{S}_4$. The measurement $\mathbf{y}^{\mathrm{U}}_{i,m,k+1}$ of state $\mathbf{x}^{\mathrm{t}}_{j_2,k+1}$ has to be considered for the estimates of $j_1$and j_2.

4.3.2.2. Updating the set of unidentified targets

One has to consider different cases to determine the updated set $\mathbb{X}^{\mathrm{U}}_{i,k+1|k+1}$ from $\mathbb{X}^{\mathrm{U}}_{i,k+1|k}$ for an unidentified target using $\mathbf{y}^{\mathrm{U}}_{i,m,k+1}$, $m \in \mathcal{D}^{\mathrm{U}}_{i,k+1}$, obtained after processing the information in $\mathbb{F}_i(\mathbf{x}^{\mathrm{u}}_{i,k+1})$ at time t_{k+1}. When evaluating $\mathbb{X}^{\mathrm{U}}_{i,k+1|k+1}$, one does not need to account for measurements $\mathbf{y}^{\mathrm{I}}_{i,j,k+1}$, $j \in \mathcal{D}^{\mathrm{I}}_{i,k+1}$.

An unidentified target may be detected again inside the set estimate of unidentified targets $\mathbb{X}^{\mathrm{U}}_{i,k+1|k}$. This hypothesis is similar to that considered in (4.6), and one obtains

$$\mathbb{S}^{\mathrm{U}}_1 = \bigcup_{m \in \mathcal{D}^{\mathrm{U}}_{i,k+1}} \left\{ \mathbf{x} \in \mathbb{X}^{\mathrm{U}}_{i,k+1|k} \,|\, \mathbf{h}_{k+1}\left(\mathbf{x}^{\mathrm{u}}_{i,k+1}, \mathbf{x}\right) \in \mathbf{y}^{\mathrm{U}}_{i,m,k+1} - [\mathbf{w}_{k+1}] \right\}. \tag{4.14}$$

Alternatively, an unidentified target may be detected for the first time in the unexplored set $\overline{\mathbb{X}}_{i,k+1|k}$. This hypothesis is similar to that leading to (4.8), and one gets

$$\mathbb{S}^{\mathrm{U}}_2 = \bigcup_{m \in \mathcal{D}^{\mathrm{U}}_{i,k+1}} \left\{ \mathbf{x} \in \overline{\mathbb{X}}_{i,k+1|k} \,|\, \mathbf{h}_{k+1}\left(\mathbf{x}^{\mathrm{u}}_{i,k+1}, \mathbf{x}\right) \in \mathbf{y}^{\mathrm{U}}_{i,m,k+1} - [\mathbf{w}_{k+1}] \right\}. \tag{4.15}$$

Contrary to (4.8) and (4.6) and due to the data association problem, $\mathbb{S}^{\mathrm{U}}_1$and $\mathbb{S}^{\mathrm{U}}_2$ contain the union of the set estimates associated to all detected targets in $\mathcal{D}^{\mathrm{U}}_{i,k+1}$. Figure 4.2 (b) and 4.3 (b) illustrate situations where $\mathbb{S}^{\mathrm{U}}_1 \subset \mathbb{F}_i(\mathbf{x}^{\mathrm{u}}_{i,k+1})$ and $\mathbb{S}^{\mathrm{U}}_2 \subset \mathbb{F}_i(\mathbf{x}^{\mathrm{u}}_{i,k+1})$ (both in cyan) are not empty.

Again, one has to account for the fact that non-detection does not occur and that all information in $\mathbb{F}_i(\mathbf{x}^{\mathrm{u}}_{i,k})$ has been processed. Therefore, $\mathbf{x}^{\mathrm{t}}_{j,k+1} \notin \mathbb{F}_i(\mathbf{x}^{\mathrm{u}}_{i,k+1}) \backslash \left(\mathbb{S}^{\mathrm{U}}_1 \cup \mathbb{S}^{\mathrm{U}}_2\right)$. Introducing,

$$\mathbb{S}^{\mathrm{U}}_3 = \mathbb{X}^{\mathrm{U}}{}_{i,k+1|k} \setminus \mathbb{F}_i\left(\mathbf{x}^{\mathrm{u}}_{i,k+1}\right), \tag{4.16}$$

which accounts for targets outside of the FoV of the UAV. The updated set estimate $\mathbb{X}^{\mathrm{U}}_{i,k+1|k+1}$ accounting for all hypotheses is then

$$\mathbb{X}^{\mathrm{U}}_{i,k+1|k+1} = \mathbb{S}^{\mathrm{U}}_1 \cup \mathbb{S}^{\mathrm{U}}_2 \cup \mathbb{S}^{\mathrm{U}}_3. \tag{4.17}$$

When all measurements from $\mathbb{F}_i(\mathbf{x}^{\mathrm{u}}_{i,k+1})$ are processed, the unexplored set $\overline{\mathbb{X}}_{i,k+1|k}$ can be updated as

$$\overline{\mathbb{X}}_{i,k+1|k+1} = \overline{\mathbb{X}}_{i,k+1|k} \setminus \mathbb{F}_i\left(\mathbf{x}^{\mathrm{u}}_{i,k+1}\right), \tag{4.18}$$

since it is assumed that false negative detection does not occur. The reduction of the size of the set estimates is in general based on the use of negative information. The set estimates can be refined even when no targets are observed. This is only possible due to the simplifying assumption that targets are always detected.

Finally, one has to update the list $\mathcal{L}_{i,k+1|k} \cup \mathcal{D}^{\mathrm{I}}_{i,k+1}$ of tracked targets after measurement update. One has to remove all targets j from the list of already detected and identified targets whose set $\mathbb{X}_{i,j,k+1|k+1}$ is empty

$$\mathcal{L}_{i,k+1|k+1} = \left\{ j \in \mathcal{L}_{i,k+1|k} \cup \mathcal{D}^{\mathrm{I}}_{i,k+1} \,|\, \mathbb{X}_{i,j,k+1|k+1} \neq \emptyset \right\}. \tag{4.19}$$

The the set $\mathbb{X}_{i,j,k+1|k+1}$ may be empty when, *e.g.*, false target ℓ was detected and misidentified as a true target $j \in \mathcal{J}^{\mathrm{t}}$ at time t_k, and new observations lead to the identification as false target at time t_{k+1}.

4.3.3. Correction step from communications

Scene 12:

Assume that two UAVs are in close range, can communicate and transmit information, e.g., *via wireless network protocols. The communication transfer takes place in both directions. One UAV starts and sends a message to another UAV. The message contains the name and location of the UAV and the estimated regions that contain the tracked cars. Subsequently, the other UAV transmits the corresponding information back. After the information exchange, both UAVs have to fuse the information about the estimated zones of the car locations.*

This section formalizes the correction step after communication as illustrated in Scene 12.

After the correction from measurements, UAV i broadcasts the sets $\mathcal{L}_{i,k+1|k+1}$, $\mathbb{X}^{\mathrm{U}}_{i,k+1|k+1}$, $\overline{\mathbb{X}}_{i,k+1|k+1}$, and $\mathcal{X}_{i,k+1|k+1} = \left\{\mathbb{X}_{i,j,k+1|k+1}\right\}_{j\in\mathcal{L}_{i,k+1|k+1}}$ to its neighbors $\ell \in \mathcal{N}_{i,k+1}$, and it receives the information related to the corresponding sets from its neighbors at the end of time step $k+1$. The information available to UAV i is then

$$\mathbb{I}_{i,k+1} = \mathbb{I}_{i,k+1|k+1} \bigcup_{\ell\in\mathcal{N}_{i,k+1}} \left\{\mathcal{L}_{\ell,k+1|k+1}, \mathcal{X}_{\ell,k+1|k+1}, \mathbb{X}^{\mathrm{U}}_{\ell,k+1|k+1}, \overline{\mathbb{X}}_{\ell,k+1|k+1}\right\}. \tag{4.20}$$

Accounting for the information exchanged with UAV i, the set of all targets which have been identified by UAV i or one of its neighbors up to time t_{k+1} is then

$$\mathcal{L}^{+}_{i,k+1|k+1} = \bigcup_{\ell\in\mathcal{N}_{i,k+1}\cup\{i\}} \mathcal{L}_{\ell,k+1|k+1}. \tag{4.21}$$

For each $j \in \mathcal{L}^{+}_{i,k+1|k+1}$, the set of neighbors $\mathcal{N}_{i,k+1}$ of UAV i can be partitioned into two subsets. The subset $\mathcal{N}^{j}_{i,k+1}$ of the neighbors who *believe* that they have detected target j up to time t_{k+1} and the subset $\overline{\mathcal{N}}^{j}_{i,k+1}$ of neighbors who are *sure* that they have *not* detected target j up to time t_{k+1}.

To further fuse the information available to UAV i before and after communication two additional sets are introduced. For all $j \in \mathcal{L}^{+}_{i,k+1|k+1}$ introduce

$$\widetilde{\mathbb{X}}_{i,j,k+1|k+1} = \mathbb{X}_0 \setminus \left\{\mathbb{X}_{i,j,k+1|k+1} \cup \mathbb{X}^{\mathrm{U}}_{i,k+1|k+1} \cup \overline{\mathbb{X}}_{i,k+1|k+1}\right)\right\}, \tag{4.22}$$

as the set *proved not to contain* the state of target j, *i.e.*, $\mathbf{x}^{\mathrm{t}}_{j,k+1} \notin \widetilde{\mathbb{X}}_{i,j,k+1|k+1}$, where, by convention, $\mathbb{X}_{i,j,k+1|k+1} = \emptyset$ when $j \notin \mathcal{L}_{i,k+1}$. Introduce also

$$\widetilde{\mathbb{X}}^{\mathrm{U}}_{i,k+1|k+1} = \mathbb{X}_0 \setminus \left(\mathbb{X}^{\mathrm{U}}_{i,k+1|k+1} \cup \overline{\mathbb{X}}_{i,k+1|k+1}\right) \tag{4.23}$$

as the set *proved not to contain* the state of any unidentified target.

Considering UAV i and any target $j \in \mathcal{L}_{i,k+1|k+1}$, one knows that either $\mathbf{x}^{\mathrm{t}}_{j,k+1} \in \mathbb{X}_{i,j,k+1|k+1}$, or $\mathbf{x}^{\mathrm{t}}_{j,k+1} \in \mathbb{X}^{\mathrm{U}}_{i,k+1|k+1}$, or $\mathbf{x}^{\mathrm{t}}_{j,k+1} \in \overline{\mathbb{X}}_{i,k+1|k+1}$. The true target state may belong to any of these sets due to the potential misidentification of false targets. Moreover, one has $\mathbf{x}^{\mathrm{t}}_{j,k+1} \notin \widetilde{\mathbb{X}}_{i,j,k+1|k+1}$. Similarly, considering UAV $\ell \in \mathcal{N}^{j}_{i,k+1}$, such that $j \in \mathcal{L}_{\ell,k+1|k+1}$, one has either $\mathbf{x}^{\mathrm{t}}_{j,k+1} \in \mathbb{X}_{\ell,j,k+1|k+1}$, or $\mathbf{x}^{\mathrm{t}}_{j,k+1} \in \mathbb{X}^{\mathrm{U}}_{\ell,k+1|k+1}$, or $\mathbf{x}^{\mathrm{t}}_{j,k+1} \in \overline{\mathbb{X}}_{\ell,k+1|k+1}$. Moreover, one knows that $\mathbf{x}^{\mathrm{t}}_{j,k+1} \notin \widetilde{\mathbb{X}}_{\ell,j,k+1|k+1}$. Consequently, for UAV i and any target $j \in \mathcal{L}^{+}_{i,k+1|k+1}$, $\mathbb{X}_{i,j,k+1}$ is evaluated as the union of all possible state values accounting for the measurements of the identified target j, deprived of the union of all sets which have been proved not to contain target j at

time t_{k+1}, *i.e.*,

$$\mathbb{X}_{i,j,k+1} = \bigcup_{\ell \in \mathcal{N}^j_{i,k+1} \cup \{i\}} \mathbb{X}_{\ell,j,k+1|k+1} \setminus \bigcup_{\ell \in \mathcal{N}_{i,k+1} \cup \{i\}} \widetilde{\mathbb{X}}_{\ell,j,k+1|k+1}. \tag{4.24}$$

The list $\mathcal{L}_{i,k+1|k+1}$ of all targets j known to UAV i is then updated from $\mathcal{L}^+_{i,k+1|k+1}$ by accounting only for estimates $\mathbb{X}_{i,j,k+1}$ which are not empty, *i.e.*,

$$\mathcal{L}_{i,k+1} = \left\{ j \in \mathcal{L}^+_{i,k+1|k+1} \,|\, \mathbb{X}_{i,j,k+1} \neq \emptyset \right\}. \tag{4.25}$$

The update of $\mathbb{X}^{\mathrm{U}}_{i,k+1|k+1}$ is evaluated as the union of the set estimates of unidentified targets reduced by the space which is proved not to contain any unidentified target, *i.e.*,

$$\mathbb{X}^{\mathrm{U}}_{i,k+1} = \bigcup_{\ell \in \mathcal{N}_{i,k+1} \cup \{i\}} \mathbb{X}^{\mathrm{U}}_{\ell,k+1|k+1} \setminus \bigcup_{\ell \in \mathcal{N}_{i,k+1} \cup \{i\}} \widetilde{\mathbb{X}}^{\mathrm{U}}_{\ell,k+1|k+1}. \tag{4.26}$$

Finally, the update of $\overline{\mathbb{X}}_{i,k+1|k+1}$ is the intersection of the unexplored space of UAV i and that of its neighbors, *i.e.*,

$$\overline{\mathbb{X}}_{i,k+1} = \bigcap_{\ell \in \mathcal{N}_{i,k+1} \cup \{i\}} \overline{\mathbb{X}}_{\ell,k+1|k+1}. \tag{4.27}$$

Figure 4.5 illustrates the sets resulting from (4.24) and (4.27) for two cases. The size of $\mathbb{X}_{i,j,k+1}$ may be smaller than $\mathbb{X}_{i,j,k+1|k+1}$ as it is the case in Figure 4.5 a), when some subsets of $\mathbb{X}_{i,j,k+1|k+1}$ have been proved by another UAV not to contain a target. It may also be larger, as is the case in Figure 4.5 b), where UAV ℓ has obtained measurements leading to another hypothesis on the state estimate of target j. The evolution of $\mathbb{X}^{\mathrm{U}}_{i,k+1}$ from $\mathbb{X}^{\mathrm{U}}_{i,k+1|k+1}$ could be illustrated with similar figures. The size of $\overline{\mathbb{X}}_{i,k+1}$ is always reduced compared to that of $\overline{\mathbb{X}}_{i,k+1|k+1}$.

4.3.4. Algorithm

Algorithm 4.1 summarizes the prediction and correction steps from both measurements and communications. It evaluates $\mathcal{L}_{i,k+1}$, $\mathcal{X}_{i,k+1}$, $\mathbb{X}^{\mathrm{U}}_{i,k+1}$, and $\overline{\mathbb{X}}_{i,k+1}$ from $\mathcal{L}_{i,k}$, $\mathcal{X}_{i,k}$, $\mathbb{X}^{\mathrm{U}}_{i,k}$, and $\overline{\mathbb{X}}_{i,k}$ at each time instant t_{k+1}.

4.3.5. Gain of information for identified targets

In Section 4.3.3, one evaluates the set estimate for identified and unidentified targets after communication and one observes that the update equations (4.24) and (4.26)

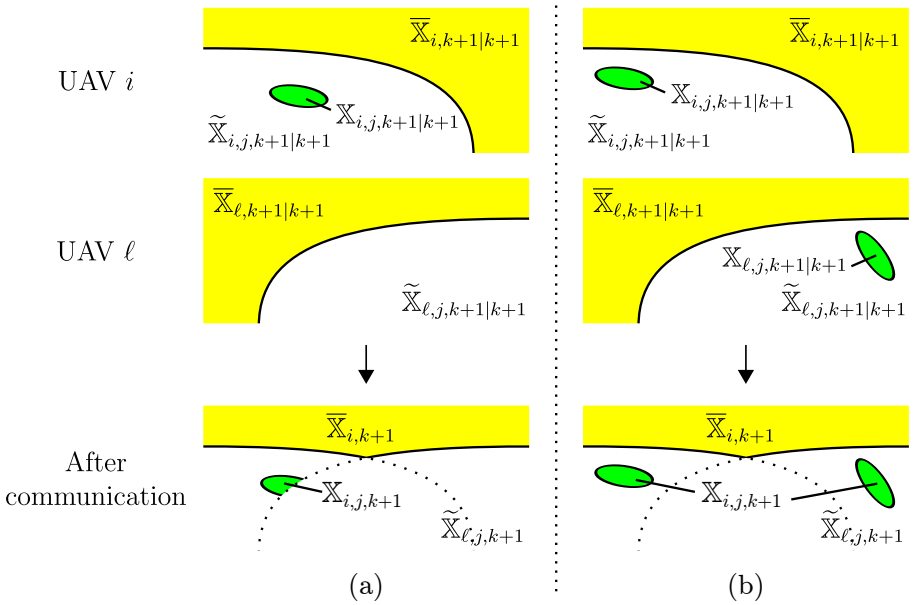

Figure 4.5.: Set estimates evaluated by UAV i and ℓ before communication (two top subfigures of each column) and after communication and update (bottom subfigures); (a) $\mathbb{X}_{i,j,k+1}$ is smaller than $\mathbb{X}_{i,j,k+1|k+1}$ since some subsets of $\mathbb{X}_{i,j,k+1|k+1}$ have been proved by UAV ℓ not to contain a target; (b) $\mathbb{X}_{i,j,k+1}$ is larger than $\mathbb{X}_{i,j,k+1|k+1}$, since UAV i has to account for the two different hypotheses on the state estimate of target j.

for $\mathbb{X}_{i,j,k}$ and $\mathbb{X}^{\mathrm{U}}_{i,k}$ have a similar structure. The aim of this section is to illustrated the fact that the size of the set estimates is smaller when targets are identified.

For unidentified targets, the information about the target locations is defined as a whole and information about the number of detected targets is lost. When the identity of a target is available, the UAVs process the information for each target separately and dispose of an estimate of the number of targets located in the ROI.

Figure 4.6 illustrates the fusion step after communications resulting from (4.24) and (4.26). When the targets are not identified, the information on the target locations is collected in a single set $\mathbb{X}^{\mathrm{U}}_{i,k}$ for each UAV, see Figure 4.6 left. A single set estimate $\mathbb{X}^{\mathrm{U}}_{i,k}$ makes it more difficult to differentiate between false and true targets (red asterisk). When the identity of the targets is known, the information for each target is processed separately, see Figure 4.6 middle and right. This facilitates the differentiation between false and true targets, and thus allows a faster reduction of the size of the set estimates, *i.e.*, the subset marked with a red asterisk could be removed.

Algorithm 4.1 Robust Cooperative Bounded-error Target Localization and Tracking

RoCoBoTLoT$\left(\mathcal{L}_{i,k}, \mathcal{X}_{i,k}, \mathbb{X}^{\mathrm{U}}_{i,k}, \overline{\mathbb{X}}_{i,k}\right)$

Input: $\mathcal{L}_{i,k}$, $\mathcal{X}_{i,k}$, $\mathbb{X}^{\mathrm{U}}_{i,k}$, and $\overline{\mathbb{X}}_{i,k}$
Output: $\mathcal{L}_{i,k+1}$, $\mathcal{X}_{i,k+1}$, $\mathbb{X}^{\mathrm{U}}_{i,k+1}$, and $\overline{\mathbb{X}}_{i,k+1}$
Prediction step
$\mathcal{L}_{i,k+1|k} = \mathcal{L}_{i,k}$
$\mathbb{X}_{i,j,k+1|k} = \mathbf{f}^{\mathrm{t}}_k\left(\mathbb{X}_{i,j,k}, [\mathbf{v}_k]\right) \cap \mathbb{X}_0$, for all $j \in \mathcal{L}_{i,k+1|k}$
$\mathbb{X}^{\mathrm{U}}_{i,k+1|k} = \mathbf{f}^{\mathrm{t}}_k\left(\mathbb{X}^{\mathrm{U}}_{i,k}, [\mathbf{v}_k]\right) \cap \mathbb{X}_0$
$\overline{\mathbb{X}}_{i,k+1|k} = \mathbf{f}^{\mathrm{t}}_k\left(\overline{\mathbb{X}}_{i,k}, [\mathbf{v}_k]\right) \cap \mathbb{X}_0$
Correction step from measurements
$\mathcal{L}^{+}_{i,k+1|k} = \mathcal{L}_{i,k+1|k} \cup \mathcal{D}^{\mathrm{I}}_{i,k}$
For all $j \in \mathcal{L}^{+}_{i,k+1|k}$
$\mathbb{X}_{i,j,k+1|k+1}$ updated as in (4.12)
$\mathcal{L}_{i,k+1|k+1} = \left\{ j \in \mathcal{L}^{+}_{i,k+1|k} \,|\, \mathbb{X}_{i,j,k+1|k+1} \neq \emptyset \right\}$
$\mathbb{X}^{\mathrm{U}}{}_{i,k+1|k+1}$ updated as in (4.17)
$\overline{\mathbb{X}}_{i,k+1|k+1} = \overline{\mathbb{X}}_{i,k+1|k} \setminus \mathbb{F}_i(\mathbf{x}^{\mathrm{u}}_{i,k+1})$
Correction step from communications
$\mathcal{L}^{+}_{i,k+1|k+1} = \bigcup_{\ell \in \mathcal{N}_{i,k+1} \cup \{i\}} \mathcal{L}_{\ell,k+1|k+1}$
For all $j \in \mathcal{L}^{+}_{i,k+1|k+1}$
$\mathbb{X}_{i,j,k+1} = \bigcup_{\ell \in \mathcal{N}^{j}_{i,k+1} \cup \{i\}} \mathbb{X}_{\ell,j,k+1|k+1} \setminus \bigcup_{\ell \in \mathcal{N}_{i,k+1} \cup \{i\}} \widetilde{\mathbb{X}}_{\ell,j,k+1|k+1}$
$\mathcal{L}_{i,k+1} = \left\{ j \in \mathcal{L}^{+}_{i,k+1|k+1} \,|\, \mathbb{X}_{i,j,k+1} \neq \emptyset \right\}$
$\mathbb{X}^{\mathrm{U}}_{i,k+1} = \bigcup_{\ell \in \mathcal{N}^{j}_{i,k+1} \cup \{i\}} \mathbb{X}^{\mathrm{U}}_{\ell,k+1|k+1} \setminus \bigcup_{\ell \in \mathcal{N}_{i,k+1} \cup \{i\}} \widetilde{\mathbb{X}}^{\mathrm{U}}_{\ell,k+1|k+1}$
$\overline{\mathbb{X}}_{i,k+1} = \overline{\mathbb{X}}_{i,k+1|k+1} \bigcap_{\ell \in \mathcal{N}_{i,k+1} \cup \{i\}} \overline{\mathbb{X}}_{\ell,k+1|k+1}$

4.3.6. Accounting for delayed information

In case of reception of delayed information from another UAV, the estimation technique has to be significantly adapted. A solution similar to the state augmentation approach considered in Lu et al. (2005) may be proposed in our set-membership estimation context. The idea is to augment the dimension of the state estimate and to keep track of the estimates at time t_k and also at time $t_{k-\delta}$, $\delta = 1, \ldots, \overline{\delta}$, where $\overline{\delta}$ is the considered time horizon in the past. Information with delay $\delta \in \left[0, \overline{\delta}\right]$ can then be used to update the estimate at time $t_{k-\delta}$. The corrected estimate at time $t_{k-\delta}$ is propagated through time to correct also the estimates at time $t_{k-\delta'}$, $\delta' = \delta - 1, \delta - 2, \ldots, 0$.

For that purpose, it is assumed that the UAVs have synchronized clocks, update their estimate periodically and synchronously, and that the transmitted data are

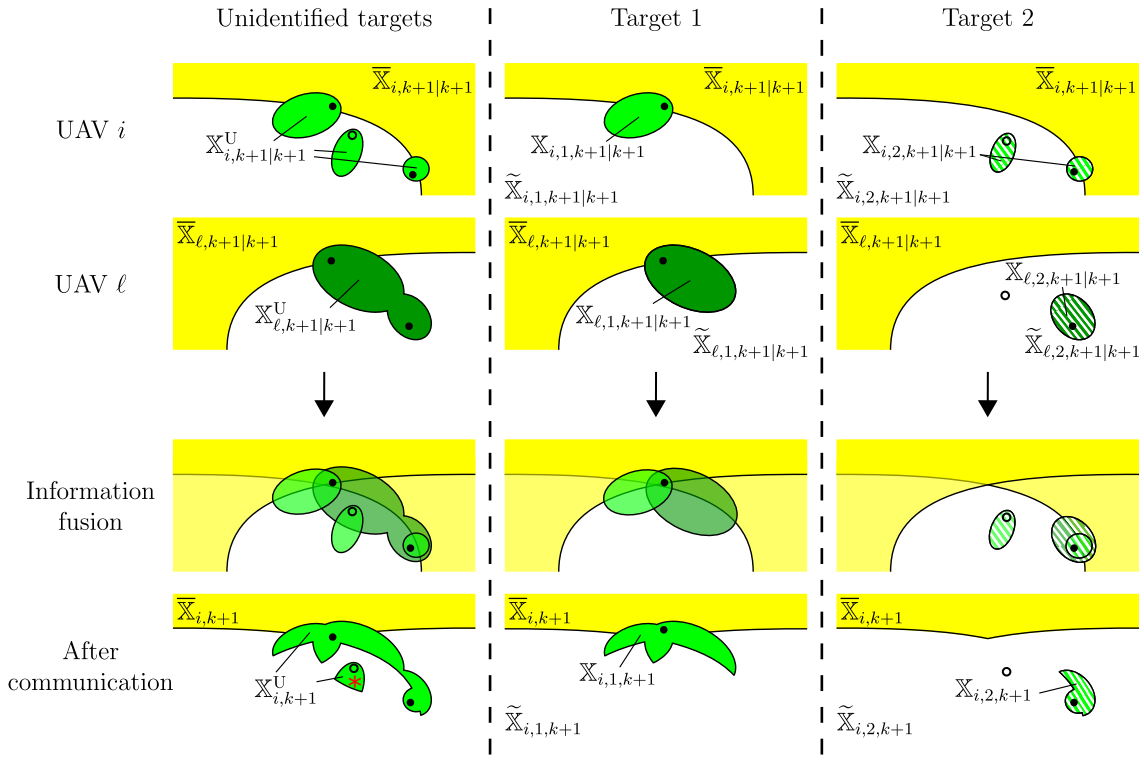

Figure 4.6.: Evaluation of the state estimates by UAV i after receiving Information from UAV ℓ: estimates evaluated by UAV i are illustrated in light green and estimates by UAV ℓ in dark green; fusion step after communications for unidentified targets (left); fusion step after communications for identified targets (middle and right).

properly time-stamped. Moreover, only information with a delay δ less or equal to some threshold $\overline{\delta}$ is processed to limit computational complexity.

At time t_k, UAV i has to maintain the sets $\mathcal{L}_{i,k-\delta}$, $\mathcal{X}_{i,k-\delta}$, $\mathbb{X}^{\mathrm{U}}_{i,k-\delta}$, and $\overline{\mathbb{X}}_{i,k-\delta}$, $\delta = 0, \ldots, \overline{\delta}$ corresponding to the estimates at time t_k as well as the estimates at time $t_{k-\delta}$, $\delta = 1, \ldots, \overline{\delta}$. Assume that UAV i receives $\mathcal{L}_{\ell,k-\delta'}$, $\mathcal{X}_{\ell,k-\delta'}$, $\mathbb{X}^{\mathrm{U}}_{\ell,k-\delta'}$, and $\overline{\mathbb{X}}_{\ell,k-\delta'}$ from UAV $\ell \neq i$ at time t_k, with $\delta' \in \left[0, \overline{\delta}\right]$. The sets $\mathcal{L}_{\ell,k-\delta'}$, $\mathcal{X}_{\ell,k-\delta'}$, $\mathbb{X}^{\mathrm{U}}_{\ell,k-\delta'}$, and $\overline{\mathbb{X}}_{\ell,k-\delta'}$ can be used to update $\mathcal{L}_{i,k-\delta'}$, $\mathcal{X}_{i,k-\delta'}$, $\mathbb{X}^{\mathrm{U}}_{i,k-\delta'}$, and $\overline{\mathbb{X}}_{i,k-\delta'}$ using the procedure described in Section 4.3.3. The corrected sets at time $t_{k-\delta'}$ are propagated trough time using the prediction step described in Section 4.3.1 and the correction steps from communication described in Section 4.3.3. These updates allow UAV i to evaluate $\mathcal{L}_{i,k-\delta}$, $\mathcal{X}_{i,k-\delta}$, $\mathbb{X}^{\mathrm{U}}_{i,k-\delta}$, and $\overline{\mathbb{X}}_{i,k-\delta}$, $\delta = \delta' - 1, \ldots, 0$. Consequently, this procedure enables UAV i to account for information from communication with a delay of $t_k - t_{k-\delta'}$ to update its estimate at time t_k. The delay $t_k - t_{k-\delta'}$ has to be a multiple of the sampling period T.

Processing delayed measurements significantly increases the computational complexity, as it is also the case in the state augmentation approaches considered in Lu et al.

(2005).

4.4. Cooperative control design

The aim of the control design for the fleet of UAVs is to decrease the estimation uncertainty as much as possible. To achieve this task, one considers the problem of determining, at each time t_k and in a distributed way, the sequence of control inputs which minimizes the predicted estimation uncertainty (3.20) at time t_{k+h}. One has

$$\overline{\Phi}_{k+h} = \frac{1}{N^{\mathrm{u}}} \sum_{i=1}^{N^{\mathrm{u}}} \Phi\left(\mathcal{X}_{i,k+h}, \mathbb{X}^{\mathrm{U}}_{i,k+h}, \overline{\mathbb{X}}_{i,k+h}\right), \tag{4.28}$$

where $h \geqslant 1$ is the considered prediction horizon. UAVs have no access to all the terms of (4.28), thus each UAV i, $i = 1, \ldots, N^{\mathrm{u}}$, will try to minimize the term $\Phi(\mathcal{X}_{i,k+h}, \mathbb{X}^{\mathrm{U}}_{i,k+h}, \overline{\mathbb{X}}_{i,k+h})$ given by (3.19).

The determination of the control inputs is performed using the distributed a MPC formalism introduced, *e.g.,* in Morari and Lee (1999); Camacho and Alba (2013). This allows to account for the prediction of the evolution of (3.19). In the proposed set-membership estimation context, some simplifications are introduced for that purpose. The description starts with an h-step ahead prediction ignoring communication between neighboring UAVs. Then the impact of communications will be taken into account in the set-membership MPC approach.

4.4.1. Control input design ignoring future communications

When the communications in time steps $k+1, \ldots, k+h$ are ignored, the control inputs of each UAV can be designed independently. Obviously, the communications which have previously occurred are taken into account.

At time t_k, UAV i has access to $\mathcal{L}_{i,k}$, $\mathcal{X}_{i,k}$, $\mathbb{X}^{\mathrm{U}}_{i,k}$, and $\overline{\mathbb{X}}_{i,k}$. Using a prediction step described in Section 4.3.1, UAV i is able to evaluate $\mathcal{L}_{i,k+1|k} = \mathcal{L}_{i,k}$, $\mathbb{X}_{i,j,k+1|k}$, $j \in \mathcal{L}_{i,k}$, $\mathbb{X}^{\mathrm{U}}_{i,k+1|k}$, and $\overline{\mathbb{X}}_{i,k+1|k}$. Then, for a given control input $\mathbf{u}_{i,k}$, UAV i is able to get a predicted value $\mathbf{x}^{\mathrm{u,P}}_{i,k+1}$ of its state $\mathbf{x}^{\mathrm{u}}_{i,k+1}$ at time t_{k+1} and to infer the corresponding FoV $\mathbb{F}_i(\mathbf{x}^{\mathrm{u,P}}_{i,k+1})$. Nevertheless, UAV i is unable to determine whether it will observe new or previously detected targets in $\mathbb{F}_i(\mathbf{x}^{\mathrm{u,P}}_{i,k+1})$. Consequently, in the updating step from measurement described in Section 4.3.2, only $\mathbb{S}_5$ in (4.11), $\mathbb{S}^{\mathrm{U}}_3$ in (4.16), and $\overline{\mathbb{X}}_{i,k+1|k+1}$ in (4.18) can be inferred accurately as follows

$$\mathbb{X}^{\mathrm{P}}_{i,j,k+1|k+1} = \mathbb{X}_{i,j,k+1|k} \setminus \mathbb{F}_i\left(\mathbf{x}^{\mathrm{u,P}}_{i,k+1}\right), j \in \mathcal{L}_{i,k} \tag{4.29}$$

$$\mathbb{X}^{\mathrm{U,P}}_{i,k+1|k+1} = \mathbb{X}^{\mathrm{U}}_{i,k+1|k} \setminus \mathbb{F}_i\left(\mathbf{x}^{\mathrm{u,P}}_{i,k+1}\right), \tag{4.30}$$

$$\overline{\mathbb{X}}^{\mathrm{P}}_{i,k+1|k+1} = \overline{\mathbb{X}}_{i,k+1|k} \setminus \mathbb{F}_i\left(\mathbf{x}^{\mathrm{u,P}}_{i,k+1}\right). \tag{4.31}$$

Here the superscript $^{\mathrm{P}}$ indicates that these are predicted values considering a given control input $\mathbf{x}^{\mathrm{u,P}}_{i,k+1}$. If $\mathbf{x}^{\mathrm{u}}_{i,k+1} = \mathbf{x}^{\mathrm{u,P}}_{i,k+1}$, then $\mathbb{X}^{\mathrm{P}}_{i,j,k+1|k+1} \subset \mathbb{X}_{i,j,k+1|k+1}$, $\mathbb{X}^{\mathrm{U,P}}_{i,k+1|k+1} \subset \mathbb{X}^{\mathrm{U}}_{i,k+1|k+1}$, and $\overline{\mathbb{X}}^{\mathrm{P}}_{i,k+1|k+1} = \overline{\mathbb{X}}_{i,k+1|k+1}$.

Figure 4.7 illustrates the prediction of possible UAV locations and their impact on the set estimates. The UAVs are not able to predict future detections of targets.

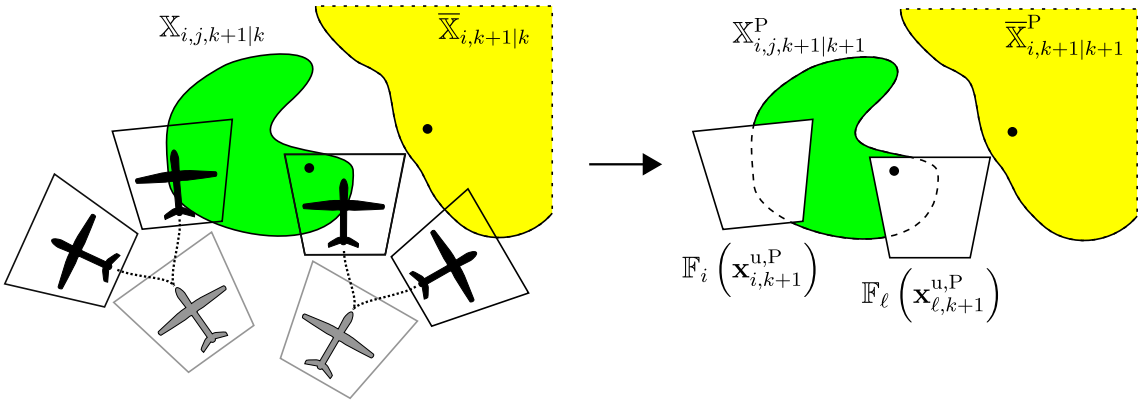

Figure 4.7.: Predicting the evolution of the set estimates: projection in $\mathbb{R}^2$ of future UAV locations $\mathbf{x}^{\mathrm{u,P}}_{i,k+1}$ (left side) and the impact on the set estimates for some selected value of $\mathbf{x}^{\mathrm{u,P}}_{i,k+1}$.

Using the previous approximations, a predicted estimation uncertainty for UAV i at time t_{k+1} may be evaluated as

$$\Phi\left(\mathcal{X}^{\mathrm{P}}_{i,k+1|k+1}, \mathbb{X}^{\mathrm{U,P}}_{i,k+1|k+1}, \overline{\mathbb{X}}^{\mathrm{P}}_{i,k+1|k+1}\right) = \phi\left(\left(\bigcup_{j\in\mathcal{L}_{i,k}} \mathbb{X}^{\mathrm{P}}_{i,j,k+1|k+1}\right) \cup \mathbb{X}^{\mathrm{U,P}}_{i,k+1|k+1} \cup \overline{\mathbb{X}}^{\mathrm{P}}_{i,k+1|k+1}\right). \quad (4.32)$$

Regarding the approximation performed in the evaluation of $\mathbb{X}^{\mathrm{P}}_{i,j,k+1|k+1}$, $j \in \mathcal{L}_{i,k}$, and $\mathbb{X}^{\mathrm{U,P}}_{i,k+1|k+1}$, the predicted uncertainty $\Phi\left(\mathcal{X}^{\mathrm{P}}_{i,k+1|k+1}, \mathbb{X}^{\mathrm{U,P}}_{i,k+1|k+1}, \overline{\mathbb{X}}^{\mathrm{P}}_{i,k+1|k+1}\right)$ is an lower bound of the uncertainty that can be achieved. The contribution of the missing part of the sets $\mathbb{X}^{\mathrm{P}}_{i,j,k+1|k+1}$ and $\mathbb{X}^{\mathrm{U,P}}_{i,k+1|k+1}$ is usually negligible compared to that of $\overline{\mathbb{X}}^{\mathrm{P}}_{i,k+1|k+1}$ in the evaluation of Φ.

In order to compute (4.32) more efficiently, at time t_k, consider the set,

$$\mathbb{X}^{\mathrm{A}}_{i,k} = \left(\bigcup_{j\in\mathcal{L}_{i,k}} \mathbb{X}_{i,j,k}\right) \cup \mathbb{X}^{\mathrm{U}}_{i,k} \cup \overline{\mathbb{X}}_{i,k}, \quad (4.33)$$

known to UAV i, *aggregating* the states of all detected targets and the states of not yet detected targets. Exploiting the target dynamics (3.2) and the common bound

on the state perturbation $[\mathbf{v}_k]$, the predicted value of $\mathbb{X}^{\mathrm{A}}_{i,k}$ in (4.33) at time t_{k+1} is

$$\mathbb{X}^{\mathrm{A}}_{i,k+1|k} = \mathbf{f}^{\mathrm{t}}_k \left(\mathbb{X}^{\mathrm{A}}_{i,k}, [\mathbf{v}_k] \right) \cap \mathbb{X}_0. \tag{4.34}$$

Considering (4.2), (4.3), and (4.4), one observes that

$$\mathbb{X}^{\mathrm{A}}_{i,k+1|k} = \left(\bigcup_{j \in \mathcal{L}_{i,k}} \mathbb{X}_{i,j,k+1|k} \right) \cup \mathbb{X}^{\mathrm{U}}_{i,k+1|k} \cup \overline{\mathbb{X}}_{i,k+1|k}. \tag{4.35}$$

Now, introducing the corrected set at time t_{k+1}

$$\mathbb{X}^{\mathrm{A,P}}_{i,k+1|k+1} = \mathbb{X}^{\mathrm{A}}_{i,k+1|k} \setminus \mathbb{F}_i \left(\mathbf{x}^{\mathrm{u,P}}_{i,k+1} \right), \tag{4.36}$$

where the superscript $^{\mathrm{P}}$ indicates that this is a predicted value of $\mathbb{X}^{\mathrm{A}}_{i,k+1|k+1}$, relying on the various assumptions considered in the proposed SM-MPC approach. Combining (4.35) and (4.36), one easily shows that

$$\mathbb{X}^{\mathrm{A,P}}_{i,k+1|k+1} = \left(\textstyle\bigcup_{j \in \mathcal{L}_{i,k}} \mathbb{X}_{i,j,k+1|k} \cup \mathbb{X}^{\mathrm{U}}_{i,k+1|k} \cup \overline{\mathbb{X}}_{i,k+1|k} \right) \setminus \mathbb{F}_i \left(\mathbf{x}^{\mathrm{u,P}}_{i,k+1} \right), \tag{4.37}$$

$$= \textstyle\bigcup_{j \in \mathcal{L}_{i,k}} \mathbb{X}^{\mathrm{P}}_{i,j,k+1|k+1} \cup \mathbb{X}^{\mathrm{U,P}}_{i,k+1|k+1} \cup \overline{\mathbb{X}}^{\mathrm{P}}_{i,k+1|k+1}. \tag{4.38}$$

Introducing $\mathbb{X}^{\mathrm{A,P}}_{i,k+1} = \mathbb{X}^{\mathrm{A,P}}_{i,k+1|k+1}$, the predicted estimation uncertainty for UAV i at time t_{k+1}, provided by (4.32), is also given by $\phi\left(\mathbb{X}^{\mathrm{A,P}}_{i,k+1}\right)$. Consequently, considering $\mathbb{X}^{\mathrm{A}}_{i,k}$, instead of $\mathcal{X}_{i,k}$, $\mathbb{X}^{\mathrm{U}}_{i,k}$, and $\overline{\mathbb{X}}_{i,k}$ and applying the prediction step (4.34) and the correction step (4.36) to $\mathbb{X}^{\mathrm{A}}_{i,k}$ is sufficient and computational advantageous to evaluate the predicted estimation uncertainty for UAV i at time t_{k+1}.

The previous approach may be applied iteratively on $\mathbb{X}^{\mathrm{A,P}}_{i,k+\kappa}$ to evaluate the impact of $\mathbf{u}_{i,k+\kappa}$, $\kappa = 1, \ldots, h-1$, on the predicted estimation uncertainty for UAV i at time $t_{k+\kappa}$, which provides $\mathbb{X}^{\mathrm{A,P}}_{i,k+h}$ when $\kappa = h-1$. Thus an estimate $\phi(\mathbb{X}^{\mathrm{A,P}}_{i,k+h}) = \Phi(\mathcal{X}^{\mathrm{P}}_{i,k+h}, \mathbb{X}^{\mathrm{U,P}}_{i,k+h}, \overline{\mathbb{X}}^{\mathrm{P}}_{i,k+h})$ of $\Phi(\mathcal{X}_{i,k+h}, \mathbb{X}^{\mathrm{U}}_{i,k+h}, \overline{\mathbb{X}}_{i,k+h})$ is deduced. Then UAV i may search the sequence of control inputs $(\mathbf{u}_{i,k}, \ldots, \mathbf{u}_{i,k+h-1})$ minimizing

$$J\left(\mathbf{u}_{i,k}, \ldots, \mathbf{u}_{i,k+h-1}\right) = \phi\left(\mathbb{X}^{\mathrm{A,P}}_{i,k+h}\right) + \alpha d\left(\mathbf{x}^{\mathrm{u,P}}_{i,k+h}, \mathbb{X}^{\mathrm{A,P}}_{i,k+h}\right), \tag{4.39}$$

where $\mathbb{X}^{\mathrm{A,P}}_{i,k+h}$ and $\mathbf{x}^{\mathrm{u,P}}_{i,k+h}$ depend on $(\mathbf{u}_{i,k}, \ldots, \mathbf{u}_{i,k+h-1})$. In (4.39), $d\left(\mathbf{x}, \mathbb{X}\right)$ represents the Hausdorff distance between the vector $\mathbf{x}$ and the set $\mathbb{X}$, which is the shortest distance from $\mathbf{x}$ to reach any point $\mathbf{x}' \in \mathbb{X}$, *i.e.*, $d\left(\mathbf{x}, \mathbb{X}\right) = \inf_{\mathbf{x}' \in \mathbb{X}} d\left(\mathbf{x}, \mathbf{x}'\right)$. The measure for the distance may be, *e.g.*, the euclidean norm such that $d\left(\mathbf{x}, \mathbf{x}'\right) = \|\mathbf{x} - \mathbf{x}'\|$. The first term of J represents the predicted estimation uncertainty for UAV i at time t_{k+h}. The second term is introduced to drive UAV i towards $\mathbb{X}^{\mathrm{A,P}}_{i,k+h}$. Cost function (4.39) is useful when the first term, $\phi\left(\mathbb{X}^{\mathrm{A,P}}_{i,k+h}\right)$, remains constant, whatever the sequence of inputs $(\mathbf{u}_{i,k}, \ldots, \mathbf{u}_{i,k+h-1})$, which may occur when the chosen prediction horizon is

not sufficient large. The parameter α adjusts the relative importance of the second term. In the simulations, sets of $\mathbb{R}^2$ are considered. The measure $\phi(\mathbb{X})$ is chosen as the area of the set $\mathbb{X}$ in that case.

4.4.2. Control input design accounting for communications

Assume that some UAVs in a subset $\mathcal{N}_{i,k}^{\mathrm{C}} \subset \mathcal{N}_{i,k}$ of neighbors of UAV i have already computed and transmitted their own control inputs $(\mathbf{u}_{\ell,k}, \ldots, \mathbf{u}_{\ell,k+h-1})$, $\ell \in \mathcal{N}_{i,k}^{\mathrm{C}}$, as well as their state $\mathbf{x}_{\ell,k}^{\mathrm{u}}$ at time t_k. To evaluate its own sequence $(\mathbf{u}_{i,k}, \ldots, \mathbf{u}_{i,k+h-1})$ of control inputs, UAV i will now account for the information that will be provided via communications at the steps $k+\kappa$ by the agents in $\mathcal{N}_{i,k+\kappa}^{\mathrm{C}}$, $\kappa = 1, \ldots, h$. Nevertheless, some UAVs in $\mathcal{N}_{i,k}^{\mathrm{C}}$ may not be able to communicate with UAV i at some prediction steps $\kappa = 1, \ldots, h$. One has to predict for each κ, the set of UAVs with which UAV i will be able to communicate. For UAV i and each UAV $\ell \in \mathcal{N}_{i,k}^{\mathrm{C}}$, consider the sequences of control inputs $(\mathbf{u}_{i,k}, \ldots, \mathbf{u}_{i,k+h-1})$ and $(\mathbf{u}_{\ell,k}, \ldots, \mathbf{u}_{\ell,k+h-1})$, as well as the states $\mathbf{x}_{i,k}^{\mathrm{u}}$ and $\mathbf{x}_{\ell,k}^{\mathrm{u}}$. UAV i can evaluate $\mathbf{x}_{\ell,k+\kappa}^{\mathrm{u,P}}$ and $\mathbf{x}_{i,k+\kappa}^{\mathrm{u,P}}$, the predicted values of $\mathbf{x}_{\ell,k+\kappa}^{\mathrm{u}}$ and $\mathbf{x}_{i,k+\kappa}^{\mathrm{u}}$, for $\kappa = 1, \ldots, h$. Then, using the communication condition (3.18), the set of UAVs with which UAV i can expect to be able to communicate at time $t_{k+\kappa}$, $\kappa = 1, \ldots, h$, is

$$\mathcal{N}_{i,k+\kappa}^{\mathrm{P}} = \left\{ \ell \in \mathcal{N}_{i,k}^{\mathrm{C}} \,|\, c\left(\mathbf{x}_{i,k+\kappa}^{\mathrm{u,P}}, \mathbf{x}_{\ell,k+\kappa}^{\mathrm{u,P}}\right) \geqslant 0 \right\}. \tag{4.40}$$

It is assumed that the UAVs have access to the value of c, which may not always be the case. If c is not available than one may assume that $\mathcal{N}_{i,k+\kappa}^{\mathrm{P}} = \mathcal{N}_{i,k}^{\mathrm{C}}$, $\kappa = 1, \ldots, h$, and UAV i can not anticipate the future communication graph. Furthermore, if $\mathbf{x}_{i,k+\kappa}^{\mathrm{u}} = \mathbf{x}_{i,k+\kappa}^{\mathrm{u,P}}$ and $\mathbf{x}_{\ell,k+\kappa}^{\mathrm{u}} = \mathbf{x}_{\ell,k+\kappa}^{\mathrm{u,P}}$, $\ell \in \mathcal{N}_{i,k}$, $\kappa = 1, \ldots, h$, then the set $\mathcal{N}_{i,k+\kappa}^{\mathrm{P}}$ is a subset of $\mathcal{N}_{i,k+\kappa}$, since UAVs that are not in $\mathcal{N}_{i,k}^{\mathrm{C}}$ may also be able to communicate with UAV i at time $t_{k+\kappa}$, $\kappa = 1, \ldots, h$.

At time $t_{k+\kappa}$, for the correction step from communications, assume that UAV i is only allowed to account for the FoV $\mathbb{F}_\ell(\mathbf{x}_{\ell,k+\kappa}^{\mathrm{u,P}})$ of UAVs with index $\ell \in \mathcal{N}_{i,k+\kappa}^{\mathrm{P}}$. All information that the neighbors of UAV i may receive from their own neighbors, not belonging to $\mathcal{N}_{i,k+\kappa}^{\mathrm{P}}$ is thus ignored.

At time t_k, UAV i can compute $\mathbb{X}_{i,k}^{\mathrm{A}}$ using (4.33). Applying the prediction step (4.34) and correction step from measurements (4.36), one gets $\mathbb{X}_{i,k+1|k}^{\mathrm{A,P}}$ and $\mathbb{X}_{i,k+1|k+1}^{\mathrm{A,P}}$. UAV i has access to $\mathbf{x}_{\ell,k}^{\mathrm{u}}$ and $\mathbf{u}_{\ell,k}$ for all UAVs with index $\ell \in \mathcal{N}_{i,k+1}^{\mathrm{P}}$, from which the FOV $\mathbb{F}_\ell(\mathbf{x}_{\ell,k+1}^{\mathrm{u,P}})$ is deduced. Ignoring possible detection of new or previously detected targets in $\mathbb{F}_\ell(\mathbf{x}_{\ell,k+1}^{\mathrm{u,P}})$, UAV i simply accounts for the reduction of the size of the search space provided by $\mathbb{F}_\ell(\mathbf{x}_{\ell,k+1}^{\mathrm{u,P}})$, $\ell \in \mathcal{N}_{i,k+1}^{\mathrm{P}}$, to evaluate $\mathbb{X}_{i,k+1}^{\mathrm{A,P}}$ similarly to (4.36), so as to get

$$\mathbb{X}_{i,k+1}^{\mathrm{A,P}} = \mathbb{X}_{i,k+1|k+1}^{\mathrm{A}} \setminus \bigcup_{\ell \in \mathcal{N}_{i,k+1}^{\mathrm{P}}} \mathbb{F}_\ell\left(\mathbf{x}_{\ell,k+1}^{\mathrm{u,P}}\right). \tag{4.41}$$

In this set-membership MPC approach, UAV i processes the FoVs of its neighbors as its own FoV.

As in Section 4.4.1, this process may be iterated from $\mathbb{X}^{\mathrm{A,P}}_{i,k+\kappa-1}$ to further evaluate the impact of $\mathbf{u}_{i,k+\kappa-1}$ and $\mathbf{u}_{\ell,k+\kappa-1}$, $\ell \in \mathcal{N}^{\mathrm{C}}_{i,k+\kappa}$, on $\mathbb{X}^{\mathrm{A,P}}_{i,k+\kappa}$, where $\kappa = 2, \ldots, h$. UAV i then searches the sequence of control inputs $(\mathbf{u}_{i,k}, \ldots, \mathbf{u}_{i,k+h-1})$ minimizing (4.39).

Remark 1. Assume that $\mathcal{L}^{\mathrm{P}}_{i,k+\kappa}$, $\mathcal{X}^{\mathrm{P}}_{i,k+\kappa}$, $\mathbb{X}^{\mathrm{U,P}}_{i,k+\kappa}$, and $\overline{\mathbb{X}}^{\mathrm{P}}_{i,k+\kappa}$ have been evaluated by UAV i for some $1 \leqslant \kappa < h$. For that purpose, UAV i has evaluated $\mathbf{x}^{\mathrm{u,P}}_{\ell,k+\kappa}$ for all $\ell \in \mathcal{N}^{\mathrm{P}}_{i,k} \cup \{i\}$. The sets $\mathcal{L}^{\mathrm{P}}_{\ell,k+\kappa}$, $\mathcal{X}^{\mathrm{P}}_{\ell,k+\kappa}$, $\mathbb{X}^{\mathrm{U,P}}_{i,k+\kappa}$, and $\overline{\mathbb{X}}^{\mathrm{P}}_{\ell,k+\kappa}$ for $\ell \in \mathcal{N}^{\mathrm{P}}_{i,k}$ are not necessarily equal to the corresponding sets evaluated by UAV i due to communication constraints. Figure 4.8 illustrates this situation, where one observes that the sets used to evaluate $\overline{\mathbb{X}}^{\mathrm{P}}_{\ell,k+1}$ and $\overline{\mathbb{X}}^{\mathrm{P}}_{\ell',k+1}$ by UAVs ℓ and ℓ' are not the same. Consequently, in general, $\overline{\mathbb{X}}^{\mathrm{P}}_{\ell,k+1} \neq \overline{\mathbb{X}}^{\mathrm{P}}_{\ell',k+1}$ and also $\mathbb{X}^{\mathrm{A,P}}_{\ell,k+1} \neq \mathbb{X}^{\mathrm{A,P}}_{\ell',k+1}$. Nevertheless, to simplify the evaluation in the considered MPC context, one assumes that the predicted sets at time $t_{k+\kappa}$ satisfy $\mathcal{L}^{\mathrm{P}}_{\ell,k+\kappa} = \mathcal{L}^{\mathrm{P}}_{i,k+\kappa}$, $\mathcal{X}^{\mathrm{P}}_{\ell,k+\kappa} = \mathcal{X}^{\mathrm{P}}_{i,k+\kappa}$, and $\overline{\mathbb{X}}^{\mathrm{P}}_{\ell,k+\kappa} = \overline{\mathbb{X}}^{\mathrm{P}}_{i,k+\kappa}$ for all $\ell \in \mathcal{N}^{\mathrm{P}}_{i,k+\kappa}$.

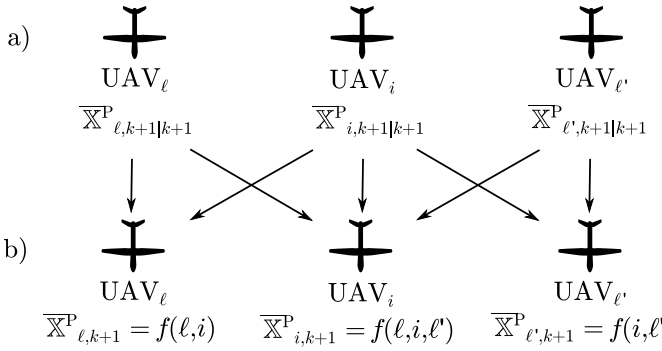

Figure 4.8.: Available estimates evaluated in the MPC approach; UAVs able to communicate directly are linked; a) before communication, estimates $\overline{\mathbb{X}}^{\mathrm{P}}_{\ell,k+1|k+1}$ of $\overline{\mathbb{X}}_{\ell,k+1|k+1}$, and b) after communication and processing, estimates $\overline{\mathbb{X}}^{\mathrm{P}}_{\ell,k+1}$ of $\overline{\mathbb{X}}_{\ell,k+1}$.

4.4.3. Control design accounting for collisions

The developed control design cannot guarantee that no collision between UAVs appears. However, the distributed controller leads to a natural repulsive behavior between the UAVs. This comes from the fact that it is inefficient for two UAVs to observe the same area. The UAVs can better reduce the estimation uncertainty if they spread over the RoI. A straightforward approach to guarantee that collision between UAVs cannot appear is to allocate each UAV to a different altitude.

Collision may also occur between UAVs and obstacles if the RoI may contain obstacles that are high enough. To account for *known* obstacles the cost function (4.39)

can be slightly changed to

$$J^*\left(\mathbf{u}_{i,k},\ldots,\mathbf{u}_{i,k+h-1}\right) = \phi\left(\mathbb{X}^{\mathrm{A,P}}_{i,k+h}\right) + \alpha d\left(\mathbf{x}^{\mathrm{u,P}}_{i,k+h},\mathbb{X}^{\mathrm{A,P}}_{i,k+h}\right) + \alpha^{\mathrm{s1}} J^{\mathrm{s}}\left(\mathbf{x}^{\mathrm{u,P}}_{i,k+1},\ldots,\mathbf{x}^{\mathrm{u,P}}_{i,k+h}\right), \quad (4.42)$$

where α^{s1} is a parameter and the term $J^{\mathrm{s}}\left(\mathbf{x}^{\mathrm{u,P}}_{i,k+1},\ldots,\mathbf{x}^{\mathrm{u,P}}_{i,k+h}\right)$ represent the risk of collision between UAVs and obstacles. It considers that a collision may occur when the distance between a UAV and the boundary of obstacle is less than some threshold d^{col}. The cost $J^{\mathrm{s}}\left(\mathbf{x}^{\mathrm{u,P}}_{i,k+1},\ldots,\mathbf{x}^{\mathrm{u,P}}_{i,k+h}\right)$ is designed in order to satisfy the following properties. Its amplitude of variations should be very small when the UAV is located far from the obstacle, and increase very fast in the vicinity of an obstacle. The function should be smooth to simplify minimization. A suitable candidate for satisfying these properties, as presented in Rochefort et al. (2014), is the following risk expression:

$$J^{\mathrm{s}}\left(\mathbf{x}^{\mathrm{u,P}}_{i,k+1},\ldots,\mathbf{x}^{\mathrm{u,P}}_{i,k+h}\right) = \sum_{\mathbf{x}\in\left\{\mathbf{x}^{\mathrm{u,P}}_{i,k+1},\ldots,\mathbf{x}^{\mathrm{u,P}}_{i,k+h}\right\}} \sum_{m=1}^{N^{\mathrm{o}}} \frac{1}{2}\left[1-\tanh\left(\frac{d\left(\mathcal{O}_{m,k},p^{\mathrm{u}}(\mathbf{x})\right)-\alpha^{\mathrm{s2}}}{\alpha^{\mathrm{s3}}}\right)\right], \quad (4.43)$$

where $d\left(\mathcal{O}_{m,k},\mathbf{x}\right)$ evaluates the distance between obstacle m and the UAV location $p^{\mathrm{u}}(\mathbf{x})$. The coefficients α^{s2} and α^{s3} are used to tune the shape of the function which varies between 0 (no risk of collision) and 1 (collision will occur). Parameter α^{s2} defines the width of the region where the criterion variations are fast and α^{s1}defines the center of this region and is related to d^{col} by $\alpha^{\mathrm{s1}} - \alpha^{\mathrm{s2}} >= d^{\mathrm{col}}$. Cost function (4.42) can reduce the risk of collision, however, it can not guarantee that collision does not occur.

4.4.4. Practical issues

The order in which the UAVs compute their control inputs at each time step t_k has to be determined. Assume that UAV i has access to $\mathcal{N}_{i,k}$ from previous communication taken place in Section 4.4.2. The selected suboptimal distributed approach for UAV i consists of computing its control inputs only once it has received the predicted control inputs from all UAVs in $\mathcal{N}_{i,k}$ with a smaller index, *i.e.*, from all UAVs with index in $\mathcal{N}^{\mathrm{C}}_{i,k} \subset \mathcal{N}_{i,k}$.

In each $\mathcal{N}_{i,k}$, $i = 1,\ldots,N^{\mathrm{u}}$, UAV i is able to determine whether it has the smallest index. If this is the case, UAV i evaluates and communicates its control inputs

$$\left(\widehat{\mathbf{u}}_{i,k},\ldots,\widehat{\mathbf{u}}_{i,k+h-1}\right) = \arg\min J\left(\mathbf{u}_{i,k},\ldots,\mathbf{u}_{i,k+h-1}\right), \quad (4.44)$$

where the minimization is over all $\mathbf{u}_{i,k} \in \mathbb{U}_0,\ldots,\mathbf{u}_{i,k+h-1} \in \mathbb{U}_{h-1}$, without accounting for the presence of its neighbors. In practice, to lighten computations, $\mathbb{U}_0,\ldots,\mathbb{U}_{h-1}$

are chosen as discrete subsets of $\mathbb{U}$, the set of admissible control inputs. Then, one of the UAVs with index $\ell \in \mathcal{N}_{i,k}$, $\ell > i$ can determine $(\widehat{\mathbf{u}}_{\ell,k}, \ldots, \widehat{\mathbf{u}}_{\ell,k+h-1})$ minimizing $J(\mathbf{u}_{\ell,k}, \ldots, \mathbf{u}_{\ell,k+h-1})$, accounting for $(\widehat{\mathbf{u}}_{i,k}, \ldots, \widehat{\mathbf{u}}_{i,k+h-1})$ provided by UAV i.

The optimization problem in (4.44) is locally non-differentiable and has multiple minima, making gradient search-based optimization methods not applicable. To solve the optimization problem, an approach similar to that in Rochefort et al. (2014) is used, where finite sets of predefined feasible control sequences are considered. The UAV evaluates the impact of all feasible control sequences and apply then the sequence that minimizes (4.44).

To understand the evolution of $J(\mathbf{u}_{i,k}, \ldots, \mathbf{u}_{i,k+h-1})$ and particularly the evolution of $\phi\left(\mathbb{X}^{\mathrm{A,P}}_{i,k+h}\right)$, a much simplified problem is considered. Figure 4.9 and 4.10 (left) show a subset of the RoI containing the set estimates $\mathbb{X}_{i,j,k}$ (green) and $\overline{\mathbb{X}}_{i,k}$ (yellow) and a UAV that is able to turn by the angle φ, *i.e.*, $\mathbf{u}_{i,k} = \varphi$. Figure 4.9 and 4.10 (right) show the corresponding evolution of the measure $\phi(\mathbb{X}^{\mathrm{A,P}}_{i,k+1}) - a_1$ (black dashed), where $\phi(\mathbb{X}^{\mathrm{A,P}}_{i,k+1})$ is the predicted evolution of the set $\mathbb{X}^{\mathrm{A}}_{i,k}$ considering the control input/heading angle φ. The constant a_1 is used as off-set, such that control inputs leading to no reduction lead to $\phi(\mathbb{X}^{\mathrm{A,P}}_{i,k+1}) - a_1 = 0$. Some angels φ are marked in both plots (left and right) to highlight the impact of the chosen control input. The sets in Figure 4.9 are simplified to obtain an less complex evolution of $\phi(\mathbb{X}^{\mathrm{A,P}}_{i,k+1})$. The sets in Figure 4.10 are taken from real simulations. One observes a much more complex evolution of $\phi(\mathbb{X}^{\mathrm{A,P}}_{i,k+1})$.

One considers also the evolution of $\phi(\mathbb{X}^{\mathrm{A,P}}_{i,k+2|k+1})$ (solid blue) which accounts for (4.34) at instant $k+2|k+1$. This is done to highlight the fact that the prediction step in (4.34) leads to a locally discontinuous evolution of the cost function when considering a prediction horizon $h > 1$.

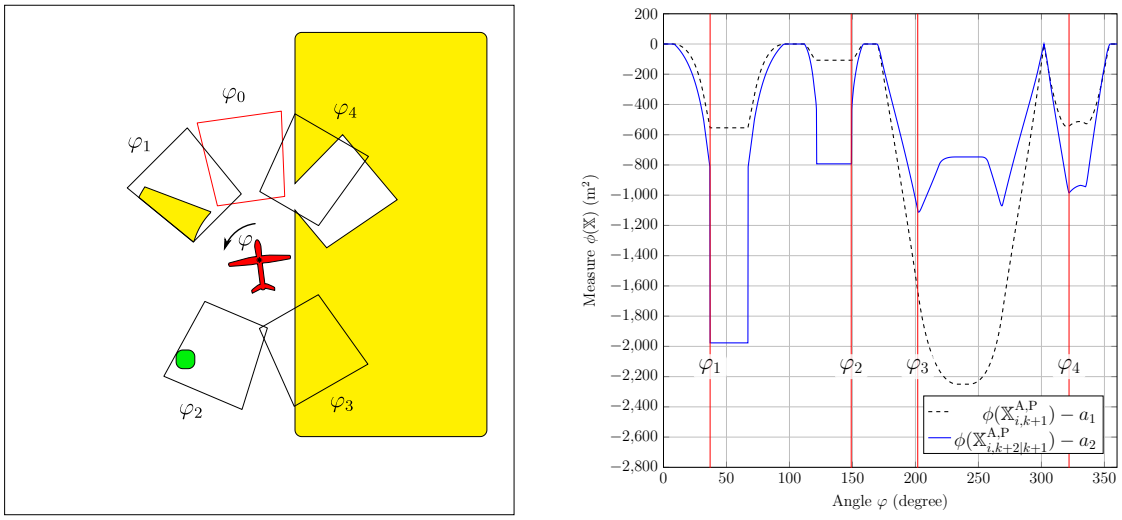

Figure 4.9.: RoI containing simplified set estimates $\mathbb{X}_{i,j,k}$ (green) and $\overline{\mathbb{X}}_{i,k}$ (yellow) and UAV able to turn by the angle φ (left). Evolution of the measures $\phi(\mathbb{X}^{\mathrm{A,P}}_{i,k+1})$ and $\phi(\mathbb{X}^{\mathrm{A,P}}_{i,k+2|k+1})$ depending on the heading of the UAV (right).

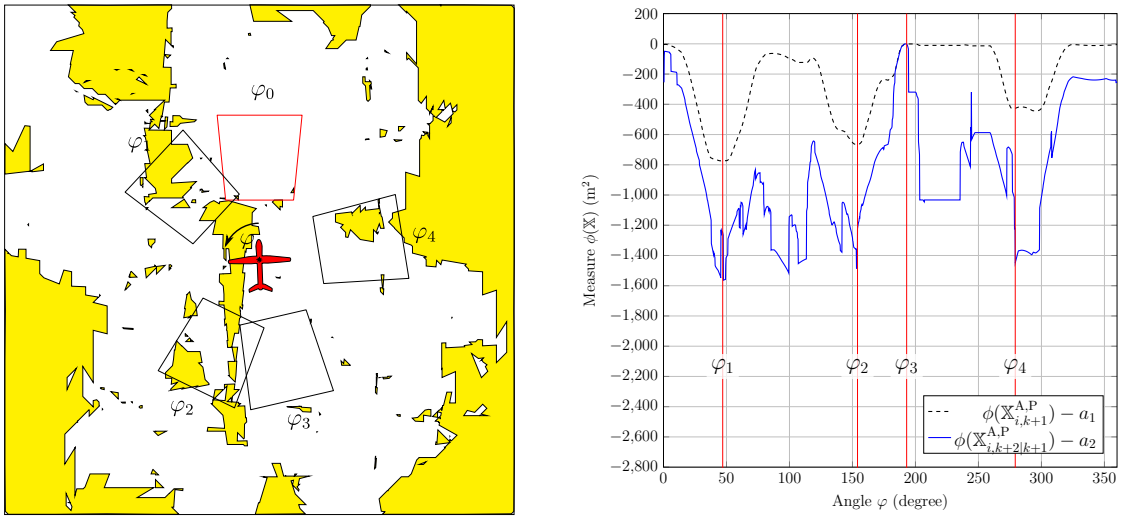

Figure 4.10.: RoI containing the set estimate $\overline{\mathbb{X}}_{i,k}$ (yellow) from real experiments and UAV able to turn by the angle φ (left). Evolution of the measures $\phi(\mathbb{X}^{\mathrm{A,P}}_{i,k+1})$ and $\phi(\mathbb{X}^{\mathrm{A,P}}_{i,k+2|k+1})$ depending on the heading of the UAV (right).

4.5. Simulations

The performance of the proposed approach is evaluated via simulations.

The targets move on the ground with a speed module V^{t} assumed constant. At time t_k, $(x^{\mathrm{t}}_{j,k,1}, x^{\mathrm{t}}_{j,k,2})^\top$ are the coordinates of target j, $x^{\mathrm{t}}_{j,k,3}$ is its heading angle, $x^{\mathrm{t}}_{j,k,4}$ its yaw rate. The yaw rate derivative $x^{\mathrm{t}}_{j,k,5}$ follows a random walk with input $v_{j,k}$ uniformly distributed in the interval $[-\pi/8, \pi/8]$ s^{-2}, *i.e.*, $v_{j,k} \sim \mathcal{U}\left(-\pi/8\,\mathrm{s}^{-2}, \pi/8\,\mathrm{s}^{-2}\right)$. The target state vector $\mathbf{x}^{\mathrm{t}}_{j,k}$ evolves according to

$$\begin{pmatrix} x^{\mathrm{t}}_{j,k+1,1} \\ x^{\mathrm{t}}_{j,k+1,2} \\ x^{\mathrm{t}}_{j,k+1,3} \\ x^{\mathrm{t}}_{j,k+1,4} \\ x^{\mathrm{t}}_{j,k+1,5} \end{pmatrix} = \begin{pmatrix} x^{\mathrm{t}}_{j,k,1} + T^{\mathrm{d}} \cos\left(x^{\mathrm{t}}_{j,k,3}\right) V^{\mathrm{t}} \\ x^{\mathrm{t}}_{j,k,2} + T^{\mathrm{d}} \sin\left(x^{\mathrm{t}}_{j,k,3}\right) V^{\mathrm{t}} \\ x^{\mathrm{t}}_{j,k,3} + T^{\mathrm{d}} x^{\mathrm{t}}_{j,k,4} \\ x^{\mathrm{t}}_{j,k,4} + T^{\mathrm{d}} x^{\mathrm{t}}_{j,k,5} \\ v_{j,k} \end{pmatrix}, \tag{4.45}$$

where $T^{\mathrm{d}} = 0.05\,\mathrm{s}$. The state of UAV i at time t_k consists of its coordinates $(x^{\mathrm{u}}_{i,k,1}, x^{\mathrm{u}}_{i,k,2}, x^{\mathrm{u}}_{i,k,3})^\top$, flight path angle $x^{\mathrm{u}}_{i,k,4}$, heading angle $x^{\mathrm{u}}_{i,k,5}$, yaw rate $x^{\mathrm{u}}_{i,k,6}$, and yaw rate derivative $x^{\mathrm{t}}_{i,k,7}$. The control input is applied to $x^{\mathrm{u}}_{i,k,7}$. The UAV state vector $\mathbf{x}^{\mathrm{u}}_{i,k}$ evolves according to

$$\begin{pmatrix} x^{\mathrm{u}}_{i,k+1,1} \\ x^{\mathrm{u}}_{i,k+1,2} \\ x^{\mathrm{u}}_{i,k+1,3} \\ x^{\mathrm{u}}_{i,k+1,4} \\ x^{\mathrm{u}}_{i,k+1,5} \\ x^{\mathrm{u}}_{i,k+1,6} \\ x^{\mathrm{u}}_{i,k+1,7} \end{pmatrix} = \begin{pmatrix} x^{\mathrm{u}}_{i,k,1} + T^{\mathrm{d}} \cos\left(x^{\mathrm{u}}_{i,k,4}\right) \cos\left(x^{\mathrm{u}}_{i,k,5}\right) V^{\mathrm{u}} \\ x^{\mathrm{u}}_{i,k,2} + T^{\mathrm{d}} \cos\left(x^{\mathrm{u}}_{i,k,4}\right) \sin\left(x^{\mathrm{u}}_{i,k,5}\right) V^{\mathrm{u}} \\ x^{\mathrm{u}}_{i,k,3} + T^{\mathrm{d}} \sin\left(x^{\mathrm{u}}_{i,k,4}\right) V^{\mathrm{u}} \\ x^{\mathrm{u}}_{i,k,4} \\ x^{\mathrm{u}}_{i,k,5} + T^{\mathrm{d}} x^{\mathrm{t}}_{i,k,6} \\ x^{\mathrm{u}}_{i,k,6} + T^{\mathrm{d}} x^{\mathrm{t}}_{i,k,7} \\ u_{i,k} \end{pmatrix}. \tag{4.46}$$

The altitude $x^{\mathrm{u}}_{i,0,3} = 100\,\mathrm{m}$, the flight path angle $x^{\mathrm{u}}_{i,0,4} = 0$, and the speed module $V^{\mathrm{u}} = 16.6$ m/s are assumed constant.

The UAVs are equipped with identical optical sensors able to detect targets within their FoV. The sensor opening angles are equal to $\pi/4$ in both azimuth and elevation. A simplified measurement model is considered, where it is assumed that the measurement function is the identity function. Only the location of the target is measured. Therefore, the noisy target location is directly available to the UAV. Consequently, a noisy measurement $\mathbf{y}_{i,j,k}$ of $(x^{\mathrm{t}}_{j,k,1}, x^{\mathrm{t}}_{j,k,2})^\top$ is obtained with a noise $\mathbf{w}_{i,j,k} \sim \mathcal{U}\left(-5\,\mathrm{m}, 5\,\mathrm{m}\right)$ when a target is detected, as described by (3.14) and (3.15). A target is detected and identified at time t_k when (3.8) is satisfied, where

$$g^{\mathrm{t}}_j\left(\mathbf{x}^{\mathrm{u}}_{i,k}, \mathbf{x}^{\mathrm{t}}_{j,k}\right) = \left(\mathbf{x}^{\mathrm{u}}_{i,k} - \mathbf{x}^{\mathrm{t}}_{j,k}\right)^\top \mathbf{a}^{\mathrm{t}}_{j,k} - \left\|\mathbf{x}^{\mathrm{u}}_{i,k} - \mathbf{x}^{\mathrm{t}}_{j,k}\right\| \left\|\mathbf{a}^{\mathrm{t}}_{j,k}\right\| \left(\cos\lambda^{\mathrm{t}}_j\right) \tag{4.47}$$

represents a half circular cone in $\mathbb{R}^3$ with a small aperture $2\lambda^{\mathrm{t}}_j = \pi/60$, to make

identification of targets more difficult. The cone vertex is $\mathbf{x}^{\mathrm{t}}_{j,k}$ and its axis is

$$\mathbf{a}^{\mathrm{t}}_{j,k} = \left(\sin\gamma_j \cos\left(x^{\mathrm{t}}_{j,k,3} + \beta_j\right), \sin\gamma_j \sin\left(x^{\mathrm{t}}_{j,k,3} + \beta_j\right), \cos\gamma_j, 0, 0, 0\right)^{\top} \tag{4.48}$$

with azimuth $\beta_j \sim \mathcal{U}(-\pi/4, \pi/4)$ and elevation angle $\gamma_j \sim \mathcal{U}(2\pi/60, 3\pi/60)$.

The false targets evolve according to the same dynamics as the true targets. False targets are detected and misidentified when (3.10) is satisfied, where

$$g^{\mathrm{f}}_{\ell}\left(\mathbf{x}^{\mathrm{u}}_{i,k}, \mathbf{x}^{\mathrm{f}}_{\ell,k}\right) = \left(\mathbf{x}^{\mathrm{u}}_{i,k} - \mathbf{x}^{\mathrm{f}}_{\ell,k}\right)^{\top} \mathbf{a}^{\mathrm{f}}_{\ell,k} - \left\|\mathbf{x}^{\mathrm{u}}_{i,k} - \mathbf{x}^{\mathrm{f}}_{\ell,k}\right\| \left\|\mathbf{a}^{\mathrm{f}}_{\ell,k}\right\| \left(\cos\lambda^{\mathrm{f,g}}_{\ell}\right), \tag{4.49}$$

and

$$q^{\mathrm{f}}_{\ell}\left(\mathbf{x}^{\mathrm{u}}_{i,k}, \mathbf{x}^{\mathrm{f}}_{\ell,k}\right) = \left(\mathbf{x}^{\mathrm{u}}_{i,k} - \mathbf{x}^{\mathrm{f}}_{\ell,k}\right)^{\top} \mathbf{a}^{\mathrm{f}}_{\ell,k} - \left\|\mathbf{x}^{\mathrm{u}}_{i,k} - \mathbf{x}^{\mathrm{f}}_{\ell,k}\right\| \left\|\mathbf{a}^{\mathrm{f}}_{\ell,k}\right\| \left(\cos\lambda^{\mathrm{f,q}}_{\ell}\right), \tag{4.50}$$

where $2\lambda^{\mathrm{f,g}}_{\ell} = \pi/30$ and $2\lambda^{\mathrm{f,q}}_{\ell} = \pi/60$. Both with axis

$$\mathbf{a}^{\mathrm{f}}_{\ell,k} = \left(\sin\gamma_{\ell} \cos\left(x^{\mathrm{f}}_{\ell,k,3} + \beta_{\ell}\right), \sin\gamma_{\ell} \cdot \sin\left(x^{\mathrm{f}}_{\ell,k,3} + \beta_{\ell}\right), \cos\gamma_{\ell}, 0, 0, 0\right)^{\top}, \tag{4.51}$$

where $\beta_{\ell} \sim \mathcal{U}(-\pi/4, \pi/4)$ and $\gamma_{\ell} \sim \mathcal{U}(2\pi/60, 3\pi/60)$.

The communication condition (3.18) is expressed as

$$c\left(\mathbf{x}^{\mathrm{u}}_{i,k}, \mathbf{x}^{\mathrm{u}}_{\ell,k}\right) = d^{\mathrm{c}} - \left\|\boldsymbol{x}^{\mathrm{u}}_{i,k} - \boldsymbol{x}^{\mathrm{u}}_{i',k}\right\|, \tag{4.52}$$

where $d^{\mathrm{c}} = 200\,\mathrm{m}$ is the maximum communication range and $\left\|\boldsymbol{x}^{\mathrm{u}}_{i,k} - \boldsymbol{x}^{\mathrm{u}}_{i',k}\right\|$ is the distance between UAV i and i'. The communication delays are neglected. The prediction horizon for the SM-MPC is $h = 2$. The control input is computed with a period $T^{\mathrm{c}} = 0.5\,\mathrm{s}$ equal to the communication period.

The RoI is a square of 400×400 m^2 and does not contain any obstacle. The simulations have been carried out in Matlab. Matlab's *Polyshapes* is used to represent sets. Polyshapes simplify the handling of sets in $\mathbb{R}^2$ regarding Boolean and geometrical operations. In higher-dimensions subpavings, *i.e.*, unions of non-overlapping interval vectors as in, *e.g.*, Kieffer et al. (2002) can be used. The considered measure $\phi(.)$ of the sets is consequently their area.

The parameter of the cost function (4.39) is $\alpha = 0.0001$, to give more importance to the reduction of the set estimates. Video sequences associated to the simulations are in the folder *Videos\Chapter_4\Simulations* or at `https://drive.google.com/drive/folders/1lFtrPrR0J2uXHquSRiZU2FSydXFXIPcB?usp=sharing`

The results for each setup of the following simulations were obtained for 30 independent simulations with uniformly distributed initial locations of the targets and UAVs in the RoI.

4.5.1. Impact of the fleet size

Figure 4.11 (left) presents, for different numbers N^{u} of UAVs, the average value and standard deviation of $\overline{\Phi}_k$ as defined in (3.20) over the 30 independent simulations, considering 3 true and 3 false targets with $V^{\mathrm{t}} = 1\,\mathrm{ms}^{-1}$.

Figure 4.11 (right) details the contribution of $\phi\left(\overline{\mathbb{X}}_k\right) = \sum_{i=1}^{N^{\mathrm{u}}} \phi\left(\overline{\mathbb{X}}_{i,k}\right)/N^{\mathrm{u}}$, $\phi\left(\mathbb{X}_k^{\mathrm{U}}\right) = \sum_{i=1}^{N^{\mathrm{u}}} \phi\left(\mathbb{X}_{i,k}^{\mathrm{U}}\right)/N^{\mathrm{u}}$, and $\phi\left(\mathbb{X}_k\right) = \sum_{i=1}^{N^{\mathrm{u}}} \phi\left(\bigcup_{\mathbb{X}_{i,j,k}\in\mathcal{X}_{i,k}} \mathbb{X}_{i,j,k}\right)/N^{\mathrm{u}}$ to $\overline{\Phi}_k$.

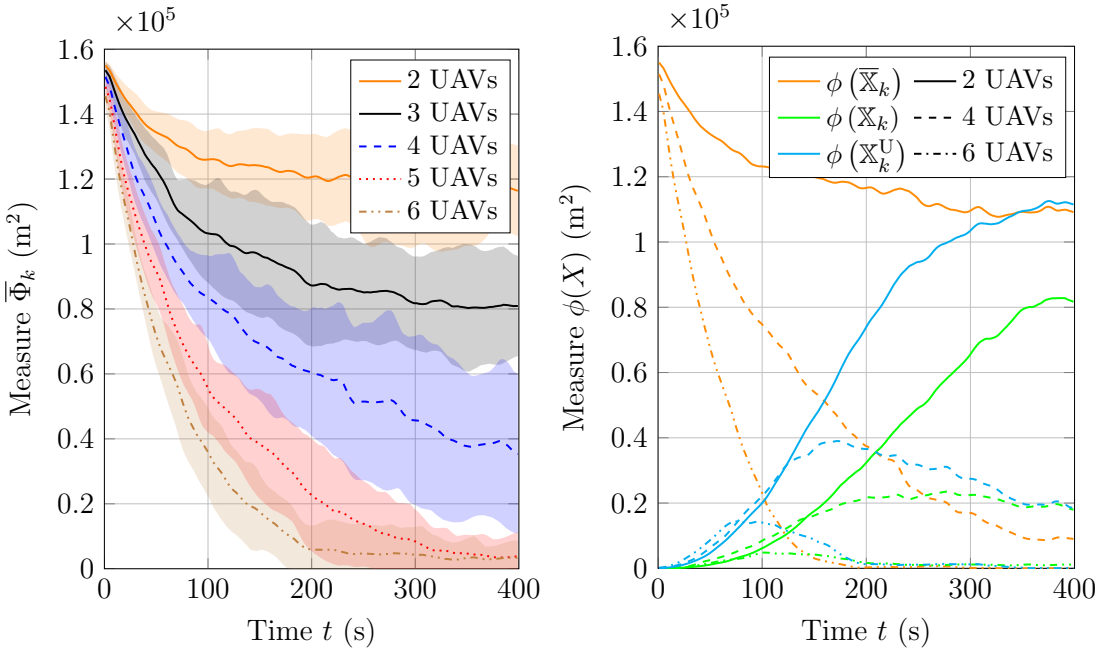

Figure 4.11.: Left: Mean values (line) and standard deviation (shaded area) of $\overline{\Phi}_k$ evaluated for 30 simulations with 3 true targets, 3 false targets, and 2 to 6 UAVs. Right: Mean values of $\phi\left(\overline{\mathbb{X}}_k\right)$, $\phi\left(\mathbb{X}_k^{\mathrm{U}}\right)$, and $\phi\left(\mathbb{X}_k\right)$ evaluated with 3 true and 3 false targets, considering 2, 4 and 6 UAVs.

Considering the size of the RoI and the relative speed of UAVs and of targets, within 400 s, from Figure 4.11, at least 5 UAVs are necessary to eliminate $\overline{\mathbb{X}}_{i,k}$. Figure 4.11 (right) shows that the growth of $\overline{\mathbb{X}}_{i,k}$ between consecutive observations is too fast to allow 3 UAVs or less to fully eliminate it. The variance of the estimation uncertainty $\overline{\Phi}_k$ is the largest for 4 UAVs: $\phi\left(\overline{\mathbb{X}}_{i,k}\right)$ may or may not converge to 0 depending on the simulations. Videos illustrate both cases (see video FleetSize_4_1 and FleetSize_4_2).

The initial growth of $\phi\left(\mathbb{X}_k^{\mathrm{U}}\right)$ in Figure 4.11 (right) is always faster then the initial growth of $\phi\left(\mathbb{X}_k\right)$ since targets are more likely to be unidentified: target identification requires additional measurements. When $\overline{\Phi}_k$ converges to 0, the size of $\mathbb{X}_k^{\mathrm{U}}$ also converges to 0 at some time instant when all false targets are identified and removed from $\mathbb{X}_k^{\mathrm{U}}$, and all true targets are identified and belong to $\mathbb{X}_k$.

Additionally, the video FleetSize_10_1 shows the performance of 10 UAVs tracking 10 true and 10 false targets.

4.5.2. Impact of the target speed

Figure 4.12 (left) shows the evolution of $\overline{\Phi}_k$ for different values of V^{t}. The simulations are carried out with 3 true targets, 3 false targets, and 6 UAVs.

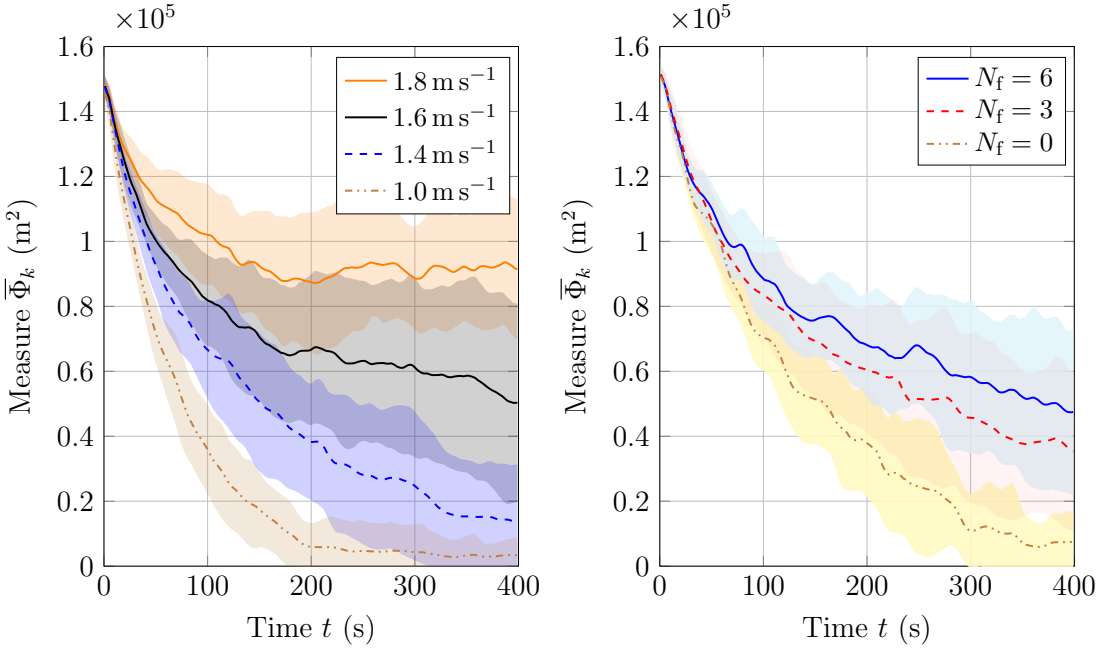

Figure 4.12.: Left: mean values (line) and standard deviation (shaded area) of $\overline{\Phi}_k$ evaluated with 3 true targets, 6 UAVs, 3 false targets, and different values of the target speed module V^{t}. Right: evolution of $\overline{\Phi}_k$ for 4 UAVs, 0 to 6 false targets, and $V^{\mathrm{t}} = 1\,\mathrm{m s}^{-1}$.

The relative speed of targets and UAVs significantly impacts the value to which $\overline{\Phi}_k$ converges. When $V^{\mathrm{t}} = 1.8\,\mathrm{m s}^{-1}$, $\phi\left(\overline{\mathbb{X}}_k\right)$ does not converge to 0 in all simulations. When $V^{\mathrm{t}} = 1.6\,\mathrm{m s}^{-1}$, $\phi\left(\overline{\mathbb{X}}_k\right)$ converges to 0 only in some simulations (see video TargetSpeed_1).

4.5.3. Impact of the number of false targets

Figure 4.12 (right) shows the evolution of $\overline{\Phi}_k$ for 0, 3, and 6 false targets. The simulations are carried out with 3 true targets, 4 UAVs, and $V^{\mathrm{t}} = 1\,\mathrm{m s}^{-1}$. The convergence speed of $\overline{\Phi}_k$ is affected by an increased N^{f}. This phenomenon is mainly due to an increase of $\phi\left(\mathbb{X}_k^{\mathrm{U}}\right)$ with N^{f}.

4.5.4. Mismatch of the measurement noise bounds

Figure 4.13 shows the mean of $\overline{\Phi}_k$ for different values for the measurement noise bounds $[\mathbf{w}_{i,j,k}]$ and different assumptions on the box $[\mathbf{w}_{i,k}]$, known to the UAVs, such that $[\mathbf{w}_{i,j,k}] \subset [\mathbf{w}_{i,k}]$. One considers 3 true targets, 0 false targets, 5 UAVs, and $V^{\mathrm{t}} = 1\,\mathrm{ms}^{-1}$.

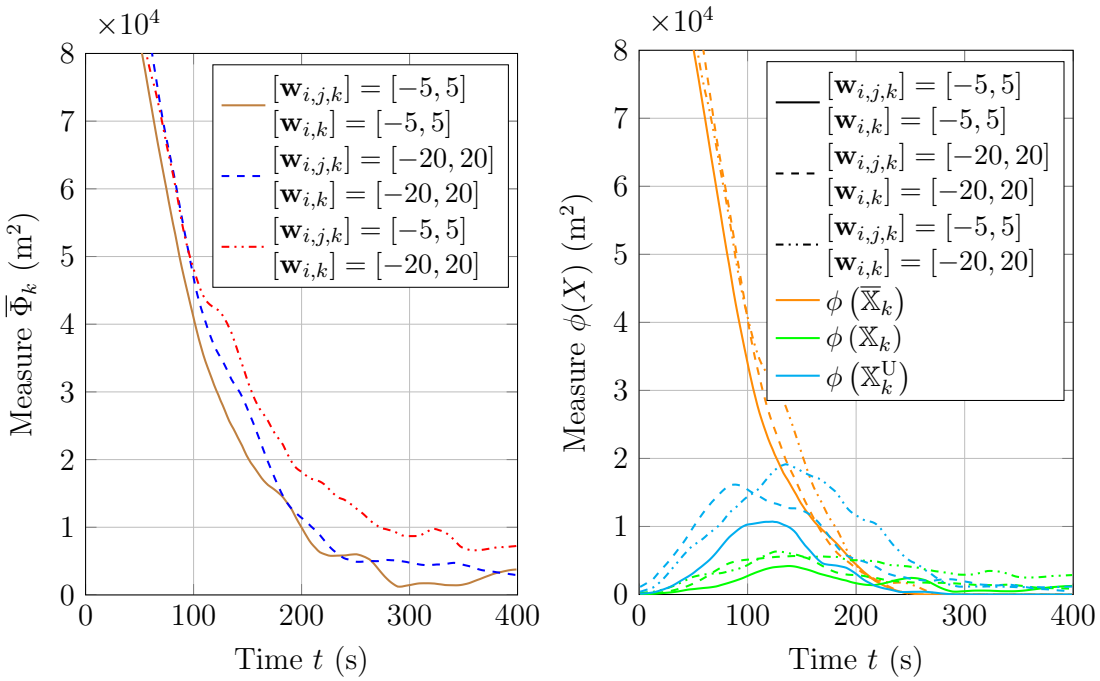

Figure 4.13.: Mean value of $\overline{\Phi}_k$ (left) and of $\phi\left(\overline{\mathbb{X}}_k\right)$, $\phi\left(\mathbb{X}_k^{\mathrm{U}}\right)$, and $\phi\left(\mathbb{X}_k\right)$ (right) evaluated for 30 simulations with 3 true targets, 0 false targets, and 5 UAVs for different measurement noise bounds $[\mathbf{w}_{i,j,k}]$ and different assumptions $[\mathbf{w}_{i,k}]$ on $[\mathbf{w}_{i,j,k}]$.

For small values of t, the decreases of $\overline{\Phi}_k$ is similar for the different setups. When $t \geqslant 100$ s, the curve of $\overline{\Phi}_k$ obtained for $[\mathbf{w}_{i,j,k}] = [\mathbf{w}_{i,k}] = [-20\,\mathrm{m}, 20\,\mathrm{m}]$ is above that for $[\mathbf{w}_{i,j,k}] = [\mathbf{w}_{i,k}] = [-5\,\mathrm{m}, 5\,\mathrm{m}]$ since large noise bounds lead to larger values of $\phi\left(\mathbb{X}_k^{\mathrm{U}}\right)$ and $\phi\left(\mathbb{X}_k\right)$, as observed in Figure 4.13 (right). A mismatch of $[\mathbf{w}_{i,j,k}]$ and $[\mathbf{w}_{i,k}]$ leads to the slowest decrease of $\overline{\Phi}_k$, due to the overestimation of $[\mathbf{w}_{i,j,k}]$ which does not allow an efficient reduction of $\phi\left(\mathbb{X}_k^{\mathrm{U}}\right)$ and $\phi\left(\mathbb{X}_k\right)$ when measurements are exploited.

The simulations show that the state of a true target was never outside the set estimates in any simulation as long as $[\mathbf{w}_{i,j,k}] \subset [\mathbf{w}_{i,k}]$. If $[\mathbf{w}_{i,j,k}] \not\subseteq [\mathbf{w}_{i,k}]$ then all targets are lost at some time instant, which provides a mean to detect erroneous estimates of the noise bounds.

The video NoiseBoundMismatch_1 shows the performance of the state estimator for a large mismatch of $[\mathbf{w}_{i,j,k}]$ and $[\mathbf{w}_{i,k}]$.

4.5.5. Impact of the communication distance

Figure 4.14 (left) illustrates the detrimental impact of a reduced communication range between UAVs on the decrease speed of $\overline{\Phi}_k$ when 6 UAVs are exploring a RoI with 3 true targets and 3 false targets. The reduction of d^{c} leads to a less efficient information sharing and thus to a redundant exploration of some areas by several UAVs unaware that these areas were already explored. A video illustrates the performance of the fleet when $d^{\mathrm{c}} = 50$ m (see video ComDist_50).

4.5.6. Processing time of the control input

Figure 4.14 (right) shows the mean and standard deviation of the evaluation time of the control input with 3 true targets, no false target and from 1 to 3 UAVs with $V^{\mathrm{t}} = 1\,\mathrm{ms}^{-1}$.

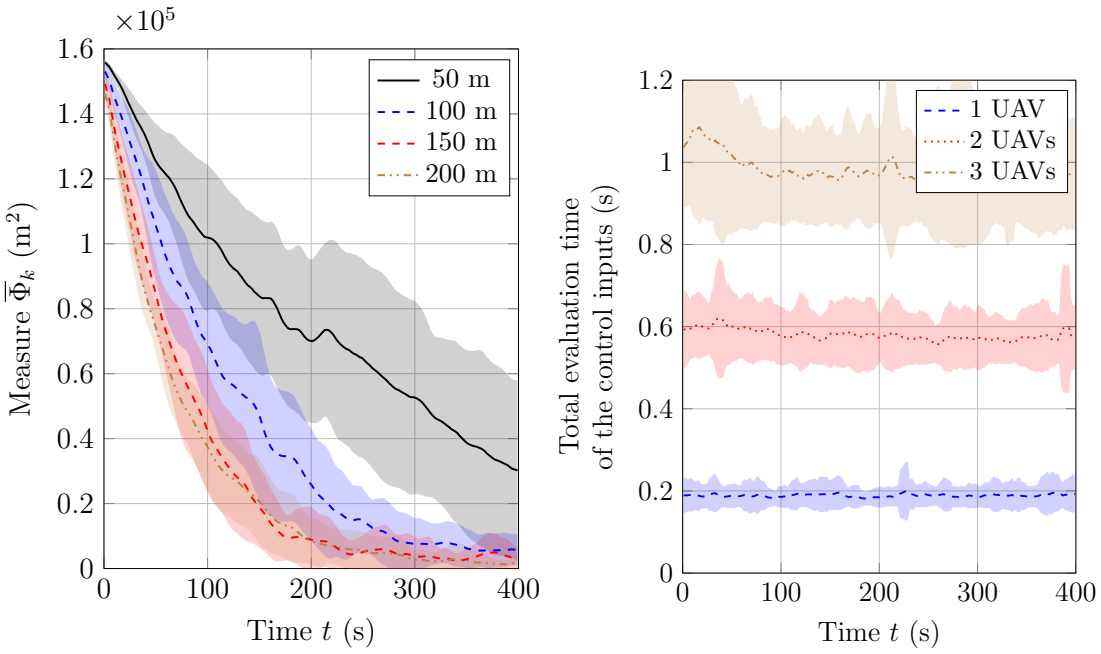

Figure 4.14.: Mean values (line) and standard deviation (shaded area) of $\overline{\Phi}_k$ evaluated for different values of the communication distances d^{c} when 6 UAVs are exploring a RoI with 3 true targets and 3 false targets (left), and of the computation time of the control inputs for 1 to 3 UAVs with 3 true targets and no false targets (right), average over 30 simulations.

One observes that the average total computing time is almost constant with time. The computing times for 2 and 3 UAVs is about three and five times that with a single UAV. This is due to the fact that in the predictive control scheme, once UAV 1 has computed its control input, UAV 2 will have to evaluate the impact of this control input when evaluating its own control input, while UAV 3 will have to evaluate the impact of the control inputs of UAVs 1 and 2.

4.5.7. Greedy control design

Some simplifications are made in the cooperative control design to predict the evaluation of (4.28), *e.g.*, the detection of targets is neglected, and it is of interest to compare the performance of the developed control scheme with a simple base line approach. For the the simple base line approach the evolution of the set estimates and the control input from the neighbors are not taken into account in the control design. Simulations show that the developed control scheme still outperforms the simple base line approach, see video SimpleBaselineMPC_1. The UAVs are not able to reduce the size of the set estimates efficiently if the controller does not account for the evolution of the set estimates and the control input coming from neighbors.

4.5.8. Occupied memory to store the set estimates

Figure 4.15 shows the evolution of the memory size that is necessary to store the sets $\overline{\mathbb{X}}_{i,k}$ and $\bigcup_{\mathbb{X}_{i,j,k}\in\mathcal{X}_{i,k}} \mathbb{X}_{i,j,k}$ maintained by one UAV. The results are averaged over 10 simulations. In this scenario, 3 UAVs are searching for 2 targets. The targets are always identified.

One observes that the maximal memory demand is less than 4000 byte for a single set, which is not that much considering a maximal package size of 1500 byte for communication over a Ethernet network. In Matlab the Polyshape-Objects are represented by a set of vertices. A vertex consists of 2 scalars each stored as double-precision floating-point values. A double-precision floating-point variable occupies 8 byte of memory. Consequently, the required memory space to store the set estimate is obtained by multiplying the number of vertices of a Polyshape-Object by 16.

4.5.9. Towards more realistic simulations

In order to obtain a more realistic rendering of the simulations, the results obtained from the MATLAB simulations have been exported and used to generate photorealistic video sequences using the simulation environment AirSim (Shah et al., 2017).

In the video sequences (see video *Sim_AirSim*), the moving targets are represented by cubes and false targets by stones. The trajectories of UAVs and targets are extracted from a MATLAB simulation. The video sequences are overlayed with the

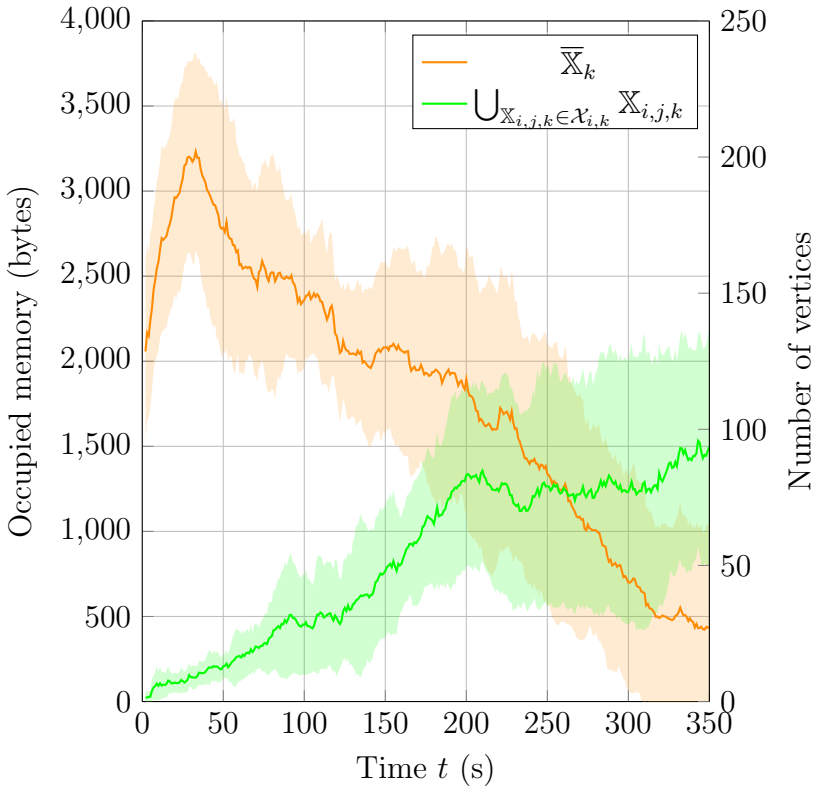

Figure 4.15.: Mean values (line) and standard deviation (shaded area) of the occupied memory of one UAV to store the set estimates $\overline{\mathbb{X}}_k$ and $\mathbb{X}_k$. 3 UAVs are exploring a RoI with 2 true targets.

evaluated estimates ($\overline{\mathbb{X}}_{i,k}$ in yellow, $\mathbb{X}_{i,j,k}$ in green, and $\mathbb{X}^{\mathrm{U}}_{i,k}$ in purple). Targets are highlighted with a circle if they are detected.

Future work will be to implement a more realistic detection model. AirSim is able to generate virtual images of the cameras of the UAVs. These images could then be processed by an image prepossessing software for object detection. This procedure allows accounting more accurately for environmental impact factors such as, *e.g.* lighting conditions and occlusion.

4.6. Experiments

Preliminary experimental studies are carried out in the experimental facilities at ONERA. The objectives are to adapt the set-membership estimation algorithm for implementation. A single UAV is considered, and the targets are static. Besides, the UAV follows a predefined search trajectory and do not use the MPC control scheme described above.

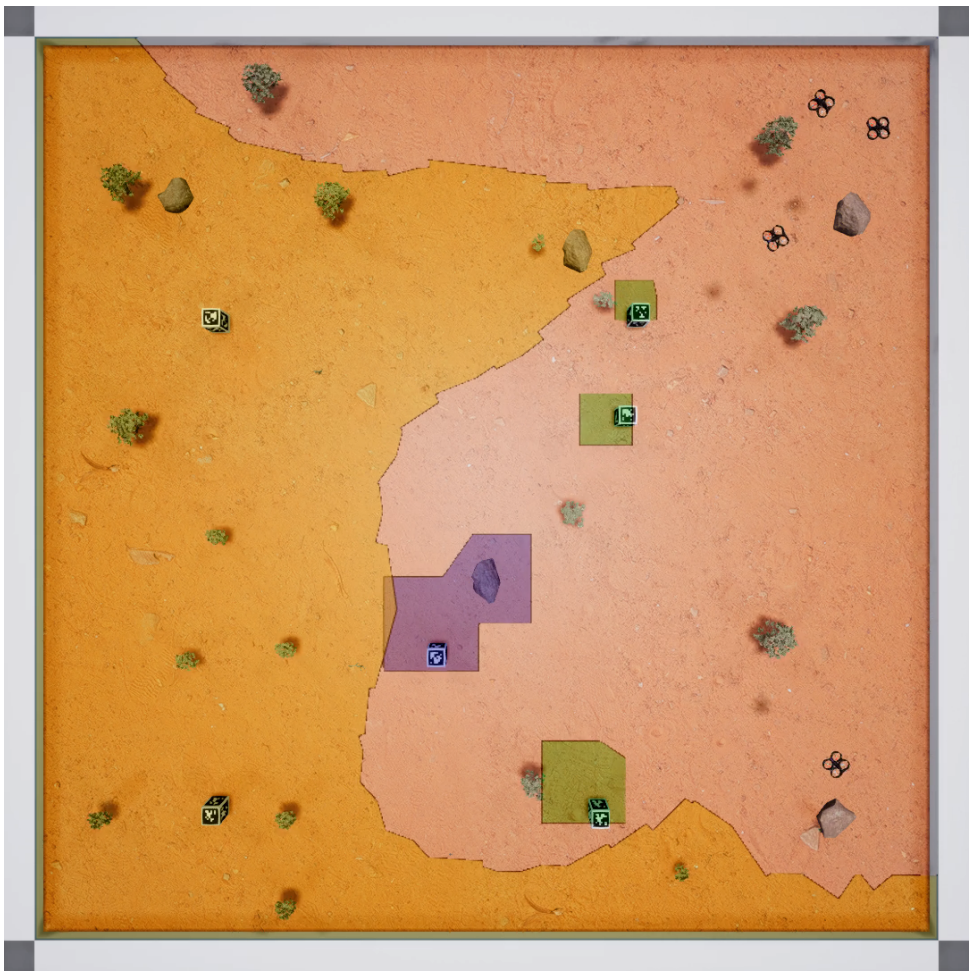

Figure 4.16.: RoI in AirSim: visualization with 4 UAVs, 6 targets (cubs), and 5 decoys (stones). The set estimates $\overline{\mathbb{X}}_{i,k}$, $\mathbb{X}^{\mathrm{U}}_{i,k}$, and $\mathbb{X}_{i,j,k}$ are shown for a single UAV.

4.6.1. Experimental setup

The experiments are carried out inside a test chamber, see Figure 4.17 (left). A Tello EDU drone is used as UAV, see Figure 4.17 (right). The drone is equipped with a front camera with a resolution of 1280×720 pixels. Other specifications of the drone are listed in Table 4.1. The camera is used to detect targets that are represented by AprilTag-markers. AprilTags are conceptually similar to QR Codes, in that they are a type of two-dimensional bar code. The marker have a size of $7 \times 7\,\mathrm{cm}$ and are distributed over a RoI of $3 \times 3\ \mathrm{m}^2$. The RoI is a vertical wall and not a ground plane (this choice was made due to the position and orientation of the camera on the drone). The UAV follows a predefined search trajectory that is shown in Figure 4.18 and holds a fixed distance of 60 cm to the wall. At this distance, the camera of the drone covers a rectangle of $110 \times 140\,\mathrm{cm}$. The size of the effective FoV $\mathbb{F}_i(\mathbf{x}^{\mathrm{u}}_{i,k})$ is

chosen as 100×100 cm to account for positioning uncertainties. The test chamber is equipped with an Optitrack motion capture system: it consists of active IR cameras and markers that allow to obtain ground-truth values of the position, orientation and velocities of the drone. The motion capture system outputs measurements with a frequency of 100 Hz and has an accuracy of about ± 2 cm for the x, y, and z-coordinates of the drone.

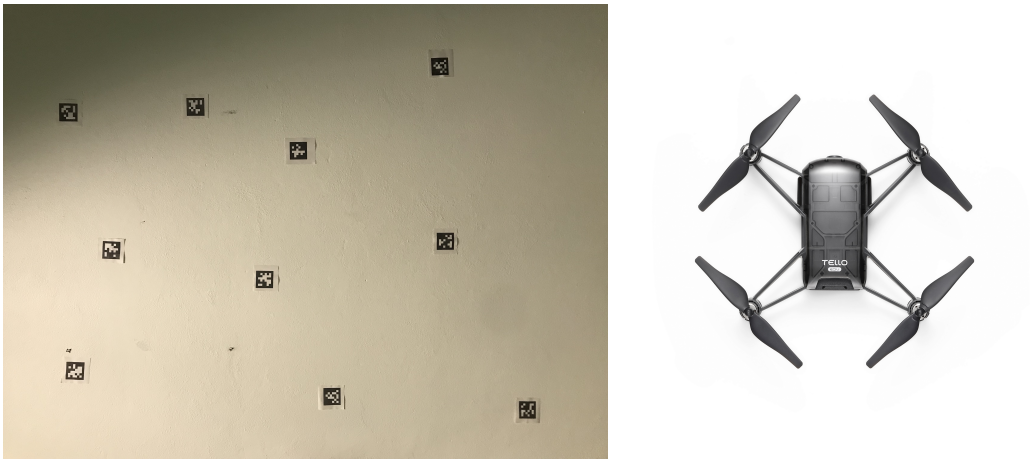

Figure 4.17.: AprilTag marker representing the targets (left) and Tello EDU drone (right)

Parameter	Value
Length(mm)	98
Width (mm)	92.5
Height (mm)	41
Weight (g)	87
Speed (m/s)	8
Max. flight time (min)	13
Camera resolution (MP)	5
Video resolution	1280×720
Frames per second	30

Table 4.1.: Specifications of the drone Tello EDU

In the experiments, the UAV collects images with an RGB camera and transmits these measurements to a stationary computer. The estimation algorithm is run on the stationary computer and implemented via the Robot Operating System (ROS) interface Quigley et al. (2009). ROS provides a structured communications layer for heterogeneous and distributed computations. Different processes (called *nodes* in ROS) can be run independently.

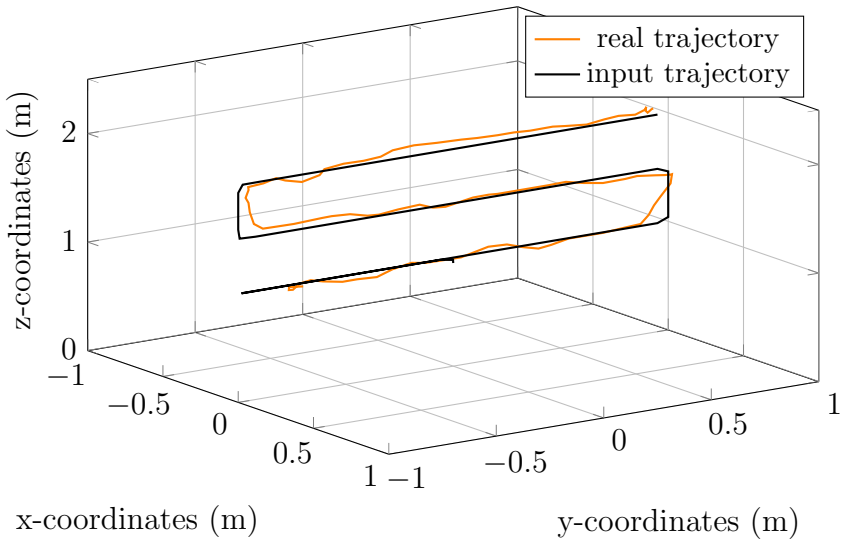

Figure 4.18.: Trajectory of the UAV

The target estimation procedure is divided into two major processes (ROS nodes) illustrated in Figure 4.19 (left). The camera of the UAV records a constant video stream that is transmitted via wireless network protocols to the stationary computer. The video stream is analyzed via the AprilTag 2 visual fiducial detection algorithm (Wang and Olson, 2016). The AprilTag detection software computes the precise 3D position, orientation, and identity of the tags relative to the camera. Its library is implemented in C with no external dependencies. It is designed to be easily included in other applications, as well as be portable to embedded devices. Real-time performance can be achieved even on cell-phone grade processors. The algorithm includes calibration scripts to setup its parameter. The pose of a detected marker is transformed from the camera frame of reference to the UAV frame and then to the global frame. For this transformation, the ground truth pose of the UAV is obtained from the Optitrack motion capture system. The AprilTag detection node has an update frequency of 30 Hz. The pose of a detected marker in the global frame is transmitted to the estimation node for the correction process of the set estimates. The estimation node has an update frequency of 1 Hz. The set estimates are represented by monochrome binary images with a resolution of 1000×1000 pixels. Consequently, the set $\mathbb{X}_0$ is discretized by the chosen resolution of the image. A single pixel represents then a square of $3 \times 3\,\mathrm{mm}^2$. This choice is made to allow fast computations of set operations. The set operations are implemented using the OpenCV library of programming functions. There are very effective numerical algorithms that allow the pixel-wise computations of unions and intersections.

Considering the control, the UAV follows a predetermined path consisting of waypoints. The waypoints are used by a guidance controller that evaluates control inputs for the UAV. This control input consists of velocities, which are used by the low-level controller of the UAV to evaluate the control input of the motors (voltages

and currents). One has no access to the design of the low level controller of the UAV. The set velocity of the UAV is chosen as 0.2 m/s and the control input of the drone in terms of velocity is bounded in $[-1, 1]$ m/s.

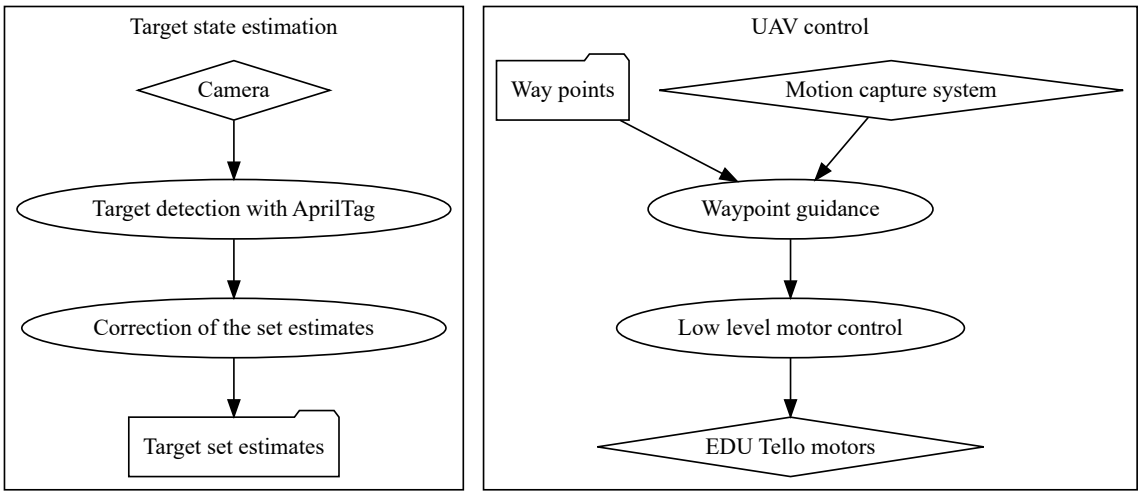

Figure 4.19.: Estimation and control processes; Illustration of the actions (diamonds), processes (ellipses) and information (folders)

In order to apply the estimation algorithm, it is necessary to determine the *a priori* noise bounds $[\mathbf{w}_{i,k}]$. These noise bounds are evaluated via experiments where the error between the estimated location of a single marker and its true location is evaluated. The estimated location is obtained from the AprilTag algorithm. The measurement noise is evaluated for a large set of UAV locations, where the UAV hovers in front of a marker. The setup is shown in Figure 4.20.

The histogram for the obtained measurement noise is shown in Figure 4.21. The measurement noise is evaluated as the signed deviation between the estimated and ground truth location of the marker. One observes that the measurement noise remains within the interval $[-3, 5]$ cm for the x-direction and $[-12, 5]$ cm for the y-direction. It seems that the noise distributions are multi modal. Future studies should analyses the noise more in detail and identify the different sources for uncertainty. Important factors that should have an impact on the measurement noise are the camera resolution and calibration, the location uncertainty of the UAV, and the lighting conditions.

The measurement noise bounds are chosen considering the Euclidean distance between the estimated and the true location of the target. The measurement noise expressed as Euclidean distance is shown in Figure 4.22. The noise bound available to the UAV for the set-membership estimator is chosen as $[0, 15]$ cm. Consequently, in the estimation process, the distance between the estimated and the true location of the target is assumed to remain in the bounds $[0, 15]$ cm, and a point measurement leads to a circular estimate with a radius of 15 cm.

Figure 4.20.: Experimental setup to estimate the noise bounds

4.6.2. Experimental results

Video sequences of the experiments are available in the folder *Videos\Chapter_4\Experiments*. The videos show the flight path of the UAV in the test chamber (*FlightTello.mp4*), the video stream of the onboard camera of the EDU Tello (*CameraTello.mp4*), and the evolution of the set estimates (*SetEstimates.mp4*). The real trajectory of the drone is also shown in Figure 4.18. A single run of the experiment takes about 100 s.

The experiment shows that the estimation algorithm runs fast enough to be used for real-time applications considering 2D location estimation of static targets. The chosen update frequency of 1 Hz of the estimation node can be maintained while the AprilTag node holds a frequency of 30 Hz.

Concerning the estimation process, one observes in the video *SetEstimates.mp4* and Figure 4.23 that the set estimates become empty. In Figure 4.23 (left), one of the detected target (green dots) is not inside the target set estimate $\mathbb{X}_{i,j,k}$ (blue area), due to previous false negative detection. Furthermore, outliers are also observed during the experiments. This indicates that the assumptions considering the absence of false negative detection and bounded measurement noise are violated. Two error sources are identified.

The first error source lies in the wireless transmission network of the video stream,

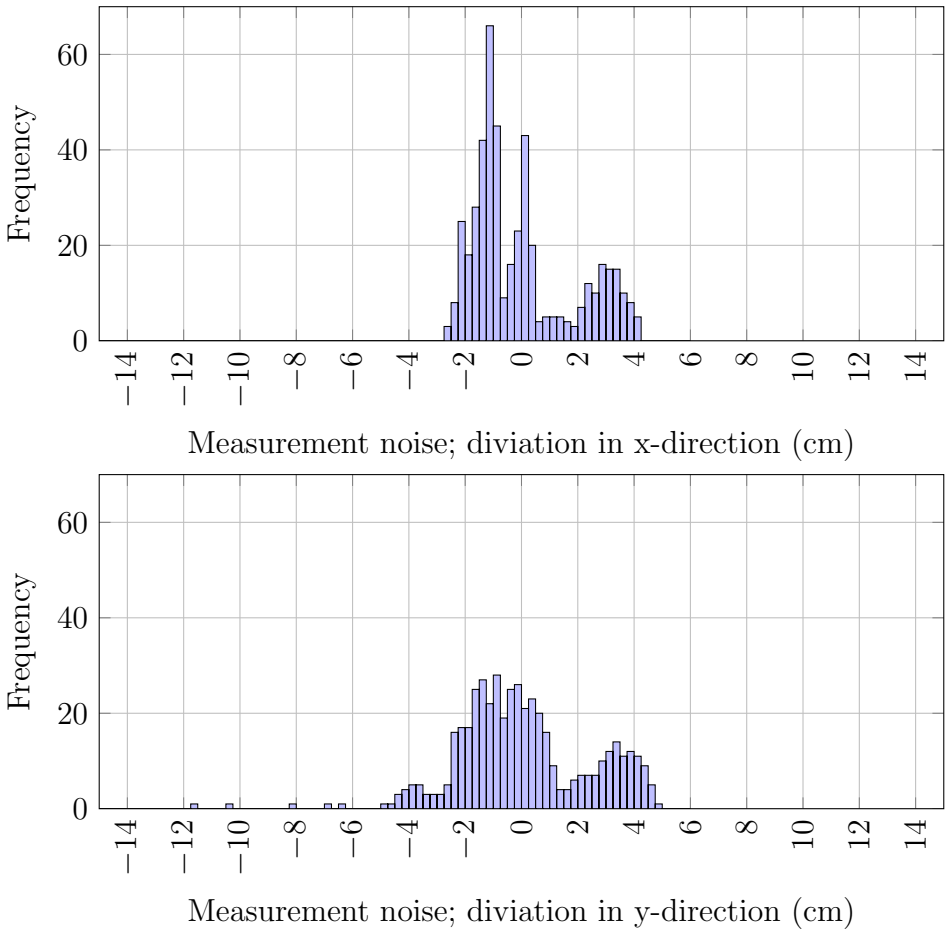

Figure 4.21.: Histogram of the measurement noise in x and y-direction.

which is not reliable and stable. Figure 4.24 shows an uncorrupted (left) and corrupted (right) image of the video stream. One observes that only some regions of the corrupted image have a high resolution, see Figure 4.24 right. The quality of other regions is strongly degraded. This disturbance might be caused by intermittent wireless network transmission and a limited bandwidth. The corrupted images may then lead to false negative detection in the AprilTag detection algorithm. A consequence is that parts of the estimates $\overline{\mathbb{X}}_{i,k}$ and $\mathbb{X}_{i,j,k}$ that contain true target locations might be removed and the locations of the targets are lost.

A second error source might be located inside the EDU Tello drone or also in the transmission network. It seems that the video stream of the camera is sometimes not updated. This means that a video frame gets stuck and is not updated over some time horizon. The same video frame is then processed repetitively by the AprilTag algorithm, which may detect the target at its old location. The problem is that the drone has already moved to a different location and the transformation function from the camera frame of reference to the global frame of reference has changed. This leads to outliers and inconsistent set estimates. This problem can

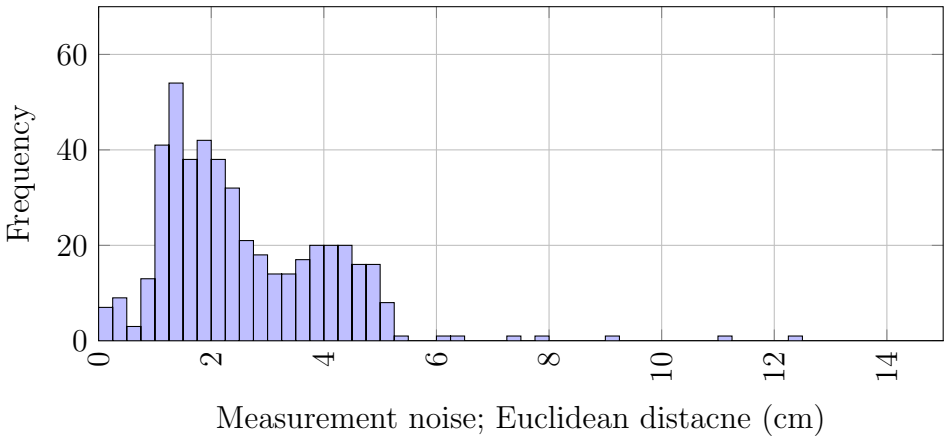

Figure 4.22.: Histogram of Euclidean distance

also be observed in Figure 4.21 where large measurement noise with an amplitude of $-12\,\mathrm{cm}$ is obtained. This outlier is probably caused by a video frame that is not updated and is outdated. A simple solution to this problem could be the enlargement of the noise bounds, however, this may not be very reasonable since the error source has a systematic nature which should be included in the measurement model.

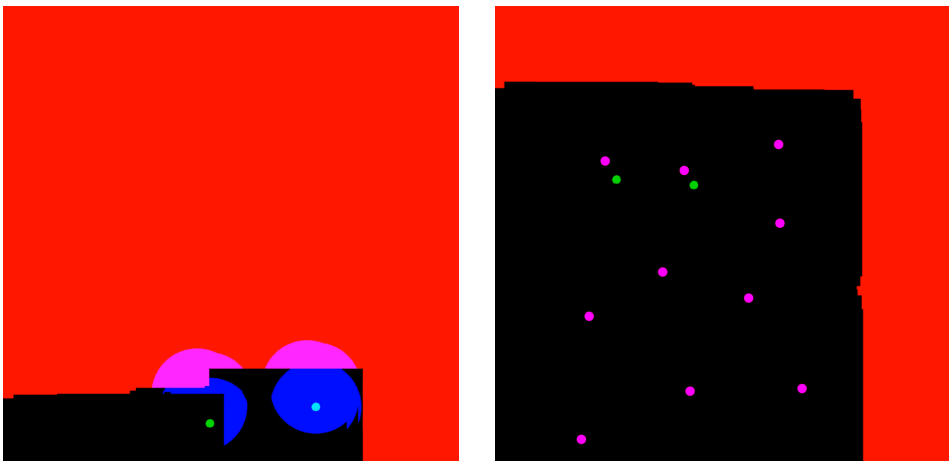

Figure 4.23.: Experimental results; RoI with set estimates $\overline{\mathbb{X}}_{i,k}$ (red), $\widetilde{\mathbb{X}}_{i,j,k}$ (black), $\mathbb{X}_{i,j,k}$ (blue), true target locations (pink dots), and detected target locations (green dots) at time $t_k = 20\,\mathrm{s}$ (left) and $t_{k'} = 90\,\mathrm{s}$ (right)

The experiments show that delayed and erroneous communication has to be considered in the estimation scheme. The transmission of a video stream is particularly problematic. An intermittent video stream can lead to erroneous measurements. A solution to this problem could be transmitting discrete time-stamped images instead of a continuous video stream. The time stamp allows to keep track of occurring delays. Alternatively, with a different type of drone, the AprilTag algorithm could

Figure 4.24.: Uncorrupted (left) and corrupted (right) camera images

be run directly onboard. This reduces the bandwidth necessary to transmit the processed information since only the locations of the drone and of detected targets need to be exchanged.

Furthermore, the experiments highlight that the estimation scheme needs to account for stochastic false negative detections for real-world applications. For an adaptation of the set-membership estimator, it may be assumed that the noise is bounded with a known probability or that the number of outliers within some time interval is limited, as suggested in the approaches in Jaulin, 2009; Drevelle and Bonnifait, 2013; Jaulin, 2011b.

The first experimental results show that real-world experiments and validations require a more elaborated estimation scheme where every error source in the measurement process is analyzed in detail. Other extension of the experiments include the online computation of optimal control input sequences to effectively reduce the target state estimation uncertainty. Additionally, it is of interest to run the complete estimation and control scheme directly on the drone. This leads to more autonomy of the drone and robustness against an intermittent communication graph. Finally, the estimation and control scheme needs to be tested for a fleet of drones. This requires an adaptation and the development of a non-synchronized estimator since the processes of the UAVs may not be synchronous. Furthermore, delayed and non-symmetric communication needs to be taken into account.

The experiments with a fleet of drones also reveal logistic challenges. Take-off and landing procedures need to be established and collision avoidance becomes inevitable. Challenges of large-scale flight operations with drones are highlighted in, *e.g.*, Chung et al., 2016. They discuss enabling technologies as well as a testbed architecture for experiments with a large number of fixed-wing aerial robots.

4.7. Conclusions and perspectives

This chapter presents a distributed set-membership approach to search and track targets using a cooperative fleet of UAVs. The presence of false targets, which may be confused with true targets, is taken into account. When a target is detected in the field of view of a UAV, it is identified as a true or false target only when observed under specific conditions. In the proposed set-membership approach, each UAV maintains several set estimates: one for each detected and identified true target, one for detected but not yet identified targets, and one for not yet detected targets. This last set estimate corresponds to the subset of the state space still to be explored. Using the information available to each UAV (provided by its sensors and information shared by its neighbors), these set estimates are updated so that, at each time step, the UAVs can have estimates as precise as possible of the states of the tracked targets.

A distributed set-membership model predictive control approach is considered for computing the trajectories of UAVs. The evolution of the set estimates for each UAV is evaluated by accounting for the impact of its own future observations and of future observations shared by its neighbors. The control inputs minimize a measure of the set-membership estimates predicted h-step ahead.

Simulation results show the efficiency of the proposed approach. The impact on its convergence of the relative speed of targets and UAVs, the number of UAVs and false targets, the communication range, and of the considered measurement noise bounds is evaluated.

In the simulation part, the UAVs were evolving at a constant altitude. Allowing UAVs to adjust their altitude is possible in the proposed framework but requires a refined model of the dependency with altitude of the detection and identification conditions and the measurement noise bounds.

Initial experimental studies show that the developed estimation scheme needs to be adapted to process real measurements that are not only noisy but also erroneous. The exact origin of all errors and uncertainties needs to be studied to derive appropriate countermeasures to make the estimator robust. Improved approaches could assume maximal numbers of errors and outliers. Furthermore, delayed communication needs to be considered for experiments with cooperating UAVs.

The presented approach accounts only for the problem where additional erroneous measurements are obtained. These erroneous measurements are modeled by considering false targets in the RoI. Further extensions should deal with the absence of measurements, *i.e.*, the potential non-detection of true targets within the field of view. The problem of *deterministic* non-detection – situations when targets are partially hidden – will be treated in the next chapter.

The presented approach in this chapter is the subject of three publications. Ibenthal et al., 2020a focuses on the problem of target search and tracking in the presence

of static false targets. Ibenthal et al., 2020b is an extension to account for moving false targets and the presence of known obstacles. Finally, Ibenthal et al., 2021a presents a generalization of the prior contributions and introduces a detailed model for deterministic detection and identification conditions for true and false targets.

5. Tracking of targets in uncertain cluttered environments

This chapter considers the cooperative search and tracking of targets by UAVs over some RoI that contains obstacles that may partly hide the targets. UAVs are not aware of the obstacle locations and cannot determine when an obstacle limits their Field of View (FoV). In the presented approaches, no map of the RoI is built, which makes it difficult to select an appropriate point of view to observe a specific part of the RoI. Showing the absence of a target at a given location of the RoI is then challenging. To address this problem, the notion of detectability sets for each point of the RoI is used, which is the set of all UAV locations from where that point is visible (notion introduced in Section 3.5). The detectability sets are unknown to the UAVs and evolve with time when the environment is time-varying. It is assumed that each detectability set contains at least one half-cone with a minimal aperture, which translates the fact that targets are never fully occluded by the environment. It is proved that a finite number of observations is sufficient to guarantee the presence or absence of targets at a given location.

Assuming again that state perturbations and measurement noises are bounded, a distributed set-membership estimator is used to evaluate set estimates for potential target locations. The trajectories of the UAVs are designed using a model predictive control approach to reduce the estimation uncertainty. Simulations illustrate the performance of the proposed approaches in the presence of unknown static and moving obstacles.

5.1. Introduction

The applications of cooperating fleets of UAVs to address CSAT of targets is particularly challenging in uncharted environments when the targets may be partially hidden by some obstacles. Classical approaches try to build a map of the environment during the CSAT of targets, and partial occlusions of targets are usually modeled via probabilities of non-detection.

This chapter considers an alternative approach to address the CSAT problem and model partial occlusions. UAVs do not try to build any map of the possibly evolving environment. This avoids frequent and resource-consuming map updates. Besides, it is not necessary to assume that UAVs are able to perceive the obstacles and to

exploit this information, which is particularly relevant in some situations, such as night observations when the contrast of the environment diminishes when using RGB or infrared cameras (Ren et al., 2018). Moreover, the ability of a UAV to detect a target depends on the location of the target and on the point of view of the UAV (both should be in the line of sight). Consequently, inspired by Pan et al. (2017), deterministic geometric target detectability conditions are used, as introduced in Section 3.5, in place of the widely-used probability of detection/non-detection as in, *e.g.*, Ur-Rehman et al. (2015).

To address this problem, L non-overlapping *conic observation subsets* of points of view are introduced for each location of the RoI. It is assumed that one of these conic subsets is included in the detectability set associated to each location of the RoI. Under this hypothesis, it is possible to guarantee that a location is free from a target when observed from L different points of view, each belonging to a different observation subset.

Based on this hypothesis, two distributed set-membership estimators are proposed that are able to provide set estimates guaranteed to contain the location of all the targets within the RoI. The first estimator allows the search of static targets in a static environment. The second estimator allows the search and tracking of moving targets in a changing environment. The estimators can be applied in a distributed UAV network. Each evaluates target locations accounting for its own measurements and for information received during communications with other UAVs. The control input for each UAV is designed using a distributed set-membership MPC approach, which aims at minimizing a measure of estimation uncertainty. The controller accounts for the impact of future measurements on the set estimates and infers future information communicated by neighbors.

The chapter is organized as follows. The considered problem and hypotheses are stated in Section 5.2. Section 5.3 presents a solution for the special case of the search of static targets in a unchanging environment. Then a solution for the search and tracking of moving targets in a changing environment is proposed in Section 5.4.

5.2. Hypotheses and problem formulation

Consider again a fleet of N^{u} UAVs searching and tracking an unknown number N^{t} of targets which are moving within a bounded RoI $\mathbb{X}_0$. The targets are distinguishable with identifiers belonging to the list $\mathcal{N}^{\mathrm{t}} = \{1, \ldots, N^{\mathrm{t}}\}$. In this chapter, it is assumed that the targets are always identified to simplify the presentation of the set-membership state estimator. Consequently, the condition $g_j^{\mathrm{t}}\left(\mathbf{x}_{i,k}^{\mathrm{u}}, \mathbf{x}_{j,k}^{\mathrm{t}}\right) \geqslant 0$ is always satisfied when $\mathbf{x}_{j,k}^{\mathrm{t}} \in \mathbb{F}_i\left(\mathbf{x}_{i,k}^{\mathrm{u}}\right)$ and a measurement $\mathbf{y}_{i,j,k}^{\mathrm{I}}$ is always obtained when target j is detected. Set $\mathbf{y}_{i,j,k} = \mathbf{y}_{i,j,k}^{\mathrm{I}}$ and $\mathcal{D}_{i,k} = \mathcal{D}_{i,k}^{\mathrm{I}}$ to simplify notations. Furthermore, it is assumed that no false targets are present in the RoI, *i.e.*, $N^{\mathrm{f}} = 0$.

The RoI is uncharted and contains unknown obstacles which may partially hide the targets. Consequently, the set $\mathbb{X}_k^{\mathrm{T}}$ (introduced in Equation 3.3) is *a priori* not known by the UAVs. The obstacles will be only static (*e.g.,* buildings) in Section 5.3 and may be static or moving (*e.g.,* buildings, cars, buses) in Section 5.4. Each UAV possesses a sensing system (*e.g.,* camera-based computer vision system) capable of detecting targets within the part of its FoV not limited by any obstacles, *i.e.*, targets in $\mathbb{F}_i^{\mathrm{D}}\left(\mathbf{x}_{i,k}^{\mathrm{u}}\right)$ (introduced in Equation 3.7) are always detected, however, $\mathbb{F}_i^{\mathrm{D}}\left(\mathbf{x}_{i,k}^{\mathrm{u}}\right)$ is not available to the UAVs.

Table 5.1 summarizes additional notations used in this chapter, some of them are introduced later.

Variable	Definition
$\mathbb{C}_\ell(\boldsymbol{x})$	Induced conic observation subsets ℓ with apex $\boldsymbol{x}$
$\mathcal{D}_{i,k} = \mathcal{D}_{i,k}^{\mathrm{I}}$	List of detected and identified targets by UAV i at time t_k
$\mathbb{F}_{i,\ell}(\mathbf{x}_{i,k}^{\mathrm{u}})$	FoV subset observed satisfying $\mathbf{x}_{i,k}^{\mathrm{u}} \in \mathbb{C}_\ell(\boldsymbol{x})$
$\underline{\mathbb{F}}(\mathcal{G}_{g,k})$	Completely observed set of group g at time t_k
$\overline{\mathbb{F}}(\mathcal{G}_{g,k})$	Partially observed set of group g at time t_k
$\mathcal{G}_{g,k}$	Set of UAV state vectors of group g at time t_k
i_g	Index of the leader of group g
N^{g}	Number of groups
$\mathcal{N}^{\mathrm{g}}$	List of groups indices
$\mathcal{N}_g$	List of UAV indices forming group g
$\mathcal{N}_{g,k}^{\mathrm{g}}$	List of groups connected to group g at time t_k
$\mathbb{S}_{g,j,k}$	Set estimate of target j from measurements
$\mathbf{y}_{i,j,k} = \mathbf{y}_{i,j,k}^{\mathrm{I}}$	Measurement of the identified true target $j \in \mathcal{D}_{i,k}$

Table 5.1.: Additional notations

5.2.1. Hypotheses on the detectability set

It is assumed that the reduced data processing capability of the sensing devices does not allow UAVs to characterize $\mathbb{D}_k(\boldsymbol{x})$. UAVs are thus unable to determine whether target occlusions occur. Figure 5.1 shows a simple box-shaped (left) and bridge-shaped (right) obstacle. The resulting detectability set $\mathbb{D}_k(\boldsymbol{x}) \subset \mathbb{R}^3$ (in red and gray) is illustrated for a point $\boldsymbol{x} = p^{\mathrm{t}}(\mathbf{x})$ (in blue), where $\mathbf{x} \in \mathbb{X}_k^{\mathrm{T}}$.

As seen in Figure 5.1 the shape of $\mathbb{D}_k(\boldsymbol{x})$ may be complex even for simple box-shaped obstacles (left). Therefore, a conic inner approximation of each $\mathbb{D}_k(\boldsymbol{x})$ is introduced to facilitate the characterization of the detectability set. For all locations $\boldsymbol{x} = p^{\mathrm{t}}(\mathbf{x})$, $\mathbf{x} \in \mathbb{X}_k^{\mathrm{T}}$ it is assumed that there are $n(\boldsymbol{x}) \geqslant 3$ unit vectors $\boldsymbol{v}_{1,k}(\boldsymbol{x}) \in$

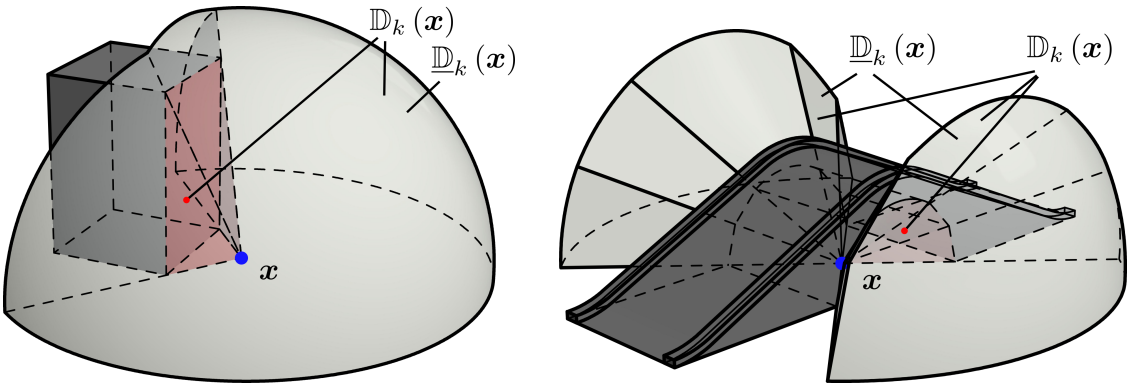

Figure 5.1.: Detectability set $\mathbb{D}_k(\boldsymbol{x}) \subset \mathbb{R}^3$ (red and gray) for a point $\boldsymbol{x} = p^{\mathrm{t}}(\mathbf{x})$ (blue), $\mathbf{x} \in \mathbb{X}_k^{\mathrm{T}}$, located close to a box-shaped (left) and a bridge-shaped (right) obstacle; The set $\underline{\mathbb{D}}_k(\boldsymbol{x})$ is the gray subset of $\mathbb{D}_k(\boldsymbol{x})$.

$\mathbb{R}^3, \ldots, \boldsymbol{v}_{n(\boldsymbol{x}),k}(\boldsymbol{x}) \in \mathbb{R}^3$ defining a half-cone of non-zero volume with apex $\boldsymbol{x}$, *i.e.*,

$$\underline{\mathbb{D}}_k(\boldsymbol{x}) = \{\boldsymbol{x} + a_1 \boldsymbol{v}_{1,k}(\boldsymbol{x}) + \cdots + a_{n(\boldsymbol{x})} \boldsymbol{v}_{n(\boldsymbol{x}),k}(\boldsymbol{x}) \mid a_i \in \mathbb{R}^+, i = 1, \ldots, n(\boldsymbol{x})\}, \quad (5.1)$$

such that $\underline{\mathbb{D}}_k(\boldsymbol{x}) \subset \mathbb{D}_k(\boldsymbol{x})$. Note that, to account for more complex environments, $\underline{\mathbb{D}}_k(\boldsymbol{x})$ may also consist of a union of several half-cones with the same apex $\boldsymbol{x}$ or of the intersection of a cone and a sphere centered in $\boldsymbol{x}$. In Figure 5.1, $\underline{\mathbb{D}}_k(\boldsymbol{x})$ consists of unions of cones. The red dot highlight the part of $\mathbb{D}_k(\boldsymbol{x})$ that does not belong to $\underline{\mathbb{D}}_k(\boldsymbol{x})$.

5.2.2. Measurements

At time t_k, let $\mathcal{D}_{i,k}$ be the set of indexes of targets detected by UAV i. When condition (3.6) is satisfied then target j is detected and also directly identified. Consequently,

$$j \in \mathcal{D}_{i,k} \iff \boldsymbol{x}_{j,k}^{\mathrm{t}} \in \mathbb{F}_i\left(\mathbf{x}_{i,k}^{\mathrm{u}}\right) \text{ and } \boldsymbol{x}_{i,k}^{\mathrm{u}} \in \mathbb{D}_k\left(\boldsymbol{x}_{j,k}^{\mathrm{t}}\right). \quad (5.2)$$

As previously assumed, UAV i is able to obtain a noisy observation of the state of each detected target $j \in \mathcal{D}_{i,k}$ as

$$\mathbf{y}_{i,j,k} = \mathbf{h}_i\left(\mathbf{x}_{i,k}^{\mathrm{u}}, \mathbf{x}_{j,k}^{\mathrm{t}}\right) + \mathbf{w}_{i,j,k}. \quad (5.3)$$

5.2.3. Problem formulation

In this chapter, the targets are always identified when detected and one has $\mathbb{X}_{i,k}^{\mathrm{U}} = \emptyset$. Consequently, only the target set estimate $\mathbb{X}_{i,j,k}$, containing all possible locations

of the detected targets that are consistent with $\mathbb{I}_{i,k}$, and the unexplored set $\overline{\mathbb{X}}_{i,k}$, containing the possible locations of targets not yet detected, are considered.

At time t_k, for UAV i, the target state estimation uncertainty accounts for all sets in which a target may be located, *i.e.*, in $\mathbb{X}_{i,j,k}$, when $j \in \mathcal{L}_{i,k}$, or in $\overline{\mathbb{X}}_{i,k}$, when $j \notin \mathcal{L}_{i,k}$. To evaluate the estimation uncertainty, a measure of the set $(\bigcup_{j\in\mathcal{L}_{i,k}} \mathbb{X}_{i,j,k}) \cup \overline{\mathbb{X}}_{i,k}$ is considered in order not to account for potential target locations twice, for example when $\mathbb{X}_{i,j,k} \cap \overline{\mathbb{X}}_{i,k} \neq \emptyset$. Consequently, at time t_k and for UAV i, the estimation uncertainty of all target locations is evaluated as $\Phi\left(\mathcal{X}_{i,k}, \mathbb{X}^{\mathrm{U}}_{i,k}, \overline{\mathbb{X}}_{i,k}\right)$, where $\mathbb{X}^{\mathrm{U}}_{i,k} = \emptyset$. Thus, the estimation uncertainty

$$\Phi\left(\mathcal{X}_{i,k}, \overline{\mathbb{X}}_{i,k}\right) = \phi\left(\left(\bigcup_{j\in\mathcal{L}^{\mathrm{t}}_{i,k}} \mathbb{X}_{i,j,k}\right) \cup \overline{\mathbb{X}}_{i,k}\right) \tag{5.4}$$

is introduced, which is consistent with (3.19). The average among the UAVs of the estimation uncertainties at time t_k is

$$\overline{\Phi}_k = \frac{1}{N^{\mathrm{u}}} \sum_{i=1}^{N^{\mathrm{u}}} \Phi\left(\mathcal{X}_{i,k}, \overline{\mathbb{X}}_{i,k}\right). \tag{5.5}$$

The aim is to evaluate sequences of control inputs for UAVs that minimize the estimation uncertainty $\overline{\Phi}_k$ as much as possible. The main difficulty compared to Chapter 4 comes from potential non-detection of *moving* targets due to the presence of *moving* unknown obstacles. The possibility of non-detection of a partially hidden target makes it difficult to prove the absence of a target at a given location and thus also to reduce the size of $\overline{\mathbb{X}}_{i,k}$. Section 5.3 presents a first solution to the special case of *static* targets and *static* unknown obstacles. The solution is then extended in Section 5.4 to the case of *moving* targets and *moving* unknown obstacles.

5.3. Special case – Time-invariant detectability set

Scene 13:

Imagine a fleet of UAVs searching for parked cars in an urban environment. The difficulty that the UAVs encounter is that the cars may be hidden behind some building or trees. To overcome this problem the UAVs may collect several observations from the same area but from different points of view. This may then lead to the detection of a car that is present in this area. The minimum number of different points of view needed to observe surely a point of the RoI depends on the environment, such as the size of the buildings, design of the streets, or the parking areas. It is much easier for the UAVs to select an appropriate point of view of observation if the UAVs could map the environment. When a map is available, the UAVs can evaluate if a parking area is visible or not. Nevertheless, this may not be possible if the sensing and processing capabilities of the UAVs are limited. The following approach presents a solution to the problem where the environment can not be mapped.

Considering Scene 13, this section presents a solution to the simplified problem of detecting partially hidden targets. It is assumed that targets and obstacles are static, *i.e.*, $\mathbf{x}^{\mathrm{t}}_{j,k} = \mathbf{x}^{\mathrm{t}}_{j,0}$, $\mathcal{O}_{m,k} = \mathcal{O}_{m,0}$, and $\mathbb{D}_k\left(p^{\mathrm{t}}(\mathbf{x})\right) = \mathbb{D}_0\left(p^{\mathrm{t}}(\mathbf{x})\right)$, $\forall k$ and $\forall \mathbf{x} \in \mathbb{X}^{\mathrm{T}}_0$. To simplify the notations, set $\mathbf{x}^{\mathrm{t}}_j = \mathbf{x}^{\mathrm{t}}_{j,0}$, $\boldsymbol{x}^{\mathrm{t}}_j = \boldsymbol{x}^{\mathrm{t}}_{j,0}$, $\mathbb{X}^{\mathrm{T}} = \mathbb{X}^{\mathrm{T}}_0$, $\mathbb{D}\left(\boldsymbol{x}\right) = \mathbb{D}_0\left(\boldsymbol{x}\right)$, and $\underline{\mathbb{D}}\left(p^{\mathrm{t}}(\mathbf{x})\right) = \underline{\mathbb{D}}_0\left(p^{\mathrm{t}}(\mathbf{x})\right)$, $\mathbf{x} \in \mathbb{X}^{\mathrm{T}}$.

The proposed solution is described in Section 5.3.1. Sections 5.3.2 and 5.3.3 present the distributed estimator and the design of the associated cooperative control strategy respectively. Section 5.3.4 introduces simulation examples illustrating the performance obtained with a fleet of UAVs. The results presented in this section are published in Ibenthal et al. (2021b).

5.3.1. Proposed solution

Consider a generic UAV with state $\mathbf{x}^{\mathrm{u}}$ and location $\boldsymbol{x}^{\mathrm{u}} = p\left(\mathbf{x}^{\mathrm{u}}\right)$ as well as a generic target with state $\mathbf{x}^{\mathrm{t}}$ and located at $\boldsymbol{x}^{\mathrm{t}} = p^{\mathrm{t}}(\mathbf{x}^{\mathrm{t}})$. Indices are omitted to lighten notations. According to the target detection model (5.2), the target is not detected when $\boldsymbol{x}^{\mathrm{u}} \notin \mathbb{D}\left(\boldsymbol{x}^{\mathrm{t}}\right)$ even if $\mathbf{x}^{\mathrm{t}}$ satisfies $\mathbf{x}^{\mathrm{t}} \in \mathbb{F}\left(\mathbf{x}^{\mathrm{u}}\right)$. The target is detected only if $\mathbf{x}^{\mathrm{t}} \in \mathbb{F}\left(\mathbf{x}^{\mathrm{u}}\right)$ *and* $\boldsymbol{x}^{\mathrm{u}} \in \mathbb{D}\left(\boldsymbol{x}^{\mathrm{t}}\right)$.

Consequently, one can conclude that there is no target located at $\boldsymbol{x} = p^{\mathrm{t}}(\mathbf{x})$ if several conditions are fulfilled. First, one must collect an observation $\mathbb{F}\left(\mathbf{x}^{\mathrm{u}}\right)$ from a UAV with state $\mathbf{x}^{\mathrm{u}}$ such that $\mathbf{x} \in \mathbb{F}\left(\mathbf{x}^{\mathrm{u}}\right)$. Second, from the observation $\mathbb{F}\left(\mathbf{x}^{\mathrm{u}}\right)$, the UAV must not detect a target with state $\mathbf{x}$. Third, the UAV location $\boldsymbol{x}^{\mathrm{u}}$ must satisfy $\boldsymbol{x}^{\mathrm{u}} \in \mathbb{D}\left(\boldsymbol{x}\right)$. If these three conditions are satisfied then there is no target located at $\boldsymbol{x}$. For a UAV, determining whether $\mathbf{x} \in \mathbb{F}\left(\mathbf{x}^{\mathrm{u}}\right)$ is easy, however, determining whether $\boldsymbol{x}^{\mathrm{u}} \in \mathbb{D}\left(\boldsymbol{x}\right)$ is impossible, since $\mathbb{D}\left(\boldsymbol{x}\right)$ is not available to that UAV.

It is assumed that the set $\underline{\mathbb{D}}(\boldsymbol{x}) \subset \mathbb{D}(\boldsymbol{x})$ is of non-zero volume. This means that there will always exist a location from where the target can be detected. Consequently, provided that $\boldsymbol{x}$ is observed from a sufficiently large but *finite* number L of different observation locations, one will prove that there exists at least one of these observation locations, $\boldsymbol{x}^{\mathrm{u}}$, such that $\boldsymbol{x}^{\mathrm{u}} \in \underline{\mathbb{D}}(\boldsymbol{x})$.

In Section 5.3.1.1, for each $\boldsymbol{x} = p^{\mathrm{t}}(\mathbf{x})$, $\mathbf{x} \in \mathbb{X}^{\mathrm{T}}$, L conic observation subsets are introduced and it is assumed that at least one of these subsets is included in $\mathbb{D}(\boldsymbol{x})$. Choosing L sufficiently large ensures that at least one of these subsets is included in $\mathbb{D}(\boldsymbol{x})$ for all $\boldsymbol{x} = p^{\mathrm{t}}(\mathbf{x})$, $\mathbf{x} \in \mathbb{X}_{\mathrm{T}}$. It is then possible to state that there is no target at location $\boldsymbol{x}$ provided that $\boldsymbol{x}$ has been observed from a location in each of the L conic observation subsets and that no target has been detected. Section 5.3.1.2 introduces L subsets of locations where no target has been detected. To account for the points of view from which the locations have been observed, each of these subsets is associated to one of the L conic observation subsets. Finally, an adapted estimation uncertainty is defined in Section 5.3.1.3, which states the target detection problem for static targets more formally.

5.3.1.1. Conic observation subsets

Consider L non-zero volume half-cones $\mathbb{C}_\ell(\mathbf{O}) \in \mathbb{R}^3$, $\ell = 1, \ldots, L$ with apex $\mathbf{O}$. Each half-cone $\mathbb{C}_\ell(\mathbf{O})$ is defined by a set of n_ℓ unit-norm vectors $\boldsymbol{v}_{\ell,1} \in \mathbb{R}^3, \ldots, \boldsymbol{v}_{\ell,n_\ell} \in \mathbb{R}^3$, such that

$$\mathbb{C}_\ell(\mathbf{O}) = \left\{ a_1 \boldsymbol{v}_{\ell,1} + \cdots + a_{n_\ell} \boldsymbol{v}_{\ell,n_\ell} \mid a_m \in \mathbb{R}^+, m = 1, \ldots, n_\ell \right\}. \tag{5.6}$$

Figure 5.2 illustrates $L = 8$ half-cones with their apex $\mathbf{O}$ realizing a partition of the half space $x_3 \geqslant 0$ from which $\mathbf{O}$ can be observed. Considering only a partition of the half space $x_3 \geqslant 0$ is reasonable when the targets evolve beneath of the UAVs or when the targets are evolving on the ground. When the targets are on the ground they can never be detected from a UAV location underground, $x_3 < 0$. Which is also not feasible for the UAVs.

Considering the half-cones $\mathbb{C}_\ell(\mathbf{O})$, $\ell = 1, \ldots, L$, one introduces for all $\boldsymbol{x} \in \mathbb{R}^3$ the translated half-cones $\mathbb{C}_\ell(\boldsymbol{x})$, $\ell = 1, \ldots, L$, of apex $\boldsymbol{x}$ such that

$$\boldsymbol{x}' \in \mathbb{C}_\ell(\boldsymbol{x}) \Leftrightarrow \boldsymbol{x}' - \boldsymbol{x} \in \mathbb{C}_\ell(\mathbf{O}), \tag{5.7}$$

where $\boldsymbol{x}' \in \mathbb{R}^3$ is any potential location of a UAV. The half-cones $\mathbb{C}_\ell(\boldsymbol{x})$, $\ell = 1, \ldots, L$, are named *conic observation subsets* of $\boldsymbol{x}$ hereafter. The mean of the vectors $\boldsymbol{v}_{\ell,1}, \ldots, \boldsymbol{v}_{\ell,n_\ell}$

$$\overline{\boldsymbol{v}}_\ell^{\mathrm{c}} = \left(\sum_{m=1,\ldots,n_\ell} \boldsymbol{v}_{\ell,m} \right) \Big/ \left\| \sum_{m=1,\ldots,n_\ell} \boldsymbol{v}_{\ell,m} \right\|, \tag{5.8}$$

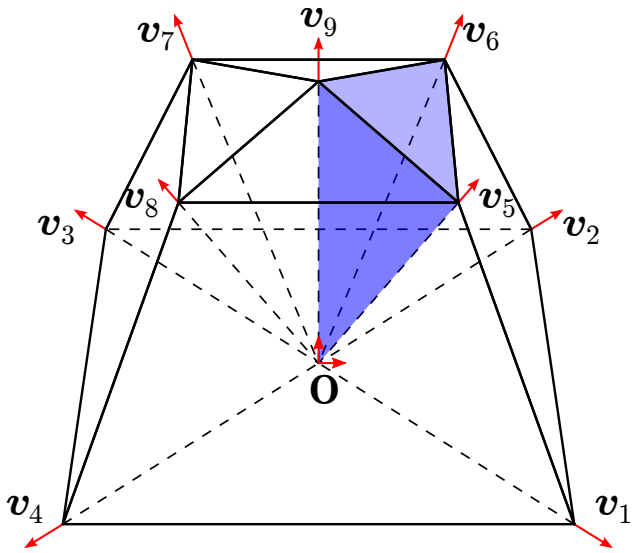

Figure 5.2.: Conic observation subsets: partition in $L = 8$ cones of the set of points of view for $\mathbf{O}$ with $x_3 \geqslant 0$; the cone $\mathbb{C}_1(\mathbf{O})$ is shown in blue; its $n_1 = 3$ vertices are $\boldsymbol{v}_5$, $\boldsymbol{v}_6$, and $\boldsymbol{v}_9$.

represents the orientation of the cones $\mathbb{C}_\ell(\mathbf{O})$ and $\mathbb{C}_\ell(\boldsymbol{x})$.

For all $\boldsymbol{x} = p^{\mathrm{t}}(\mathbf{x})$, $\mathbf{x} \in \mathbb{X}^{\mathrm{T}}$, it is assumed that the half-cones $\mathbb{C}_1(\boldsymbol{x}), \ldots, \mathbb{C}_L(\boldsymbol{x})$ are such that

$$\exists \ell \in \{1, \ldots, L\}, \mathbb{C}_\ell(\boldsymbol{x}) \subset \underline{\mathbb{D}}(\boldsymbol{x}), \tag{5.9}$$

i.e., for every possible target location $\boldsymbol{x} = p^{\mathrm{t}}(\mathbf{x})$, $\mathbf{x} \in \mathbb{X}^{\mathrm{T}}$, there exists a half-cone $\mathbb{C}_\ell(\boldsymbol{x})$ included in $\underline{\mathbb{D}}(\boldsymbol{x})$, and thus also included in $\mathbb{D}(\boldsymbol{x})$.

Assumption (5.9) is essential in the proposed approach. It translates the fact that a target is never fully occluded by obstacles and my be visible by a UAV located in one of the conic observation subsets. Some insight on the choice of L and $\mathbb{C}_1(\boldsymbol{x}), \ldots, \mathbb{C}_L(\boldsymbol{x})$ is provided in Section 5.4.4.1.

Figure 5.3 illustrates Assumption (5.9) for the detectability set $\mathbb{D}(\boldsymbol{x})$ (light gray), its inner approximation $\underline{\mathbb{D}}(\boldsymbol{x})$ (green cone), and the cone $\mathbb{C}_{\ell'}(\boldsymbol{x})$ (blue cone), satisfying $\mathbb{C}_{\ell'}(\boldsymbol{x}) \subset \underline{\mathbb{D}}(\boldsymbol{x})$. The illustrated inner approximation $\underline{\mathbb{D}}(\boldsymbol{x})$ is and example for a possible choice of $\underline{\mathbb{D}}(\boldsymbol{x})$. One observes that $\mathbb{C}_{\ell'}(\boldsymbol{x})$ is included in $\underline{\mathbb{D}}(\boldsymbol{x})$ and that $\underline{\mathbb{D}}(\boldsymbol{x})$ is included in $\mathbb{D}(\boldsymbol{x})$.

When $\mathbb{D}(\boldsymbol{x})$ consists of the intersection of one or several cones with a sphere, one should consider observation subsets consisting of the intersection of a cone with a sphere. The radius of this sphere should be smaller than the radius of the spheres considered in $\underline{\mathbb{D}}(\boldsymbol{x})$ for all $\boldsymbol{x} = p^{\mathrm{t}}(\mathbf{x})$, $\mathbf{x} \in \mathbb{X}^{\mathrm{T}}$.

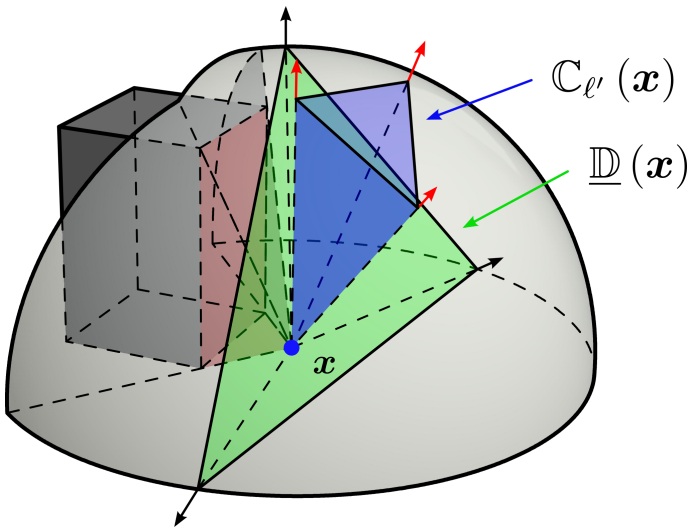

Figure 5.3.: Detectability set $\mathbb{D}(\boldsymbol{x})$ (light gray), its inner approximation $\underline{\mathbb{D}}(\boldsymbol{x})$ (green cone), and the cone $\mathbb{C}_{\ell'}(\boldsymbol{x})$ (blue cone), satisfying $\mathbb{C}_{\ell'}(\boldsymbol{x}) \subset \underline{\mathbb{D}}(\boldsymbol{x})$.

5.3.1.2. Subsets of the FoV

Scene 14:

An UAV observes a potential car location and does not detect a car. The UAV should now store the information that this zone was observed with a specific point of view. This is not that simple since almost every point within the observed zone is observed from a different point of view, i.e., *there are infinite lines of sight connecting the UAV with all the points within the observed zone. Hereafter, to simplify the storage of this information, the FoV of the UAV will be partitioned depending on discretized points of view.*

To formalize the idea described in Scene 14, consider the state $\mathbf{x}_{i,k}^{\mathrm{u}}$ of UAV i at time t_k and its FoV $\mathbb{F}_i(\mathbf{x}_{i,k}^{\mathrm{u}})$. The conic observation subsets $\mathbb{C}_1(\boldsymbol{x}), \ldots, \mathbb{C}_L(\boldsymbol{x})$ introduced in Section (5.3.1.1) induce a subdivision of the FoV $\mathbb{F}_i(\mathbf{x}_{i,k}^{\mathrm{u}})$ into the following subsets

$$\mathbb{F}_{i,\ell}\left(\mathbf{x}_{i,k}^{\mathrm{u}}\right) = \left\{\mathbf{x} \in \mathbb{F}_i\left(\mathbf{x}_{i,k}^{\mathrm{u}}\right) \mid \boldsymbol{x}_{i,k}^{\mathrm{u}} \in \mathbb{C}_\ell(\boldsymbol{x}), \boldsymbol{x} = p^{\mathrm{t}}(\mathbf{x})\right\}, \tag{5.10}$$

$\ell \in \{1, \ldots, L\}$. $\mathbb{F}_{i,\ell}(\mathbf{x}_{i,k}^{\mathrm{u}})$ is the subset of states $\mathbf{x}$ observed from the point of view $\boldsymbol{x}_{i,k}^{\mathrm{u}} \in \mathbb{C}_\ell(\boldsymbol{x})$, where $\boldsymbol{x} = p^{\mathrm{t}}(\mathbf{x})$. If $\boldsymbol{x}_{i,k}^{\mathrm{u}} \notin \mathbb{C}_\ell(\boldsymbol{x})$ for all $\mathbf{x} \in \mathbb{F}_i\left(\mathbf{x}_{i,k}^{\mathrm{u}}\right)$, with $\boldsymbol{x} = p^{\mathrm{t}}(\mathbf{x})$, then $\mathbb{F}_{i,\ell}(\mathbf{x}_{i,k}^{\mathrm{u}}) = \emptyset$.

Figure 5.4 provides an example of $L = 8$ conic observation subsets $\mathbb{C}_1, \ldots, \mathbb{C}_8$ and of the intersection with a horizontal plane of the induced subsets $\mathbb{F}_{i,1}(\mathbf{x}_{i,k}^{\mathrm{u}}), \ldots, \mathbb{F}_{i,8}(\mathbf{x}_{i,k}^{\mathrm{u}})$ of the FoV $\mathbb{F}_i(\mathbf{x}_{i,k}^{\mathrm{u}})$ for two different values of the states $\mathbf{x}_{i,k}^{\mathrm{u}}$ of UAV i. Since $\mathbb{C}_1, \ldots, \mathbb{C}_8$ are not overlapping, a point $\boldsymbol{x} \in \mathbb{F}_i(\mathbf{x}_{i,k}^{\mathrm{u}})$ can only belong to a single set $\mathbb{F}_{i,\ell}(\mathbf{x}_{i,k}^{\mathrm{u}})$. In this example, the subsets $\mathbb{F}_{i,\ell}(\mathbf{x}_{i,k}^{\mathrm{u}})$, $\ell \in \{1, 6, 7, 8\}$ are empty, see

Figure 5.4 (left).

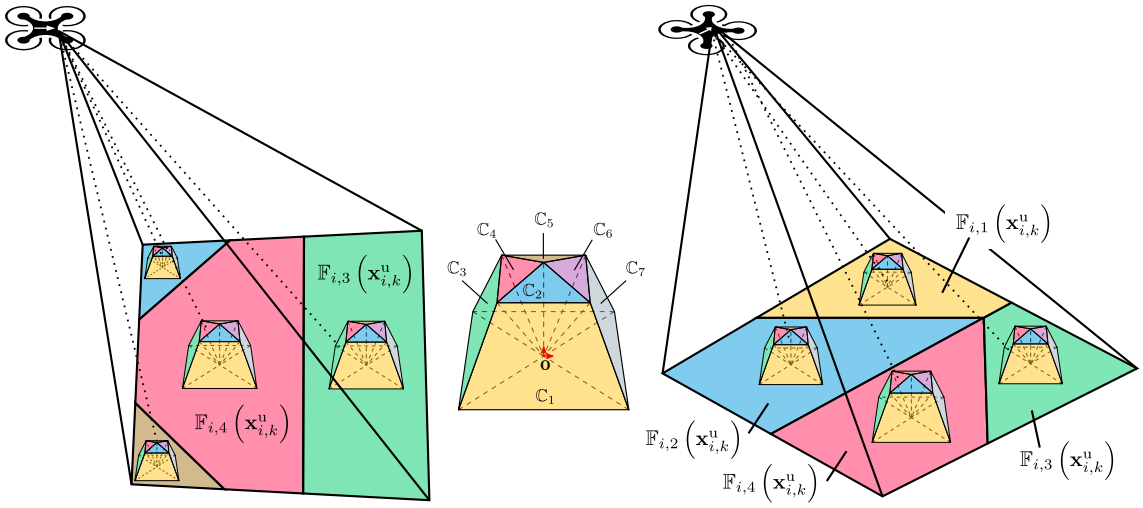

Figure 5.4.: Subsets of the FoV: conic observation subsets $\mathbb{C}_1, \ldots, \mathbb{C}_8$ and intersection with a horizontal plane of the induced subsets $\mathbb{F}_{i,1}(\mathbf{x}^{\mathrm{u}}_{i,k}), \ldots, \mathbb{F}_{i,8}(\mathbf{x}^{\mathrm{u}}_{i,k})$ of the FoV $\mathbb{F}_i(\mathbf{x}^{\mathrm{u}}_{i,k})$ for two different values of the state $\mathbf{x}^{\mathrm{u}}_{i,k}$ of UAV i.

Processing the information available from $\mathbb{F}_i(\mathbf{x}^{\mathrm{u}}_{i,k})$ at time t_k, one gets the list of detected targets $\mathcal{D}_{i,k}$ and a measurement $\mathbf{y}_{i,j,k}$ for each $j \in \mathcal{D}_{i,k}$. Using (5.2) and (5.3), one can conclude that no target is detected at position $\boldsymbol{x}$ when observed from a location $\boldsymbol{x}^{\mathrm{u}}_{i,k} = p^{\mathrm{u}}(\mathbf{x}^{\mathrm{u}}_{i,k})$ belonging to $\mathbb{C}_\ell(\boldsymbol{x})$ either when $\mathcal{D}_{i,k} = \emptyset$ or when $\forall j \in \mathcal{D}_{i,k}, \mathbf{h}_i(\mathbf{x}^{\mathrm{u}}_{i,k}, \boldsymbol{x}) \notin [\mathbf{y}_{i,j,k}]$, where $[\mathbf{y}_{i,j,k}] = \mathbf{y}_{i,j,k} - [\mathbf{w}_i]$. The latter condition indicates that the candidate target location $\boldsymbol{x}$ is not consistent with the measurement $\mathbf{y}_{i,j,k}$, the measurement function $\mathbf{h}_i$, and the noise bound $[\mathbf{w}_i]$. From these conditions, introduce

$$c_\ell\left(\mathbf{x}^{\mathrm{u}}_{i,k}, \mathbf{x}\right) = \begin{cases} 0 & \text{if } \mathbf{x} \in \mathbb{F}_{i,\ell}(\mathbf{x}^{\mathrm{u}}_{i,k}) \text{ and } \mathcal{D}_{i,k} = \emptyset, \\ 0 & \text{if } \mathbf{x} \in \mathbb{F}_{i,\ell}(\mathbf{x}^{\mathrm{u}}_{i,k}) \\ & \quad \text{and } \forall j \in \mathcal{D}_{i,k}, \mathbf{h}_i(\mathbf{x}^{\mathrm{u}}_{i,k}, \mathbf{x}) \notin [\mathbf{y}_{i,j,k}] \\ 1 & \text{else.} \end{cases}$$

When $c_\ell(\mathbf{x}^{\mathrm{u}}_{i,k}, \mathbf{x}) = 0$, no target is detected at location $\boldsymbol{x} = p^{\mathrm{t}}(\mathbf{x})$ when observed from $\boldsymbol{x}^{\mathrm{u}}_{i,k} = p(\mathbf{x}^{\mathrm{u}}_{i,k})$ belonging to $\mathbb{C}_\ell(\boldsymbol{x})$. Otherwise, no decision can be made.

Proposition 2. *Consider some state $\mathbf{x} \in \mathbb{X}^T$ and location $\boldsymbol{x} = p^t(\mathbf{x})$ with detectability set $\mathbb{D}(\boldsymbol{x})$, L conic observations subsets $\mathbb{C}_\ell(\boldsymbol{x})$, and a set of L UAV states $\mathbf{x}^u_\ell$, $\ell = 1, \ldots, L$, such that $\boldsymbol{x}^u_\ell = p(\mathbf{x}^u_\ell) \in \mathbb{C}_\ell(\boldsymbol{x})$ and $\mathbf{x} \in \mathbb{F}_\ell(\mathbf{x}^u_\ell)$. Assuming that $\mathbb{C}_\ell(\boldsymbol{x})$, $\ell = 1, \ldots, L$ satisfy (5.9), if $c_\ell(\mathbf{x}^u_\ell, \mathbf{x}) = 0$ for all $\ell = 1, \ldots, L$, then there is no target at location $\boldsymbol{x}$.*

Proof. Assume that target j with state $\mathbf{x}$ is located at $\boldsymbol{x} = p^{\mathrm{t}}(\mathbf{x})$, *i.e.*, $\mathbf{x}^{\mathrm{t}}_j = \mathbf{x}$ and $\boldsymbol{x}^{\mathrm{t}}_j = \boldsymbol{x}$, and that $c_\ell(\mathbf{x}^{\mathrm{u}}_\ell, \mathbf{x}) = 0$ for all $\ell = 1, \ldots, L$. Since $\exists \ell$ such that $\mathbb{C}_\ell(\boldsymbol{x}) \subset$

$\mathbb{D}(\boldsymbol{x})$, one has $\boldsymbol{x}_\ell^{\mathrm{u}} \in \mathbb{C}_\ell(\boldsymbol{x}) \subset \mathbb{D}(\boldsymbol{x})$. Moreover, as $\mathbf{x} \in \mathbb{F}_\ell(\mathbf{x}_\ell^{\mathrm{u}})$, according to (5.2), target j should have been detected, *i.e.*, $j \in \mathcal{D}_\ell$ and a measurement $\mathbf{y}_{\ell,j} = \mathbf{h}_\ell\left(\mathbf{x}_\ell^{\mathrm{u}}, \mathbf{x}_j^{\mathrm{t}}\right) + \mathbf{w}_{\ell,j}$, with $\mathbf{w}_{\ell,j} \in [\mathbf{w}_\ell]$ should be available. Thus $\mathbf{h}_\ell(\mathbf{x}_{\ell,k}^{\mathrm{u}}, \mathbf{x}) \in [\mathbf{y}_{\ell,j,k}]$ and $c_\ell(\mathbf{x}_{\ell,k}^{\mathrm{u}}, \mathbf{x}) = 1$, which contradicts the initial assumptions. □

The observations obtained from UAVs with states $\mathbf{x}_\ell^{\mathrm{u}}$, $\ell = 1, \ldots, L$, could be taken by different UAVs and at different time instants. Proposition 2 gives us now means to prove the absence of a target at a location $\boldsymbol{x}$.

5.3.1.3. Extended set estimates

Additionally to the introduced set estimates $\mathcal{X}_{i,k}$ and $\overline{\mathbb{X}}_{i,k}$, UAV i maintains the set estimate $\overline{\mathbb{X}}_{i,\ell,k} \subset \mathbb{X}_0$, $\ell = 1, \ldots, L$, of potential target states $\mathbf{x}$ that have not been observed from a point of view belonging to the cone $\mathbb{C}_\ell(\boldsymbol{x})$, $\boldsymbol{x} = p^{\mathrm{t}}(\mathbf{x})$, up to time t_k. The subsets $\overline{\mathbb{X}}_{i,\ell,k}$, $\ell = 1, \ldots, L$, are collected in the list $\overline{\mathcal{X}}_{i,k} = \left\{\overline{\mathbb{X}}_{i,\ell,k}\right\}_{\ell=1,\ldots,L}$. One has

$$\overline{\mathbb{X}}_{i,k} = \bigcup_{\ell \in \{1,\ldots,L\}} \overline{\mathbb{X}}_{i,\ell,k}. \tag{5.11}$$

The set estimate $\overline{\mathbb{X}}_{i,k}$ can now be interpreted as the set of potential target locations $\boldsymbol{x}$ which have not been observed from at least one point of view in *each* cone $\mathbb{C}_\ell(\boldsymbol{x})$, $\ell = 1, \ldots, L$.

At time t_k, instead of minimizing the estimation uncertainty (5.4), UAV i minimizes

$$\Phi^{\mathrm{C}}\left(\mathcal{X}_{i,k}, \overline{\mathcal{X}}_{i,k}\right) = \sum_{j \in \mathcal{L}_{i,k}} \phi\left(\mathbb{X}_{i,j,k}\right) + \frac{1}{L} \sum_{\ell=1}^{L} \phi\left(\overline{\mathbb{X}}_{i,\ell,k}\right). \tag{5.12}$$

The estimation uncertainty $\Phi^{\mathrm{C}}\left(\mathcal{X}_{i,k}, \overline{\mathcal{X}}_{i,k}\right)$ accounts for the set estimates $\mathbb{X}_{i,j,k}$, $j \in \mathcal{L}_{i,k}$, of detected targets and for the sets $\overline{\mathbb{X}}_{i,\ell,k}$, $\ell = 1, \ldots, L$. The difference between (5.4) and (5.12) is, that (5.12) accounts for the conic observation subset from where some subsets of $\mathbb{X}_0$ are explored. The sum $\sum_{\ell=1}^{L} \phi\left(\overline{\mathbb{X}}_{i,\ell,k}\right)$ is considered instead of the measure of the union $\phi(\bigcup_{\ell \in \{1,\ldots,L\}} \overline{\mathbb{X}}_{i,\ell,k})$, since $\sum_{\ell=1}^{L} \phi\left(\overline{\mathbb{X}}_{i,\ell,k}\right)$ is more sensitive to the reduction of each set $\overline{\mathbb{X}}_{i,\ell,k}$, $\ell = 1, \ldots, L$. The measurements allow the UAVs to directly reducing the size of $\overline{\mathbb{X}}_{i,\ell,k}$, while the reduction of the size of $\bigcup_{\ell \in \{1,\ldots,L\}} \overline{\mathbb{X}}_{i,\ell,k}$ appears delayed.

The average estimation uncertainty among all UAVs at time t_k is then

$$\Phi_k^{\mathrm{C}} = \frac{1}{N^{\mathrm{u}}} \sum_{i=1}^{N^{\mathrm{u}}} \Phi^{\mathrm{C}}\left(\mathcal{X}_{i,k}, \overline{\mathcal{X}}_{i,k}\right). \tag{5.13}$$

Similarly to Chapter 4, each UAV has to evaluate a sequence of control inputs that minimizes the estimation uncertainty. The main difficulty compared to Chapter 4 lies in the fact that L sets $\overline{\mathbb{X}}_{i,\ell,k}$ are taken into account, each associated with a specific cone $\mathbb{C}_\ell$, $\ell = 1, \ldots, L$, thus, measurements have to be taken with a specific point of view. This requires first to be able to determine the evolution of the various set estimates managed by the UAVs when new measurements are available.

5.3.2. Evolution of the set estimates

UAV i manages the sets $\mathcal{L}_{i,k}$, $\mathcal{X}_{i,k}$, $\overline{\mathcal{X}}_{i,k}$, and $\overline{\mathbb{X}}_{i,k}$ introduced in Section 5.3.1.3. These sets are initialized at time $t_{k=0}$ as $\mathcal{L}_{i,0} = \emptyset$, $\mathcal{X}_{i,0} = \emptyset$, $\overline{\mathbb{X}}_{i,\ell,0} = \mathbb{X}_0$, $\overline{\mathbb{X}}_{i,k} = \mathbb{X}_0$, where $\ell = 1, ..., L$, for $i = 1, \ldots, N^{\mathrm{u}}$. In what follows, the evolution of the set estimates is described when new measurements are taken into account, either coming from UAV i or from its neighbors.

5.3.2.1. Accounting for measurements

Assume that at time t_{k+1}, after processing the information in $\mathbb{F}_i(\mathbf{x}^{\mathrm{u}}_{i,k+1})$, UAV i obtains a measurement $\mathbf{y}_{i,j,k+1}$ for each detected target $j \in \mathcal{D}_{i,k+1}$. Consequently, the information gathered in $\mathbb{I}_{i,k+1|k+1}$ is

$$\mathbb{I}_{i,k+1|k+1} = \mathbb{I}_{i,k} \cup \left\{ \mathcal{D}_{i,k+1}, \{\mathbf{y}_{i,j,k+1}\}_{j \in \mathcal{D}_{i,k+1}} \right\}. \tag{5.14}$$

Using the new information in $\mathbb{I}_{i,k+1|k+1}$ and $\mathbb{F}_i(\mathbf{x}^{\mathrm{u}}_{i,k+1})$, three cases have to be considered for updating the sets $\mathcal{X}_{i,k}$, and $\overline{\mathcal{X}}_{i,k}$.

Case 1 When $j \in \mathcal{L}_{i,k}$ and $j \in \mathcal{D}_{i,k+1}$, a known target j is observed again. The new measurement $\mathbf{y}_{i,j,k+1}$ has to be consistent with the previous target set estimate $\mathbb{X}_{i,j,k}$. Consequently,

$$\mathbb{X}_{i,j,k+1|k+1} = \left\{ \mathbf{x} \in \mathbb{X}_{i,j,k} \,|\, \mathbf{h}_i \left(\mathbf{x}^{\mathrm{u}}_{i,k+1}, \mathbf{x} \right) \in \mathbf{y}_{i,j,k+1} - [\mathbf{w}_{i,k+1}] \right\}. \tag{5.15}$$

Case 2 When $j \notin \mathcal{L}_{i,k}$ and $j \in \mathcal{D}_{i,k+1}$, a new target is detected. The target location belongs to one of the non-empty subsets $\mathbb{F}_{i,\ell}(\mathbf{x}^{\mathrm{u}}_{i,k})$ of the FoV $\mathbb{F}_i(\mathbf{x}^{\mathrm{u}}_{i,k})$, and to one of the corresponding set $\overline{\mathbb{X}}_{i,\ell,k}$. Since determining which of these sets contains the target is difficult, one gets

$$\mathbb{X}_{i,j,k+1|k+1} = \bigcup_{\substack{\ell=\{1,\ldots,L\}, \\ \mathbb{F}_{i,\ell}(\mathbf{x}^{\mathrm{u}}_{i,k}) \neq \emptyset}} \left\{ \mathbf{x} \in \overline{\mathbb{X}}_{i,\ell,k} \mid \mathbf{h}_i \left(\mathbf{x}^{\mathrm{u}}_{i,k+1}, \mathbf{x} \right) \in \mathbf{y}_{i,j,k+1} - [\mathbf{w}_{i,k+1}] \right\}. \tag{5.16}$$

One could also consider $\overline{\mathbb{X}}_{i,k}$ instead of $\overline{\mathbb{X}}_{i,\ell,k}$ as in (4.8). However, considering each set $\overline{\mathbb{X}}_{i,\ell,k}$, $\ell = 1, ..., L$, independently and only the sets with index ℓ, where $\mathbb{F}_{i,\ell}(\mathbf{x}^{\mathrm{u}}_{i,k}) \neq \emptyset$, may lead to a more precise set estimate $\mathbb{X}_{i,j,k+1|k+1}$.

Case 3 When $j \in \mathcal{L}_{i,k}$ and $j \notin \mathcal{D}_{i,k+1}$, a previously detected and known target j is not detected at time instant t_{k+1} and

$$\mathbb{X}_{i,j,k+1|k+1} = \mathbb{X}_{i,j,k}. \tag{5.17}$$

In that case it is not implemented to reduce the size of $\mathbb{X}_{i,j,k}$ using $\mathbb{F}_{i,\ell}(\mathbf{x}^{\mathrm{u}}_{i,k})$. The measure $\phi\left(\mathbb{X}_{i,j,k}\right)$ remains always small since the targets are static and accounting for the observed subsets $\mathbb{F}_{i,\ell}(\mathbf{x}^{\mathrm{u}}_{i,k})$ would require the introduction of additional set estimates and would not be worthwhile.

Once all information in $\mathbb{F}_{i,\ell}(\mathbf{x}^{\mathrm{u}}_{i,k+1})$ has been exploited, one may update the sets $\overline{\mathbb{X}}_{i,\ell,k}$, $\ell = 1, \ldots, L$, by removing the states $\mathbf{x} \in \mathbb{F}_{i,\ell}(\mathbf{x}^{\mathrm{u}}_{i,k+1})$ observed from $\boldsymbol{x}^{\mathrm{u}}_{i,k+1} \in \mathbb{C}_\ell\left(\boldsymbol{x}\right)$, $\boldsymbol{x} = p^{\mathrm{t}}(\mathbf{x})$, thus

$$\overline{\mathbb{X}}_{i,\ell,k+1|k+1} = \overline{\mathbb{X}}_{i,\ell,k} \backslash \mathbb{F}_{i,\ell}\left(\mathbf{x}^{\mathrm{u}}_{i,k+1}\right). \tag{5.18}$$

According to (5.11), one gets

$$\overline{\mathbb{X}}_{i,k+1|k+1} = \bigcup_{\ell \in \{1,\ldots,L\}} \overline{\mathbb{X}}_{i,\ell,k+1|k+1}. \tag{5.19}$$

Based on Proposition 2 the subset $\left(\overline{\mathbb{X}}_{i,k+1|k+1} \setminus \overline{\mathbb{X}}_{i,k}\right)$ is now proved to not contain any undetected targets.

Figure 5.5 shows different sets $\overline{\mathbb{X}}_{i,\ell,k}$ at time t_k considering four cones $\mathbb{C}_\ell\left(\mathbf{O}\right)$, $\ell \in \{1, ..., 4\}$. The newly explored space $\overline{\mathbb{X}}_{i,\ell,k} \cap \mathbb{F}_{i,\ell}(\mathbf{x}^{\mathrm{u}}_{i,k+1})$ at time t_k is shown in orange for each UAV i and each conic observation subset ℓ. The vertices of the associated cone $\mathbb{C}_\ell\left(\boldsymbol{x}\right)$ are highlighted in red. Figure 5.5 (right) shows the resulting set $\overline{\mathbb{X}}_{i,k}$. One observes that the orientation of the FoV of each UAV determines the index ℓ of the set $\overline{\mathbb{X}}_{i,\ell,k}$ which size will be the most significantly reduced using the measurement at time t_{k+1}. For example, the FoV of the red UAV has an orientation opposite to the one of the cone $\mathbb{C}_2$, leading to a significant reduction of $\overline{\mathbb{X}}_{i,2,k}$. The reduction of the size of $\overline{\mathbb{X}}_{i,4,k}$ is null, due to the relatively close orientation of the FoV of the red UAV and that of the cone $\mathbb{C}_4$. This property will have to be taken into account in the design of the control inputs of the UAVs. One observes also that reduction of some of the sets $\overline{\mathbb{X}}_{i,\ell,k}$, $\ell = 1, \ldots, L$ is quite large, however, the reduction of $\overline{\mathbb{X}}_{i,k}$ is quite small. This observation lead us also to introducing the cost function (5.12).

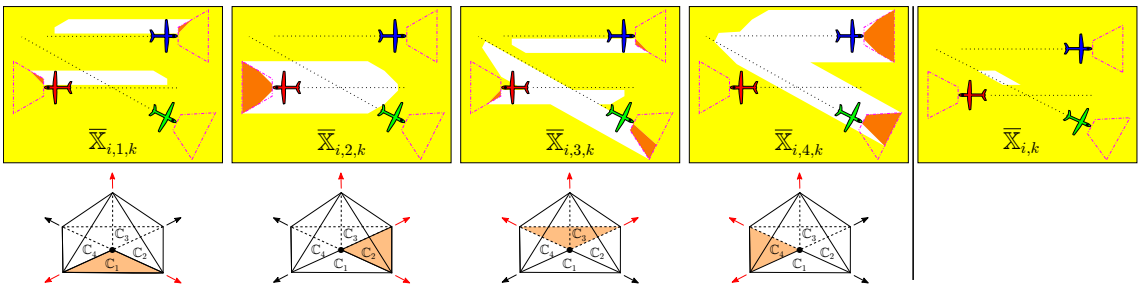

Figure 5.5.: Evolution of $\overline{\mathbb{X}}_{i,\ell,k}$, $\ell \in \{1,...,4\}$ when considering 3 UAVs; Each column shows a set $\overline{\mathbb{X}}_{i,\ell,k}$ in yellow and the corresponding cone $\mathbb{C}_\ell(\mathbf{O})$, $\ell \in \{1,...,4\}$; The last column represents $\overline{\mathbb{X}}_{i,k}$; The orange area indicates the set $\overline{\mathbb{X}}_{i,\ell,k} \cap \mathbb{F}_{i,\ell}(\mathbf{x}^{\mathrm{u}}_{i,k+1})$ at time t_k.

5.3.2.2. Accounting for communications

After the measurement correction step, UAV i receives the information $\mathbb{I}_{n,k+1|k+1}$ from each UAV $n \in \mathcal{N}_{i,k}$. Using that information, UAV i first updates the list of known targets as $\mathcal{L}_{i,k+1} = \bigcup_{n\in\mathcal{N}_{i,k}\cup\{i\}} \mathcal{L}_{n,k+1|k+1}$. Then for each $j \in \mathcal{L}_{i,k+1}$, the corrected target set estimate $\mathbb{X}_{i,j,k+1}$ is evaluated as

$$\mathbb{X}_{i,j,k+1} = \bigcap_{n\in\mathcal{N}_{i,k}\cup\{i\} \,|\, j\in\mathcal{L}_{n,k+1|k+1}} \mathbb{X}_{n,j,k+1|k+1}, \tag{5.20}$$

since $\mathbb{X}_{i,j,k+1}$ has to be consistent with all observations from the UAVs which have detected target j. The intersection of $\mathbb{X}_{n,j,k+1|k+1}$, among $n \in \mathcal{N}_{i,k} \cup \{i\}$, is evaluated since false detection and misidentification are not considered in this chapter. Consequently, the true state value of the target has to lie within the intersection.

If, for some $\ell \in \{1,...,L\}$, UAV i or one of its neighbors have observed $\mathbf{x} \in \mathbb{X}_0$ from a location $\boldsymbol{x}' \in \mathbb{C}_\ell(\boldsymbol{x})$, it is not necessary to observe $\mathbf{x}$ again from a location in $\mathbb{C}_\ell(\boldsymbol{x})$. A target has either been detected, leading to one of the sets $\mathbb{X}_{i,j,k+1}$, $j \in \mathcal{L}_{n,k+1|k+1}$, or no target has been detected. In both cases, $\mathbf{x}$ can be removed from $\overline{\mathbb{X}}_{i,\ell,k+1|k+1}$. Consequently, for each $\ell \in \{1,...,L\}$,

$$\overline{\mathbb{X}}_{i,\ell,k+1} = \bigcap_{n\in\mathcal{N}_{i,k}\cup\{i\}} \overline{\mathbb{X}}_{n,\ell,k+1|k+1}. \tag{5.21}$$

Finally, one has $\overline{\mathbb{X}}_{i,k+1} = \bigcup_{\ell=1}^{L} \overline{\mathbb{X}}_{i,\ell,k+1}$.

The update process in Section 5.3.2.1 and 5.3.2.2 is applied iteratively at each time instant t_k to update the different set estimates. The next section considered the cooperative control design for the fleet of UAVs. Each UAV has now to account for its point of view when evaluating its control input.

5.3.3. Cooperative control design

The aim of the control input design is to compute, in a distributed way, a sequence of control inputs $\mathbf{u}_{i,k:k+h-1} = (\mathbf{u}_{i,k}, \ldots, \mathbf{u}_{i,k+h-1})$ for each UAV $i \in \{1, \ldots, N^{\mathrm{u}}\}$ that minimizes the predicted estimation uncertainty (5.13),

$$\Phi^{\mathrm{C}}_{k+h} = \frac{1}{N^{\mathrm{u}}} \sum_{i=1}^{N^{\mathrm{u}}} \Phi^{\mathrm{C}} \left(\mathcal{X}_{i,k+h}, \overline{\mathcal{X}}_{i,k+h} \right), \tag{5.22}$$

at time t_{k+h} where $h \geqslant 1$ is the prediction horizon and $\mathcal{X}_{i,k+h}$ and $\overline{\mathcal{X}}_{i,k+h}$ depend on $\mathbf{u}_{i,k:k+h-1}$. The set-membership estimator described in Section 5.3.2 is again combined with a Model Predictive Control approach to design of the control inputs.

It is assumed that the UAVs compute their control inputs sequentially. Once UAV i has evaluated $\mathbf{u}_{i,k:k+h-1}$, it is broadcast to its neighbors, which then compute their sequence of control inputs accounting for those evaluated by their neighbors. The order in which the evaluations are done may clearly be optimized, but is left for future research.

5.3.3.1. Control input design

One assumes that UAV i has to evaluate $\mathbf{u}_{i,k:k+h-1}$ accounting for the sequences of control inputs already evaluated by a subset $\mathcal{N}^{\mathrm{c}}_{i,k} \subset \mathcal{N}_{i,k}$ of its neighbors. Thus, one assumes that all UAVs $n \in \mathcal{N}^{\mathrm{c}}_{i,k}$ have broadcast their sequence $\mathbf{u}_{n,k:k+h-1}$ as well as their states $\mathbf{x}^{\mathrm{u}}_{n,k}$, at time t_k. Consequently, at time t_k, UAV i has access to $\mathcal{L}_{i,k}$, $\mathcal{X}_{i,k}$, $\overline{\mathcal{X}}_{i,k}$, $\mathbf{u}_{n,k:k+h-1}$, and $\mathbf{x}^{\mathrm{u}}_{n,k}$, $n \in \mathcal{N}^{\mathrm{c}}_{i,k}$. When UAV i has to evaluate the sequence of control inputs minimizing Φ^{C}_{k+h}, it has in fact to evaluate

$$\widehat{\mathbf{u}}_{i,k:k+h-1} = \arg \min_{\mathbf{u}_{i,k:k+h-1}} \Phi^{\mathrm{C}} \left(\mathcal{X}^{\mathrm{P}}_{i,k+h}, \overline{\mathcal{X}}^{\mathrm{P}}_{i,k+h} \right). \tag{5.23}$$

Since one is unable to predict whether new targets will be detected between time t_k and t_{k+h}, the predicted values of $\mathcal{L}_{i,k+\kappa}$ are set to $\mathcal{L}^{\mathrm{P}}_{i,k+\kappa} = \mathcal{L}_{i,k}$, $\kappa = 1, \ldots, h$. Moreover, in the considered set-membership MPC approach, the impact of the control input sequence on $\mathbb{X}_{i,j,k+\kappa}$, $\kappa = 1, \ldots, h$, is difficult to ealuate. In the set-membership estimator the value of $\mathbb{X}_{i,j,k}$ is only updated when a target is detected which can not be predict. Thus, the contribution of $\mathbb{X}_{i,j,k+\kappa}$, $\kappa = 1, \ldots, h$, in (5.23) will be neglected. This approximation is reasonable, since most of the time, the contribution of $\mathcal{X}_{i,k+h}$ to Φ^{C}_{k+h} is negligible compared to that of $\overline{\mathcal{X}}_{i,k+h}$. This also means that the UAVs will not try to track targets that are in $\mathcal{L}_{i,k}$, but as said before, the targets are static and refining their set estimates is less important. Thus, the focus lies on the evolution of the components of $\overline{\mathcal{X}}_{i,k+\kappa}$, $\kappa = 1, \ldots, h$, from the control input sequences provided by UAV i and its neighbors $n \in \mathcal{N}^{\mathrm{c}}_{i,k}$. Consequently, (5.23) can

be simplified to

$$\widehat{\mathbf{u}}_{i,k:k+h-1} = \arg \min_{\mathbf{u}_{i,k:k+h-1}} \sum_{\ell=1}^{L} \phi \left(\overline{\mathbb{X}}^{\mathrm{P}}_{i,\ell,k+h} \right). \tag{5.24}$$

In the following, the impact of the control input sequences of UAV i and of its neighbors $n \in \mathcal{N}^{\mathrm{c}}_{i,k}$ on the predicted sets $\overline{\mathbb{X}}^{\mathrm{P}}_{i,\ell,k+h}$ is evaluated. For all $n \in \mathcal{N}^{\mathrm{c}}_{i,k}$, UAV i predicts iteratively $\mathbf{x}^{\mathrm{u,P}}_{n,k+1}, ..., \mathbf{x}^{\mathrm{u,P}}_{n,k+h}$ from $\mathbf{x}^{\mathrm{u}}_{n,k}$ and $\mathbf{u}_{n,k:k+h-1}$ using (3.1). From $\mathbf{x}^{\mathrm{u,P}}_{n,k+1}$, UAV i derives $\mathbb{F}_{n,\ell}(\mathbf{x}^{\mathrm{u,P}}_{n,k+1})$ as in (5.10). Each UAV $n \in \mathcal{N}^{\mathrm{c}}_{i,k}$ will contribute to the reduction of $\overline{\mathbb{X}}_{i,\ell,k}$ as follows

$$\overline{\mathbb{X}}^{\mathrm{P}}_{i,\ell,k+} = \overline{\mathbb{X}}_{i,\ell,k} \setminus \bigcup_{n \in \mathcal{N}^{\mathrm{c}}_{i,k}} \mathbb{F}_{n,\ell} \left(\mathbf{x}^{\mathrm{u,P}}_{n,k+1} \right), \tag{5.25}$$

$\ell \in \{1, ..., L\}$. The previous approach can be applied iteratively on $\overline{\mathbb{X}}^{\mathrm{P}}_{i,\ell,k+}$ to evaluate the impact of $\mathbf{u}_{n,k+\kappa-1}$, $n \in \mathcal{N}^{\mathrm{c}}_{i,k}$ and $\kappa = 1, \ldots, h$, as

$$\overline{\mathbb{X}}^{\mathrm{P}}_{i,\ell,k+\kappa+} = \overline{\mathbb{X}}^{\mathrm{P}}_{i,\ell,k+\kappa-1+} \setminus \bigcup_{n \in \mathcal{N}^{\mathrm{c}}_{i,k}} \mathbb{F}_{n,\ell} \left(\mathbf{x}^{\mathrm{u,P}}_{n,k+\kappa} \right). \tag{5.26}$$

Finally, one may write

$$\overline{\mathbb{X}}^{\mathrm{P}}_{i,\ell,k+h+} = \overline{\mathbb{X}}_{i,\ell,k} \setminus \bigcup_{\kappa=1}^{h} \bigcup_{n \in \mathcal{N}^{\mathrm{c}}_{i,k}} \mathbb{F}_{n,\ell} \left(\mathbf{x}^{\mathrm{u,P}}_{n,k+\kappa} \right). \tag{5.27}$$

In the same way, and for any control input sequence $\mathbf{u}_{i,k:k+h-1}$, UAV i can predict iteratively $\mathbf{x}^{\mathrm{u,P}}_{i,k+1}, ..., \mathbf{x}^{\mathrm{u,P}}_{i,k+h}$ from $\mathbf{x}^{\mathrm{u}}_{i,k}$ and can derive $\mathbb{F}_{i,\ell}(\mathbf{x}^{\mathrm{u,P}}_{i,k+\kappa}), \kappa = 1, ..., h$, which contributes to the reduction of $\overline{\mathbb{X}}^{\mathrm{P}}_{i,\ell,k+h+}$ to get $\overline{\mathbb{X}}^{\mathrm{P}}_{i,\ell,k+h}$. One has

$$\overline{\mathbb{X}}^{\mathrm{P}}_{i,\ell,k+h} = \overline{\mathbb{X}}^{\mathrm{P}}_{i,\ell,k+h+} \setminus \bigcup_{\kappa=1}^{h} \mathbb{F}_{i,\ell} \left(\mathbf{x}^{\mathrm{u,P}}_{i,k+\kappa} \right). \tag{5.28}$$

Hence, (5.24) can finally be written as

$$\widehat{\mathbf{u}}_{i,k:k+h-1} = \arg \min_{\mathbf{u}_{i,k:k+h-1}} \sum_{\ell=1}^{L} \phi \left(\overline{\mathbb{X}}^{\mathrm{P}}_{i,\ell,k+h} \right) \tag{5.29}$$

$$= \arg \min_{\mathbf{u}_{i,k:k+h-1}} \sum_{\ell=1}^{L} \phi \left(\overline{\mathbb{X}}^{\mathrm{P}}_{i,\ell,k+h+} \setminus \bigcup_{\kappa=1}^{h} \mathbb{F}_{i,\ell} \left(\mathbf{x}^{\mathrm{u,P}}_{i,k+\kappa} \right) \right) \tag{5.30}$$

$$= \arg \max_{\mathbf{u}_{i,k:k+h-1}} \sum_{\ell=1}^{L} \phi \left(\overline{\mathbb{X}}^{\mathrm{P}}_{i,\ell,k+h+} \cap \bigcup_{\kappa=1}^{h} \mathbb{F}_{i,\ell} \left(\mathbf{x}^{\mathrm{u,P}}_{i,k+\kappa} \right) \right). \tag{5.31}$$

The resulting sequence of control inputs leads to the maximum average reduction

of the size of $\overline{\mathbb{X}}^{\mathrm{P}}_{i,\ell,k+h+}$. The optimization problem (5.29) can be rewritten, and one may ether minimize the size of the set $\overline{\mathbb{X}}^{\mathrm{P}}_{i,\ell,k+h+} \setminus \bigcup_{\kappa=1}^{h} \mathbb{F}_{i,\ell}\left(\mathbf{x}^{\mathrm{u,P}}_{i,k+\kappa}\right)$, as in (5.30), or maximize the intersection of the predicted FoV $\bigcup_{\kappa=1}^{h} \mathbb{F}_{i,\ell}\left(\mathbf{x}^{\mathrm{u,P}}_{i,k+\kappa}\right)$ with the set $\overline{\mathbb{X}}^{\mathrm{P}}_{i,\ell,k+h+}$, as in (5.31).

In general, the evaluation of (5.29) is much less computational demanding compared to minimizing (4.39) since the targets are static. This is due to the fact that one does not need to account for the evolution of the target state and the impact of the FoV of the neighbors can be evaluated beforehand since $\overline{\mathbb{X}}^{\mathrm{P}}_{i,\ell,k+h+}$ does not depend on $\mathbf{u}_{i,k:k+h-1}$.

5.3.3.2. Practical issues

In practice, obtaining $\hat{\mathbf{u}}_{i,k:k+h-1}$ from (5.31), when h is limited may prove to be inefficient, especially when $\overline{\mathbb{X}}^{\mathrm{P}}_{i,\ell,k+h+} \cap (\bigcup_{\kappa=1}^{h} \mathbb{F}_{i,\ell}(\mathbf{x}^{\mathrm{u,P}}_{i,k+\kappa})) = \emptyset$ for all $\ell = 1, \ldots, L$, whatever the sequence of control inputs. Such situation may occur, *e.g.*, when a UAV reaches the boundary of $\mathbb{X}_0$.

To address this issue, one observes that the orientation of $\mathbb{F}_i(\mathbf{x}^{\mathrm{u}}_{i,k+1})$ and of the cone $\mathbb{C}_\ell$ are quite different when $\overline{\boldsymbol{v}}^{\mathrm{F}}_i(\mathbf{x}^{\mathrm{u}}_{i,k+1})^{\mathrm{T}}\overline{\boldsymbol{v}}^{\mathrm{c}}_\ell < 0$. In that case, $\phi(\mathbb{F}_{i,\ell}(\mathbf{x}^{\mathrm{u}}_{i,k+1}))$ is likely to be large and the UAV may get observations able to reduce $\overline{\mathbb{X}}_{i,\ell,k}$, provided that $\overline{\mathbb{X}}_{i,\ell,k} \cap \mathbb{F}_{i,\ell}(\mathbf{x}^{\mathrm{u}}_{i,k+1}) \neq \emptyset$. This is, for example, the case with the red UAV in Figure 5.5 for $\mathbb{C}_2$ and $\overline{\mathbb{X}}_{i,2,k}$.

When $\overline{\boldsymbol{v}}^{\mathrm{F}}_i(\mathbf{x}^{\mathrm{u}}_{i,k+1})^{\mathrm{T}}\overline{\boldsymbol{v}}^{\mathrm{c}}_\ell > 0$, the orientation of $\mathbb{F}_i(\mathbf{x}^{\mathrm{u}}_{i,k+1})$ is close to that of the cone $\mathbb{C}_\ell$. In that case, $\phi(\mathbb{F}_{i,\ell}(\mathbf{x}^{\mathrm{u}}_{i,k+1}))$ is likely to be small. The observation performed at time t_{k+1} is likely to leave $\overline{\mathbb{X}}_{i,\ell,k}$ unchanged. This is the case with the red UAV in Figure 5.5 for $\mathbb{C}_4$ and $\overline{\mathbb{X}}_{i,4,k}$.

In order to get an efficient reduction of $\overline{\mathbb{X}}_{i,\ell,k}$ or $\overline{\mathbb{X}}^{\mathrm{P}}_{i,\ell,k+h+}$, it may thus be of interest to control UAV i in such a way that $\overline{\boldsymbol{v}}^{\mathrm{F}}_i(\mathbf{x}^{\mathrm{u}}_{i,k+\kappa})^{\mathrm{T}}\overline{\boldsymbol{v}}^{\mathrm{c}}_\ell$ is as negative as possible for some $\ell \in \{1, \ldots, L\}$. This is nevertheless not sufficient, since one should have, *e.g.*, $\overline{\mathbb{X}}_{i,\ell,k} \cap \mathbb{F}_{i,\ell}(\mathbf{x}^{\mathrm{u}}_{i,k+1}) \neq \emptyset$. Hence, when $\overline{\mathbb{X}}^{\mathrm{P}}_{i,\ell,k+h+} \cap (\bigcup_{\kappa=1}^{h} \mathbb{F}_{i,\ell}(\mathbf{x}^{\mathrm{u,P}}_{i,k+\kappa})) = \emptyset$ for all $\ell = 1, \ldots, L$ whatever the input sequences, while $\overline{\mathbb{X}}^{\mathrm{P}}_{i,\ell,k+h+} \neq \emptyset$ for some ℓ, it may be of interest to find a control input that drives UAV i to a point of $\overline{\mathbb{X}}^{\mathrm{P}}_{i,\ell,k+h+}$ which may lead to future reductions via observations such that $\overline{\boldsymbol{v}}^{\mathrm{F}}_i\,(\mathbf{x}^{\mathrm{u}}_i)^{\mathrm{T}}\,\overline{\boldsymbol{v}}^{\mathrm{c}}_\ell < 0$.

The point

$$\boldsymbol{x}^{*}_{i,\ell,k+h} = \arg \max_{\boldsymbol{x} \in \overline{\mathbb{X}}^{\mathrm{P}}_{i,\ell,k+h+}} \boldsymbol{x}^{\mathrm{T}}\overline{\boldsymbol{v}}^{\mathrm{c}}_\ell, \tag{5.32}$$

is a good candidate for that purpose as it is the farthest point of $\overline{\mathbb{X}}^{\mathrm{P}}_{i,\ell,k+h+}$ from the origin along $\overline{\boldsymbol{v}}^{\mathrm{c}}_\ell$.

For each cone $\mathbb{C}_\ell$, $\ell = 1, \ldots, L$, one may then introduce the cost function

$$\begin{aligned} J_\ell\left(\mathbf{u}_{i,k}, \ldots, \mathbf{u}_{i,k+h-1}\right) =& \phi\left(\overline{\mathbb{X}}^{\mathrm{P}}_{i,\ell,k+h+} \cap \left(\bigcup_{\kappa=1}^{h} \mathbb{F}_{i,\ell}\left(\mathbf{x}^{\mathrm{u,P}}_{i,k+\kappa}\right)\right)\right) \\ & - \alpha_1 \left\| \boldsymbol{x}^{*}_{i,\ell,k+h} - \left(\boldsymbol{x}^{\mathrm{u,P}}_{i,k+h} + \lambda \overline{\boldsymbol{v}}^{\mathrm{F}}_{i}\left(\mathbf{x}^{\mathrm{u,P}}_{i,k+h}\right)\right)\right\| \\ & - \alpha_2 \overline{\boldsymbol{v}}^{\mathrm{F}}_{i}\left(\mathbf{x}^{\mathrm{u,P}}_{i,k+h}\right)^{\mathrm{T}} \overline{\boldsymbol{v}}^{\mathrm{c}}_{\ell}. \end{aligned} \tag{5.33}$$

On the right-hand side of (5.33), the first term represents the reduction of the measure of $\overline{\mathbb{X}}^{\mathrm{P}}_{i,\ell,k+h+}$ that may be obtained from successive measurements, as in (5.31). The second term accounts for the Euclidean distance between $\boldsymbol{x}^{*}_{i,\ell,k+h}$ and a point $\boldsymbol{x}^{\mathrm{u,P}}_{i,k+h} + \lambda \overline{\boldsymbol{v}}^{\mathrm{F}}_{i}(\mathbf{x}^{\mathrm{u,P}}_{i,k+h})$ in the FoV of UAV i when it is located at $\boldsymbol{x}^{\mathrm{u,P}}_{i,k+h}$. The parameter λ can be tuned to select specific locations in the FoV. Choosing $\lambda > 0$ proves to be more efficient in practice. The last term favors $\overline{\boldsymbol{v}}^{\mathrm{F}}_{i}(\mathbf{x}^{\mathrm{u,P}}_{i,k+h})^{\mathrm{T}} \overline{\boldsymbol{v}}^{\mathrm{c}}_{\ell} < 0$ as J_ℓ is maximized. This term accounts for relative orientation of the FoV which is necessary to collect an observation from a point of view in the cone $\mathbb{C}_\ell$. The tuning parameters α_1 and α_2 adjust the weight of each term in the cost function. The second and third terms of the right-hand side of (5.33) are most often negligible compared to the first term.

The control input for UAV i is obtained as the first element of the control sequence

$$\widehat{\mathbf{u}}_{i,k:k+h-1} = \arg \max_{\mathbf{u}_{i,k:k+h-1}} \left(\max_{\ell} \left(J_\ell\left(\mathbf{u}_{i,k}, \ldots, \mathbf{u}_{i,k+h-1}\right)\right)\right). \tag{5.34}$$

The cone $\mathbb{C}_\ell$ for which the reduction of the size of $\overline{\mathbb{X}}_{i,\ell,k}$ is maximum is selected. This avoids changing too frequently the orientation of the UAVs. The control inputs belong to the set $\mathbb{U}$ of admissible control inputs. In practice, to lighten computations, $\mathbb{U}$ is partitioned into discrete subsets $\mathbb{U}_0, \ldots, \mathbb{U}_{h-1}$.

5.3.4. Simulations

In the proposed simulation, $\mathbb{X}_0$ is taken as $[0, 300] \times [0, 300] \times [0, 100]$ m^3. Obstacles, modeled as boxes, are randomly placed with a minimal distance of 20 m from each other. They are uniformly scattered over $[0, 300] \times [0, 300]$ m^2. Their lengths and widths are uniformly distributed in $[40\,\mathrm{m}, 60\,\mathrm{m}] \times [40\,\mathrm{m}, 60\,\mathrm{m}]$. Their heights are uniformly distributed in $[80\,\mathrm{m}, 90\,\mathrm{m}]$. Only static targets at an altitude 0 m are considered in the RoI, *i.e.*, $\mathbb{X}_{\mathrm{T}} = [0, 300] \times [0, 300] \times [0, 0]$. The location of the j-th target is then $\boldsymbol{x}^{\mathrm{t}}_{j} = (x_{j,1}, x_{j,2}, 0)^{\mathrm{T}}$, $j = 1, \ldots, N_{\mathrm{t}}$. The locations are generated by distributing the targets uniformly inside $\mathbb{X}_{\mathrm{T}}$ and discarding locations inside or too far from the obstacles. The targets have maximal distance of 5 m to the obstacles to make the search more difficult.

The state of UAV i at time t_k consists of its location $\boldsymbol{x}^{\mathrm{u}}_{i,k} = (x^{\mathrm{u}}_{i,k,1}, x^{\mathrm{u}}_{i,k,2}, x^{\mathrm{u}}_{i,k,3})^{\top}$, flight path angle $x^{\mathrm{u}}_{i,k,4}$, heading angle $x^{\mathrm{u}}_{i,k,5}$, yaw rate $x^{\mathrm{u}}_{i,k,6}$, and yaw rate derivative

$x^{\mathrm{u}}_{i,k,7}$. The control input is applied to $x^{\mathrm{u}}_{i,k,7}$. The UAV state vector $\mathbf{x}^{\mathrm{u}}_{i,k}$ evolves according to (4.46). The altitude $x^{\mathrm{u}}_{i,k,3} = 100\,\mathrm{m}$, the flight path angle $x^{\mathrm{u}}_{i,k,4} = 0$, and the speed module $V^{\mathrm{u}} = 16.6$ m/s are assumed constant.

The UAVs are equipped with identical optical seekers able to observe a subset of the RoI. The angle between the longitudinal axis of the UAV and the orientation of the seeker is $3\pi/8$. The apertures of the seekers are equal to $\pi/4$ in azimuth and in elevation. A set of 8 observation cones is chosen as in Figure 5.2. The vertices are at $\pi/4$, $3\pi/4$, $5\pi/4$, and $7\pi/4$ for the azimuth and at 0, $\pi/3$, and π for the elevation. Consequently, $\boldsymbol{v}_1 = (1/\sqrt{2}, -1/\sqrt{2}, 0)^{\mathrm{T}}$, $\boldsymbol{v}_2 = (1/(2\sqrt{2}), -1/(2\sqrt{2}), \sqrt{3}/2)^{\mathrm{T}}$,... and $\boldsymbol{v}_9 = (0, 0, 1)^{\mathrm{T}}$.

A noisy measurement of the first two components of $\boldsymbol{x}_j$ is obtained when target j is detected by UAV i at time t_k. The noise is bounded in $[-5\,\mathrm{m}, 5\,\mathrm{m}]$.

The communication condition (3.18) is defined as in (4.52) where $d^{\mathrm{c}} = 200\,\mathrm{m}$. The prediction horizon for the set-membership MPC is $h = 2$. The control input is computed with a period $T^{\mathrm{c}} = 0.5\,\mathrm{s}$ and is equal to the communication period. The parameters of (5.33) are $\alpha_1 = 0.002$, $\alpha_2 = 1$, and $\lambda = 100$. The values of α_1 and α_2 are chosen so that $\phi(.)$ in (5.33) remains the most important term. More importance is given to the orientation with which the FoV reaches the set to be explored, thus $\alpha_2 \gg \alpha_1$ – this choice ensures a more efficient uncertainty reduction. The simulations have been carried out in Matlab where Matlab's *Polyshapes* are used to represent sets.

Figure 5.6 shows an example of the resulting simulation with 7 obstacles (gray boxes), 10 targets (black circles) and 4 UAVs. The plot on the left illustrates the simulation scenario and the occluded area (darker gray) for the red UAV. This information is not accessible for the UAVs. The plot on the right shows the set estimates $\mathbb{X}_{i,j,k}$ (green) and $\overline{\mathbb{X}}_{i,\ell,k}$ (yellow) known to the red UAV.

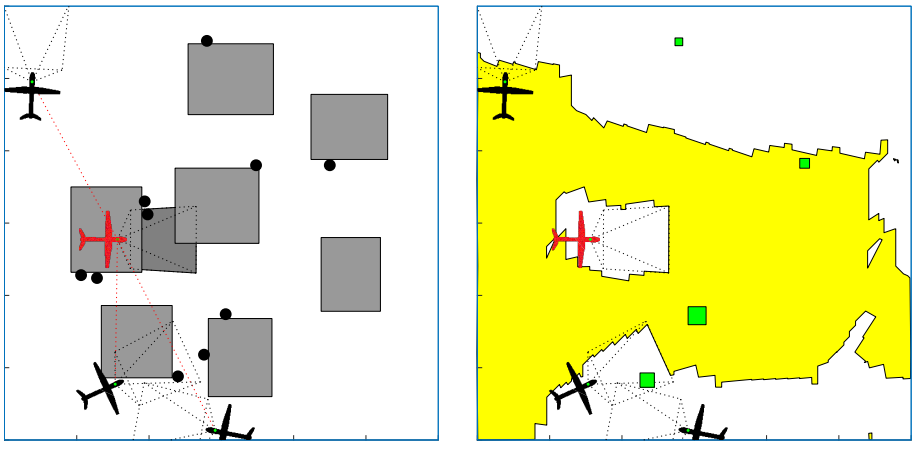

Figure 5.6.: Map of the simulated environment with obstacles, targets, and UAVs (left side). Estimates $\overline{\mathbb{X}}_{1,2,191}$ (yellow) and $\mathcal{X}_{1,191}$ (green) of UAV 1 (red) (right side)

The results in Figure 5.7 are obtained for 30 independent simulations with the same number of obstacles, targets, and UAVs. The initial locations of the obstacles, targets, and UAVs are changed in each simulation. Figure 5.7 shows the evolution with time of $\phi\left(\overline{\mathbb{X}}_k\right) = \sum_{i=1}^{N^{\mathrm{u}}} \phi\left(\overline{\mathbb{X}}_{i,k}\right)/N^{\mathrm{u}}$ and of the contribution to $\overline{\Phi}_k^{\mathrm{C}}$ of $\phi\left(\overline{\mathbb{X}}_{\ell,k}\right) = \sum_{i=1}^{N^{\mathrm{u}}} \phi\left(\overline{\mathbb{X}}_{i,\ell,k}\right)/N^{\mathrm{u}}$, $\ell \in \{1, ..., L\}$, and $\phi\left(\mathbb{X}_k\right) = \sum_{i=1}^{N^{\mathrm{u}}} \phi(\bigcup_{\mathbb{X}_{i,j,k} \in \mathcal{X}_{i,k}} \mathbb{X}_{i,j,k})/N^{\mathrm{u}}$. The conic observation subsets are grouped into cones of indices in the set $\mathcal{L}^{**} = \{1, 2, 3, 4\}$, with elevation bounds $[0, \pi/3]$, and into cones of indices in the set $\mathcal{L}^{*} = \{5, 6, 7, 8\}$, with elevation bounds $[\pi/3, \pi/2]$.

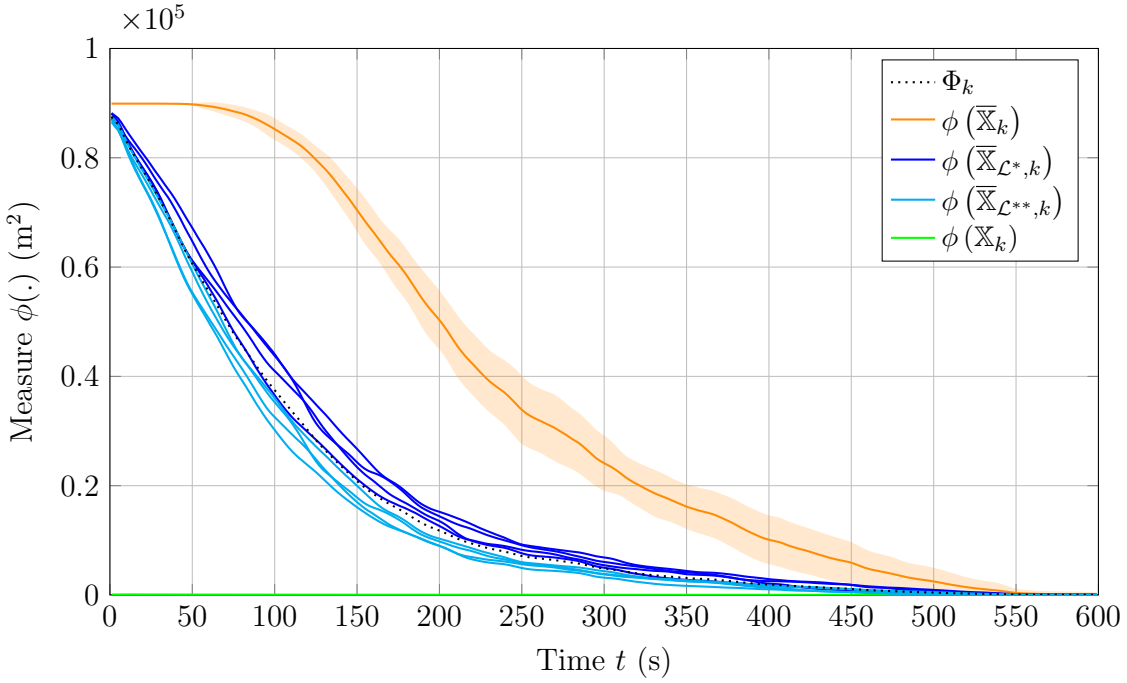

Figure 5.7.: Mean value of $\phi\left(\mathbb{X}_k\right)$, $\phi\left(\overline{\mathbb{X}}_{\mathcal{L}^*,k}\right)$, and $\phi\left(\overline{\mathbb{X}}_{\mathcal{L}^{**},k}\right)$ for 30 simulations; 10 targets, 7 obstacles, and 4 UAVs; Mean values (line) and root-mean-square error (area) of $\phi\left(\overline{\mathbb{X}}_k\right)$.

In Figure 5.7, one can see that the evolution of $\phi(\overline{\mathbb{X}}_{\ell,k})$ is similar for all $\ell \in \{1, ..., L\}$. One observes a slightly faster decrease of $\phi(\overline{\mathbb{X}}_{\mathcal{L}^{**},k})$ of cones of indices in $\mathcal{L}^{**}$ – with elevation in $[0, \pi/3]$ – compared to $\phi(\overline{\mathbb{X}}_{\mathcal{L}^{*},k})$ of cones of indices in $\mathcal{L}^{*}$ – with elevation in $[\pi/3, \pi/2]$. This is caused by the elevation of the FoV that leads to larger intersection with $\overline{\mathbb{X}}_{i,\mathcal{L}^{**},k}$ for cones with a low value for the elevation.

Regarding the target set estimate, one observes that $\phi(\mathbb{X}_k)$ remains small compared to $\phi(\overline{\mathbb{X}}_{\ell,k})$ and that the assumptions considered in Section 5.3.3.1 are reasonable.

The reduction of $\phi(\overline{\mathbb{X}}_k)$ appears only after an area has been explored from locations belonging to the L different observation cones since $\overline{\mathbb{X}}_{i,k} = \bigcup_{\ell \in \{1,...,L\}} \overline{\mathbb{X}}_{i,\ell,k}$. This explains the initially flat slope of $\phi(\overline{\mathbb{X}}_k)$. It takes more time to completely explore an area from a point of view in every conic observation subset.

The computation time for a time horizon of 600 s is 2121 s with an Intel Xeon W-2123 processor with 16 GB of RAM running Windows 10. Video sequences of the simulations are in the folder *Videos\Chapter_5\5.3...* or at `https://drive.google.com/drive/folders/1djk7qQJCGBYPKVwD8nAey7C9f4bbQ65I?usp=sharing`

Note that in the video sequences some UAVs are leaving the RoI during the search. This allows UAVs to turn and better reduce the size of the unexplored sets.

This section proposed and illustrated via simulations an algorithm for cooperative search of ground targets by a fleet of UAVs. The approach accounts for potential occultation of targets by unknown obstacles. To assess the presence or absence of targets it is necessary to collect observations from a variety of points of view.

Instead of considering a probability of non-detection that could be difficult to tailor to the various relative positions of the targets and obstacles, the notion of *detectability set* for a target was introduced. A robust distributed set-membership estimator provides set estimates of the target locations. The resulting set estimates are guaranteed to contain the locations of all the targets within the search area. The search strategy is be adapted to provide trajectories that sweep the different points of view required to conclude the effective presence or absence of a target at a given location. An MPC approach determines the control inputs that minimize a measure of the set estimates accounting for the detection performance. The distributed algorithms take advantage of communications of data among neighboring UAVs. The performance of the resulting method is illustrated via simulations.

5.4. General case – Time-variant detectability set

After having presented a solution to search static partially hidden targets in Section 5.3, the more general case is considered where the targets and obstacles are evolving with time, thus, the target state $\mathbf{x}_{j,k}^{\mathrm{t}}$, the obstacle $\mathcal{O}_{m,k}$, and detectability set $\mathbb{D}_k(\boldsymbol{x})$ are changing with t_k. The main difficulty compared to Section 5.3 comes from the fact the evolution of the detectability set $\mathbb{D}_k(\boldsymbol{x})$ is unknown. The information collected in the set estimate $\overline{\mathbb{X}}_{i,\ell,k}$ in Section 5.3.1.3 at time t_k can not be used at time t_{k+1}. It is not possible to observe a location gradually from different points of view since the targets are moving.

To address this problem it is assumed that each detectability set contains at least one non-zero volume half-cone at each time instant. This translates again the fact that targets are never fully occluded by the environment. The absence of a map of the environment and the unknown detectability sets makes it particularly challenging for UAVs to conclude the absence of a moving target when they observe only a part of the RoI.

To state that a location in the RoI is clear from any target, one has to observe this location simultaneously with a sufficient diversity of points of view. The fleet of

UAVs is partitioned into groups to reach this diversity, where each UAV is in charge of observing the RoI with a given point of view. Once a target is detected, it is again assumed that its location is obtained with some bounded uncertainty. The distributed set-membership state estimator presented in Section 5.3 is extended to evaluate sets guaranteed to contain target locations within the RoI, and a set that is proven to be clear from any target. Contrary to the approach in Section 5.3, the new estimator is able to guarantee the detection of partly hidden *moving* targets in a *changing* environment. In order to solve the non-detection issues, an approach where UAVs have to cooperate significantly more than in Section 5.3 is presented. The proposed solution is to organize them into dedicated groups in which they stay in formation.

5.4.1. Proposed solution

Following the same reasoning as in Section 5.3.1 one introduces, for each $\mathbf{x} \in \mathbb{X}_k^{\mathrm{T}}$, L conic observation subsets $\mathbb{C}_\ell(\boldsymbol{x})$, where $\boldsymbol{x} = p^{\mathrm{t}}(\mathbf{x})$. It is additionally assumed that for all k the detectability set $\underline{\mathbb{D}}_k(\boldsymbol{x}) \subset \mathbb{D}_k(\boldsymbol{x})$ is of non-zero volume and that at least one conic observation subset is included in $\mathbb{D}_k(\boldsymbol{x})$, *i.e.*,

$$\exists \ell \in \{1, \ldots, L\}, \mathbb{C}_\ell(\boldsymbol{x}) \subset \underline{\mathbb{D}}_k(\boldsymbol{x}), \forall k. \tag{5.35}$$

Consequently, provided that $\mathbf{x}$ is *simultaneously* observed from a sufficiently large but *finite* number L of different observation locations, one can prove again that there exists at least one of these observation locations $\boldsymbol{x}^{\mathrm{u}}$ – of a generic UAV with state $\mathbf{x}^{\mathrm{u}}$ and location $\boldsymbol{x}^{\mathrm{u}} = p(\mathbf{x}^{\mathrm{u}})$ – such that $\boldsymbol{x}^{\mathrm{u}} \in \underline{\mathbb{D}}_k(\boldsymbol{x})$.

To prove the absence of a moving target at some location $\boldsymbol{x}$, Proposition 2 in Section 5.3.1.2 is adapted.

Proposition 3. *At time t_k, consider some state $\mathbf{x} \in \mathbb{X}^T$ and location $\boldsymbol{x} = p^t(\mathbf{x})$ with detectability set $\mathbb{D}_k(\boldsymbol{x})$, L conic observations subsets $\mathbb{C}_\ell(\boldsymbol{x})$ satisfying (5.35). Assume that a set of $N \geqslant L$ UAVs with states $\mathbf{x}_{i,k}^u$, $i = 1, \ldots, N$, is such that for all $\ell = 1, \ldots, L$ there exists $i_\ell \in \{1, \ldots, N\}$ satisfying $\boldsymbol{x}_{i_\ell,k}^u = p(\mathbf{x}_{i_\ell,k}^u) \in \mathbb{C}_\ell(\boldsymbol{x})$ and $\mathbf{x} \in \mathbb{F}_\ell(\mathbf{x}_{i_\ell,k}^u)$. If $c_\ell(\mathbf{x}_{i_\ell,k}^u, \mathbf{x}) = 0$ for all $\ell = 1, \ldots, L$, then there is no target at $\boldsymbol{x}$.*

Proof. At time t_k, assume that target j with state $\mathbf{x}$ is located at $\boldsymbol{x}$, *i.e.*, $\mathbf{x}_{j,k}^{\mathrm{t}} = \mathbf{x}$ and $\boldsymbol{x}_{j,k}^{\mathrm{t}} = \boldsymbol{x}$, and that $c_\ell(\mathbf{x}_{i,k}^{\mathrm{u}}, \mathbf{x}) = 0$ for all $\ell = 1, \ldots, L$ and $i = 1, \ldots, N$. Since there exists ℓ such that $\mathbb{C}_\ell(\boldsymbol{x}) \subset \mathbb{D}_k(\boldsymbol{x})$ and there exists $i_\ell \in \{1, \ldots, N\}$ such that $\boldsymbol{x}_{i_\ell,k}^{\mathrm{u}} \in \mathbb{C}_\ell(\boldsymbol{x})$, one has $\boldsymbol{x}_{i_\ell,k}^{\mathrm{u}} \in \mathbb{C}_\ell(\boldsymbol{x}) \subset \mathbb{D}_k(\boldsymbol{x})$. Moreover, as $\mathbf{x} \in \mathbb{F}_\ell(\mathbf{x}_{i_\ell,k}^{\mathrm{u}})$, according to (5.2), target j should have been detected, *i.e.*, $j \in \mathcal{D}_\ell$ and a measurement $\mathbf{y}_{i_\ell,j} = \mathbf{h}_{i_\ell}(\mathbf{x}_{i_\ell,k}^{\mathrm{u}}, \mathbf{x}_{j,k}^{\mathrm{t}}) + \mathbf{w}_{i_\ell,j}$, with $\mathbf{w}_{i_\ell,j} \in [\mathbf{w}_{i_\ell}]$ should be available. Thus $\mathbf{h}_{i_\ell}(\mathbf{x}_{i_\ell,k}^{\mathrm{u}}, \mathbf{x}) \in [\mathbf{y}_{i_\ell,j,k}]$ and $c_{i_\ell}(\mathbf{x}_{i_\ell,k}^{\mathrm{u}}, \mathbf{x}) = 1$, which contradicts the initial assumptions. □

Proposition 3 states that observations acquired simultaneously from at least L UAVs with states $\mathbf{x}^{\mathrm{u}}_{i_\ell,k}$, $\ell = 1, \ldots, L$, are sufficient to prove the absence of a target located at $\boldsymbol{x}$. This property is illustrated hereafter and leads us to the introduction of groups of UAVs with at least L members in Section 5.4.1.1.

A single UAV can explore the RoI and collect gradually a sufficient amount of observations to detect every target as done in Section 5.3.1 only when the detectability set $\mathbb{D}_k(\boldsymbol{x})$ is constant over time for each $\mathbf{x} \in \mathbb{X}^{\mathrm{T}}_k$ and when targets are not moving. This is no more possible when $\mathbb{D}_k(\boldsymbol{x})$ is time-dependent or when targets are moving as illustrated in Figure 5.8. In Figure 5.8 a), a single UAV searches for a moving target (black dot) in a cluttered environment. Even if the UAV moves around the obstacle, provided that the target remains in the shadow of the obstacle (gray area), it will never be detected. Two UAVs collecting measurements simultaneously are not enough too, as illustrated in Figure 5.8 b), the target may remain undetected in the red area. In that case, a clever control design may allow the detection of the target with only two UAVs, provided that they move in opposite directions around the pillar. Nevertheless, this requires knowing the obstacle's shape and location. Figure 5.8 c) shows that three properly positioned UAVs observing *simultaneously* the area around a pillar are sufficient to guarantee the target detection.

In Figure 5.8, the part of the FoV occulted by the obstacle has been emphasized (gray and red areas). In practice, in the proposed approach, the knowledge of the obstacle locations and the thereby hidden areas is not needed. Only Assumption (5.9) needs to be satisfied.

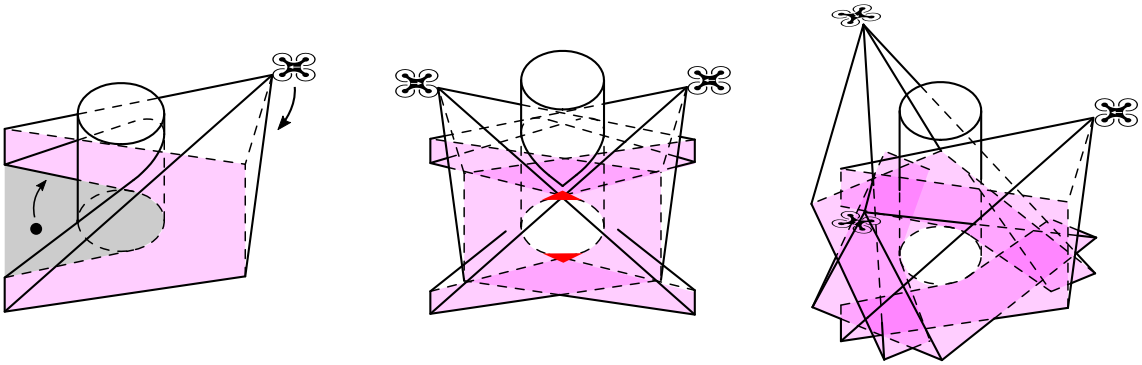

Figure 5.8.: UAVs searching for a target (black dot) in presence of an obstacle (pillar); When considering only one or two UAVs, a target can easily hide behind the pillar in the shadow of the obstacle (gray or red area) and may never be inside visible area (pink); Here, three cooperating UAVs are sufficient to guarantee the target detection.

In Section 5.4.1.1, the fleet of UAVs is partitioned into groups to ensure the diversity of observation points of view. Finally, Section 5.4.1.2 and 5.4.1.3 characterize the

observed subsets of each group and the set estimate that is obtained when measurements are collected.

5.4.1.1. Groups of UAVs to search and track moving targets

As stated in Proposition 3, when L conic observation subsets are considered, at least L UAVs have to simultaneously gather observations from L different points of view to prove the absence of a target at some location. The choice is to partition the fleet of UAVs into N^{g} groups of L UAVs each, *i.e.,* $N^{\mathrm{u}} = N^{\mathrm{g}}L$. The UAVs with indices in the set $\mathcal{N}_g = (g-1)\,L + \{1,\ldots,L\}$ form group g. UAVs of the same group are assumed to share the same amount of information, *i.e.*, the communication inside a group is perfect and instantaneous. At time t_k, the list of UAV states of group g is

$$\mathcal{G}_{g,k} = \left\{ \mathbf{x}^{\mathrm{u}}_{i,k} \mid i \in \mathcal{N}_g \right\}. \tag{5.36}$$

5.4.1.2. Observed subsets by a group of UAVs

In this section, two types of subsets of $\mathbb{X}_0$ from observations obtained by the UAVs of a group g are introduced. At time t_k, the subset of points observed by the group from the conic observation subset $\mathbb{C}_\ell$ is

$$\mathbb{F}_\ell\left(\mathcal{G}_{g,k}\right) = \bigcup_{\mathbf{x}^{\mathrm{u}}_{i,k} \in \mathcal{G}_{g,k}} \mathbb{F}_{i,\ell}\left(\mathbf{x}^{\mathrm{u}}_{i,k}\right), \tag{5.37}$$

for $\ell = 1,\ldots,L$. Using $\mathbb{F}_\ell\left(\mathcal{G}_{g,k}\right)$, one introduces the *completely observed set*

$$\underline{\mathbb{F}}\left(\mathcal{G}_{g,k}\right) = \bigcap_{\ell \in \{1,\ldots,L\}} \mathbb{F}_\ell\left(\mathcal{G}_{g,k}\right), \tag{5.38}$$

as the set of all points observed simultaneously from L different conic observation subsets. One can also evaluate the *partially observed set*

$$\overline{\mathbb{F}}\left(\mathcal{G}_{g,k}\right) = \bigcup_{\ell \in \{1,\ldots,L\}} \mathbb{F}_\ell\left(\mathcal{G}_{g,k}\right), \tag{5.39}$$

as the set of points observed by at least one UAV of the group. A target cannot be detected at time t_k if it is located outside $\overline{\mathbb{F}}\left(\mathcal{G}_{g,k}\right)$. Using Proposition 4, one can prove the absence of targets in $\underline{\mathbb{F}}\left(\mathcal{G}_{g,k}\right)$ when no target is detected.

Proposition 4. *If at time t_k, $\mathcal{D}_{i,k} = \emptyset$ for all $i \in \mathcal{N}_g$ then $\underline{\mathbb{F}}\left(\mathcal{G}_{g,k}\right)$ does not contain undetected targets.*

Proof. At time t_k, assume that some target j has state $\mathbf{x} \in \mathbb{X}^{\mathrm{T}}$,with location $\boldsymbol{x} = p^{\mathrm{t}}(\mathbf{x})$, such that $\mathbf{x} \in \underline{\mathbb{F}}\left(\mathcal{G}_{g,k}\right)$, *i.e.*, $\mathbf{x}^{\mathrm{t}}_{j,k} = \mathbf{x}$ and $\boldsymbol{x}^{\mathrm{t}}_{j,k} = \boldsymbol{x}$, and that $\mathcal{D}_{i,k} = \emptyset$ for all $i = 1,\ldots,L$. As $\mathbf{x} \in \underline{\mathbb{F}}\left(\mathcal{G}_{g,k}\right)$, from (5.38), one has $\mathbf{x} \in \mathbb{F}_\ell\left(\mathcal{G}_{g,k}\right)$ for all $\ell = 1,\ldots,L$.

Moreover, from (5.37), for all $\ell = 1, \ldots, L$ there exists at least one UAV i such that $\mathbf{x} \in \mathbb{F}_{i,\ell}(\mathbf{x}^{\mathrm{u}}_{i,k})$. According to Proposition 3, since $\mathcal{D}_{i,k} = \emptyset$ for all $i = 1, \ldots, L$, there is no target located at $\boldsymbol{x}$, which contradicts the initial assumption. □

The shape of $\underline{\mathbb{F}}(\mathcal{G}_{g,k})$ depends on the conic observation subsets, on the shape of the FoV, and on the state of each UAV of the group g as illustrated by Figure 5.9. Figure 5.9 shows the intersection of the subsets $\mathbb{F}_{i,\ell}(\mathbf{x}^{\mathrm{u}}_{i,k})$ with two horizontal planes with different altitude. The orientation of the group is changed in each of the three subplots. The colors of the subsets $\mathbb{F}_{i,\ell}(\mathbf{x}^{\mathrm{u}}_{i,k})$ are those of the corresponding conic observation subsets $\mathbb{C}_1, \ldots, \mathbb{C}_4$ shown in Figure 5.9. The completely observed subset $\underline{\mathbb{F}}(\mathcal{G}_{g,k})$ (dark gray) is the set of locations where the individual FoVs overlap. The shape of $\underline{\mathbb{F}}(\mathcal{G}_{g,k})$ depends on the constraints regarding the FoV or the point of view. A group formation that is not optimized with respect to conic observation subsets, leads to a subset $\underline{\mathbb{F}}(\mathcal{G}_{g,k})$ with reduced volume (middle) or even to $\underline{\mathbb{F}}(\mathcal{G}_{g,k}) = \emptyset$ (right). One observes that the size of $\underline{\mathbb{F}}(\mathcal{G}_{g,k})$ is maximized when the size of $\mathbb{F}_{i,\ell}(\mathbf{x}^{\mathrm{u}}_{i,k})$ is maximized for some ℓ. Since $\underline{\mathbb{F}}(\mathcal{G}_{g,k})$ is a subset of $\mathbb{F}_{\ell}(\mathcal{G}_{g,k})$ for all $\ell = 1, \ldots, L$, the group may detect targets outside of $\underline{\mathbb{F}}(\mathcal{G}_{g,k})$. The subset $\overline{\mathbb{F}}(\mathcal{G}_{g,k})$ is illustrated in Figure 5.9 in light gray. Even if $\mathcal{D}_{i,k} = \emptyset$ for all $i \in \mathcal{N}_g$, the absence of target in $\overline{\mathbb{F}}(\mathcal{G}_{g,k}) \setminus \underline{\mathbb{F}}(\mathcal{G}_{g,k})$ cannot be guaranteed.

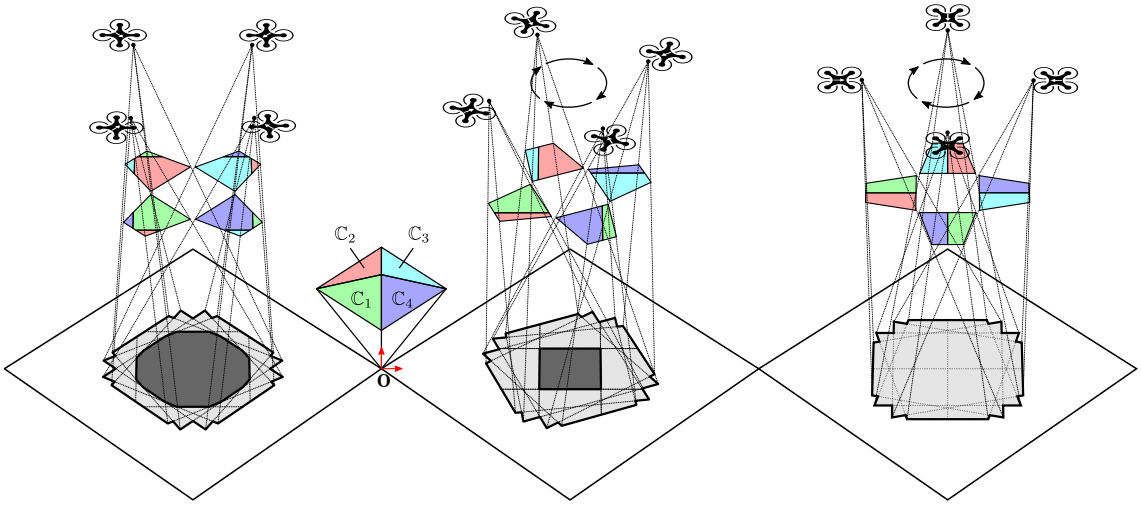

Figure 5.9.: FoV subsets $\mathbb{F}_{i,\ell}(\mathbf{x}^{\mathrm{u}}_{i,k})$ of individual UAVs with colors corresponding to the associated half-cones $\mathbb{C}_1, \ldots, \mathbb{C}_4$. FoV subsets $\underline{\mathbb{F}}(\mathcal{G}_{g,k})$ (dark gray) and $\overline{\mathbb{F}}(\mathcal{G}_{g,k})$ (light gray) when the individual FoVs overlap (subplots on the right) for different orientations of group of UAVs.

5.4.1.3. Estimates from group measurements

This section describes the set estimates which may be obtained gathering information collected by each UAV in a group g. It is assumed that the UAVs in a group are

complete connected and share their information instantaneously. Section 5.4.4.3 discusses practical issues related to information exchange between UAVs of the group and between groups.

At time instant t_k, assume that UAV i in group g has detected targets with indices in $\mathcal{D}_{i,k}$. After sharing this information with the group, the list of targets detected by the group g at time t_k is

$$\mathcal{D}^{\mathrm{t}}_{g,k} = \bigcup_{i \in \mathcal{N}_g} \mathcal{D}_{i,k}. \tag{5.40}$$

The superscript $^{\mathrm{t}}$ indicates collected information about the targets available to the group. For any $j \in \mathcal{D}^{\mathrm{t}}_{g,k}$, the subset $\mathcal{N}_{g,j,k} = \{i \in \mathcal{N}_g \mid j \in \mathcal{D}_{i,k}\}$ contains indices of UAVs which detect target j at time t_k. For all $i \in \mathcal{N}_{g,j,k}$, the state $\mathbf{x}^{\mathrm{t}}_{j,k}$ of target j at time t_k has to belong to $\mathbb{F}_i(\mathbf{x}^{\mathrm{u}}_{i,k})$ and can be estimated as

$$\mathbb{S}_{i,j,k} = \left\{ \mathbf{x} \in \mathbb{F}_i\left(\mathbf{x}^{\mathrm{u}}_{i,k}\right) \mid \mathbf{h}_i\left(\mathbf{x}^{\mathrm{u}}_{i,k}, \mathbf{x}\right) \in \mathbf{y}_{i,j,k} - [\mathbf{w}_i] \right\}, \tag{5.41}$$

which is the set of target locations consistent with the measurement $\mathbf{y}_{i,j,k}$ obtained by UAV i, the measurement equation (5.3), and the measurement noise bound $[\mathbf{w}_i]$. The set estimate of $\mathbf{x}^{\mathrm{t}}_{j,k}$ obtained by the group g is then the set of target states consistent with all measurements from the UAVs in $\mathcal{N}_{g,j,k} \subset \mathcal{N}_g$ and is defined as the intersection of the sets $\mathbb{S}_{i,j,k}$, $i \in \mathcal{N}_{g,j,k}$, *i.e.*,

$$\mathbb{S}^{\mathrm{t}}_{g,j,k} = \bigcap_{i \in \mathcal{N}_{g,j,k}} \mathbb{S}_{i,j,k}. \tag{5.42}$$

Figure 5.10 shows the estimates $\mathbb{S}_{i,j,k}$ (left) obtained by different UAVs of group g and the resulting estimates $\mathbb{S}^{\mathrm{t}}_{g,j,k}$ obtained gathering the information of each member of group g (right). The figure illustrates a case where $L = 4$ and $|\mathcal{N}_{g,j,k}| = 3$. Here the detected target lies in $\underline{\mathbb{F}}(\mathcal{G}_{g,k})$, however, targets can be also detected in $\overline{\mathbb{F}}(\mathcal{G}_{g,k})$.

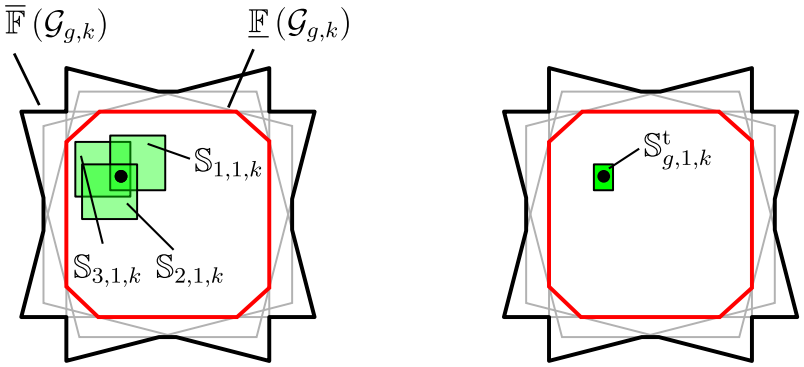

Figure 5.10.: Set estimate $\mathbb{S}_{i,1,k}$ processed by different UAVs $i \in \{1, 2, 3\}$ of group g (left) and resulting group estimate $\mathbb{S}^{\mathrm{t}}_{g,1,k}$ for target $j = 1$ (right).

5.4.2. Evolution of the target set estimates

It is assumed that each UAV i of a group g has the same information $\mathbb{I}^{\mathrm{t}}_{g,k}$ as the other UAVs in the group, *i.e.*, $\mathbb{I}_{i,k} = \mathbb{I}^{\mathrm{t}}_{g,k}$, $i \in \mathcal{N}_g$. Let $\mathcal{L}^{\mathrm{t}}_{g,k}$ be the list of indices of targets already detected by the group g, $\mathcal{X}^{\mathrm{t}}_{g,k}$ be the list of set estimates of already detected targets, and $\overline{\mathbb{X}}^{\mathrm{t}}_{g,k}$ be the set of possible locations of targets not yet detected for group g. The aim is to minimize the target estimation uncertainty $\Phi\left(\mathcal{X}^{\mathrm{t}}_{g,k}, \overline{\mathbb{X}}^{\mathrm{t}}_{g,k}\right)$ of group g, similarly to (5.4).

Remark 5. The evolution of $\mathbb{I}^{\mathrm{t}}_{g,k}$, $\mathcal{X}^{\mathrm{t}}_{g,k}$, and $\overline{\mathbb{X}}^{\mathrm{t}}_{g,k}$ may be either evaluated and maintained by all UAVs or by some leader. For simplification it is assumed that all UAVs in a group evaluate these estimates and that there is some virtual group entity, that maintains the values $\mathbb{I}^{\mathrm{t}}_{g,k}$, $\mathcal{X}^{\mathrm{t}}_{g,k}$, and $\overline{\mathbb{X}}^{\mathrm{t}}_{g,k}$. This may increase robustness to the loss of UAVs, but it also demands more communication and synchronization between UAVs.

Section 5.4.2.1 presents the evolution of $\mathbb{I}^{\mathrm{t}}_{g,k}$, $\mathcal{L}^{\mathrm{t}}_{g,k}$, and of the set estimates $\mathcal{X}^{\mathrm{t}}_{g,k}$ and $\overline{\mathbb{X}}^{\mathrm{t}}_{g,k}$ when new information is available to group g. For the initialization, one has $\mathcal{L}^{\mathrm{t}}_{g,0} = \emptyset$, $\mathcal{X}^{\mathrm{t}}_{g,0} = \emptyset$, $\overline{\mathbb{X}}^{\mathrm{t}}_{g,0} = \mathbb{X}_0$ for each group $g = 1, \ldots, N^{\mathrm{g}}$ at time t_0. The following approach is an adaptation of the estimator presented in Section 5.3.2 to set estimates managed by groups. The state estimator starts with the prediction of the sets followed by a correction from measurements and information received from neighboring groups.

5.4.2.1. Prediction step

At time t_k, group g has access to $\mathbb{I}^{\mathrm{t}}_{g,k}$, $\mathcal{L}^{\mathrm{t}}_{g,k}$, $\mathcal{X}^{\mathrm{t}}_{g,k}$, and $\overline{\mathbb{X}}^{\mathrm{t}}_{g,k}$. Accounting for the dynamics of the targets, the predicted value $\mathbb{X}^{\mathrm{t}}_{g,j,k+1|k}$ of $\mathbb{X}^{\mathrm{t}}_{g,j,k+1}$ at time t_{k+1} is obtained as

$$\begin{aligned}\mathbb{X}^{\mathrm{t}}_{g,j,k+1|k} &= \left\{\mathbf{f}^{\mathrm{t}}_k(\mathbf{x}, \mathbf{v}) \mid \mathbf{x} \in \mathbb{X}^{\mathrm{t}}_{g,j,k}, \mathbf{v} \in [\mathbf{v}]\right\} \cap \mathbb{X}_0 \\ &= \mathbf{f}^{\mathrm{t}}_k\left(\mathbb{X}^{\mathrm{t}}_{g,j,k}, [\mathbf{v}]\right) \cap \mathbb{X}_0. \end{aligned} \tag{5.43}$$

The possible target states of a detected target $j \in \mathcal{L}^{\mathrm{t}}_{g,k}$ are evaluated from the dynamics (3.2) and the bound $[\mathbf{v}]$ of the state perturbations. One assumes here that the targets do not leave the RoI $\mathbb{X}_0$. The set of all predicted target set estimates is then $\mathcal{X}^{\mathrm{t}}_{g,k+1|k} = \left\{\mathbb{X}^{\mathrm{t}}_{g,j,k+1|k}\right\}_{j \in \mathcal{L}^{\mathrm{t}}_{g,k}}$.

The predicted value $\overline{\mathbb{X}}^{\mathrm{t}}_{g,k+1|k}$ of $\overline{\mathbb{X}}^{\mathrm{t}}_{g,k+1}$ is obtained similarly as all targets are assumed to share the same dynamics (3.2) and the same bound $[\mathbf{v}]$ of the state perturbations. Consequently,

$$\overline{\mathbb{X}}^{\mathrm{t}}_{g,k+1|k} = \mathbf{f}^{\mathrm{t}}_k\left(\overline{\mathbb{X}}^{\mathrm{t}}_{g,k}, [\mathbf{v}]\right) \cap \mathbb{X}_0. \tag{5.44}$$

5.4.2.2. Correction step after measurements

At time t_{k+1}, group g observes the subspace $\overline{\mathbb{F}}(\mathcal{G}_{g,k+1})$, detects targets with indices in $\mathcal{D}^{\mathrm{t}}_{g,k+1}$, and obtains an estimate $\mathbb{S}^{\mathrm{t}}_{g,j,k+1}$ for each detected target j in $\mathcal{D}^{\mathrm{t}}_{g,k+1}$ based on the measurements of UAVs in $\mathcal{N}_{g,j,k+1}$. This is based on the assumption that the UAVs of a group share all their information and are able to evaluate $\mathbb{S}^{\mathrm{t}}_{g,j,k+1}$. This information is gathered in $\mathbb{I}^{\mathrm{t}}_{g,k+1|k+1}$ as

$$\mathbb{I}^{\mathrm{t}}_{g,k+1|k+1} = \mathbb{I}^{\mathrm{t}}_{g,k} \cup \left\{ \mathcal{D}^{\mathrm{t}}_{g,k+1}, \left\{ \mathbb{S}^{\mathrm{t}}_{g,j,k+1} \right\}_{j \in \mathcal{D}^{\mathrm{t}}_{g,k+1}} \right\}. \tag{5.45}$$

The updated list of detected targets is

$$\mathcal{L}^{\mathrm{t}}_{g,k+1|k+1} = \mathcal{L}^{\mathrm{t}}_{g,k} \cup \mathcal{D}^{\mathrm{t}}_{g,k+1}. \tag{5.46}$$

Three cases have then to be considered when updating $\mathbb{X}^{\mathrm{t}}_{g,j,k+1|k}$. The group may either detect a new target, detect a known target again, or not detect a known target again.

Case 1 When $j \in \mathcal{D}^{\mathrm{t}}_{g,k+1}$ and $j \notin \mathcal{L}^{\mathrm{t}}_{g,k}$, a new target is detected. This target may only be located in $\overline{\mathbb{X}}^{\mathrm{t}}_{g,k+1|k}$, and the target is observed by at least one UAV of the group and the estimate $\mathbb{S}^{\mathrm{t}}_{g,j,k+1}$ is obtained as described in (5.42). The set estimate for this new target is then

$$\mathbb{X}^{\mathrm{t}}_{g,j,k+1|k+1} = \overline{\mathbb{X}}^{\mathrm{t}}_{g,k+1|k} \cap \mathbb{S}^{\mathrm{t}}_{g,j,k+1}. \tag{5.47}$$

The set $\mathbb{X}^{\mathrm{t}}_{g,j,k+1|k+1}$ accounts for the predicted potential locations of undetected targets in $\overline{\mathbb{X}}^{\mathrm{t}}_{g,k+1|k}$ from (5.44) and the obtained measurements of the group.

Case 2 When $j \in \mathcal{D}^{\mathrm{t}}_{g,k+1}$ and $j \in \mathcal{L}^{\mathrm{t}}_{g,k}$, the previously detected target j is detected again. Target j has to be located in the predicted set $\mathbb{X}^{\mathrm{t}}_{g,j,k+1|k}$. As above, the target is observed by at least one UAV leading to the estimate $\mathbb{S}^{\mathrm{t}}_{g,j,k+1}$. The corrected target set estimate is then

$$\mathbb{X}^{\mathrm{t}}_{g,j,k+1|k+1} = \mathbb{X}^{\mathrm{t}}_{g,j,k+1|k} \cap \mathbb{S}^{\mathrm{t}}_{g,j,k+1}. \tag{5.48}$$

Case 3 When $j \notin \mathcal{D}^{\mathrm{t}}_{g,k+1}$ and $j \in \mathcal{L}^{\mathrm{t}}_{g,k}$, a detected target is not detected again. Group g observes the subset $\overline{\mathbb{F}}(\mathcal{G}_{g,k+1})$ but only the subset $\underline{\mathbb{F}}(\mathcal{G}_{g,k+1})$ is proved not to contain undetected targets. Since $\mathbf{x}^{\mathrm{t}}_{j,k+1} \notin \underline{\mathbb{F}}(\mathcal{G}_{g,k+1})$ when $j \notin \mathcal{D}^{\mathrm{t}}_{g,k+1}$, the corrected target set estimate is evaluated as

$$\mathbb{X}^{\mathrm{t}}_{g,j,k+1|k+1} = \mathbb{X}^{\mathrm{t}}_{g,j,k+1|k} \setminus \underline{\mathbb{F}}(\mathcal{G}_{g,k+1}). \tag{5.49}$$

All measurements of detected targets in $\overline{\mathbb{F}}(\mathcal{G}_{g,k+1})$ are processed and taken into account to evaluate $\mathbb{X}^{\mathrm{t}}_{g,j,k+1|k+1}$, for all $j \in \mathcal{L}^{\mathrm{t}}_{g,k+1|k+1}$. One can now update the set $\overline{\mathbb{X}}^{\mathrm{t}}_{g,k+1|k}$ of potential target states of undetected targets. As in (5.49), only $\underline{\mathbb{F}}(\mathcal{G}_{g,k+1})$ is proved not to contain undetected targets. Consequently, the corrected set of potential target states of undetected targets is

$$\overline{\mathbb{X}}^{\mathrm{t}}_{g,k+1|k+1} = \overline{\mathbb{X}}^{\mathrm{t}}_{g,k+1|k} \setminus \underline{\mathbb{F}}(\mathcal{G}_{g,k+1}). \tag{5.50}$$

5.4.2.3. Correction step after communication between groups of UAVs

After having processed the collected measurements, each group exchanges its information with neighboring groups $n \in \mathcal{N}^{\mathrm{g}}_{g,k+1}$, where

$$\mathcal{N}^{\mathrm{g}}_{g,k+1} = \left\{ n \in \{1, \ldots, N^{\mathrm{g}}\} \mid \exists \ell \in \mathcal{N}_n, \exists \ell' \in \mathcal{N}_g, \left(\ell, \ell'\right) \in \mathcal{E}_{k+1} \right\}. \tag{5.51}$$

This means means that two groups are assumed to be able to exchange information as soon as at least one UAV in one group is able to communicate with at least one UAV of the other group.

Group g sends its information $\mathbb{I}^{\mathrm{t}}_{g,k+1|k+1}$ and receives the corresponding information $\mathbb{I}^{\mathrm{t}}_{n,k+1|k+1}$ from each group $n \in \mathcal{N}^{\mathrm{g}}_{g,k+1}$. For group g, the available information and the list of known targets can be updated as

$$\mathbb{I}^{\mathrm{t}}_{g,k+1} = \bigcup_{n \in \mathcal{N}^{\mathrm{g}}_{g,k+1} \cup \{g\}} \mathbb{I}^{\mathrm{t}}_{n,k+1|k+1} \tag{5.52}$$

and

$$\mathcal{L}^{\mathrm{t}}_{g,k+1} = \bigcup_{n \in \mathcal{N}^{\mathrm{g}}_{g,k+1} \cup \{g\}} \mathcal{L}^{\mathrm{t}}_{n,k+1|k+1}. \tag{5.53}$$

The updated set estimates after communication are obtained as the intersection of the set estimates obtained by each group. Consequently, the corrected target set estimate $\mathbb{X}^{\mathrm{t}}_{g,j,k+1}$ is updated as

$$\mathbb{X}^{\mathrm{t}}_{g,j,k+1} = \bigcap_{n \in \mathcal{N}^{\mathrm{g}}_{g,k+1} \cup \{g\} | j \in \mathcal{L}^{\mathrm{t}}_{n,k+1|k+1}} \mathbb{X}^{\mathrm{t}}_{n,j,k+1|k+1}, \tag{5.54}$$

to account for the set estimates of groups n who have detected targets $j \in \mathcal{L}^{\mathrm{t}}_{g,k+1}$ that were received from neighboring groups. The list of all target set estimates is then $\mathcal{X}^{\mathrm{t}}_{g,k+1} = \left\{ \mathbb{X}^{\mathrm{t}}_{g,j,k+1} \right\}_{j \in \mathcal{L}^{\mathrm{t}}_{g,k+1}}$. Similarly, one can update the remaining unexplored set as

$$\overline{\mathbb{X}}^{\mathrm{t}}_{g,k+1} = \bigcap_{n \in \mathcal{N}^{\mathrm{g}}_{g,k+1} \cup \{g\}} \overline{\mathbb{X}}^{\mathrm{t}}_{n,k+1|k+1}. \tag{5.55}$$

The update processes in Section 5.4.2.1, 5.4.2.2, and 5.4.2.3 can be applied by each group at any time t_{k+1} to evaluate the set $\mathcal{X}^{\mathrm{t}}_{g,k+1}$, and $\overline{\mathbb{X}}^{\mathrm{t}}_{g,k+1}$ from the set $\mathcal{X}^{\mathrm{t}}_{g,k}$, and $\overline{\mathbb{X}}^{\mathrm{t}}_{g,k}$ at time t_k.

5.4.3. Cooperative control design

The objective of the control design is to displace the fleet such that the global uncertainty $\Phi_k = \frac{1}{N^{\mathrm{g}}} \sum_{g=1}^{N^{\mathrm{g}}} \Phi\left(\mathcal{X}^{\mathrm{t}}_{g,k}, \overline{\mathbb{X}}^{\mathrm{t}}_{g,k}\right)$ diminishes as much as possible. As in Section 5.3.3, an MPC approach is adapted to the considered set estimation context to evaluate a sequence of control inputs for each UAV. The aim is to minimize the estimation uncertainty Φ_{k+h} over a prediction horizon of h steps. The optimization problem to solve is

$$\left\{\widehat{\mathbf{u}}_{i,k:k+h-1}\right\}_{i\in\mathcal{N}^{\mathrm{u}}} = \underset{\left\{\mathbf{u}_{i,k:k+h-1}\in\mathbb{U}^h\right\}_{i\in\mathcal{N}^{\mathrm{u}}}}{\arg\min} \frac{1}{N^{\mathrm{g}}} \sum_{g=1}^{N^{\mathrm{g}}} \Phi\left(\mathcal{X}^{\mathrm{t}}_{g,k+h}, \overline{\mathbb{X}}^{\mathrm{t}}_{g,k+h}\right), \tag{5.56}$$

where $\widehat{\mathbf{u}}_{i,k:k+h-1}$ is the sequence of control inputs applied to UAV i at the time instants $\{t_k, t_{k+1} \ldots, t_{k+h-1}\}$. In (5.56), the values of $\mathcal{X}^{\mathrm{t}}_{g,k+h}$ and of $\overline{\mathbb{X}}^{\mathrm{t}}{}_{g,k+h}$ depend on the evolution of the UAVs and thus on $\mathbf{u}_{i,k+\kappa}$, $\kappa = 0, \ldots, h-1$, $i \in \mathcal{N}^{\mathrm{u}}$. From (5.56), one can obtain the control input for each UAV i, $i \in \mathcal{N}^{\mathrm{u}}$, that leads to the smallest global uncertainty Φ_{k+h} after h steps. Nevertheless, the solution of (5.56) is computationally too demanding and requires many communications between UAVs. Consequently, more practical approaches is proposed in what follows.

5.4.3.1. Towards more practical solutions

The size of the various set estimates managed by a group g is mainly reduced via the completely observed subsets $\underline{\mathbb{F}}\left(\mathcal{G}_{g,k}\right)$, as seen in (5.49) and (5.50). The positions and orientations of the UAVs of a group g at time t_k with respect to the orientation of conic observation subsets determine the size of $\underline{\mathbb{F}}\left(\mathcal{G}_{g,k}\right)$ which has to be maximized, as illustrated in Figure 5.9.

Consider a one-step-ahead MPC approach, *i.e.*, $h = 1$. A first practical solution can be obtained by evaluating the set of control inputs of each group independently. Neglecting the contribution to the estimation uncertainty of new measurements related to already or newly detected targets, the set of control inputs of the UAVs of group g can be obtained as

$$\begin{aligned}\left\{\widehat{\mathbf{u}}_{i,k}\right\}_{i\in\mathcal{N}_g} = \arg\min_{\left\{\mathbf{u}_{i,k}\in\mathbb{U}\right\}_{i\in\mathcal{N}_g}} \\ \phi\left(\left(\overline{\mathbb{X}}^{\mathrm{t}}_{g,k+1|k} \setminus \underline{\mathbb{F}}\left(\mathcal{G}_{g,k+1}\right)\right) \cup \bigcup_{j\in\mathcal{L}^{\mathrm{t}}_{g,k}} \left(\mathbb{X}^{\mathrm{t}}_{g,j,k+1|k} \setminus \underline{\mathbb{F}}\left(\mathcal{G}_{g,k+1}\right)\right)\right),\end{aligned} \tag{5.57}$$

where $\mathcal{G}_{g,k+1}$ depends on $\{\mathbf{u}_{i,k}\}_{i\in\mathcal{N}_g}$. This may be rewritten as

$$\{\widehat{\mathbf{u}}_{i,k}\}_{i\in\mathcal{N}_g} = \arg\min_{\{\mathbf{u}_{i,k}\in\mathbb{U}\}_{i\in\mathcal{N}_g}} \phi\left(\left(\overline{\mathbb{X}}^{\mathrm{t}}_{g,k+1|k} \cup \bigcup_{j\in\mathcal{L}^{\mathrm{t}}_{g,k+1}} \mathbb{X}^{\mathrm{t}}_{g,j,k+1|k}\right) \setminus \underline{\mathbb{F}}\left(\mathcal{G}_{g,k+1}\right)\right) \tag{5.58}$$

$$\{\widehat{\mathbf{u}}_{i,k}\}_{i\in\mathcal{N}_g} = \arg\max_{\{\mathbf{u}_{i,k}\in\mathbb{U}\}_{i\in\mathcal{N}_g}} \phi\left(\left(\overline{\mathbb{X}}^{\mathrm{t}}_{g,k+1|k} \cup \bigcup_{j\in\mathcal{L}^{\mathrm{t}}_{g,k+1}} \mathbb{X}^{\mathrm{t}}_{g,j,k+1|k}\right) \cap \underline{\mathbb{F}}\left(\mathcal{G}_{g,k+1}\right)\right) \tag{5.59}$$

which evidences the fact that the size of $\underline{\mathbb{F}}\left(\mathcal{G}_{g,k+1}\right)$ has to be maximized. Solving (5.59) is still computationally demanding since one tries to determine jointly the control input for all UAVs in the group g.

To further simplify the control input design, the choice is to assign a single conic observation subset of index $\ell\left(i\right)$ to each UAV i of group g. UAV i handles the measurement collection from a point of view in $\mathbb{C}_{\ell(i)}$. The structure of $\underline{\mathbb{F}}\left(\mathcal{G}_{g,k}\right)$, see (5.38), imposes that the mapping $\ell\left(i\right)$ fulfills $\bigcup_{i\in\mathcal{N}_g}\{\ell\left(i\right)\} = \{1,\ldots,L\}$ to have $\underline{\mathbb{F}}\left(\mathcal{G}_{g,k}\right)$ not empty, which means that every UAV is associated to a different conic observation subset. A leader with index $i_g \in \mathcal{N}_g$ is chosen for group g at each time t_k. Since $\underline{\mathbb{F}}\left(\mathcal{G}_{g,k+1}\right) \subset \mathbb{F}_{i,\ell(i)}(\mathbf{x}^{\mathrm{u}}_{i,k+1})$, in order to get an approximate solution of (5.59), the leader evaluates

$$\widehat{\mathbf{u}}_{i_g,k} = \arg\max_{\mathbf{u}} \phi\left(\left(\overline{\mathbb{X}}^{\mathrm{t}}_{g,k+1|k} \cup \bigcup_{j\in\mathcal{L}^{\mathrm{t}}_{g,k}} \mathbb{X}^{\mathrm{t}}_{g,j,k+1|k}\right) \cap \mathbb{F}_{i_g,\ell(i_g)}\left(\mathbf{f}^{\mathrm{u}}_k\left(\mathbf{x}^{\mathrm{u}}_{i_g,k},\mathbf{u}\right)\right)\right). \tag{5.60}$$

This control input can be obtained in the same way as in Section 4.4 or 5.3.3.1 for a single UAV. Then, the other UAVs in the group evaluate their control input such that $\mathbb{F}_{i_g,\ell(i_g)}(\mathbf{x}^{\mathrm{u}}_{i_g,k+1}) \cap \mathbb{F}_{i,\ell(i)}(\mathbf{x}^{\mathrm{u}}_{i,k+1})$ is as large as possible. The control inputs of the followers is then evaluated as

$$\begin{aligned}\{\widehat{\mathbf{u}}_{i,k}\}_{i\in\mathcal{N}_g,i\neq i_g} = \arg &\max_{\{\mathbf{u}_i\}_{i\in\mathcal{N}_g,i\neq i_g}} \\ &\phi\left(\mathbb{F}_{i_g,\ell(i_g)}\left(\mathbf{f}^{\mathrm{u}}_k\left(\mathbf{x}^{\mathrm{u}}_{i_g,k},\widehat{\mathbf{u}}_{i_g,k}\right)\right) \cap \bigcap_{i\in\mathcal{N}_g,i\neq i_g} \mathbb{F}_{i,\ell(i)}\left(\mathbf{f}^{\mathrm{u}}_k\left(\mathbf{x}^{\mathrm{u}}_{i,k},\mathbf{u}_i\right)\right)\right).\end{aligned} \tag{5.61}$$

This still requires coordination and consequently communications among agents in a same group, once the leader has evaluated $\widehat{\mathbf{u}}_{i_g,k}$. Therefore, instead of (5.61), it is proposed that each UAV $i \in \mathcal{N}_g, i \neq i_g$ evaluates

$$\widehat{\mathbf{u}}_{i,k} = \arg\max_{\mathbf{u}} \left(\mathbb{F}_{i_g,\ell(i_g)}\left(\mathbf{f}^{\mathrm{u}}_k\left(\mathbf{x}^{\mathrm{u}}_{i_g,k},\widehat{\mathbf{u}}_{i_g,k}\right)\right) \cap \mathbb{F}_{i,\ell(i)}\left(\mathbf{f}^{\mathrm{u}}_k\left(\mathbf{x}^{\mathrm{u}}_{i,k},\mathbf{u}\right)\right)\right). \tag{5.62}$$

Once UAV i_g has evaluated $\widehat{\mathbf{u}}_{i_g,k}$ using (5.61), each UAV of group g, as soon as it has access to $\mathbb{F}_{i_g,\ell(i_g)}(\mathbf{f}^{\mathrm{u}}_k(\mathbf{x}^{\mathrm{u}}_{i_g,k},\widehat{\mathbf{u}}_{i_g,k}))$, can evaluate (5.62) independently from the

other UAVs of the group. The latter approach is thus amenable to a distributed evaluation of the control inputs. An additional advantage is that only the leader needs to account for the set estimates $\overline{\mathbb{X}}^{\mathrm{t}}_{g,k+1|k}$ and $\mathbb{X}^{\mathrm{t}}_{g,j,k+1|k}$, $j \in \mathcal{L}^{\mathrm{t}}_{g,k}$, which may be less computational demanding.

5.4.3.2. Predicting the impact of the control input

From (5.60) and (5.62) in Section 5.4.3.1 one can evaluate a set of control inputs for all UAVs of a single group that maximizes the intersection of the FoV subsets $\mathbb{F}_{i,\ell(i)}$ with the set estimates $\overline{\mathbb{X}}^{\mathrm{t}}_{g,k+1|k}$ and $\mathbb{X}^{\mathrm{t}}_{g,j,k+1|k}$ after one time step. In this section, the aim is to evaluate the impact of the set of control inputs of group g and of neighboring groups ℓ on the set estimates maintained by group g in order to determine the set of control inputs $\{\widehat{\mathbf{u}}_{i,k+1}\}_{i\in\mathcal{N}_g}$. This prediction process is then applied iteratively on the predicted set estimates to evaluate the impact of $\{\widehat{\mathbf{u}}_{i,k+\kappa}\}_{i\in\mathcal{N}_g}$, $\kappa = 0, \ldots, h-1$.

At time t_k, the values of $\mathbb{I}^{\mathrm{t}}_{g,k}$, $\mathcal{L}^{\mathrm{t}}_{g,k}$, $\mathcal{X}^{\mathrm{t}}_{g,k}$, and $\overline{\mathbb{X}}^{\mathrm{t}}_{g,k}$ are available to group g. Following Section 5.4.2.1, the leader can evaluate the predicted set $\mathcal{X}^{\mathrm{t}}_{g,k+1|k}$ and $\overline{\mathbb{X}}^{\mathrm{t}}_{g,k+1|k}$ starting from $\mathcal{X}^{\mathrm{t}}_{g,k}$ and $\overline{\mathbb{X}}^{\mathrm{t}}_{g,k}$.

For the correction step from measurements the leader predicts the completely observed subset $\underline{\mathbb{F}}(\mathcal{G}_{g,k})$ of the group for a given set of control inputs $\{\widehat{\mathbf{u}}_{i,k}\}_{i\in\mathcal{N}_g}$. The leader evaluates $\mathcal{G}_{g,k+1}$ using (3.1) and (5.36). Then, it deduces the future FoV $\underline{\mathbb{F}}(\mathcal{G}_{g,k+1})$ at t_{k+1}. Compared to Section 5.4.2.2, one cannot determine whether a target will be detected except if a predicted set estimate $\mathbb{X}^{\mathrm{t}}_{g,j,k+1|k}$ for some target j is included in $\underline{\mathbb{F}}(\mathcal{G}_{g,k+1})$. Consequently, it is considered that $\mathbb{I}^{\mathrm{t}}_{g,k}$ and $\mathcal{L}^{\mathrm{t}}_{g,k}$ remain unchanged and the predicted value of $\mathbb{X}^{\mathrm{t}}_{g,j,k+1|k+1}$ is simply

$$\mathbb{X}^{\mathrm{p}}_{g,j,k+1|k+1} = \mathbb{X}^{\mathrm{t}}_{g,j,k+1|k} \setminus \underline{\mathbb{F}}(\mathcal{G}_{g,k+1}), \tag{5.63}$$

for all $j \in \mathcal{L}^{\mathrm{t}}_{g,k}$, where the superscript $^{\mathrm{p}}$ indicates predicted variables. Similarly, the predicted value of $\overline{\mathbb{X}}^{\mathrm{t}}_{g,k+1|k+1}$ is taken as

$$\overline{\mathbb{X}}^{\mathrm{p}}_{g,k+1|k+1} = \overline{\mathbb{X}}^{\mathrm{t}}_{g,k+1|k} \setminus \underline{\mathbb{F}}(\mathcal{G}_{g,k+1}). \tag{5.64}$$

$\overline{\mathbb{X}}^{\mathrm{t}}_{g,k+1|k+1} = \overline{\mathbb{X}}^{\mathrm{p}}_{g,k+1|k+1}$ since measurements are not used when updating $\overline{\mathbb{X}}^{\mathrm{t}}_{g,k+1|k+1}$.

Assume now that the predicted states at time t_{k+1} of UAVs in neighboring groups that have already evaluated their control input are available. Let $\mathcal{N}^{\mathrm{c}}_{g,k} \subset \mathcal{N}^{\mathrm{g}}_{g,k}$ be the list of indices of neighboring groups that have already evaluated their control input, see Remark 6. Using the predicted states of group $n \in \mathcal{N}^{\mathrm{c}}_{g,k}$, one can predict the values of $\mathcal{G}_{n,k+1}$ and $\mathcal{E}_{k+1}$, and thus determine the groups able to communicate at t_{k+1} as

$$\mathcal{N}^{\mathrm{p}}_{g,k+1} = \left\{ n \in \mathcal{N}^{\mathrm{c}}_{g,k} \mid \exists \ell \in \mathcal{N}_n, \exists \ell' \in \mathcal{N}_g, \left(\ell, \ell'\right) \in \mathcal{E}_{k+1} \right\}. \tag{5.65}$$

The corrected set estimates accounting for the FoV of groups belonging to $\mathcal{N}^{\mathrm{p}}_{g,k+1}$ are given by

$$\mathbb{X}^{\mathrm{p}}_{g,j,k+1} = \mathbb{X}^{\mathrm{p}}_{g,j,k+1|k+1} \setminus \bigcup_{n \in \mathcal{N}^{\mathrm{p}}_{g,k+1}} \underline{\mathbb{F}}\left(\mathcal{G}^{\mathrm{u}}_{n,k+1}\right), \tag{5.66}$$

for all $j \in \mathcal{L}^{\mathrm{t}}_{g,k}$, and

$$\overline{\mathbb{X}}^{\mathrm{p}}_{g,k+1} = \overline{\mathbb{X}}^{\mathrm{p}}_{g,k+1|k+1} \setminus \bigcup_{n \in \mathcal{N}^{\mathrm{p}}_{g,k+1}} \underline{\mathbb{F}}\left(\mathcal{G}^{\mathrm{u}}_{n,k+1}\right). \tag{5.67}$$

After processing $\mathbb{X}^{\mathrm{p}}_{g,j,k+1}$ and $\overline{\mathbb{X}}^{\mathrm{p}}_{g,k+1}$ the leader of group g can again evaluate (5.60) and the followers evaluate (5.62) considering the predicted set estimates at time t_{k+1} to obtain the set of control inputs $\{\widehat{\mathbf{u}}_{i,k+1}\}_{i \in \mathcal{N}_g}$. The prediction process may be applied iteratively on $\mathbb{X}^{\mathrm{p}}_{g,j,k+\kappa}$ and $\overline{\mathbb{X}}^{\mathrm{p}}_{g,k+\kappa}$ to evaluate the impact of $\{\widehat{\mathbf{u}}_{i,k+\kappa}\}_{i \in \mathcal{N}_g}$, $\kappa = 0, \ldots, h-1$, which provides $\mathbb{X}^{\mathrm{p}}_{g,j,k+h}$ and $\overline{\mathbb{X}}^{\mathrm{p}}_{g,k+h}$ when $\kappa = h-1$. The predicted estimation uncertainty at time $k+\kappa$ is evaluated as

$$\Phi^{\mathrm{p}}_{k+h} = \frac{1}{N^{\mathrm{u}}} \sum_{i=1}^{N^{\mathrm{u}}} \Phi\left(\mathcal{X}^{\mathrm{p}}_{g,k+h}, \overline{\mathbb{X}}^{\mathrm{p}}_{g,k+h}\right), \tag{5.68}$$

where $\mathcal{X}^{\mathrm{p}}_{g,k+h} = \left\{\mathbb{X}^{\mathrm{p}}_{g,j,k+h}\right\}_{j \in \mathcal{L}^{\mathrm{t}}_{g,k}}$.

Similarly to (4.39), instead of using the predicted estimation uncertainty, the cost function to minimize may be expressed as

$$J\left(\mathbf{u}_{i_g,k:k+h-1}\right) = \Phi\left(\mathcal{X}^{\mathrm{p}}_{g,k+h}, \overline{\mathbb{X}}^{\mathrm{p}}_{g,k+h}\right) + \alpha d\left(\boldsymbol{x}^{\mathrm{g}}_{i_g,k+h}, \bigcup_{j \in \mathcal{L}^{\mathrm{t}}_{g,k}} \mathbb{X}^{\mathrm{p}}_{g,j,k+h} \cup \overline{\mathbb{X}}^{\mathrm{p}}_{g,k+h}\right), \tag{5.69}$$

where $d(\boldsymbol{x}, \mathbb{X})$ is the Hausdorff distance between point $\boldsymbol{x}$ and set $\mathbb{X}$. The third term is introduced to drive group g towards $\mathbb{X}^{\mathrm{p}}_{g,j,k+h} \cup \overline{\mathbb{X}}^{\mathrm{p}}_{g,k+h}$ when the first term of the cost function remains constant due to the limited prediction horizon. The tuning parameter $\alpha \in \mathbb{R}$ increases the importance of the next closest set relatively to the group g.

Remark 6. Considering group g, the assumption on the availability of the predicted states of the neighboring group $n \in \mathcal{N}^{\mathrm{c}}_{g,k}$ relies on a suboptimal distributed approach, where group g computes its control inputs only once it has received the predicted states from all groups in $\mathcal{N}^{\mathrm{g}}_{g,k}$ with a smaller index, *i.e.*, groups in $\mathcal{N}^{\mathrm{c}}_{g,k} = \left\{n \in \mathcal{N}^{\mathrm{g}}_{g,k} \mid n < g\right\}$. In each $\mathcal{N}^{\mathrm{g}}_{g,k}$, $g = 1, \ldots, N_{\mathrm{g}}$, group g is able to determine whether it has the smallest index due to prior communication at time step t_k. If this

is the case, group g evaluates its control input without accounting for the presence of its neighbors.

5.4.4. Practical issues

This section addresses some practical issues that have to be considered when applying the presented approach. It starts by giving insights on the design of the conic observation subsets in Section 5.4.4.1. Then, Section 5.4.4.2 proposes a simplified control design where the followers from Section 5.4.3.1 are organized in a rigid formation around the leader. This omits solving the optimization problem (5.62) for every UAV $i \in \mathcal{N}_g \setminus \{i_g\}$ and is less computationally demanding. Finally, Section 5.4.4.3 briefly presents a possible communication protocol.

5.4.4.1. Choosing the conic observation subsets

In the proposed approach, the conic observation subsets $\mathbb{C}_\ell$ have to be chosen such that (5.9) is satisfied. In this section, the impact of the aperture and orientation of the conic observation subsets on the potential satisfaction of (5.9) is illustrated.

In the following three figures, only the visibility of points on the ground plane is evaluated. In Figure 5.11, two conic observation subsets are considered: $\mathbb{C}_1$ with a large aperture and $\mathbb{C}_2$ with a small aperture. For a given UAV state $\mathbf{x}^{\mathrm{u}}$ and location $\boldsymbol{x}^{\mathrm{u}}$, the green set contains all $\boldsymbol{x}$ on the ground plane such that $\boldsymbol{x}^{\mathrm{u}} \in \mathbb{C}_1(\boldsymbol{x})$ (left) and $\boldsymbol{x}^{\mathrm{u}} \in \mathbb{C}_2(\boldsymbol{x})$ (right). The green set will contain $\mathbb{F}_{i,\ell}(\mathbf{x}^{\mathrm{u}})$ (darker green). When the cone aperture is reduced (Figure 5.11 right), the size of the green set reduces, and $\mathbb{F}_{i,\ell}(\mathbf{x}^{\mathrm{u}}_{i,k})$ reduces too, when the aperture gets too small.

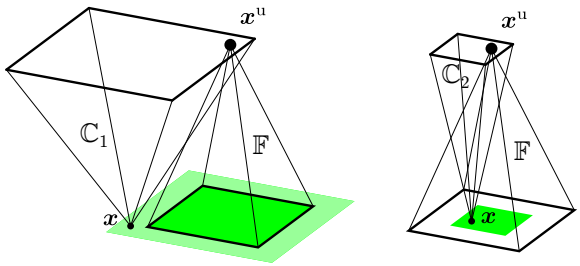

Figure 5.11.: Conic observation subsets with large ($\mathbb{C}_1$) and small ($\mathbb{C}_2$) aperture and resulting locations $\boldsymbol{x}$ on the ground plane (green) that are observed from a point of view $\mathbf{x}^{\mathrm{u}}_{i,k}$ belonging to $\mathbb{C}_1(\boldsymbol{x})$ or $\mathbb{C}_2(\boldsymbol{x})$.

Figure 5.12 illustrates the impact of the presence of an obstacle $\mathcal{O}$ on the locations $\boldsymbol{x}$ on the ground plane for which $\mathbb{C}_\ell(\boldsymbol{x}) \subset \underline{\mathbb{D}}(\boldsymbol{x})$ is satisfied (in green) and unsatisfied (in pink), considering the two previous conic observation subsets $\mathbb{C}_1$ (left) and $\mathbb{C}_2$ (right). $\underline{\mathbb{D}}(\boldsymbol{x})$ is not represented to keep the figure readable. A larger cone aperture leads to larger regions that do not satisfy $\mathbb{C}_1(\boldsymbol{x}) \subset \underline{\mathbb{D}}(\boldsymbol{x})$ (red).

Figure 5.11 and 5.12 show that the aperture of a conic observation subset $\mathbb{C}_\ell$ has to be chosen so as to satisfy a trade-off between the size of $\mathbb{F}_{i,\ell}$ and the size of the set of points $\boldsymbol{x}$ satisfying $\mathbb{C}_\ell(\boldsymbol{x}) \subset \underline{\mathbb{D}}(\boldsymbol{x})$.

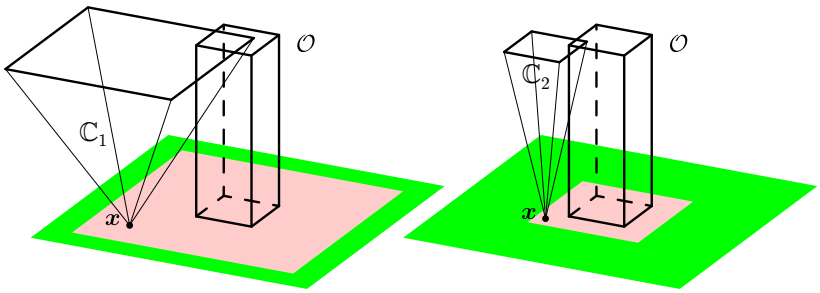

Figure 5.12.: Conic observation subset with large ($\mathbb{C}_1$) and small ($\mathbb{C}_2$) opening angle in presence of an obstacle and resulting locations on the ground plane (green) that are satisfying $\mathbb{C}_1(\boldsymbol{x}) \subset \underline{\mathbb{D}}(\boldsymbol{x})$ (left) or $\mathbb{C}_2(\boldsymbol{x}) \subset \underline{\mathbb{D}}(\boldsymbol{x})$ (right).

Finally, considering again obstacle $\mathcal{O}$, Figure 5.13 (left and middle) illustrates the impact of the orientation of the conic observation subsets on the size of the set of points $\boldsymbol{x}$ for which $\mathbb{C}_\ell(\boldsymbol{x}) \subset \underline{\mathbb{D}}(\boldsymbol{x})$ is satisfied (in green) or unsatisfied (in pink). Considering the two conic observation subsets $\mathbb{C}_1$ and $\mathbb{C}_2$ (right part of Figure 5.13) increases of the size of the green set for which $\mathbb{C}_1(\boldsymbol{x}) \subset \underline{\mathbb{D}}(\boldsymbol{x})$ or $\mathbb{C}_2(\boldsymbol{x}) \subset \underline{\mathbb{D}}(\boldsymbol{x})$.

As discussed in Section 5.3.1.2, a point needs to be observed simultaneously from every conic observation subsets to be guaranteed not to contain undetected targets. This means that at least as many UAVs as conic observation subsets are necessary, and indeed the number L is chosen as the number of UAVs in each team in Section 5.4.1.1.

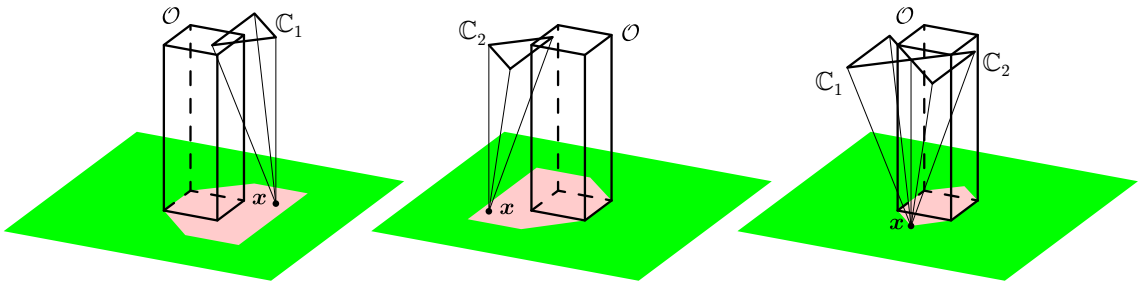

Figure 5.13.: Conic observation subsets ($\mathbb{C}_1$ and $\mathbb{C}_2$) with different orientations in presence of an obstacle and resulting locations on the ground plane (green) that are satisfying $\mathbb{C}_1(\boldsymbol{x}) \subset \underline{\mathbb{D}}(\boldsymbol{x})$ (left), $\mathbb{C}_2(\boldsymbol{x}) \subset \underline{\mathbb{D}}(\boldsymbol{x})$ (middle), and $\mathbb{C}_1(\boldsymbol{x}) \subset \underline{\mathbb{D}}(\boldsymbol{x}) \vee \mathbb{C}_2(\boldsymbol{x}) \subset \underline{\mathbb{D}}(\boldsymbol{x})$ (right), where $\vee$ is the logical conjunction function.

5.4.4.2. Rigid Formation design

Consider group g with leader index i_g. Solving the optimization problem (5.62) for every UAV $i \in \mathcal{N}_g \backslash \{i_g\}$ and at every time step $t_{k+\kappa}$ in the prediction horizon relies on set computations which can be computationally demanding. This section suggests to consider a further simplified suboptimal design of the control by imposing on the group that the followers are organized as a rigid formation around the leader.

The state of UAV i may be written as $\mathbf{x}^{\mathrm{u}}_{i,k} = (\boldsymbol{x}^{\mathrm{u}\top}_{i,k}, \dot{\boldsymbol{x}}^{\mathrm{u}\top}_{i,k}, \boldsymbol{q}^{\mathrm{u}\top}_{i,k}, \dot{\boldsymbol{q}}^{\mathrm{u}\top}_{i,k})^\top$, where $\boldsymbol{q}^{\mathrm{u}}_{i,k} \in \mathbb{R}^3$ represents its orientation in $(\mathbf{O}, \mathcal{F})$. Assume that all UAVs fly at a *constant* altitude a, *i.e.*, $\boldsymbol{x}_{i,k} = (x_{1,k}, x_{2,k}, a)$, that their orientation $\boldsymbol{q}^{\mathrm{u}}_{i,k}$ is constant, and that

$$\begin{aligned} \Delta\boldsymbol{x}_i &= \boldsymbol{x}^{\mathrm{u}}_{i_g,k} - \boldsymbol{x}^{\mathrm{u}}_{i,k}, \\ \Delta\boldsymbol{q}_i &= \Delta_{\mathrm{ori}}\left(\boldsymbol{q}^{\mathrm{u}}_{i_g,k}, \boldsymbol{q}^{\mathrm{u}}_{i,k}\right), \end{aligned} \tag{5.70}$$

are constant with time, where Δ_{ori} is a function expressing the relative orientation of $\boldsymbol{q}^{\mathrm{u}}_{i,k}$ compared to $\boldsymbol{q}^{\mathrm{u}}_{i_g,k}$ which depends on the representation used, *i.e.*, Euler-angles or quaternions. Consequently, the formation is rigid and the relative distances and orientations of the UAVs with respect to the group leader i_g needs only to be evaluated during the initialization process. Assuming that the FoV only depends on $\boldsymbol{x}^{\mathrm{u}}_{i,k}$ and $\boldsymbol{q}^{\mathrm{u}}_{i,k}$, then, when a UAV moves from one location to an other, the evolution of its FoV is only a translation of its apex. Thus, the optimal formation may be obtained by the solving

$$\begin{aligned} \left\{ \begin{pmatrix} \boldsymbol{x}^{\mathrm{u}}_{i,0} \\ \boldsymbol{q}^{\mathrm{u}}_{i,0} \end{pmatrix} \right\}_{i \in \mathcal{N}_g \backslash \{i_g\}} = \arg \max_{\left\{\boldsymbol{x}^{\mathrm{u}}_i, \boldsymbol{q}^{\mathrm{u}}_i\right\} \in \mathbb{S}^{\mathrm{u}}_i, i \in \mathcal{N}_g \backslash \{i_g\}} \\ \phi \left(\mathbb{F}_{i_g, \ell(i_g)} \begin{pmatrix} \boldsymbol{x}^{\mathrm{u}}_{i_g,0} \\ \boldsymbol{q}^{\mathrm{u}}_{i_g,0} \end{pmatrix} \cap \bigcap_{i \in \mathcal{N}_g \backslash \{i_g\}} \mathbb{F}_{i,\ell(i)} \begin{pmatrix} \boldsymbol{x}^{\mathrm{u}}_i \\ \boldsymbol{q}^{\mathrm{u}}_i \end{pmatrix} \right), \end{aligned} \tag{5.71}$$

where $\mathbb{S}^{\mathrm{u}}_i$ is the set of admissible positions and orientations of the UAVs. Then $\Delta\boldsymbol{x}_i$ and $\Delta\boldsymbol{q}_i$ are obtained from (5.71) using (5.70).

With this approach, during the search, only the leader evaluates its control input accounting for the set estimates. The followers then simply apply formation control techniques (see, *e.g.,* Liu and Bucknall 2018; Sun et al. 2015; Viel et al. 2019) to keep the relative distance $\Delta\boldsymbol{x}_i$ and orientation $\Delta\boldsymbol{q}_i$ with respect to the leader. This simplification of a rigid formation is considered in the simulations.

5.4.4.3. Practical communication issues

This section details the information that needs to be exchanged inside and between the groups and a tentative communication protocol. The introduced set-membership target state estimator evaluates target state set estimates in a distributed way regarding different groups and in a more centralized way inside a single group g.

Figure 5.14 shows an example of UAV network at time t_k with edges $\mathcal{E}_k$ (solid lines) for two groups with leaders $i_g \in \{1, 5\}$ (red UAVs). The edges $\{(1,2), (1,3), (1,4)\}$ within the first group are constant. The edge $(2, 8)$ between the groups, may change with time.

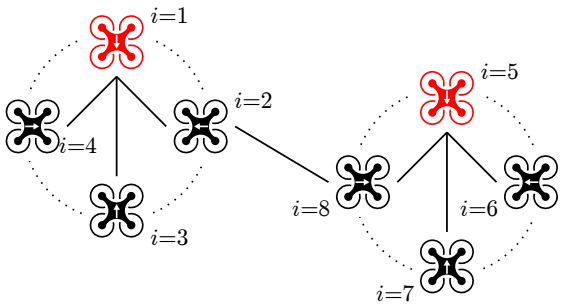

Figure 5.14.: UAV network at time t_k with edges $\mathcal{E}_k$ (solid lines) for two teams, where $\mathcal{N}_1 = \{1, 2, 3, 4\}$ and $\mathcal{N}_2 = \{5, 6, 7, 8\}$, with leaders $i_1 = 1$ and $i_2 = 5$ (red UAVs).

The sequential information flow inside group g with leader i_g for a network as in Figure 5.14 is described in Table 5.2. One observes that the leader communicates five times with each member of the group and that each member of the group may communicate three times with UAVs from other groups during the period T. This shows that the introduction of groups increases the communication demand compared to prior approaches, *e.g.*, Chapter 4. This also shows that a well-designed communication protocol is needed to ensure efficient information exchange, *i.e.*, with reduced latency.

Information flow		
1	P	At time t_k, UAVs in $\mathcal{N}_g$ collect measurement.
2	C_{in}	UAVs in $\mathcal{N}_g \setminus \{i_g\}$ transmit their states and measurements to leader i_g.
3	P	UAV i_g processes $\mathbb{F}(\mathcal{G}_{g,k})$, $\mathbb{S}^{t}_{g,j,k}$, and $\mathcal{D}^{t}_{g,k}$ to get the set estimates accounting for (local) measurements ($\mathbb{I}^{t}_{g,k+1\|k+1}$, $\mathcal{L}^{t}_{g,k+1\|k+1}$, $\mathcal{X}^{t}_{g,k+1\|k+1}$, and $\overline{\mathbb{X}}^{t}_{g,k+1\|k+1}$).
4	C_{in}	UAV i_g transmits $\mathbb{I}^{t}_{g,k+1\|k+1}$, $\mathcal{L}^{t}_{g,k+1\|k+1}$, $\mathcal{X}^{t}_{g,k+1\|k+1}$, and $\overline{\mathbb{X}}^{t}_{g,k+1\|k+1}$ to UAVs in $\mathcal{N}_g \setminus \{i_g\}$.
5	C_{out}	UAVs of group g broadcast $\mathbb{I}^{t}_{g,k+1\|k+1}$, $\mathcal{L}^{t}_{g,k+1\|k+1}$, $\mathcal{X}^{t}_{g,k+1\|k+1}$, and $\overline{\mathbb{X}}^{t}_{g,k+1\|k+1}$; the connected UAVs from group $n \in \mathcal{N}^{g}_{g,k}$ receive this information and broadcast themselves the corresponding information.
6	C_{in}	UAVs in $\mathcal{N}_g \setminus \{i_g\}$ transmit the received information from group $n \in \mathcal{N}^{g}_{g,k}$ to UAV i_g.
7	P	UAV i_g updates the set estimates using the information from other groups.
		If $g < g', \forall g' \in \mathcal{N}^{g}_{g,k}$
8	P	UAV i_g evaluates the sequence of control input $\{\widehat{\mathbf{u}}_{i_g,k:k+h-1}\}$
9	C_{in}	UAV i_g transmits $\{\widehat{\mathbf{u}}_{i_g,k:k+h-1}\}$ to UAVs in $\mathcal{N}_g \setminus \{i_g\}$.
10	C_{out}	UAVs in $\mathcal{N}_g$ broadcast $\{\widehat{\mathbf{u}}_{i_g,k:k+h-1}\}$.
		else
11	C_{out},C_{in}	Group g waits until receiving $\{\widehat{\mathbf{u}}_{i_g,k:k+h-1}\}$ from groups $n \in \mathcal{N}^{c}_{g,k}$.
12	P	UAV i_g evaluates the sequence of control input $\{\widehat{\mathbf{u}}_{i_g,k:k+h-1}\}$ accounting for neighboring groups.
13	C_{out},C_{in}	UAV i_g transmits $\{\widehat{\mathbf{u}}_{i_g,k:k+h-1}\}$ to UAVs in $\mathcal{N}_g \setminus \{i_g\}$. UAVs in $\mathcal{N}_g$ broadcast $\{\widehat{\mathbf{u}}_{i_g,k:k+h-1}\}$.
14	P	Group g applies its control input. Restart the procedure at time t_{k+1}

Table 5.2.: Sequential information flow for group g with leader i_g; Partitioning in information update Processes (P), Communication inside the group (C_{in}) and Communication outside (C_{out}) the group.

5.4.5. Simulations

The proposed approach is evaluated via simulations. The impact of the choice of the conic observation subsets and the impact of static and dynamic environments on the search performance is studied.

The algorithm is implemented using Matlab. The sets are represented using Matlab's *polyshapes*. Video sequences of the simulations can be found in the folder

Videos\Chapter_5\5.4... or at: `https://drive.google.com/drive/folders/1SlM2FT6LQrNpfgtHBLhaysG8O1Hya1Hp?usp=sharing`

The videos illustrate the UAV locations, their FoVs (dotted lines), and the target locations (black filled circles). Additionally, the local estimates $\overline{\mathbb{X}}^{\mathrm{t}}_{g,k}$ (yellow) and $\mathbb{X}^{\mathrm{t}}_{g,j,k}$ (green) maintained by the red team ($g = 1$) are shown.

5.4.5.1. Impact of the design of the conic observation subsets

Two different designs for the conic observation subsets are considered in this section. The RoI $\mathbb{X}_0$ is taken as $[0, 300] \times [0, 300] \times [0, 100]$ m^3 and attached to the frame $\mathcal{F}$. Obstacles are modeled as boxes with a square base of 50×50 m. $N^{\mathrm{o}} = 9$ static obstacles are regularly placed within the RoI with a minimal distance of 25 m from each other. Two scenarios for the environment are considered. The obstacles have a height of $h_{\mathrm{o}} = 25$ m (scenario 1) and $h_{\mathrm{o}} = 65$ m (scenario 2 and 3).

The UAVs search for $N^{\mathrm{t}} = 9$ targets moving on the ground with a speed of constant module $V^{\mathrm{t}} = 1\,\mathrm{ms}^{-1}$. Target j moves on the ground around obstacle j. The distance between target j and the boundary of obstacle j is the j-th element of $\{0.5\,\mathrm{m}, 1\,\mathrm{m}, 2\,\mathrm{m}, 5\,\mathrm{m}, 10\,\mathrm{m}, 15\,\mathrm{m}, 20\,\mathrm{m}, 24\,\mathrm{m}, 24\,\mathrm{m}\}$.

The search is carried out by $N^{\mathrm{u}} = 20$ UAVs divided into $N^{\mathrm{g}} = 5$ groups of $L = 4$ UAVs each. The state of UAV i at time t_k consists of its location $\boldsymbol{x}^{\mathrm{u}}_{i,k} = (x^{\mathrm{u}}_{i,k,1}, x^{\mathrm{u}}_{i,k,2}, x^{\mathrm{u}}_{i,k,3})^{\top}$, flight speed along the roll axis $x^{\mathrm{u}}_{i,k,4}$, along the pitch axis $x^{\mathrm{u}}_{i,k,5}$, and along the yaw axis $x^{\mathrm{u}}_{i,k,6}$, orientation $\boldsymbol{q}^{\mathrm{u}}_{i,k}$ in $\mathcal{F}$ and its derivative $\dot{\boldsymbol{q}}^{\mathrm{u}}_{i,k}$. The UAVs are modeled as point mass that can accelerate along two axis with constant orientation and move on a plane with a constant altitude of $x^{\mathrm{u}}_{i,0,3} = 100\,\mathrm{m}$. The values for the flight speed $x^{\mathrm{u}}_{i,k,4}$ and $x^{\mathrm{u}}_{i,k,5}$ are bounded in $[-14, 14]$ m/s. Consequently, the UAV state vector $\mathbf{x}^{\mathrm{u}}_{i,k}$ evolves according to

$$\begin{pmatrix} x^{\mathrm{u}}_{i,k+1,1} \\ x^{\mathrm{u}}_{i,k+1,2} \\ x^{\mathrm{u}}_{i,k+1,3} \\ x^{\mathrm{u}}_{i,k+1,4} \\ x^{\mathrm{u}}_{i,k+1,5} \\ x^{\mathrm{u}}_{i,k+1,6} \\ \boldsymbol{q}^{\mathrm{u}}_{i,k+1} \\ \dot{\boldsymbol{q}}^{\mathrm{u}}_{i,k+1} \end{pmatrix} = \begin{pmatrix} x^{\mathrm{u}}_{i,k,1} + T^{\mathrm{d}} x^{\mathrm{u}}_{i,k,4} \\ x^{\mathrm{u}}_{i,k,2} + T^{\mathrm{d}} x^{\mathrm{u}}_{i,k,5} \\ x^{\mathrm{u}}_{i,k,3} \\ x^{\mathrm{u}}_{i,k,4} + T^{\mathrm{d}} u_{i,k,1} \\ x^{\mathrm{u}}_{i,k,5} + T^{\mathrm{d}} u_{i,k,2} \\ 0 \\ \boldsymbol{q}^{\mathrm{u}}_{i,k} \\ (0,0,0)^{\top} \end{pmatrix}, \tag{5.72}$$

where $u_{i,k,1}$ and $u_{i,k,2}$ are the control inputs applied to $x^{\mathrm{u}}_{i,k,4}$ and $x^{\mathrm{u}}_{i,k,5}$ and $T^{\mathrm{d}} = 0.5\,\mathrm{s}$ is the sampling period.

The communication range for the UAVs is limited to $d^{\mathrm{c}} = 200\,\mathrm{m}$ and the communication condition (3.18) is

$$c\left(\mathbf{x}^{\mathrm{u}}_{i,k}, \mathbf{x}^{\mathrm{u}}_{i',k}\right) = d^{\mathrm{c}} - \left\| \boldsymbol{x}^{\mathrm{u}}_{i,k} - \boldsymbol{x}^{\mathrm{u}}_{i',k} \right\|.$$

The prediction horizon of the MPC controller is set to $h = 3$. The control input is computed with a period of 0.5 s which is equal to the communication period. The update period for the UAV and target states is 0.05 s. The parameter α in the cost function (5.69) is set to $\alpha = 1.5$, to encourage UAVs to leave areas where targets were already detected.

The UAVs possess optical seekers able to detect targets. The opening angles of the FoV of the seekers are equal to $\pi/8$ in azimuth and in elevation. The angle between the roll axis of the UAV and the center line of the sensor is $\gamma_{\text{FoV}} = 3\pi/8$ (scenario 1 and 3) or $\gamma_{\text{FoV}} = 7\pi/16$ (scenario 2), when rotated around the pitch axis (see illustration in Figure 5.15). The optical seekers of the UAVs of a group have the same elevation but different azimuths. The azimuth, angle between the roll axis and the main axis of the sensor when rotating around the yaw axis, is $\pi/4$, $3\pi/4$, $5\pi/4$, and $7\pi/4$ for the 4 UAVs of each group. When a target is detected, a noisy measurement $\mathbf{y}_{i,j,k}$ of $\boldsymbol{x}^{\text{t}}_{j,k}$ is obtained with a uniformly distributed noise bounded in $[-5\,\text{m}, 5\,\text{m}]$ in the first two components of $\boldsymbol{x}^{\text{t}}_{j,k}$.

$L = 4$ conic observation subsets are chosen as described in Figure 5.9. The orientations of the vertices are $\pi/4$, $3\pi/4$, $5\pi/4$, and $7\pi/4$ for the azimuth and $\pi/4$ (scenario 1 and 3) or $\pi/3$ (scenario 2) for the elevation. The resulting vertices of the conic observation subsets are listed in Table 5.3.

Remark 7. Some insights regarding the choice of the conic observation subsets are given in Section 5.4.4.1. The design of $\mathbb{C}_\ell$ becomes easier when some knowledge about the RoI is available, *e.g.,* in the case of cars, minimal roads width, maximal obstacles heights, maximal width of bridges. This knowledge helps in the choice of $\mathbb{C}_\ell$.

Scenario	h_{o}	γ_{FoV}	Vertices of $\mathbb{C}_\ell$
1	25	$3\pi/8$	$\boldsymbol{v}_5 = (0,0,1)^\top$, $\boldsymbol{v}_{\{1,2,3,4\}} = \left(\pm 1/2, \pm 1/2, 1/\sqrt{2}\right)^\top$
2	65	$7\pi/16$	$\boldsymbol{v}_5 = (0,0,1)^\top$, $\boldsymbol{v}_{\{1,2,3,4\}} = \left(\pm 1/2\sqrt{2}, \pm 1/2\sqrt{2}, \sqrt{3}/2\right)^\top$
3	65	$3\pi/8$	$\boldsymbol{v}_5 = (0,0,1)^\top$, $\boldsymbol{v}_{\{1,2,3,4\}} = \left(\pm 1/2, \pm 1/2, 1/\sqrt{2}\right)^\top$

Table 5.3.: Parameters of the three simulation scenarios

For each of the three simulation scenarios in Table 5.3, 30 independent runs were performed, with random initial locations of the groups of UAVs. The number of obstacles, targets, and UAVs remains constant.

Figure 5.16 shows the evolution with time of the mean value of $\overline{\Phi}_k$ (black), $\phi\left(\overline{\mathbb{X}}_k\right) = \frac{1}{N^{\text{g}}} \sum_{g=1}^{N^{\text{g}}} \phi\left(\overline{\mathbb{X}}^{\text{t}}_{g,k}\right)$ (orange), $\phi\left(\mathbb{X}_k\right) = \frac{1}{N^{\text{g}}\left|\mathcal{L}^{\text{t}}_{g,k}\right|} \sum_{i=1}^{N^{\text{g}}} \sum_{j \in \mathcal{L}^{\text{t}}_{g,k}} \phi\left(\mathbb{X}^{\text{t}}_{g,j,k}\right)$ (green), and the

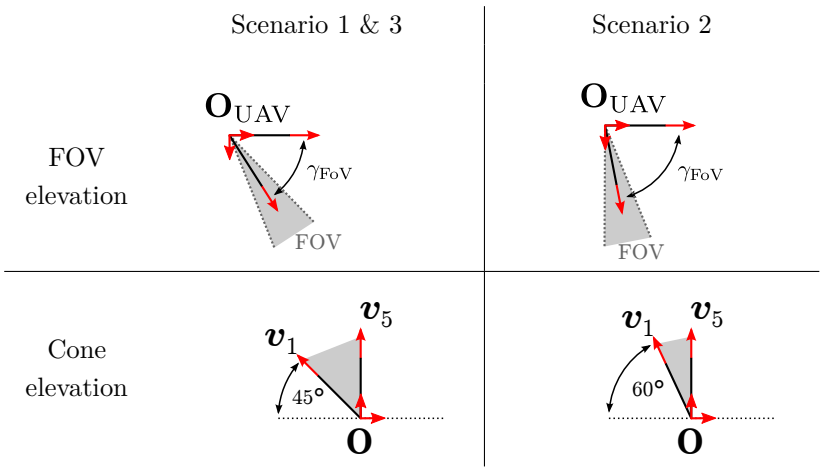

Figure 5.15.: FOV elevation γ_{FoV} and cone $\mathbb{C}_1$ elevation in the simulation scenarios

mean of the number of tracked targets $\mathcal{L}_k = \frac{1}{N^{\mathrm{g}}} \sum_{i=1}^{N^{\mathrm{g}}} \left| \mathcal{L}_{g,k}^{\mathrm{t}} \right|$ (dashed, blue) over 30 simulations with parameters in Scenario 1, see Table 5.3. See also the video *SimSet_1*. The measure of the estimation uncertainty $\overline{\Phi}_k$ decreases from $8 \times 10^4\,\mathrm{m}^2$ to $\sim 1 \times 10^4\,\mathrm{m}^2$ (black line). The variance of $\overline{\Phi}_k$ reaches a minimum at 300 s and grows afterwards again (gray area). This comes from the fact that the number of targets is larger than the number of groups. The groups are attracted by the targets they are observing which limits their re-exploration of the rest of the RoI, until the resulting uncertainty overcomes a certain limit. Nevertheless, the mean estimation uncertainty per target $\phi\left(\mathbb{X}_k\right)$ remains always smaller than $2 \times 10^3\,\mathrm{m}^2$. The groups are able to find and track all targets within the RoI after an average time of 100 s (dashed blue line).

Figure 5.17 shows the results of the simulations of Scenario 2. See also the video *SimSet_2*. Compared to Scenario 1, obstacles are taller which makes target detection more challenging. Nevertheless, the groups are able to find and track all targets within the RoI after an average time of 300 s (dashed blue line). As shown in Figure 5.17, and contrary to Figure 5.16, one can never prove, however, that all targets are detected since the unexplored space $\overline{\mathbb{X}}_k$ is never empty. The estimation uncertainty decreases only from $8.5 \times 10^4\,\mathrm{m}^2$ to $6.5 \times 10^4\,\mathrm{m}^2$ (black line). The reduced performance of the groups – compared to Figure 5.16 – comes from the fact that the size of the completely observed subset $\underline{\mathbb{F}}_g(\mathcal{G}_{g,k})$ is much smaller. This is due to the smaller aperture of the cones $\mathbb{C}_\ell$, $\ell = \{1, 2, 3, 4\}$. In general, the performance of the proposed approach depends on the shape and size of $\underline{\mathbb{F}}\left(\mathcal{G}_{g,k}\right)$, which itself depends on the design of the conic observation subsets.

The video sequences ConeElevation_1, ConeElevation_2, and *ConeElevation_3* present the change of the size of $\underline{\mathbb{F}}_g(\mathcal{G}_{g,k})$ when the elevation of $\boldsymbol{v}_{\{1,2,3,4\}}$ of the conic observation subsets is chosen as 45°, 50°, or 60° respectively, see also Figure 5.11.

Figure 5.18 shows the results of the simulations for Scenario 3, see also the video *SimSet_3*. In this scenario the visibility assumption (5.9) is not satisfied for all

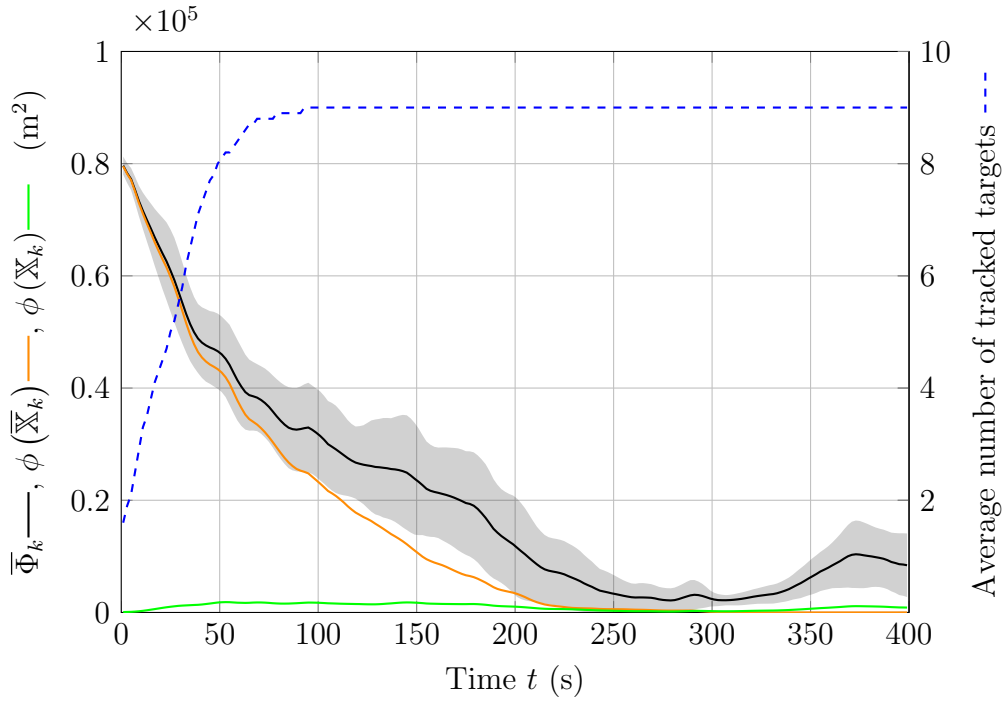

Figure 5.16.: Scenario 1 (obstacles with low height - $h_o = 25\,\mathrm{m}$): Mean values (line) and root-mean-square error (area) of $\overline{\Phi}_k$ (black), $\phi\left(\overline{\mathbb{X}}_k\right)$ (orange), $\phi\left(\mathbb{X}_k\right)$ (green), and $\mathcal{L}_k$ (dashed, blue) averaged over 30 simulations.

points in the RoI. In Figure 5.18, one observes that the average estimation uncertainty (black line) reduces significantly. The average number of detected and tracked targets (dashed blue line) reaches a maximum after 80 s and starts to decrease after 200 s. This is due to the fact that a target located at a point where the visibility condition is not satisfied may not be detected when observed by a group of UAVs. The group may then conclude the absence of a target at that point and possibly lose track of a previously detected target.

The minimal number of tracked targets within the 30 independent runs is zero after 300 s. This means that for some simulations, all targets detected during the simulation are lost at the end. Figure 5.19 (right) illustrates an inner approximation (in pink) of the area that is not satisfying the visibility condition (5.9). One observes that every target trajectory enters the pink area, hence, the UAVs may lose track of all targets.

5.4.5.2. Impact of dynamic environments

This section presents two more challenging scenarios where the environment is evolving with time. The evolution of the environment and the design of the conic observation subsets are such that the visibility assumption (5.9) remains satisfied at all

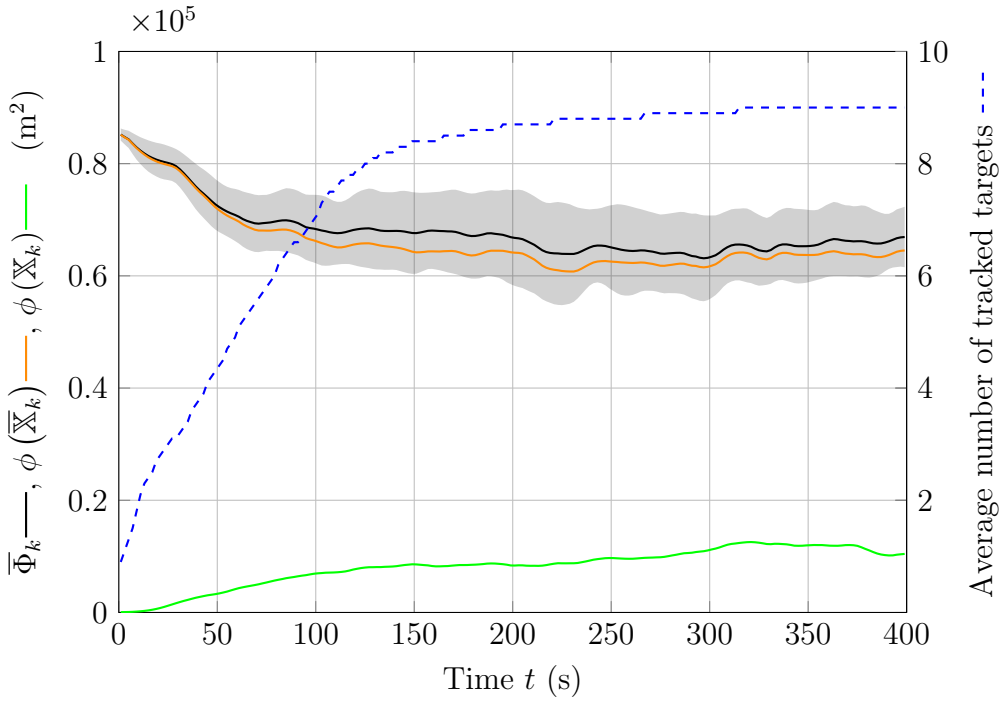

Figure 5.17.: Scenario 2 (obstacles with large height - $h_{\mathrm{o}} = 65\,\mathrm{m}$): Mean values (line) and root-mean-square error (area) of $\overline{\Phi}_k$ (black), $\phi\left(\overline{\mathbb{X}}_k\right)$ (orange), $\phi\left(\overline{\mathbb{X}}_k\right)$ (green), and $\mathcal{L}_k$ (dashed, blue) averaged over 30 simulations.

time instants. In both scenarios, the search is carried out by $N^{\mathrm{u}} = 20$ UAVs whose dynamics are given by (5.72). The fleet is divided into $N^{\mathrm{g}} = 5$ groups of $L = 4$ UAVs. The values for the flight speed $x^{\mathrm{u}}_{i,k,4}$ and $x^{\mathrm{u}}_{i,k,5}$ are bounded in $[-14, 14]$ m/s. The seeker of the UAVs are taken as in Scenario 1, see Table 5.3.

The first scenario consists of a mission where the fleet searches $N^{\mathrm{t}} = 9$ floating targets on the ocean surface. The RoI is again taken as $[0, 300] \times [0, 300] \times [0, 100]$ m^3 and the UAVs fly at constant altitude of $x^{\mathrm{u}}_{i,0,3} = 100\,\mathrm{m}$. Conic observation subsets are taken as in Scenario 1, see Table 5.3. The RoI is cluttered with $N^{\mathrm{o}} = 40$ floating obstacles *(e.g.*, debris) which may partially hide the targets. Each debris is modeled by a box which length, width, and height are uniformly distributed in $[7, 15] \times [7, 15] \times [8, 8]$ m^3. The targets and obstacles are moving, due to, *e.g.*, the oceans current and wind. Their speed module is assumed to be constant, $V^{\mathrm{t}} = V^{\mathrm{o}} = 1.0\,\mathrm{m\,s^{-1}}$. Their motion follows a straight line, except when collision occurs or when they may leave the RoI. In that case, the targets and obstacles change randomly their speed direction. The collision distance between two obstacles is assumed to be 4 m. The evolution of UAVs, targets and obstacles as well as set estimates can be seen at *SimDebris*. The sampling period is $T^{\mathrm{d}} = 0.5\,\mathrm{s}$. Figure 5.20 shows the evolution of the volume of the set estimates for this scenario. The results show that the size of the set estimates can be effectively reduced and that the UAVs never lose track of targets in $\mathcal{L}_k$.

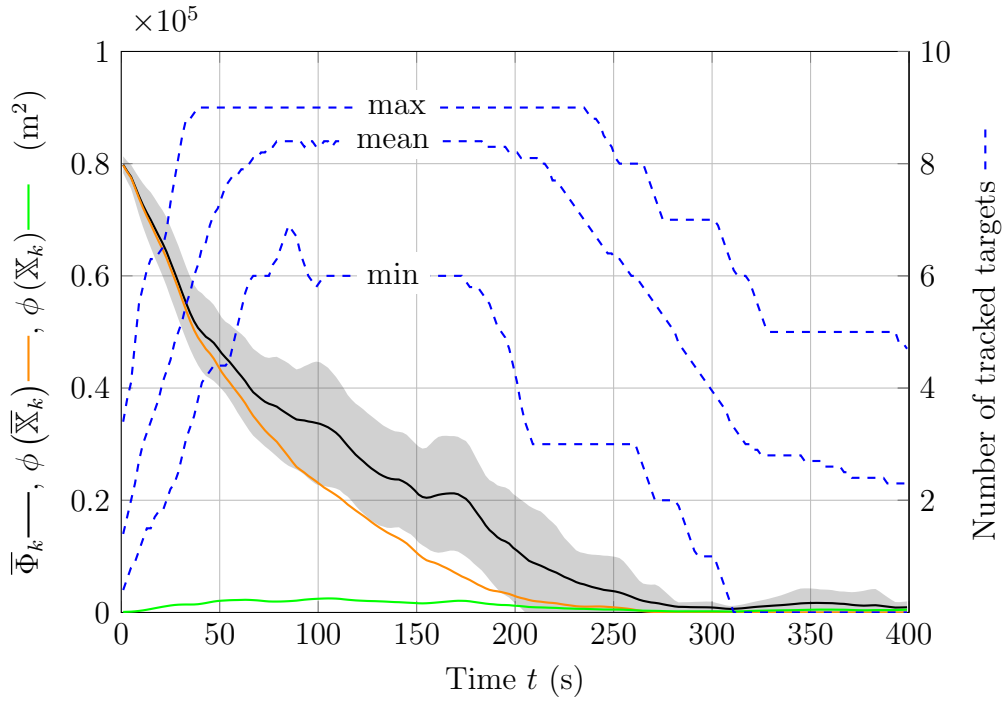

Figure 5.18.: Scenario 3 (visibility assumption (5.9) not always satisfied): Mean values over 30 simulations of $\overline{\Phi}_k$ (black), $\phi\left(\overline{\mathbb{X}}_k\right)$ (orange), $\phi\left(\overline{\mathbb{X}}_k\right)$ (green); mean value plus or minus standard deviation of $\overline{\Phi}_k$ (gray area); minimum, mean and maximum values of $\mathcal{L}_k$ (dashed, blue).

For the second scenario, the target search is made more difficult by the presence of clouds floating over the RoI between the UAVs and the targets. The RoI is now taken as $[0, 3000] \times [0, 3000] \times [0, 1000]$ m^3 and the UAVs fly at constant altitude of $x^{\mathrm{u}}_{i,0,3} = 1000\,\mathrm{m}$. The conic observation subsets are based on Scenario 1, see Table 5.3, however the vector $\boldsymbol{v}_5$ is changed and not perpendicular to the ground plane but inclined by 15° to reduce the aperture of each cone. The clouds move at a constant speed of $4.0\,\mathrm{m\,s^{-1}}$ at an altitude of 700 m. Clouds are represented by boxes with length randomly chosen in $[300, 1500]$ m. They have a width of 300 m and a height of 100 m. The clouds are aligned in rows where the distance between the rows is 850 m. The $N^{\mathrm{t}} = 9$ targets evolve according to random walk dynamics as in Ibenthal et al. (2021a). They move on the ground with constant speed module $V^{\mathrm{t}} = 1.0\,\mathrm{m\,s^{-1}}$. The sampling period for the simulations is $T^{\mathrm{d}} = 5\,\mathrm{s}$. The evolution of UAVs, targets and obstacles as well as set estimates can be seen at *SimClouds*. Figure 5.21 shows the evolution of the set estimates for this scenario. The results show that the size of the set estimates can be effectively reduced and that the UAVs never lose track of targets in $\mathcal{L}_k$.

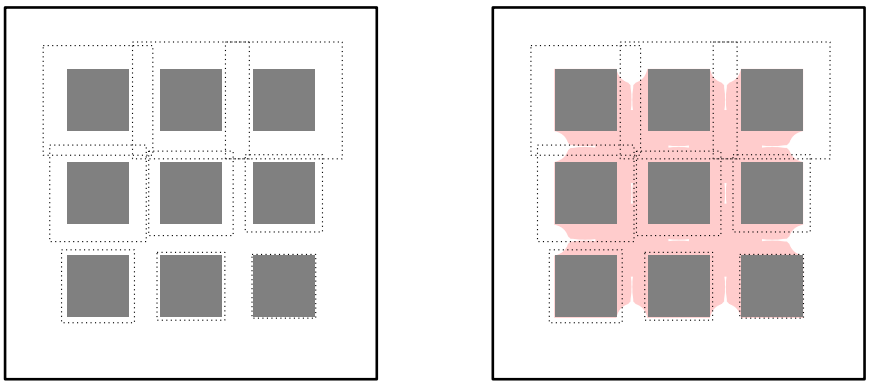

Figure 5.19.: Ground-projection of the RoI, the $N^{\text{o}} = 9$ static obstacles (gray), and the target trajectories (dotted lines); Inner approximation (in pink) of the points not satisfying visibility assumption (5.9) for Scenario 1 (left) and Scenario 3 (right).

5.4.6. Conclusion and perspectives

This chapter addresses the problem of cooperative search and track of static and moving targets using a fleet of UAVs collecting measurements corrupted by bounded noise. The search environment is unknown and cluttered with static or moving obstacles that may partially hide the targets. The UAVs have no *a priori* knowledge about the location and shape of the obstacles. Therefore, they are unable to determine whether a target located in their FoV is hidden behind an obstacle and thus not detected.

As an alternative to classical probabilistic non-detection models, the detectability set for each point in the RoI is introduced. The detectability set is the set of all UAV locations from where a target located at that point can be deterministically detected. This set is unknown but assumed to be always non-empty, which means that targets are never entirely hidden. The absence of a target at some zone is then proven, given that enough observations of that zone are collected with a sufficient variety of points of view. These observations may be collected gradually in the case of static targets or simultaneously in the case of moving targets. The requirement of simultaneous observations from different points of view led to structuring the fleet of UAVs into groups that jointly observe a subset of the RoI.

A distributed set-membership estimator is then used to evaluate set estimates of the target locations and a set clear from any target. The trajectories of the groups of UAVs are designed to reduce the estimation uncertainty using a model predictive control approach. Several simulations illustrate the performance of the proposed approach in various scenarios.

Future work includes elaborating a more sophisticated control scheme to account for more flexible formations, state perturbation of the UAVs, and the risk of collision between UAVs. Furthermore, the idea of the detectability set could be extended.

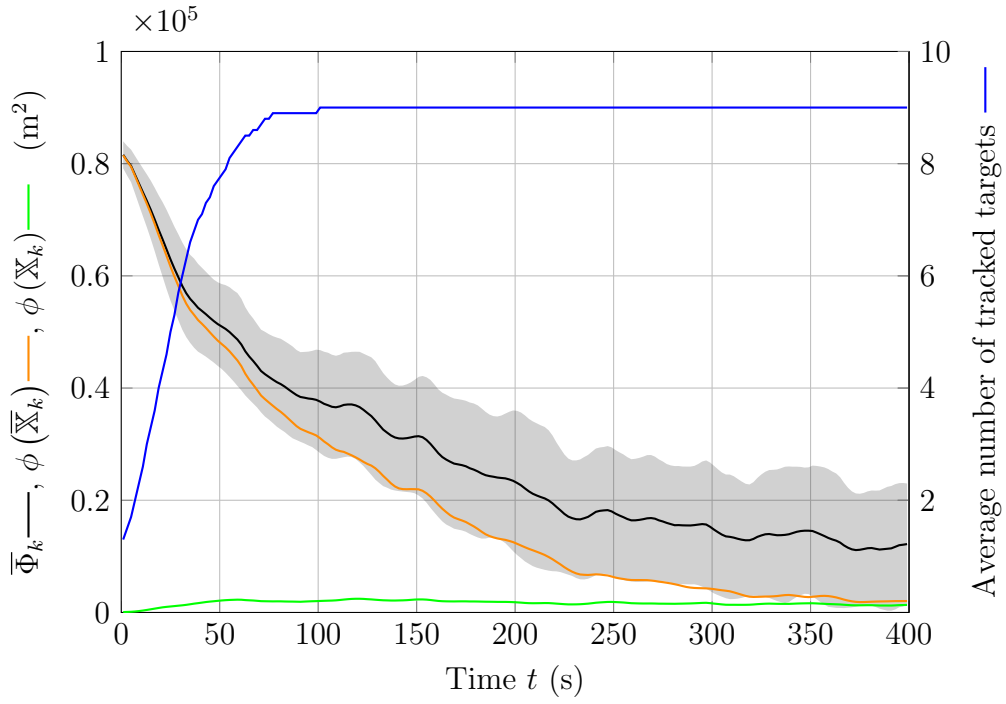

Figure 5.20.: Results for a target search in presence of floating debris; Mean values (line) and root-mean-square error (area) of $\overline{\Phi}_k$ (black), $\phi\left(\overline{\mathbb{X}}_k\right)$ (orange), $\phi\left(\mathbb{X}_k\right)$ (green), and $\mathcal{L}_k$ (blue) averaged over 30 simulations.

For some sensors, the detectability of a target depends on the relative difference between the target and sensor state. This is, *e.g.*, the case for Pulse-Doppler radars which can lose track of targets due to their clutter rejection filter, *i.e.*, targets flying perpendicular to the radar beam may be filtered out. It would be of great interest to extend the idea of detectability sets to address this problem.

The presented approaches in this chapter are subject of one publication. Ibenthal et al., 2021b is based on the estimation algorithm presented Section 5.3. Furthermore, another article based on the approach in Section 5.4 is submitted to the journal Transactions on Robotics (IEEE).

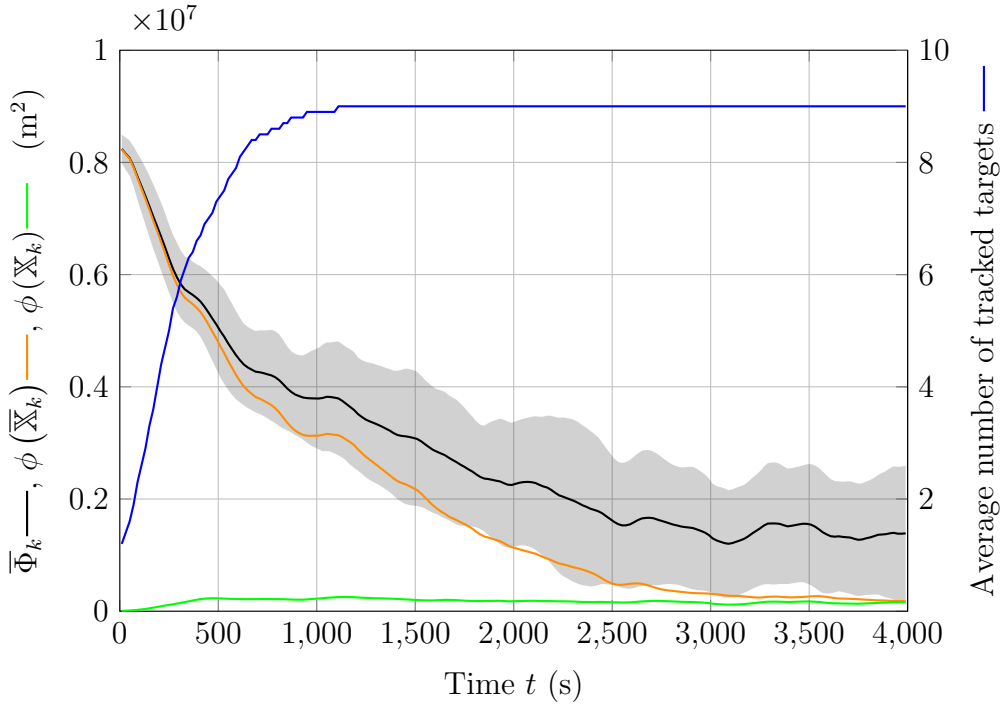

Figure 5.21.: Results for a target search in presence of floating clouds; Mean values (line) and root-mean-square error (area) of $\overline{\Phi}_k$ (black), $\phi\left(\overline{\mathbb{X}}_k\right)$ (orange), $\phi\left(\mathbb{X}_k\right)$ (green), and $\mathcal{L}_k$ (blue) averaged over 30 simulations.

6. Comparison of set-membership and stochastic approaches for target localization

The objective of this chapter is to compare the performances of set-membership and stochastic Bayesian estimation techniques for target search and tracking for scenarios integrating false alarms. For this purpose, an estimation scheme is presented for each technique. The performance of the estimators in terms of the ability to find real targets and not to be deceived by false targets or an imperfect sensor are compared in simulations.

6.1. Introduction

Consider N^{u} identical UAVs searching for an unknown but constant number $N^{\mathrm{t}} \leqslant |\mathcal{J}^{\mathrm{t}}|$ of moving ground targets. The targets evolve in a delimited RoI $\mathbb{X}_0$. In this chapter, it is assumed that $\mathbb{X}_0 \subset \mathbb{R}^2$ and that the UAVs are unable to identify the targets. Furthermore, similarly to the problem described in Chapter 4, it is assumed that false positive detection (false alarm) may occur and that targets are always detected when observed (absence of false negative detection). Consequently, $p^{\mathrm{u}}(\mathbf{x}^{\mathrm{u}}_{i,k}) \in \mathbb{D}_k\left(\boldsymbol{x}^{\mathrm{t}}_{j,k}\right)$, where $\mathbf{x}^{\mathrm{u}}_{i,k} \in \mathbb{R}^{n^{\mathrm{u}}}$, is always satisfied. That is, the UAVs are always located inside the detectability set of the targets, and the targets are never hidden behind any obstacle.

Each UAV estimates the location of the targets using its measurements and information received from other UAVs. The aim of the fleet is to find all targets in the RoI and to estimate their locations as precisely as possible.

6.1.1. Target representation

The target dynamics are simplified compared to Section 3.2 and assumed to be linear. The location $\boldsymbol{x}^{\mathrm{t}}_{j,k} \in \mathbb{X}_0$ at time t_k of target j evolves as

$$\boldsymbol{x}^{\mathrm{t}}_{j,k+1} = \boldsymbol{x}^{\mathrm{t}}_{j,k} + T\mathbf{v}_{j,k}, \tag{6.1}$$

where $\mathbf{v}_{j,k}$ is the unknown target velocity over the time interval $[t_k, t_{k+1}]$. The unknown target heading angle $\gamma(\mathbf{v}_{j,k})$ is assumed to be bounded in $[0, 2\pi[$, and the magnitude $\|\mathbf{v}_{j,k}\|$ of its velocity is assumed to be bounded in $[0, v]$.

6.1.2. Measurements

The targets are supposed to remain unidentified. Consequently, after processing the information in the FoV $\mathbb{F}_i\left(\mathbf{x}^{\mathrm{u}}_{i,k}\right)$, UAV i obtains the measurements $\mathbf{y}^{\mathrm{U}}_{i,m,k}$, $m \in \mathcal{D}^{\mathrm{U}}_{i,k}$, as defined in (3.11). These measurements are collected in the list $\mathcal{Y}_{i,k} = \left\{\mathbf{y}^{\mathrm{U}}_{i,m,k}\right\}_{m\in\mathcal{D}^{\mathrm{U}}_{i,k}}$. Since the targets in the FoV are always detected, one has

$$\boldsymbol{x}^{\mathrm{t}}_{j,k} \in \mathbb{F}_i\left(\mathbf{x}^{\mathrm{u}}_{i,k}\right) \Rightarrow \exists \mathbf{y} \in \mathcal{Y}_{i,k} \text{ such that } \mathbf{y} = \mathbf{y}_{i,j,k}. \tag{6.2}$$

UAV i is unable to determine which target is associated with a given measurement since they can not identify the targets. Consequently, from $\mathcal{Y}_{i,k}$, UAV i obtains only information about the locations of detected targets, but not about their identity. Considering $\mathcal{Y}_{i,k}$, the measurement model (3.17), and the assumed bounds on the measurement noise, the set containing all noise-free measurements is thus defined as

$$\mathbb{Y}_{i,k} = \{\mathbf{y} - \mathbf{w} \mid \mathbf{y} \in \mathcal{Y}_{i,k}, \mathbf{w} \in [\mathbf{w}]\}. \tag{6.3}$$

Proposition 8. *Assume that UAV i has obtained a list of $\left|\mathcal{D}^{U}_{i,k}\right|$ measurements $\mathbf{y} \in \mathcal{Y}_{i,k}$ at time t_k. Then one has*

$$\boldsymbol{x}^{t}_{j,k} \in \mathbb{F}_i\left(\mathbf{x}^{u}_{i,k}\right) \cap \mathbb{X}_0 \Rightarrow \mathbf{h}_i\left(\mathbf{x}^{u}_{i,k}, \boldsymbol{x}^{t}_{j,k}\right) \in \mathbb{Y}_{i,k}. \tag{6.4}$$

Proof. At time t_k, assume that $\boldsymbol{x}^{\mathrm{t}}_{j,k} \in \mathbb{F}_i\left(\mathbf{x}^{\mathrm{u}}_{i,k}\right) \cap \mathbb{X}_0$, only one target is detected, and $\mathbf{h}_i\left(\mathbf{x}^{\mathrm{u}}_{i,k}, \boldsymbol{x}^{\mathrm{t}}_{j,k}\right) \notin \mathbb{Y}_{i,k}$. Since $\boldsymbol{x}^{\mathrm{t}}_{j,k} \in \mathbb{F}_i\left(\mathbf{x}^{\mathrm{u}}_{i,k}\right) \cap \mathbb{X}_0$ and due to (6.2) a measurement $\mathbf{y}_{i,j,k}$ as in (3.17) is obtained. From (3.17) and (6.3) one deduces that $\mathbf{h}_i\left(\mathbf{x}^{\mathrm{u}}_{i,k}, \boldsymbol{x}^{\mathrm{t}}_{j,k}\right) = \mathbf{y}_{i,j,k} - \mathbf{w}_{i,j,k}$ and $\mathbb{Y}_{i,k} = \{\mathbf{y}_{i,j,k} - \mathbf{w} \mid \mathbf{w} \in [\mathbf{w}]\}$ respectively. Therefore, $\mathbf{y}_{i,j,k} - \mathbf{w}_{i,j,k} \in \{\mathbf{y}_{i,j,k} - \mathbf{w} \mid \mathbf{w} \in [\mathbf{w}]\}$ since $\mathbf{w}_{i,j,k} \in [\mathbf{w}]$, which contradicts the initial assumption. □

It is assumed that false positive detection may occur due to, *e.g.*, decoys confused with targets, changing environmental conditions (such as natural lighting), or imperfections of the image processing system. As a consequence, the list $\mathcal{Y}_{i,k}$ may contain measurements that do not correspond to a true target. At this point, no specific model for false positive detection is assumed. False positive detection may be deterministic or probabilistic.

In what follows, two approaches for target search and tracking are presented. Both approaches are able to account for potential false positive detection of targets in their estimation scheme. The state perturbation bounds of $\gamma(\mathbf{v}_{j,k})$ and $\|\mathbf{v}_{j,k}\|$ and the measurement noise bounds $[\mathbf{w}]$ are available for both approaches.

6.2. Guaranteed set-membership estimation

This section describes a simplified set-membership estimator based on the estimator presented in Section 4.3. At time t_k, each UAV maintains the three set estimates $\mathbb{X}^{\mathrm{U}}_{i,k}$, $\overline{\mathbb{X}}_{i,k}$, and $\widetilde{\mathbb{X}}_{i,k}$ (introduced in Section 3.9). Due to potential false positive detection, estimates that are not consistent with actual target locations may also belong to $\mathbb{X}^{\mathrm{U}}_{i,k}$.

The relative estimation uncertainty for UAV i is expressed as

$$\Phi^{\mathrm{S}}\left(\mathbb{X}^{\mathrm{U}}_{i,k}, \overline{\mathbb{X}}_{i,k}\right) = \phi\left(\mathbb{X}^{\mathrm{U}}_{i,k} \cup \overline{\mathbb{X}}_{i,k}\right) / \phi\left(\mathbb{X}_0\right). \tag{6.5}$$

The aim of each UAV i is to reduce $\Phi^{\mathrm{S}}\left(\mathbb{X}^{\mathrm{U}}_{i,k}, \overline{\mathbb{X}}_{i,k}\right)$ as much as possible. The superscript $^{\mathrm{S}}$ will be used to indicate quantities and parameters of the set-membership estimator.

6.2.1. Evolution of the set estimates

Assume that at time t_k, UAV i has evaluated $\mathbb{X}^{\mathrm{U}}_{i,k}$ and $\overline{\mathbb{X}}_{i,k}$. This section describes the way UAV i evaluates the sets $\mathbb{X}^{\mathrm{U}}_{i,k+1}$ and $\overline{\mathbb{X}}_{i,k+1}$ at time t_{k+1} using the target evolution model (6.1), the collected measurement set $\mathbb{Y}_{i,k}$ from (6.3), and the information received from neighbors in $\mathcal{N}_{i,k}$.

For the initialization at time t_0, UAV i considers $\mathbb{X}^{\mathrm{U}}_{i,k} = \emptyset$ and $\overline{\mathbb{X}}_{i,0} = \mathbb{X}_0$.

6.2.1.1. Prediction step

At time t_k, similarly to (4.3), UAV i evaluates the set of target locations

$$\mathbb{X}^{\mathrm{U}}_{i,k+1|k} = \left\{\boldsymbol{x} + T\mathbf{v} \,|\, \boldsymbol{x} \in \mathbb{X}^{\mathrm{U}}_{i,k}, \mathbf{v} \in \mathbb{R}^2, \|\mathbf{v}\| < v, \gamma(\mathbf{v}) \in [0, 2\pi[\right\} \cap \mathbb{X}_0, \tag{6.6}$$

that can be reached from any $\boldsymbol{x} \in \mathbb{X}^{\mathrm{U}}_{i,k}$ at time t_{k+1}, knowing (6.1), $\|\mathbf{v}\| < v$, and $\gamma(\mathbf{v}) \in [0, 2\pi[$. The value of $\overline{\mathbb{X}}_{i,k+1|k}$ is evaluated as

$$\overline{\mathbb{X}}_{i,k+1|k} = \left\{\boldsymbol{x} + T\mathbf{v} \,|\, \boldsymbol{x} \in \overline{\mathbb{X}}_{i,k}, \mathbf{v} \in \mathbb{R}^2, \|\mathbf{v}\| < v, \gamma(\mathbf{v}) \in [0, 2\pi[\right\} \cap \mathbb{X}_0, \tag{6.7}$$

similarly to (4.4).

6.2.1.2. Correction step from measurements

At time t_{k+1}, UAV i observes the subset $\mathbb{F}_i\left(\mathbf{x}^{\mathrm{u}}_{i,k+1}\right)$, collects measurements, and obtains $\mathbf{y}^{\mathrm{U}}_{i,m,k}$, $m \in \mathcal{D}^{\mathrm{U}}_{i,k}$. The updated target set estimate $\mathbb{X}^{\mathrm{U}}_{i,k+1|k+1}$ and the updated unexplored set $\overline{\mathbb{X}}_{i,k+1|k+1}$ can be obtained as in Section 4.3.2.2.

6.2.1.3. Correction step from communication

After the measurement process, UAV i communicates and exchanges the set estimates $\mathbb{X}^{\mathrm{U}}_{i,k+1|k+1}$, $\overline{\mathbb{X}}_{i,k+1|k+1}$, and $\widetilde{\mathbb{X}}_{i,k+1|k+1}$ with other neighboring UAVs, with index $\ell \in \mathcal{N}_{i,k}$, and receives the corresponding sets $\mathbb{X}^{\mathrm{U}}_{\ell,k+1|k+1}$, $\overline{\mathbb{X}}_{\ell,k+1|k+1}$, and $\widetilde{\mathbb{X}}_{\ell,k+1|k+1}$. After communication, the set estimates $\mathbb{X}^{\mathrm{U}}_{i,k+1}$ and $\overline{\mathbb{X}}_{i,k+1}$ are obtained as in Section 4.3.3, see (4.26) and (4.27) respectively.

6.2.2. Cooperative control design

The aim of the control design for each UAV is to decrease the estimation uncertainty as much as possible. At each time t_k, UAV i should determine the sequence of control inputs $\mathbf{u}_{i,k:k+h-1} = (\mathbf{u}_{i,k}, \ldots, \mathbf{u}_{i,k+h-1})$ which minimizes the predicted estimation uncertainty (6.5) at time t_{k+h}, $\Phi^{\mathrm{S}}\left(\mathbb{X}^{\mathrm{U}}_{i,k+h}, \overline{\mathbb{X}}_{i,k+h}\right)$ where $h \geqslant 1$ is the considered prediction horizon.

The predicted evolution of the sets $\mathbb{X}^{\mathrm{U}}_{i,k+h}$ and $\overline{\mathbb{X}}_{i,k+h}$ is evaluated as in Section 4.4, where $\mathbb{X}_{i,j,k+h} = \emptyset$. Using (4.41), an predicted estimate $\Phi^{\mathrm{S}}\left(\mathbb{X}^{\mathrm{P}}_{i,k+h}, \overline{\mathbb{X}}^{\mathrm{P}}_{i,k+h}\right) = \phi(\mathbb{X}^{\mathrm{A,P}}_{i,k+h})$ of $\Phi^{\mathrm{S}}\left(\mathbb{X}_{i,k+h}, \overline{\mathbb{X}}_{i,k+h}\right)$ can be deduced. The superscript $^{\mathrm{A}}$ and $^{\mathrm{P}}$ indicate aggregated and predicted set estimates, respectively. Then, UAV i searches for the sequence of control inputs $(\mathbf{u}_{i,k}, \ldots, \mathbf{u}_{i,k+h-1})$ minimizing

$$J^{\mathrm{S}}(\mathbf{u}_{i,k}, \ldots, \mathbf{u}_{i,k+h-1}) = \phi(\mathbb{X}^{\mathrm{A,P}}_{i,k+h}) + \alpha^{\mathrm{S}} d\left(\mathbf{x}^{\mathrm{u,P}}_{i,k+h}, \mathbb{X}^{\mathrm{A,P}}_{i,k+h}\right), \tag{6.8}$$

where $\mathbf{x}^{\mathrm{u,P}}_{i,k+h}$, $\mathbb{X}^{\mathrm{P}}_{i,k+h}$, and $\overline{\mathbb{X}}^{\mathrm{P}}_{i,k+h}$ depend on $(\mathbf{u}_{i,k}, \ldots, \mathbf{u}_{i,k+h-1})$, and where each element in $(\mathbf{u}_{i,k}, \ldots, \mathbf{u}_{i,k+h-1})$ belongs, *e.g.*, to a set of admissible control inputs $\mathcal{U}$. The parameter α^{S} adjusts the importance of the second term. The relative weighting tends to favor the reduction of $\phi(\mathbb{X}^{\mathrm{A,P}}_{i,k+h})$.

6.3. Bayesian state estimation in a stochastic context

This section presents a derivation of the Bayesian state estimation approach in a stochastic context for target search and tracking as introduced in Hu et al. (2014, 2012). The approach evaluates the *a posteriori* probability for the presence of a

target in a discrete probability grid of the RoI. The approach is extended to account for known target dynamics and constrained target control inputs. For this approach, it is assumed that $\mathbf{w}_{i,j,k}$ is uniformly distributed in $[\mathbf{w}]$, *i.e.*, $\mathbf{w}_{i,j,k} \sim \mathcal{U}(\underline{\mathbf{w}}, \overline{\mathbf{w}})$, and that $\gamma(\mathbf{v}_{j,k})$ and $\|\mathbf{v}_{j,k}\|$ are uniformly distributed in $[0, 2\pi[$ and $[0, v]$ respectively, *i.e.*, $\gamma(\mathbf{v}_{j,k}) \sim \mathcal{U}(0, 2\pi)$ and $\|\mathbf{v}_{j,k}\| \sim \mathcal{U}(0, v)$.

Following the approach in Hu et al. (2014), the RoI $\mathbb{X}_0$ is partitioned into N^{c} rectangular cells $\mathcal{C}_m \subset \mathbb{X}_0$, where $m \in \mathcal{N}^{\mathrm{c}} = \{1, \ldots, N^{\mathrm{c}}\}$ and $\mathbb{X}_0 = \bigcup_{m \in \mathcal{N}^{\mathrm{c}}} \mathcal{C}_m$. Assume that there is at most one target in each cell. At time t_k, let $\theta_{m,k}$ be a Bernoulli random variable indicating the presence ($\theta_{m,k} = 1$) or absence ($\theta_{m,k} = 0$) of a target in cell $\mathcal{C}_m$. The UAVs have no access to $\theta_{m,k}$ and $\theta_{m,k}$ is changing with time due to target motions.

Let $p_{i,m,k} = \Pr(\theta_{m,k} = 1 \mid \mathcal{I}_{i,k})$ be the posterior probability of presence of a target in $\mathcal{C}_m$, *i.e.*, $p_{i,m,k}$ is the probability of having $\theta_m = 1$ for cell $\mathcal{C}_m$. The posterior probability $p_{i,m,k}$ is evaluated considering all information $\mathcal{I}_{i,k}$ available to UAV i up to time t_k, *i.e.*, the measurements collected by UAV i, the measurement noise distribution, the target state transition probability, and the information coming from the rest of the fleet. UAV i gathers the values of $p_{i,m,k}$ in the set of posterior probabilities $\mathcal{P}_{i,k} = \{p_{i,m,k}\}_{m=1,\ldots,N^{\mathrm{c}}}$, called the *probability map* of the RoI.

In this stochastic estimation context, the evolution of the target state from one cell to another between two measurement times has to be described by a transition probability function. Assume that at time t_k the continuous pdf of the location of a target is $p_k(\boldsymbol{x})$. Furthermore, let $\pi(\boldsymbol{x}'|\boldsymbol{x})$ be the target transition pdf from $\boldsymbol{x}$ to $\boldsymbol{x}'$ during a time interval of duration T. Then, the pdf of the predicted location pdf $p_{k+1|k}(\boldsymbol{x})$ at time t_{k+1} is obtained from $p_k(\boldsymbol{x})$ and $\pi(\boldsymbol{x}'|\boldsymbol{x})$ via the Chapman-Kolmogorov equation as

$$p_{k+1|k}(\boldsymbol{x}) = \int_{\mathbb{X}_0} \pi(\boldsymbol{x}' \mid \boldsymbol{x})\, p_k(\boldsymbol{x})\, \mathrm{d}\boldsymbol{x}, \tag{6.9}$$

The transition probability $\pi(\boldsymbol{x}' \mid \boldsymbol{x})$ is derived from the target dynamics (6.1). Assuming that no target is entering or escaping $\mathbb{X}_0$, consider some $a > 0$ and

$$\mu(\boldsymbol{x}'|\boldsymbol{x}) = \begin{cases} a & \text{if } \|\boldsymbol{x}' - \boldsymbol{x}\| < vT \text{ and } \boldsymbol{x}' \in \mathbb{X}_0 \text{ and } \boldsymbol{x} \in \mathbb{X}_0, \\ 0 & \text{else,} \end{cases} \tag{6.10}$$

then the transition probability can be evaluated as

$$\pi(\boldsymbol{x}'|\boldsymbol{x}) = \frac{\mu(\boldsymbol{x}'|\boldsymbol{x})}{\mu_0(\boldsymbol{x})}, \tag{6.11}$$

where

$$\mu_0(\boldsymbol{x}) = \int_{\mathbb{X}_0} \mu(\boldsymbol{x}'|\boldsymbol{x})\, d\boldsymbol{x}' \tag{6.12}$$

is a normalization constant. If for some $\boldsymbol{x}$, all $\boldsymbol{x}'$ satisfying $\|\boldsymbol{x}' - \boldsymbol{x}\| < vT$ are such that $\boldsymbol{x}' \in \mathbb{X}_0$, then

$$\pi\left(\boldsymbol{x}'|\boldsymbol{x}\right) = \begin{cases} \frac{1}{\pi(vT)^2} & \|\boldsymbol{x}' - \boldsymbol{x}\| < vT, \\ 0 & \text{else}, \end{cases} \tag{6.13}$$

which is similar to the transition pdf considered in, *e.g.*, Zhen et al. (2020).

The transition probability $\Pr\left(\theta_{n,k+1} = 1 \mid \theta_{m,k} = 1\right) = \Pr\left(\boldsymbol{x}' \in \mathcal{C}_n, \boldsymbol{x} \in \mathcal{C}_m\right)$ needs to be evaluated to model the probability of a target moving from cell m to cell n after the time period T, one has

$$\Pr\left(\theta_{n,k+1} = 1 \mid \theta_{m,k} = 1\right) = \frac{\Pr\left(\theta_{n,k+1} = 1, \theta_{m,k} = 1\right)}{\Pr\left(\theta_{m,k} = 1\right)}, \tag{6.14}$$

where

$$\Pr\left(\theta_{m,k} = 1\right) = \int_{\mathcal{C}_m} p_k\left(\boldsymbol{x}\right) \mathrm{d}\boldsymbol{x} \tag{6.15}$$

and

$$\Pr\left(\theta_{n,k+1} = 1, \theta_{m,k} = 1\right) = \int_{\mathcal{C}_n} \int_{\mathcal{C}_m} \pi\left(\boldsymbol{x}'|\boldsymbol{x}\right) p_k\left(\boldsymbol{x}\right) \mathrm{d}\boldsymbol{x} \mathrm{d}\boldsymbol{x}' \tag{6.16}$$

are obtained from the assumption that there is a single target in each cell. The transition probability (6.14) simplifies to

$$\Pr\left(\theta_{n,k+1} = 1 \mid \theta_{m,k} = 1\right) = \frac{\int_{\mathcal{C}_n} \int_{\mathcal{C}_m} \pi\left(\boldsymbol{x}'|\boldsymbol{x}\right) \mathrm{d}\boldsymbol{x} \mathrm{d}\boldsymbol{x}'}{\int_{\mathcal{C}_m} \mathrm{d}\boldsymbol{x}}, \tag{6.17}$$

since the pdf $p_k\left(\boldsymbol{x}\right)$ is assumed uniform over $\mathcal{C}_m$.

At time t_k, UAV i may observe $\mathcal{C}_m$ and obtain the observation result $z_{i,m,k} \in \{0, 1\}$, where $z_{i,m,k} = 1$ indicates that a target is detected and $z_{i,m,k} = 0$ that no target is detected. The probability of the detection of a target within each cell is modeled as a Bernoulli distribution . It is assumed that the true positive detection probability is $\Pr\left(z_{i,m,k} = 1|\theta_m = 1\right) = p$ and the false positive detection probability is $\Pr\left(z_{i,m,k} = 1|\theta_m = 0\right) = q$. One has $p = 1$ since targets located inside the FoV are always detected, see (6.2), and $q > 0$ since it is assumed that false positive detection of targets may appear. Conditioned on $\theta_{m,k}$, the random variables $z_{i,m,k}$ are assumed to be time-independent.

At time t_k, to evaluate the estimation performance, Hu et al. (2012) introduces the uncertainty on the probability of a target being in $\mathcal{C}_m$ as

$$\eta_{i,m,k} = e^{-\alpha_1^{\mathrm{B}}\left|q_{i,m,k}\right|}, \tag{6.18}$$

where

$$q_{i,m,k} = \ln\left(\frac{1 - p_{i,m,k}}{p_{i,m,k}}\right), \tag{6.19}$$

is the logarithm of the *a posteriori* ratio of the target presence probability and α_1^{B} is a positive tuning parameter. The value of $\eta_{i,m,k}$ is small when $p_{i,m,k}$ is close to 0 or 1, and is maximal when $p_{i,m,k} = 0.5$, *i.e.*, when $p_{i,m,k} = 0.5$ then UAV i is unsure about the presence or absence of a target in $\mathcal{C}_m$. The uncertainty associated to the complete map $\mathcal{P}_{i,k}$ of UAV i at time t_k is

$$\Phi^{\mathrm{B}}\left(\mathcal{P}_{i,k}\right) = \frac{1}{N^{\mathrm{c}}} \sum_{m \in \mathcal{N}^{\mathrm{c}}} \eta_{i,m,k}. \tag{6.20}$$

As in (6.5) the aim of each UAV i is to reduce (6.20) as much as possible.As in (6.5) the aim of each UAV i is to reduce (6.20) as much as possible. The superscript $^{\mathrm{B}}$ will be used to indicate quantities and parameters of the stochastic Bayesian estimator.

To obtain a measure comparable with (6.5), one introduces additionally

$$\Phi^{\mathrm{B}}\left(\mathcal{P}_{i,k}, \underline{p}\right) = \frac{\left|\left\{m \in \mathcal{N}^{\mathrm{c}} \mid p_{i,m,k} > \underline{p}\right\}\right| \phi\left(\mathcal{C}\right)}{N^{\mathrm{c}} \phi\left(\mathcal{C}\right)}, \tag{6.21}$$

where $\phi\left(\mathcal{C}\right)$ is the area of a single cell. The function $\Phi^{\mathrm{B}}\left(\mathcal{P}_{i,k}, \underline{p}\right)$ is the relative measure of the cells where the estimator assumes the presence of a target with a probability larger than a threshold $\underline{p}$, *i.e.*, the ratio between the area of the cells where the probability for the presence of a target is larger than $\underline{p}$ and the total area of the cells. A potential choice for $\underline{p}$ is $\underline{p} = \alpha_2^{\mathrm{B}} + 0.5$. The tuning parameter $0.5 > \alpha_2^{\mathrm{B}} > 0$ sets the symmetric threshold of the probability in a cell to consider a target as present or absent in this cell.

6.3.1. Evolution of the probability map

Starting at time t_k, each UAV i applies a three-step procedure similar to that in Section 6.2. First, UAVs have to account for the evolution of the targets. Second, the probability map is updated using the collected measurements. Third, the information received from the neighboring UAVs is taken into account.

For the initialization at time t_0, it is assumed that the probability of presence of a target is constant over cells of the RoI, *i.e.*, $p_{i,m,k} = p_0 = 0.5$, $m \in \mathcal{N}^{\mathrm{c}}$.

6.3.1.1. Prediction step

Considering the evolution of the targets, one can evaluate the probability $p_{i,n,k+1} = \Pr\left(\theta_{i,n,k+1} = 1 \mid \mathcal{I}_k\right)$ of having a target in cell n at time t_{k+1} using the map $\mathcal{P}_{i,k}$ at

time t_k and the conditional transition probability $\Pr(\theta_{n,k+1} = 1 \mid \theta_{m,k} = 1)$ as

$$p_{i,n,k+1|k} = \sum_{m \in \mathcal{N}^{\mathrm{c}}} \Pr(\theta_{n,k+1} = 1 \mid \theta_{m,k} = 1)\, p_{i,m,k}. \tag{6.22}$$

This evaluation may be performed for all cells $\mathcal{C}_n$ of the map. The prediction step for the whole map may be compactly written as

$$\mathcal{P}_{i,k+1|k} = M(\mathcal{P}_{i,k}), \tag{6.23}$$

where $\mathcal{P}_{i,k+1|k} = \left\{p_{i,n,k+1|k}\right\}_{n \in \mathcal{N}^{\mathrm{c}}}$ and the function M is defined from (6.22). The function M can be evaluated offline as the state transition probability is independent of the target state values. Similar map update procedures are considered in Bertuccelli and How (2006a); Frew and Elston (2008).

6.3.1.2. Correction step from measurements

At time t_{k+1}, UAV i observes the set $\mathbb{F}_i\left(\mathbf{x}^{\mathrm{u}}_{i,k+1}\right)$ and evaluates the list of completely observed cells as

$$\mathcal{O}_{i,k+1} = \left\{m \in \mathcal{N}^{\mathrm{c}} \mid \mathcal{C}_m \subset \mathbb{F}_i\left(\mathbf{x}^{\mathrm{u}}_{i,k+1}\right)\right\}. \tag{6.24}$$

Furthermore, UAV i obtains the measurements set $\mathbb{Y}_{i,k}$ from $\mathbb{F}_i\left(\mathbf{x}^{\mathrm{u}}_{i,k+1}\right)$. The measurements set $\mathbb{Y}_{i,k}$ can be mapped into the discretized map of $\mathbb{X}_0$ with the cells $\mathcal{C}_m$, $m = 1, \ldots, N^{\mathrm{c}}$, to evaluate the list of cells where a target is detected

$$\mathcal{L}_{i,k+1} = \left\{m \in \mathcal{N}^{\mathrm{c}} \mid \exists \boldsymbol{x} \in \mathcal{C}_m, \mathbf{h}_i\left(\mathbf{x}^{\mathrm{u}}_{i,k+1}, \boldsymbol{x}\right) \in \mathbb{Y}_{i,k}\right\}. \tag{6.25}$$

From the lists $\mathcal{O}_{i,k+1}$ and $\mathcal{L}_{i,k+1}$ one can now evaluate the observation result $z_{i,m,k+1}$ known to UAV i for cell m considering the measurements set $\mathbb{Y}_{i,k}$ as

$$z_{i,m,k+1} = \begin{cases} 0 & \text{if } m \in \mathcal{O}_{i,k+1} \text{ and } m \notin \mathcal{L}_{i,k+1}, \\ 1 & \text{if } m \in \mathcal{L}_{i,k+1}. \end{cases} \tag{6.26}$$

Then, UAV i can correct its probability map $\mathcal{P}_{i,k+1|k}$ using Bayes' rule to incorporate the observation result $z_{i,m,k+1}$, where the corrected probability $p_{i,m,k+1|k+1}$ of each cell $\mathcal{C}_m$, $m \in \mathcal{N}^{\mathrm{c}}$, is evaluated as

$$p_{i,m,k+1|k+1} = \frac{\Pr(z_{i,m,k+1}|\theta_m = 1)\, p_{i,m,k+1|k}}{\Pr(z_{i,m,k+1}|\theta_m = 1)\, p_{i,m,k+1|k} + \Pr(z_{i,m,k+1}|\theta_m = 0)\left(1 - p_{i,m,k+1|k}\right)}, \tag{6.27}$$

which can be specialized in three cases of events, *i.e.*,

$$p_{i,m,k+1|k+1} = \begin{cases} \frac{pp_{i,m,k+1|k}}{pp_{i,m,k+1|k}+q\left(1-p_{i,m,k+1|k}\right)} & \text{if } m \in \mathcal{O}_{i,k+1} \text{ and } z_{i,m,k+1} = 1, \\ \frac{(1-p)p_{i,m,k}}{(1-p)p_{i,m,k+1|k}+(1-q)\left(1-p_{i,m,k+1|k}\right)} & \text{if } m \in \mathcal{O}_{i,k+1} \text{ and } z_{i,m,k+1} = 0, \\ p_{i,m,k+1|k} & \text{if } m \notin \mathcal{O}_{i,k+1}. \end{cases} \tag{6.28}$$

This classical map update process for multi target search has been considered also in several other works as , *e.g.*, Yang et al. (2004); Vidal et al. (2001); Khan et al. (2015); Bertuccelli and How (2006b); Kuhlman et al. (2017).

The nonlinear update process in (6.28) can be transformed into a linear update function using (6.19). As in Hu et al. (2012), update equation (6.28) becomes then

$$q_{i,m,k+1|k+1} = q_{i,m,k+1|k} + \upsilon_{i,m,k+1}, \tag{6.29}$$

where

$$\upsilon_{i,m,k+1} \triangleq \begin{cases} \ln \frac{q}{p} & \text{if } m \in \mathcal{O}_{i,k+1} \text{ and } z_{i,m,k+1} = 1, \\ \ln \frac{1-q}{1-p} & \text{if } m \in \mathcal{O}_{i,k+1} \text{ and } z_{i,m,k+1} = 0, \\ 0 & \text{if } m \notin \mathcal{O}_{i,k+1}. \end{cases} \tag{6.30}$$

Assuming that the detection probability is $p = 1$, equation (6.28) and (6.30) simplify to

$$p_{i,m,k+1|k+1} = \begin{cases} \frac{p_{i,m,k+1|k}}{p_{i,m,k+1|k}+q\left(1-p_{i,m,k+1|k}\right)} & \text{if } m \in \mathcal{O}_{i,k+1} \text{ and } z_{i,m,k+1} = 1, \\ 0 & \text{if } m \in \mathcal{O}_{i,k+1} \text{ and } z_{i,m,k+1} = 0, \\ p_{i,m,k+1|k} & \text{if } m \notin \mathcal{O}_{i,k+1}, \end{cases} \tag{6.31}$$

and

$$\upsilon_{i,m,k+1} \triangleq \begin{cases} \ln q & \text{if } m \in \mathcal{O}_{i,k+1} \text{ and } z_{i,m,k+1} = 1, \\ +\inf & \text{if } m \in \mathcal{O}_{i,k+1} \text{ and } z_{i,m,k+1} = 0, \\ 0 & \text{if } m \notin \mathcal{O}_{i,k+1}. \end{cases} \tag{6.32}$$

This means that when no target is detected in cell $\mathcal{C}_m$ the probability of having a target in that cell becomes directly zero, *i.e.*, $p_{i,m,k+1|k+1} = 0$. Furthermore, $q_{i,m,k}$ is a nonlinear bijective transformation of $p_{i,m,k}$, *i.e.*, when $p_{i,m,k} = 1$ then $q_{i,m,k} = -\inf$ and when $p_{i,m,k} = 0$ then $q_{i,m,k} = +\inf$. This is consistent with (6.32).

6.3.1.3. Correction step from communication

After collecting the measurements and updating $q_{i,m,k+1|k}$, each UAV i broadcasts $q_{i,\ell,k+1|k+1}$ to UAV $\ell \in \mathcal{N}_{i,k}$ and receives the corresponding information. As in Hu et al. (2012), the corrected estimate $q_{i,m,k+1}$ after communication is

$$q_{i,m,k+1} = \sum_{\ell \in \mathcal{N}_{i,k} \cup \{i\}} w_{i,\ell,k} q_{i,\ell,k+1|k+1}, \tag{6.33}$$

where $w_{i,i,k} = 1 - ((|\mathcal{N}_{i,k}| - 1)/N^{\mathrm{u}})$ and $w_{i,\ell,k} = 1/N^{\mathrm{u}}$, $\ell \in \mathcal{N}_{i,k}$. Using (6.19), UAV i transforms $q_{i,m,k+1}$ to $p_{i,m,k+1}$ to obtain $\mathcal{P}_{i,k+1}$.

6.3.2. Control design

As in the control design in Section 6.2.2, the aim is for each UAV is to decrease the uncertainty as much as possible. In the stochastic Bayesian context, UAV i seeks for the sequence of control inputs $\mathbf{u}_{i,k:k+h-1} = (\mathbf{u}_{i,k}, \ldots, \mathbf{u}_{i,k+h-1})$ which minimizes the predicted uncertainty $\Phi^{\mathrm{B}}(\mathcal{P}_{i,m,k+h})$ at time $k+h$.

To obtain comparable results, the control design is based on the same assumptions as in Section 6.2.2: (1) the UAVs compute their control inputs sequentially, (2) once $\mathbf{u}_{i,k:k+h-1}$ is evaluated, it is broadcast, (3) UAV i accounts for the control sequences of neighbors in $\ell \in \mathcal{N}^{\mathrm{c}}_{i,k} \subseteq \mathcal{N}_{i,k}$, and (4) the evolution of $\Phi^{\mathrm{B}}(\mathcal{P}_{i,m,k+h})$ is performed via a model predictive control approach.

At time t_k, UAV i has access to $\mathcal{P}_{i,m,k}$ and $u_{\ell,k:k+h-1}$, $\ell \in \mathcal{N}^{\mathrm{c}}_{i,k}$. UAV i can predict $\mathbf{x}^{\mathrm{u,P}}_{i,k+1}$ of $\mathbf{x}^{\mathrm{u}}_{i,k+1}$ for a given control input $\mathbf{u}_{i,k}$ using (3.1). Similarly, it can evaluate the location $\mathbf{x}^{\mathrm{u,P}}_{\ell,k+1}$ of the neighbors in $\mathcal{N}^{\mathrm{c}}_{i,k}$. The predicted probabilities $p^{\mathrm{P}}_{i,m,k+1|k}$ of $p_{i,m,k+1|k}$ can be evaluated using (6.23).

Considering the correction from measurements, the predicted sets of cells that UAV i or the neighbors in $\mathcal{N}^{\mathrm{c}}_{i,k}$ observe are

$$\mathcal{O}^{\mathrm{P}}_{\ell,k+1} = \left\{ m \in \mathcal{N}^{\mathrm{c}} \mid \mathcal{C}_m \subset \mathbb{F}_\ell\left(\mathbf{x}^{\mathrm{u}}_{\ell,k+1}\right) \cap \mathbb{X}_0 \right\},$$

where $\ell \in \mathcal{N}^{\mathrm{c}}_{i,k} \cup \{i\}$. As in Section 6.2.2, each UAV is unable to predict if a target will be detected at t_{k+1}, consequently the predicted value of $\mathcal{L}_{\ell,k+1}$ is $\mathcal{L}^{\mathrm{P}}_{\ell,k+1} = \emptyset$ and of $z_{\ell,m,k+1}$ is $z^{\mathrm{P}}_{\ell,m,k+1} = 0$, for $m \in \mathcal{O}^{\mathrm{P}}_{\ell,k+1}$ and $\ell \in \mathcal{N}^{\mathrm{c}}_{i,k} \cup \{i\}$.

One can now transform $p^{\mathrm{P}}_{i,m,k+1|k}$ to $q^{\mathrm{P}}_{i,m,k+1|k}$ using (6.19). The predicted measurements are incorporated as

$$q^{\mathrm{P}}_{i,m,k+1} = q^{\mathrm{P}}_{i,m,k+1|k} + \sum_{\ell \in \mathcal{N}^{\mathrm{c}}_{i,k} \cup \{i\}} w_{i,\ell,k} \upsilon^{\mathrm{P}}_{\ell,m,k+1}, \tag{6.34}$$

where

$$\upsilon^{\mathrm{P}}_{\ell,m,k+1} \triangleq \begin{cases} +\inf & \text{if } m \in \mathcal{O}_{\ell,k+1}, \\ 0 & \text{if } m \notin \mathcal{O}_{\ell,k+1}, \end{cases} \tag{6.35}$$

$\ell \in \mathcal{N}^{\mathrm{c}}_{i,k} \cup \{i\}$, and where $w_{i,i,k} = 1 - \left(\left|\mathcal{N}^{\mathrm{c}}_{i,k}\right| - 1\right)/N^{\mathrm{u}}$ and $w_{i,\ell,k} = 1/N^{\mathrm{u}}$, $\ell \in \mathcal{N}^{\mathrm{c}}_{i,k}$. The update (6.34) directly fuses the measurements that are collected by UAV i , as in (6.29), and by its neighbors in $\mathcal{N}^{\mathrm{c}}_{i,k}$, as in (6.33). One can then transform $q^{\mathrm{P}}_{i,m,k+1}$ using the inverse of (6.19) to obtain $p^{\mathrm{P}}_{i,m,k+1}$ and $\mathcal{P}^{\mathrm{P}}_{i,m,k+1}$.

The one-step ahead prediction of $\mathcal{P}^{\mathrm{P}}_{i,m,k+1}$, described above, can be applied recursively on $\mathcal{P}^{\mathrm{P}}_{i,m,k+\kappa-1}$ to evaluate the impact of $\mathbf{u}_{i,k+\kappa}$, $\kappa = 1, \ldots, h-1$ on the predicted estimation uncertainty for UAV i at time $t_{k+\kappa}$, which provides $\mathcal{P}^{\mathrm{P}}_{i,m,k+h}$ when $\kappa = h-1$. This allows UAV i to evaluate the impact of the sequence $\mathbf{u}_{i,k+\kappa}$, $\kappa = 1, \ldots, h-1$ on the estimation uncertainty $\Phi^{\mathrm{B}}\left(\mathcal{P}^{\mathrm{P}}_{i,m,k+h}\right)$. UAV i can then search for the control input sequence $\mathbf{u}_{i,k:k+h-1}$ minimizing $\Phi^{\mathrm{B}}\left(\mathcal{P}^{\mathrm{P}}_{i,m,k+h}\right)$. When the value of h is small, $\mathbf{u}_{i,k:k+h-1}$ may have no impact on $\Phi^{\mathrm{B}}\left(\mathcal{P}^{\mathrm{P}}_{i,m,k+h}\right)$. This is why an alternative cost function

$$J^{\mathrm{B}}\left(\mathbf{u}_{i,k}, \ldots, \mathbf{u}_{i,k+h-1}\right) = \Phi^{\mathrm{B}}\left(\mathcal{P}^{\mathrm{P}}_{i,m,k+h}\right) + \alpha^{\mathrm{B}}_3 d^{\mathrm{B}}\left(\boldsymbol{x}^{\mathrm{u,P}}_{i,k+h}, \mathcal{P}^{\mathrm{P}}_{i,m,k+h}\right), \tag{6.36}$$

is introduced, where

$$d^{\mathrm{B}}\left(\boldsymbol{x}^{\mathrm{u,P}}_{i,k+h}, \mathcal{P}^{\mathrm{P}}_{i,m,k+h}\right) = \min_{m \in \mathcal{N}^{\mathrm{c}} \mid \left|p^{\mathrm{P}}_{i,m,k+h} - 0.5\right| < \alpha^{\mathrm{B}}_2} \left\| c_m - \boldsymbol{x}^{\mathrm{u,P}}_{i,k+h} \right\|,$$

where c_m is the center of cell $\mathcal{C}_m$. The weight α^{B}_3 tunes the importance of the minimal distance $d^{\mathrm{B}}\left(\boldsymbol{x}^{\mathrm{u,P}}_{i,k+h}, \mathcal{P}^{\mathrm{P}}_{i,m,k+h}\right)$ between the UAV location $\boldsymbol{x}^{\mathrm{u,P}}_{i,k+h}$ and the cells $m \in \mathcal{N}^{\mathrm{c}}$.

6.4. Practical issues

Some design parameters need to be defined for the different approaches presented.

For the set-membership target search process one parameter needs to be chosen in (6.8). The value α^{S} should be designed such that $\alpha^{\mathrm{S}} d\left(\mathbf{x}^{\mathrm{u,P}}_{i,k+h}, \mathbb{X}^{\mathrm{P}}_{i,j,k+h} \cup \overline{\mathbb{X}}^{\mathrm{P}}_{i,k+h}\right)$ remains always small compared to $\Phi^{\mathrm{S}}\left(\mathbb{X}^{\mathrm{P}}_{i,j,k+h}, \overline{\mathbb{X}}^{\mathrm{P}}_{i,k+h}\right)$, to emphasize the reduction of the size of the sets.

Regarding the stochastic Bayesian search approach 4 parameters need to be chosen. The tuning parameter α^{B}_1 characterizes the uncertainty for the presence or absence of a target considering the probability $p_{i,m,k}$ of each cell $\mathcal{C}_m$. The parameter α^{B}_1 is linked to α^{B}_2, which is the threshold for $p_{i,m,k}$ to consider a target present or absent in a cell. The weight α^{B}_3 has a similar meaning as α^{S} and should be chosen such that $\alpha^{\mathrm{B}}_3 d^{\mathrm{B}}\left(\boldsymbol{x}^{\mathrm{u,P}}_{i,k+h}, \mathcal{P}^{\mathrm{P}}_{i,m,k+h}\right)$ remains small compared to $\Phi^{\mathrm{B}}\left(\mathcal{P}_{i,m,k+h}\right)$. Finally, for

the stochastic estimator the false detection probability q needs to be selected. This probability depends on the quality of observation and thus on the sensor, the image processing system, and environmental conditions. Finding *a priori* appropriate values for q may be difficult, however, q may be derived from prior simulations and experiments analyzing the probabilistic properties of the sensor system in various conditions.

6.5. Simulations

Simulations are carried out to compare both approaches. The sampling period is $T = 0.5\,\mathrm{s}$. The RoI is taken as a square of $500 \times 500\,\mathrm{m}^2$. A fleet of $N^{\mathrm{u}} = 4$ UAVs searches for $N^{\mathrm{t}} = 10$ *static* ground targets uniformly distributed in the RoI.

The state of UAV i at time t_k consists of its location $\boldsymbol{x}^{\mathrm{u}}_{i,k} = (x^{\mathrm{u}}_{i,k,1}, x^{\mathrm{u}}_{i,k,2}, x^{\mathrm{u}}_{i,k,3})^{\top}$, flight path angle $x^{\mathrm{u}}_{i,k,4}$, heading angle $x^{\mathrm{u}}_{i,k,5}$, yaw rate $x^{\mathrm{u}}_{i,k,6}$, and yaw rate derivative $x^{\mathrm{t}}_{i,k,7}$. The UAVs move on a plane with a constant altitude of $h = 100\,\mathrm{m}$ and fly with a constant speed of $V = 16.6\,\mathrm{m/s}$. The control input $u_{i,k}$ is then limited to the yaw rate $x^{\mathrm{u}}_{i,k,7}$. The state vector $\mathbf{x}^{\mathrm{u}}_{i,k}$ evolves according to (4.46).

The FoV of each UAV has an identical aperture of $\pi/4$ for the azimuth and elevation. Its inclination, defined as in Figure 5.15, is $\gamma_{\mathrm{FoV}} = 3\pi/8$. When a target is detected, a noisy measurement of the target coordinates is obtained, with a noise uniformly distributed in $[-5, 5] \times [-5, 5]\,\mathrm{m}^2$. The measurement noise bound available to the UAVs is chosen as $[\mathbf{w}] = [-7, 7] \times [-7, 7]\,\mathrm{m}^2$ to reflect situations where the noise bounds are over estimated.

The prediction horizon for the control design is $h = 3$ for both control schemes. A complete connected communication graph is assumed.

The RoI is divided into 125×125 cells for the probability map of the stochastic estimator. Each cell has then a size of $4 \times 4\,\mathrm{m}$. The parameter are chosen as $\alpha^{\mathrm{S}} = 0.0001$, $\alpha^{\mathrm{B}}_1 = 0.5$, $\alpha^{\mathrm{B}}_2 = 0.49$ and $\alpha^{\mathrm{B}}_3 = 0.0001$. The results for each setup of the following simulations were obtained for 30 independent simulations with uniformly distributed initial locations of the targets and UAVs in the RoI.

In the fist scenario, the estimation performance of both estimation schemes is evaluated without false positive detection. Figure 6.2 (left) presents the evolution of the performance criteria $\overline{\Phi}^{\mathrm{S}}_k = \frac{1}{N^{\mathrm{u}}} \sum_{i=1}^{N^{\mathrm{u}}} \Phi^{\mathrm{S}} \left(\mathbb{X}^{\mathrm{U}}_{i,k}, \overline{\mathbb{X}}_{i,k} \right)$ (for the set-membership estimator) and $\overline{\Phi}^{\mathrm{B}}_k \left(\underline{p} \right) = \frac{1}{N^{\mathrm{u}}} \sum_{i=1}^{N^{\mathrm{u}}} \Phi^{\mathrm{B}} \left(\mathcal{P}_{i,k}, \underline{p} \right)$ (for the stochastic estimator), where the threshold $\underline{p}$ varies in the set $\underline{p} = \{0.6, 0.9, 0.99\}$. These criteria correspond to the size of the area where the estimators indicate the presence of the targets. For the stochastic Bayesian state estimation, the values for the probabilities of false positive detection are compared, *i.e.*, $q = \{0.1, 0.5, 0.9\}$. These values are chosen very large to highlight their impact on the estimation performance.

In Figure 6.1 (left), one observes that $\overline{\Phi}_k^{\mathrm{S}}$ monotonically decreases with t_k. The proposed set-membership estimator evaluates guaranteed estimates, consequently, $\overline{\Phi}_k^{\mathrm{S}}$ is an upper bound for the estimation uncertainty that can be obtained. The optimal value of $\overline{\Phi}_k^{\mathrm{S}}$ is 0.064×10^{-2}, which is the number of true targets ($N^{\mathrm{t}} = 10$) times the measure of the mismatch of the noise bound ($4 \times 4\,\mathrm{m}^2$) divided by the measure of the RoI ($500 \times 500\,\mathrm{m}^2$).

For the stochastic estimator, one observes that the criterion $\overline{\Phi}_k^{\mathrm{B}}\left(\underline{p}\right)$ converges towards different values depending on $q = \{0.1, 0.5, 0.9\}$. The optimal value of $\overline{\Phi}_k^{\mathrm{B}}\left(\underline{p}\right)$ is identical to that of $\overline{\Phi}_k^{\mathrm{S}}$. The optimal value of $\overline{\Phi}_k^{\mathrm{B}}\left(\underline{p}\right)$ is the number of true targets ($N^{\mathrm{t}} = 10$) times the measure of a single cell ($4 \times 4\,\mathrm{m}^2$) divided by the measure of the RoI ($500 \times 500\,\mathrm{m}^2$). Nevertheless, due to the mismatch of the noise bound, a single target may lead to a constant detection in neighboring cells. Assuming that a single target leads to a detection in 3 neighboring cells leads to a optimal value of 0.192×10^{-2}, which is very close to the value that is obtained for $\overline{\Phi}_k^{\mathrm{B}}(0.99)$, for $q = 0.9$. The stochastic estimator when $q = 0.9$ performs better since it removes more efficiently these detections in neighboring cells.

Figure 6.1 (right) presents the number of tracked targets. For the set-membership estimator, the number of tracked targets corresponds to the number of targets that are located in $\mathbb{X}_{i,k}^{\mathrm{U}}$ (solid, black, SME). The targets are always located in $\mathbb{X}_{i,k}^{\mathrm{U}} \cup \overline{\mathbb{X}}_{i,k}$. For the stochastic estimator, the number of tracked targets is the number of targets that are in cells where $p_{i,m,k} > \underline{p}$, where $\underline{p} = \{0.6, 0.9, 0.99\}$. One observes that the stochastic estimator when $q = 0.9$ needs a much larger number of observations to identify the cells where the targets are located. This is reasonable since the higher probability of false positive detections makes it necessary to collect more measurements of the same cell to increase $p_{i,m,k}$.

Hereafter, in the simulations, the estimation performance of the set-membership and stochastic estimator are compared for three different sources of errors of false positive detections. Section 6.5.1 reports results for simulations where false positive detection appears due to the presence of false targets, where the detection is modeled as in (3.10). Subsequently, Section 6.5.2 and 6.5.3 report results for simulations where it is assumed that false positive detections can be modeled by realizations of random variables and appear due to a defective/imperfect sensor and changing environmental conditions.

6.5.1. Deterministic false positive detection

This section compares the estimation performance of both estimation schemes considering the presence of static false targets that may be confused with true targets. Similar to (3.10), a false target at location $\boldsymbol{x}_{\ell}^{\mathrm{f}}$ is detected when $\boldsymbol{x}_j^{\mathrm{t}} \in \mathbb{F}_i\left(\mathbf{x}_{i,k}^{\mathrm{u}}\right)$ and $\boldsymbol{x}_{i,k}^{\mathrm{u}} \in \mathbb{D}_k\left(\boldsymbol{x}_j^{\mathrm{t}}\right)$, where $\boldsymbol{x}_{i,k}^{\mathrm{u}} \in \mathbb{D}_k\left(\boldsymbol{x}_j^{\mathrm{t}}\right)$ is assumed to be always satisfied. When

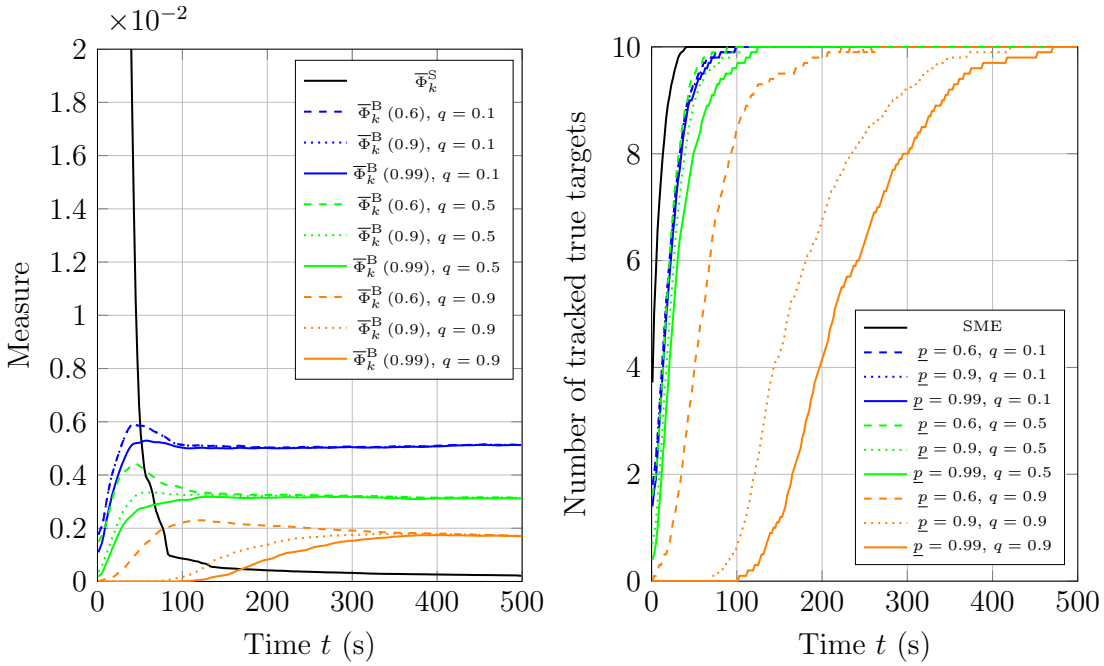

Figure 6.1.: Performance without false detection. Left: Mean values of $\overline{\Phi}_k^{\mathrm{S}}$ and $\overline{\Phi}_k^{\mathrm{B}}\left(\underline{p}\right)$ for 30 simulations with 10 true targets and 4 UAVs. Right: Mean values of the number of true targets that are tracked.

detected, similarly to $g_\ell^{\mathrm{f}}\left(\mathbf{x}_{i,k}^{\mathrm{u}}, \mathbf{x}_{\ell,k}^{\mathrm{f}}\right)$ in (3.12), false target ℓ is recognized as a true target when $\boldsymbol{x}_{i,k}^{\mathrm{u}} \notin \mathbb{G}_\ell$, where

$$\mathbb{G}_\ell = \left\{ \begin{pmatrix} \boldsymbol{x}_\ell^{\mathrm{f}} \\ 0 \end{pmatrix} + a_1 \boldsymbol{v}_{\ell,1} + a_2 \boldsymbol{v}_{\ell,2} + a_3 \boldsymbol{v}_{\ell,3} \mid a_m \in \mathbb{R}^+, m = 1,2,3 \right\},$$

is a cone spanned by vectors $\boldsymbol{v}_{\ell,1}$, $\boldsymbol{v}_{\ell,2}$, and $\boldsymbol{v}_{\ell,3} \in \mathbb{R}^3$. The vector $\boldsymbol{v}_{\ell,1}$ is $(0,0,1)^\top$. The angle between the vectors are $\angle\left(\boldsymbol{v}_{\ell,1}, \boldsymbol{v}_{\ell,2}\right) = \pi/4$, $\angle\left(\boldsymbol{v}_{\ell,1}, \boldsymbol{v}_{\ell,3}\right) = \pi/4$, and $\angle\left(\boldsymbol{v}_{\ell,2}, \boldsymbol{v}_{\ell,3}\right) = \pi/4$. The orientation/angle of the cone $\angle\left(\boldsymbol{v}_{\ell,2}, (1,0,0)^\top\right)$ is uniformly distributed in $[0, 2\pi[$. When $\boldsymbol{x}_{i,k}^{\mathrm{u}} \in \mathbb{G}_\ell$, the measurement is discarded. Consequently, for $\mathcal{Y}_{i,k}$ in (6.2) one has

$$\mathbf{x}_{\ell,k}^{\mathrm{f}} \in \mathbb{F}_i\left(\mathbf{x}_{i,k}^{\mathrm{u}}\right) \text{ and } \boldsymbol{x}_{i,k}^{\mathrm{u}} \in \mathbb{D}_k\left(\mathbf{x}_{\ell,k}^{\mathrm{f}}\right) \text{ and } \boldsymbol{x}_{i,k}^{\mathrm{u}} \notin \mathbb{G}_\ell \Rightarrow \exists \mathbf{y} \in \mathcal{Y}_{i,k} \mid \mathbf{y} = \mathbf{y}_{i,m,k}^{\mathrm{U}}, \quad (6.37)$$

where $\mathbf{y}_{i,m,k}^{\mathrm{U}}$ is the measurement of the location $\boldsymbol{x}_j^{\mathrm{f}}$ of false target ℓ according to (3.17). The RoI contains 10 uniform distributed false targets.

In Figure 6.2 (left), one observes that the evolution of $\overline{\Phi}_k^{\mathrm{S}}$ – compared to Figure 6.1 – is not much affected by the presence of false targets. For the stochastic estimator, $\overline{\Phi}_k^{\mathrm{B}}\left(\underline{p}\right)$ converges to different values compared to Figure 6.1. The estimator when $q = 0.1$ is strongly affected by the presence of the false targets and the performance

criterion converges to $\overline{\Phi}_k^{\mathrm{B}}(0.99) \approx 0.85 \times 10^{-2}$ (compared to $\overline{\Phi}_k^{\mathrm{B}}(0.99) \approx 0.35 \times 10^{-2}$ in Figure 6.1).

Figure 6.2 (right) presents the evolution of the number of tracked true targets. The presence of 10 false targets does not have a visible impact on the evolution of the number of tracked true targets for the set-membership estimator. Results similar to those in Figure 6.1 (right) are obtained. The stochastic estimator shows also a similar behavior. However, it is of high interest to notice that the number of tracked targets for the estimator when $\underline{p} = 0.99$ and $q = 0.9$ is increasing faster at $t = 200$ than in Figure 6.1. Repetitive observations of false targets seem to lead also to more observations of true targets and thus to improved detection of the true targets.

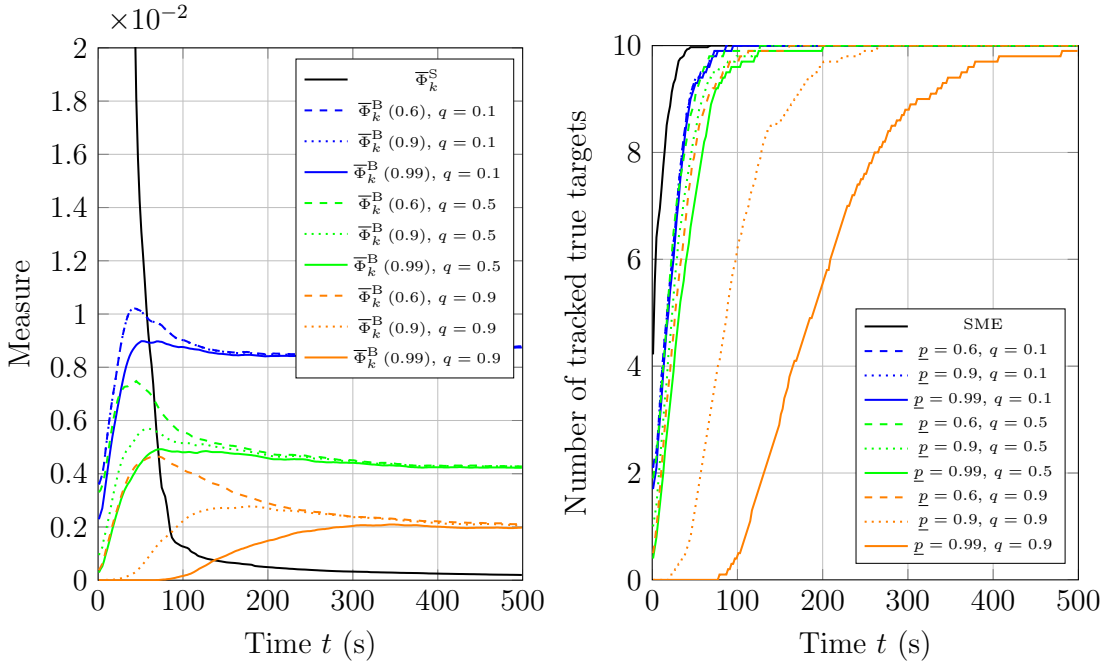

Figure 6.2.: Left: Mean values of $\overline{\Phi}_k^{\mathrm{S}}$ and $\overline{\Phi}_k^{\mathrm{B}}\left(\underline{p}\right)$ for 30 simulations with 10 true targets, 10 false targets, and 4 UAVs. Right: Mean values of the number of true targets that are tracked.

Figure 6.3 presents the mean values of the number of tracked false targets, *i.e.*, false targets that are inside the set estimates $\mathbb{X}_{i,k}^{\mathrm{U}} \cup \overline{\mathbb{X}}_{i,k}$ (for the set-membership estimator) or inside a cell m, where $p_{i,m,k} > \underline{p}$ (for the stochastic estimator). One observes that the stochastic estimator when $q = 0.9$ is the most efficient in discarding locations of false targets, and performs the worst when $q = 0.1$. A high probability of false positive detection forces the UAVs to update the probability of each cell many times to reach $p_{i,m,k} > \alpha_2^{\mathrm{B}} + 0.5$ as in (6.36), since the presence or absence of a target is considered uncertain if $|p_{i,m,k} - 0.5| < \alpha_2^{\mathrm{B}}$. The frequent updates lead to changing points of view when collecting observations, and the UAVs are prone to attain configurations where $\boldsymbol{x}_{i,k}^{\mathrm{u}} \in \mathbb{G}_j$ and can finally discard the false targets.

The stochastic estimators when $q < 0.5$ perform worse than the set-membership estimator. This might be partially due to numerical approximations. The probability $p_{i,m,k}$ in each cell may be rounded to either 0 or 1 after a finite number of observations, which leads to $q_{i,m,k}$ either $+\inf$ or $-\inf$ and then to $\eta_{i,m,k} = 0$. As a consequence, the cost function (6.36) can become zero what ever the control input sequence.

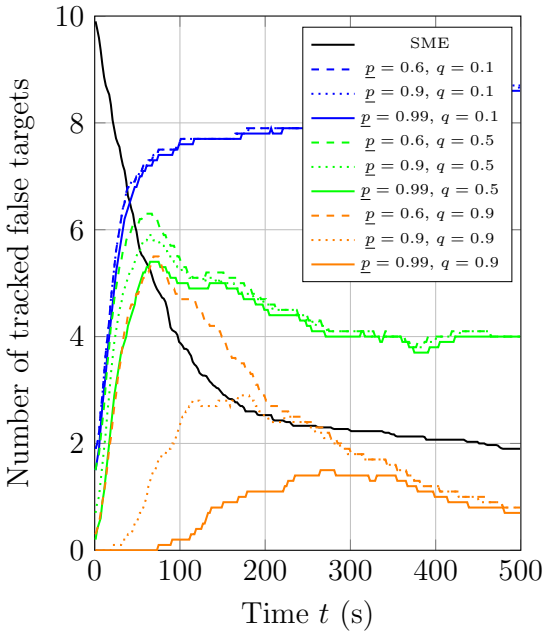

Figure 6.3.: Mean values of the number of tracked false targets.

6.5.2. Stochastic false positive detection – Poisson modeling

This section compares the estimation performance of both estimation schemes considering false positive detections due to a defective/imperfect sensor and computer vision system. At each time t_k, it is assumed that UAV i may obtain $N^{\mathrm{f}}_{i,k}$ false positive detections in the FoV. The number of false positive detections $N^{\mathrm{f}}_{i,k}$ is random and the probability of occurrence of this event is modeled by a Poisson probability distribution, *i.e.*, $\mathrm{Pois}\left(\lambda_i\right)$ with parameter λ_i. It is assumed that the parameter λ_i may depend on the quality of the computer vision system of UAV i. The probability, at time t_k, for UAV i to obtain $N^{\mathrm{f}}_{i,k}$ false positive detections is then

$$P\left(N^{\mathrm{f}}_{i,k} \mid \lambda_i\right) = \frac{\lambda_i^{N^{\mathrm{f}}_{i,k}} \mathrm{e}^{-\lambda_i}}{N^{\mathrm{f}}_{i,k}!}.$$

The location of the $N^{\mathrm{f}}_{i,k}$ false detections is uniformly distributed in $\mathbb{F}_i\left(\mathbf{x}^{\mathrm{u}}_{i,k}\right)$. Each false positive detection generates a measurement $\mathbf{y}$ in $\mathcal{Y}_{i,k}$.

Figure 6.4 and 6.5 present the estimation performance of the estimators for $\lambda_i = 10$ and $\lambda_i = 20$ respectively. One observes that the choice of λ_i has only a minor impact on the estimation performance of the set-membership estimator. Nevertheless, the decrease of $\Phi_k^{\mathrm{S}}\left(\mathbb{X}_{i,k}^{\mathrm{U}}, \overline{\mathbb{X}}_{i,k}\right)$ is slower for $\lambda_i = 20$ at $t \approx 100\,\mathrm{s}$. The evolution of the number of tracked targets of set-membership estimator in Figure 6.4 and 6.5 (right) is very similar for both cases. The stochastic estimator when $q = 0.9$ converges for both scenarios towards similar values $\overline{\Phi}_k^{\mathrm{B}}(0.99) \approx 0.2 \times 10^{-2}$. One observes that targets are detected earlier for a higher probability of false positive detection – as can be seen by comparing the number of tracked targets at $t \approx 200$ in Figure 6.4 (right) when $\lambda_i = 10$ and Figure 6.5 (right) where $\lambda_i = 20$ –. The chosen values of λ_i have a strong impact on the performance of the stochastic estimator when $q = 0.1$ or $q = 0.5$. One observes a strong overshoot of $\overline{\Phi}_k^{\mathrm{B}}(0.99)$ when $q = 0.1$ and $\lambda_i = 10$ or when $q = 0.5$ and $\lambda_i = 20$. This indicates that the chosen probability of false positive detection ($q = 0.1$ or $q = 0.5$) is too small and the real probability of false positive detection is higher. In general, an appropriate choice of q should lead to an evolution of $\Phi^{\mathrm{B}}\left(\mathcal{P}_{i,k}, \underline{p}\right)$ that does not present any overshoots.

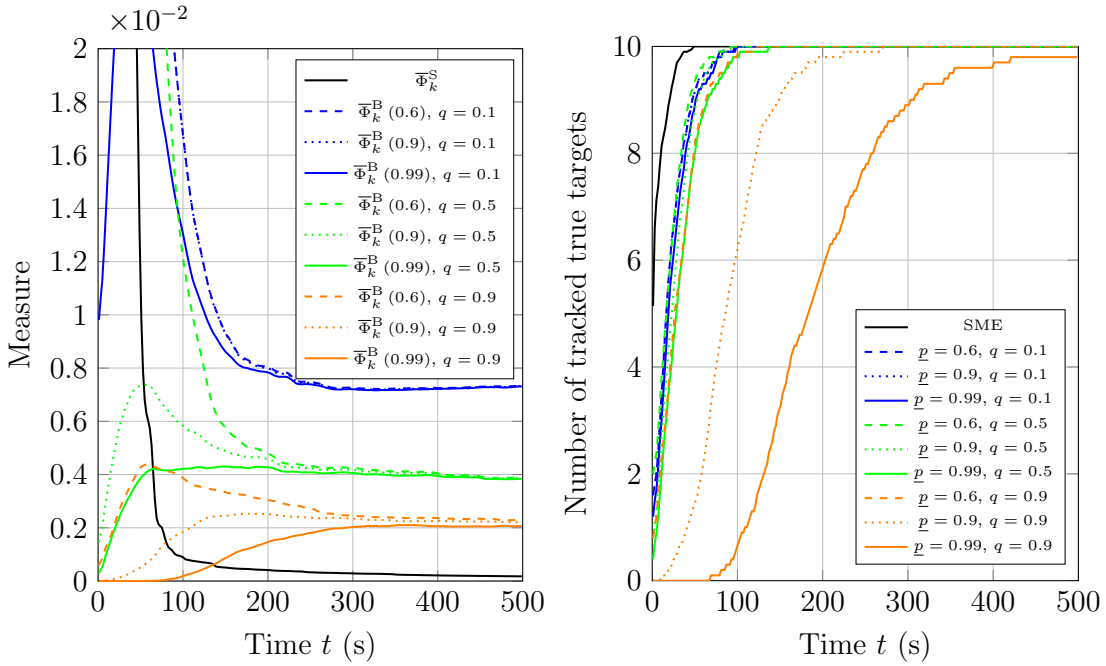

Figure 6.4.: Results of simulations when $\lambda_i = 10$. Left: Mean values of $\overline{\Phi}_k^{\mathrm{S}}$ and $\overline{\Phi}_k^{\mathrm{B}}\left(\underline{p}\right)$ for 30 simulations with 10 true targets, and 4 UAVs. Right: Mean values of the number of true targets that are tracked.

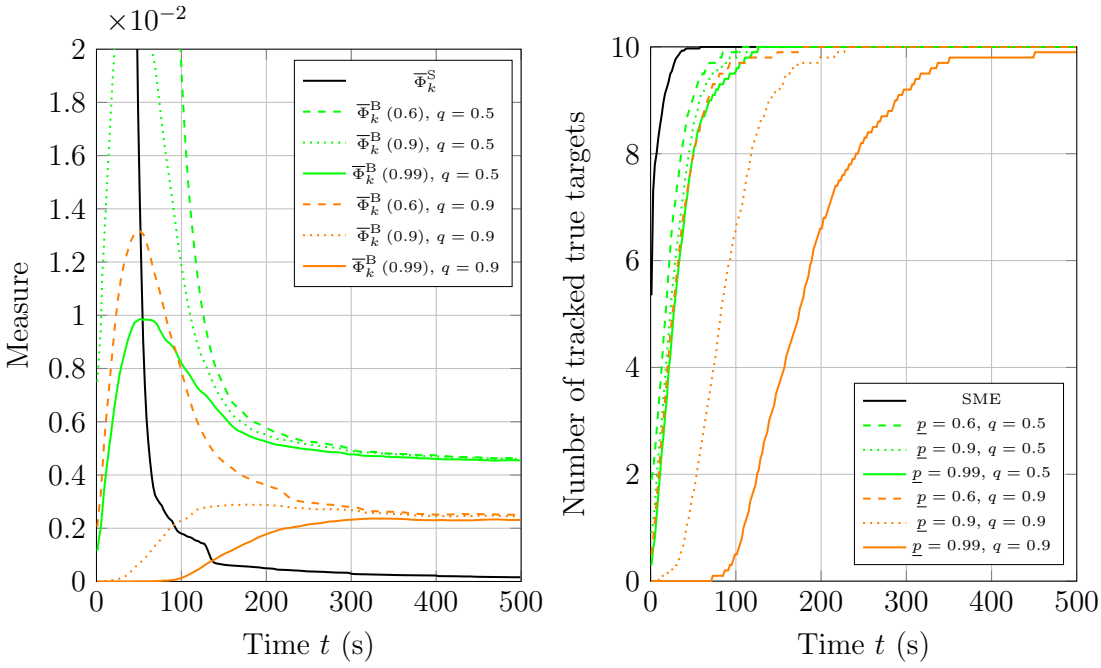

Figure 6.5.: Results of simulations when $\lambda_i = 20$. Left: Mean values of $\overline{\Phi}_k^{\mathrm{S}}$ and $\overline{\Phi}_k^{\mathrm{B}}\left(\underline{p}\right)$ for 30 simulations with 10 true targets, and 4 UAVs. Right: Mean values of the number of true targets that are tracked.

6.5.3. Stochastic false positive detection – Markov modeling

This section compares the estimation performance of both estimation schemes considering false positive detections due to changing environmental conditions. It is assumed that false positive detections in the cells $\mathcal{C}_m$, $m \in \mathcal{N}^{\mathrm{c}}$, are modeled by a Markov process. At time t_k, let $\theta_{m,k}^{\mathrm{f}}$ be a Bernoulli random variable indicating potential false positive detection of a target in $\mathcal{C}_m$. When $\theta_{m,k}^{\mathrm{f}} = 1$, a target will be erroneously detected in cell $\mathcal{C}_m$ when $\mathcal{C}_m$ is observed. When $\theta_{m,k}^{\mathrm{f}} = 0$, the cell can be correctly observed and false positive detection does not appear. The UAVs have no access to $\theta_{m,k}^{\mathrm{f}}$, and $\theta_{m,k}^{\mathrm{f}}$ is changing with time due to changing environmental conditions. The evolution of $\theta_{m,k}^{\mathrm{f}}$ with time is modeled by a Markov process, where $\Pr\left(\theta_{m,k+1}^{\mathrm{f}} = 1 \mid \theta_{m,k}^{\mathrm{f}} = 1\right) = p_{11}$, $\Pr\left(\theta_{m,k+1}^{\mathrm{f}} = 0 \mid \theta_{m,k}^{\mathrm{f}} = 0\right) = p_{00}$, $\Pr\left(\theta_{m,k+1}^{\mathrm{f}} = 0 \mid \theta_{m,k}^{\mathrm{f}} = 1\right) = 1 - p_{11}$, and $\Pr\left(\theta_{m,k+1}^{\mathrm{f}} = 1 \mid \theta_{m,k}^{\mathrm{f}} = 0\right) = 1 - p_{00}$ are the transition probabilities between the states $\theta_{m,k}^{\mathrm{f}}$ at t_k and $\theta_{m,k+1}^{\mathrm{f}}$at t_{k+1}. Consider UAV i and cell m, when $\mathcal{C}_m \subset \mathbb{F}_i\left(\mathbf{x}_{i,k+1}^{\mathrm{u}}\right)$ and $\theta_{m,k}^{\mathrm{f}} = 1$ then false positive detection appears and UAV i collects a measurement $\mathbf{y}$ that corresponds to the detection of a target at the center of $\mathcal{C}_m$.

Figure 6.6 present the estimation performances of the two estimators when $p_{11} = 0,99$ and $p_{00} = 0,99999$. This choice of p_{11} and p_{00} is made such that the search area contains in average 15 cells where false positive detection can appear and such

that the cells seldom change their state. In Figure 6.6 (left), one observes that the evolution of $\overline{\Phi}_k^{\mathrm{S}}$ – compared to Figure 6.1 – is not much affected by the Markov modeling of stochastic false positive detections. For the stochastic estimator, $\overline{\Phi}_k^{\mathrm{B}}\left(\underline{p}\right)$ converges to different values compared to Figure 6.1. The estimator when $q = 0.1$ is strongly affected by stochastic false positive detections and the performance criterion converges to $\overline{\Phi}_k^{\mathrm{B}}(0.99) \approx 0.65 \times 10^{-2}$ (compared to $\overline{\Phi}_k^{\mathrm{B}}(0.99) \approx 0.5 \times 10^{-2}$ in Figure 6.1). One observes again strong overshoots of $\overline{\Phi}_k^{\mathrm{B}}(0.99)$ for the estimators when $q = 0.1$ and $q = 0.5$. This indicates again that the chosen probabilities of false positive detection are too small and the real probability of false positive detection is higher.

Figure 6.6 (right) presents the evolution of the number of tracked true targets. The presence of cells leading to random false detection does not have a visible impact on the evolution of the number of tracked true targets for the set-membership and stochastic estimator estimator. Results similar to those in Figure 6.1 (right) are obtained.

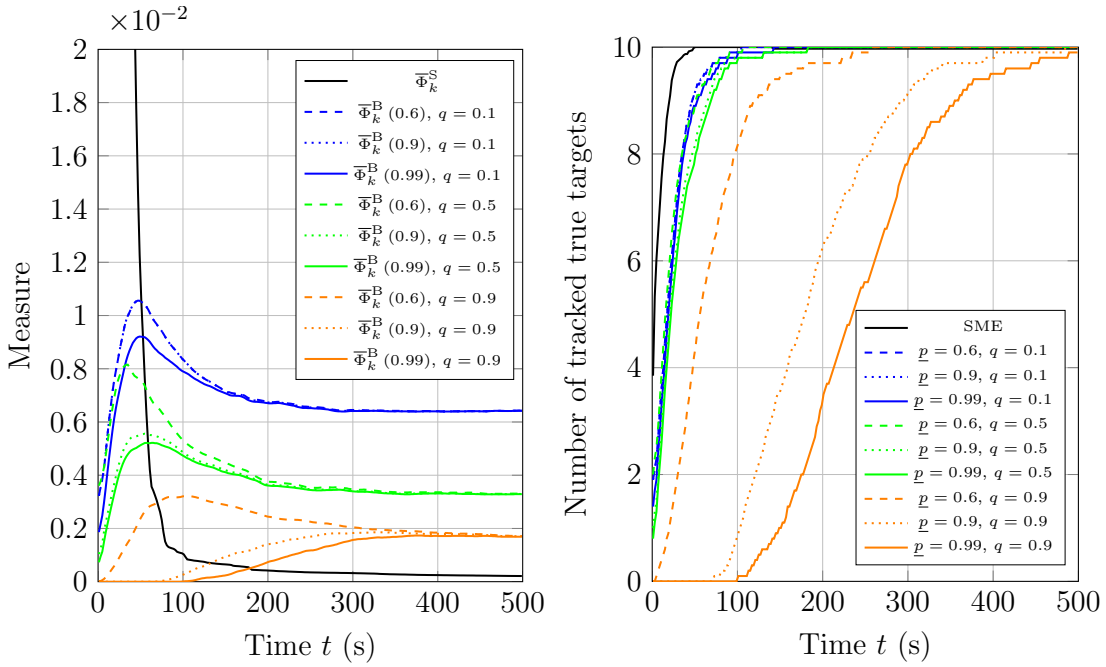

Figure 6.6.: Results of simulations when $p_{11} = 0,99999$ and $p_{00} = 0,99$. Left: Mean values of $\overline{\Phi}_k^{\mathrm{S}}$ and $\overline{\Phi}_k^{\mathrm{B}}\left(\underline{p}\right)$ for 30 simulations with 10 true targets, and 4 UAVs. Right: Mean values of the number of true targets that are tracked.

6.6. Conclusion and perspectives

This chapter compares set-membership and stochastic Bayesian state estimators for target search and tracking. Both estimation techniques are applied to search scenarios with three different error sources considering false positive detection, namely false targets a potentially defective/imperfect computer vision system, and changing environmental conditions. It is assumed that the detection of false targets is deterministic and depends on the points of view of the UAVs when an observation is taken. Stochastic false positive detection is assumed to be caused by a defective/imperfect computer vision system, where the false positive detections appear uniformly distributed in the FoV or are modeled by a Markov chain model. The results show that the set-membership estimator is not very sensitive to the considered sources of a false positive detection. The stochastic estimator presents a higher sensitivity.

Furthermore, the choice of the assumed probability of false positive detection q impacts the estimation uncertainty considerably. Consequently, q is an additional parameter that must be carefully chosen when using a stochastic estimation method. The stochastic estimator shows the potential to remove more effectively false targets from the estimates when choosing a very high probability of false positive detection. Nevertheless, this retards also the estimation of the location of true targets.

Further extensions of the comparison include simulation with moving targets and other noise sources. Only false positive detection is considered in this chapter. It would be very interesting to adapt and compare both estimation techniques for scenarios where false negative detection of targets may appear. The adaptation of the stochastic estimator in this context seems to be simpler than for the set-membership estimator.

7. Conclusion and future research

7.1. Conclusion

This thesis addresses the problem of searching and tracking mobile targets using a fleet of cooperative UAVs. The estimation schemes assume that target state perturbations and measurement noises are bounded. Distributed set-membership state estimators have been developed and used to evaluate set estimates that are guaranteed to contain the target states. The trajectories of the UAVs are designed using control laws obtained by model predictive control approaches.

Another contribution of the thesis to the cooperative target search and tracking research field consists of proposing alternative detection and identification conditions of the targets. Deterministic geometric target detectability conditions are introduced in place of the widely-used probability of detection/non-detection. The new detection conditions model the target detection is based on geometric considerations and accounts for the UAV, target state, and environmental obstacles. The new identification conditions account for the target and UAV states and model the identification and confusion of true and false targets.

A new cooperative target search and tracking scheme is proposed for scenarios where the identity of a target is not always available. The robust distributed set-membership estimator run by each UAV determines *i*) set estimates containing the state of each *identified* target, *ii*) a set estimate containing the states of *detected* but *not yet identified* (true and false) targets, and *iii*) a set possibly containing targets remaining to be detected (the part of the search area still to be explored). Issues related to false detection and misidentification of false targets and potential non-identification of true targets are considered. The performance of this approach is evaluated via simulations, and preliminary experimental studies are carried out. The experiments have illustrated some limitations of the approach and highlight that real-world experiments and validations require a detailed study of error sources in the measurement process.

An alternative model considering potential non-detection of targets due to partial occlusions has been proposed. UAVs do not try to build any map of the possibly evolving environment to avoid frequent and resource-consuming map updates. This avoids assuming that UAVs can perceive and identify the feature of the obstacles and exploit this information. For each possible target location in the RoI, one introduces its detectability set as the set of all UAV locations from where the target is visible.

This set is unknown but assumed to be always non-empty, meaning that targets are never entirely hidden. One can then prove the absence of a target at a given zone when enough observations of that zone are collected with a sufficient variety of points of view. The absence of a map of the environment and the unknown detectability sets makes it particularly challenging for the UAVs to conclude the absence of a moving target when they observe a part of the RoI. A solution is proposed where the fleet of UAVs is partitioned into groups that observe a subset of the RoI simultaneously.

The adapted control scheme relies on a distributed MPC approach, which accounts for future predicted observations and communication. The control aims at minimizing the volume of the set estimates and accounts for the points of view of the UAVs when collecting an observation.

Finally, the developed set-membership estimation scheme is compared with existing classical search and tracking approaches that rely on a stochastic description of the problem. Both approaches are compared in Simulations illustrating their performances and different properties. In the simulation results, the stochastic estimator (compared to the set-membership estimator) shows a higher sensitivity towards user-chosen parameters and the modeling of false positive detections.

7.2. Perspectives

The contributions of this thesis address some relevant issues and drawbacks of cooperative target search and tracking approaches. Nevertheless, there are still many problems that remain open. The essential research directions in this field include improving the realism of the models, developing decentralized embedded algorithms, and strengthening the validation process. Problems that arise directly from the contributions in this thesis are discussed hereafter.

The notion of detectability sets and conic observation subsets present a new model for detectability conditions of targets. The simulation results illustrate the potential of this approach for an unknown time-evolving structured environment. One of the major strengths is that the approach does not require any *a priori* or online map of the environment. However, this is not strictly true because of assumption (5.35). One needs enough half-cones to ensure visibility. Though satisfying (5.35) can be guaranteed by choosing a large value for L, it is not practical since it increases the group size of the UAVs. A question to answer is what *a priori* knowledge of the environment is necessary to effectively design the conic observation subsets. Simple guidelines and design rules for the conic observation subsets based on classes of environments would make this approach more practical.

The idea of detectability sets can be extended to account for additional sensor limitations. For some sensors, the detectability of a target depends on the relative

positions and velocities of the target and the sensor. This is the case, *e.g.*, for Pulse-Doppler radars which can lose track of targets due to their clutter rejection filter, *i.e.*, targets flying perpendicular to the radar beam may be filtered out. It would be interesting to treat this problem using the notion of detectability sets.

The developed control design exhibits a satisfying performance in the simulations. Nevertheless, the control scheme assumes time synchronized UAVs which is not realistic in real-world applications. Furthermore, the control input is evaluated in a sequential manner, at least for locally connected UAVs. This sequential evaluation will not scale well for larger numbers of connected UAVs.

Another limitation concerns collision avoidance in the control design. The developed control schemes can reduce the risk of collision with obstacles and between UAVs. However, a safe operation can not be guaranteed. The deployment of groups of UAVs makes this issue even more critical.

The final optimization problem in the control design is defined through several approximations and simplifications. Though the proposed control scheme outperforms a greedy algorithm, the losses should be studied more in detail. A rigorous study or empirical evaluation that shows how much is earned/lost with each simplification would be of interest.

The effectiveness of the estimation and control scheme was only shown for targets that are much slower than the UAVs. Targets with higher mobility would lead to faster growth of the size of the set estimates and thus to situations where the UAVs can not effectively explore the search zone, especially if the targets outnumber them. The fact that uncertainties grow fast when propagating estimates of uncertain systems is well known for set-membership and bounded error estimation techniques. The guaranteed results are obtained by accounting for worst-case situations. This conservatism leads to the fast growth of uncertainties. The only way to restrict the fast growth is by introducing additional constraints and having minimal bounds of the unknown target state perturbations.

Another problem related to set-membership estimation techniques is the *curse of dimensionality*, which refers to the issue that the computational complexity of set operations increases exponentially with the number of considered dimensions. This particularly impacts the control design since the optimization problem to solve includes recursive operations on sets. The performance could be improved by evaluating relevant subdomains beforehand and solving the optimization problem within these subdomains.

Preliminary experimental studies show that the developed estimation scheme needs to be adapted to process real measurements that are not only noisy but also erroneous. The exact origin of all errors and uncertainties must be studied to derive appropriate countermeasures and design a robust estimator. Improved approaches could assume maximal numbers of errors and outliers. This issue is also related to the choice of the measurement noise bounds and their confidence. Bounds cho-

sen too small lead to outliers, and bounds chosen too large lead to a pessimistic evaluation of the set estimates.

An important motivation for the studies in this thesis was to explore the capabilities of set-membership estimation techniques in the context of target search and tracking. An advantage of set-membership estimation over stochastic estimation is that no knowledge about the probability density distributions describing the process and the noise is necessary. Nevertheless, the set-membership estimator accounts for worst-case characteristics due to the exploitation of less information, which may lead to larger uncertainties. Consequently, there is a trade-off between the required amount of *a priori* knowledge and the estimation uncertainty.

A. Résumé étendu en français

Cette thèse se concentre sur le problème de la Recherche, l'Acquisition et le Suivi Coopératifs (Cooperative Search Acquisition and Tracking; CSAT) de cibles à l'aide d'une flotte de drones. Chaque drone est équipé de capteurs pour détecter et localiser les cibles dans la zone de recherche. Le présent travail propose une modélisation détaillée des conditions de détection et d'identification des cibles, conditions qui dépendent des cibles et de l'environnement. Cette modélisation est une alternative à la description probabiliste largement utilisée dans ce domaine de recherche. De plus, des hypothèses alternatives de bruit et d'incertitude sont considérées: en effet, au lieu de définir une fonction de densité de probabilité caractérisant la distribution du bruit et des incertitudes, on suppose uniquement que ces derniers sont bornés, de bornes connues *a priori*. Les techniques d'estimation ensembliste sont alors utilisées pour estimer les états des cibles. Ces estimations sont données sous forme d'ensembles garantis de contenir les vrais états des cibles, sous réserve que les erreurs sont absolument bornées. Les contributions de la thèse sont les suivantes.

Le chapitre 2 fournit des informations de base pour les études menées dans cette thèse. Il comprend la définition et la caractérisation du problème général et une revue des approches existantes. En outre, les méthodes d'estimation de l'état de la cible et les techniques de commande du robot pour la recherche et le suivi de cibles sont abordées.

Le chapitre 3 formule le problème général considéré dans la thèse. Les conditions déterministes et géométriques de détection, de reconnaissance (distinction entre les vraies et les fausses cibles) et d'identification des cibles sont introduites à la place des classiques probabilités de détection/non-détection largement utilisées par ailleurs dans la littérature. Ces nouvelles conditions tiennent compte de la présence potentielle d'obstacles dans l'environnement, et des états de la cible et du drone. Pour chaque cible détectée, on suppose qu'une mesure incertaine de son état est disponible. Le bruit d'observation est supposé borné par des bornes connues, qui peuvent dépendre des conditions d'observation.

Le chapitre 4 présente un nouveau schéma coopératif de recherche et de suivi de cibles. Lorsqu'une cible est détectée, on suppose que son identité n'est obtenue que si certaines conditions d'observation sont satisfaites. Cette situation est typiquement rencontrée lorsqu'on utilise des caméras : l'identité d'une cible n'est disponible que lorsqu'elle est observée depuis un ou plusieurs points de vue spécifiques. De plus, on suppose que de fausses cibles, telles que des leurres ou des artefacts issus des fouillis environnementaux ou , sont présentes. Ces fausses cibles peuvent être identifiées à

tort comme de vraies cibles, mais elles s'en distinguent lorsqu'elles sont observées dans des conditions spécifiques. Pour chaque cible détectée (vraie et fausse), on suppose qu'une mesure incertaine de son état est disponible. Le bruit d'observation est supposé borné par des bornes connues, qui peuvent dépendre des conditions d'observation. On propose une méthode d'estimation distribuée et robuste exécutée par chaque UAV, qui permet de déterminer

- une estimation d'ensemble contenant l'état de chaque cible *identifiée*,
- une estimation d'ensemble contenant les états des cibles *détectées* mais non encore *identifiées* (vraies et fausses),
- et un ensemble contenant éventuellement les cibles restant à détecter (la partie de la zone de recherche restant à explorer).

L'estimateur est capable de traiter les mesures associées aux cibles détectées mais non identifiées avant leur identification à des instants ultérieurs. L'estimateur alterne les prédictions et les corrections en utilisant les mesures du capteur de chaque drone et les mesures reçues lors des communications avec ses voisins. Les entrées de commande de chaque drone sont calculées à l'aide d'une méthode de Commande Prédictive par Modèle (Model Predictive Control, MPC) adaptée au contexte de l'estimation ensembliste, qui vise à minimiser le volume des ensembles d'estimation. L'approche MPC tient compte de l'impact des mesures futures sur ces ensembles et prédit les informations futures communiquées par les voisins. Une portée de communication limitée est également prise en compte. En résumé, l'estimateur ensembliste proposé au chapitre 4 permet la détection et le suivi de cibles mobiles en présence de fausses cibles mobiles. Les problèmes liés à la fausse détection et à la mauvaise identification des fausses cibles, ainsi qu'à la non-identification potentielle des vraies cibles, sont examinés. La distinction entre vraies et fausses cibles repose sur certaines conditions d'observation déterministes. L'approche MPC distribuée tient compte de l'évolution des estimations de l'ensemble, des informations provenant des voisins et des communications limitées entre les drones. Des simulations de scénarios, incluant la présence de fausses cibles, illustrent la capacité de l'approche proposée à rechercher et à suivre efficacement un nombre inconnu de cibles mobiles dans une zone de recherche délimitée. De plus, les résultats obtenus lors d'expérimentations préliminaires sont présentés.

Le chapitre 5 contribue à la recherche et au suivi coopératifs de cibles dans des environnements non cartographiés lorsque les cibles sont en mouvement et peuvent être partiellement cachées. Dans un tel contexte, de nombreuses approches tentent de construire une carte de l'environnement pendant la mission de recherche, et les occlusions partielles de cibles sont généralement modélisées par des probabilités de non-détection. Une approche alternative modélisant les occlusions partielles et abordant le problème de la recherche et du suivi est proposée. La construction d'une carte de l'environnement susceptible d'évoluer nécessitant des mises à jour fréquentes et consommatrices de ressources devient inutile. Il n'est, de plus, pas nécessaire de supposer que les drones soient capables de percevoir les obstacles et d'exploiter

cette information, ce qui est particulièrement en adéquation pour des observations nocturnes effectuées à l'aide de caméras RVB (modèle de couleurs rouge, vert et bleu) ou infrarouge, lorsque le contraste de l'environnement diminue . En outre, la capacité d'un drone à détecter des cibles dépend de l'emplacement de la cible et du point de vue du drone.

Pour chaque emplacement possible de la cible dans la Région d'Intérêt (RdI), on introduit son *ensemble de détectabilité* comme l'ensemble de tous les emplacements du drone d'où la cible est visible, c'est à dire qu'il existe une ligne de vue reliant la cible et le drone. En raison de l'environnement non cartographié qui est susceptible d'évoluer dans le temps, les ensembles de détectabilité sont inconnus des drones et évoluent également dans le temps. On suppose qu'à chaque instant, chaque ensemble de détectabilité contient au moins un demi-cône de volume non nul. Cela signifie que les cibles ne sont jamais complètement occultées par l'environnement. L'absence de carte de l'environnement et les ensembles de détectabilité inconnus rendent particulièrement difficile pour les drones de conclure à l'absence d'une cible mobile lorsqu'ils observent une partie de la RdI.

Dans un premier temps, une solution à ce problème est proposée en supposant que les cibles et les obstacles sont statiques. Pour résoudre ce problème, on introduit la notion de *sous-ensembles coniques* de lieux d'observation. On suppose par la suite que l'un de ces sous-ensembles coniques est inclus dans l'ensemble de détectabilité associé à chaque emplacement du RdI. Sous cette hypothèse, il est possible de garantir qu'un emplacement est exempt de cible lorsqu'il est observé depuis différents points de vue, chacun appartenant à un sous-ensemble d'observation différent. Par conséquent, les drones peuvent explorer progressivement la zone de recherche à partir de différents points de vue et conclure à l'absence de cibles.

Cette solution est ensuite étendue au cas général où les cibles et les obstacles peuvent se déplacer. Pour affirmer qu'un emplacement de la RdI est libre de toute cible, il faut observer cet emplacement simultanément avec une diversité suffisante de points de vue. Pour atteindre cette diversité, une solution proposée est de diviser la flotte de drones en groupes, où chaque drone d'un même groupe est chargé d'observer le RdI depuis un point de vue donné. Une fois qu'une cible est détectée, on suppose à nouveau que sa localisation est obtenue avec une certaine incertitude bornée. L'estimateur d'état ensembliste distribué est adapté pour évaluer, d'une part, des ensembles garantis comme contenant des emplacements de cibles dans la RdI et, d'autre part, un ensemble dont il est prouvé qu'il est libre de toute cible. Contrairement au chapitre 4, l'approche proposée est capable de garantir la détection de cibles *mobiles* partiellement cachées dans un environnement inconnu et *changeant* (les obstacles pouvant être mobiles). La trajectoire de chaque groupe de drones est à nouveau conçue de manière distribuée en minimisant une mesure de l'incertitude de l'estimation de l'état de la cible via une approche MPC.

Le chapitre 6 compare l'estimateur d'état de cibles proposé avec un schéma d'estimation stochastique classique et souligne les différences entre les approches. Les deux

approches sont comparées dans des simulations avec des cibles terrestres statiques. Les avantages et les inconvénients sont discutés.

Le chapitre 7 conclut la thèse et introduit les directions de recherche et les perspectives envisagées à la suite de ce travail.

Bibliography

A. Alexopoulos, T. Schmidt, and E. Badreddin. Cooperative pursue in pursuit-evasion games with unmanned aerial vehicles. In *Proc. IEEE/RSJ IROS*, pages 4538–4543, 2015.

B. Allik. Tracking of multiple targets across distributed platforms with fov constraints. In *Proc. IEEE 58th CDC*, pages 6044–6049, 2019.

S. Baek and G. York. Optimal sensor management for multiple target tracking using cooperative unmanned aerial vehicles. In *Proc. IEEE ICUAS*, pages 1294–1300, 2020.

X. Bai, Z. Wang, L. Zou, and Z. Zhang. Target tracking for wireless localization systems using set-membership filtering: A component-based event-triggered mechanism. *Automatica*, 132:109795, 2021. ISSN 0005-1098. doi: 10.1016/j.automatica.2021.109795.

Y. Bar-Shalom, P. K. Willett, and X. Tian. *Tracking and Data Fusion*, volume 11. YBS publishing Storrs, CT, USA:, 2011.

S. Bertrand, J. Marzat, H. Piet-Lahanier, A. Kahn, and Y. Rochefort. MPC Strategies for Cooperative Guidance of Autonomous Vehicles. *AerospaceLab*, 19(8), 2014.

L. F. Bertuccelli and J. How. Robust UAV search for environments with imprecise probability maps. In *Proc. IEEE CDC*, pages 5680–5685, 2005.

L. F. Bertuccelli and J. P. How. Search for dynamic targets with uncertain probability maps. In *Proc. American Contr. Conf.*, pages 6–pp, 2006a.

L. F. Bertuccelli and J. P. How. UAV search for dynamic targets with uncertain motion models. In *Proc. IEEE CDC*, pages 5941–5946. IEEE, 2006b.

S. S. Blackman. Multiple hypothesis tracking for multiple target tracking. *IEEE Aerospace and Electronic Systems Magazine*, 19(1):5–18, 2004.

W. Blanding, W. Koch, and U. Nickel. Tracking through jamming using negative information. In *Proc. IEEE FUSION*, pages 1–8, 2006.

E. Blasch and B. Kahler. Multiresolution EO/IR target tracking and identification. In *Proc. IEEE FUSION*, volume 1, pages 8–pp, 2005.

J. Blinn. Me and my (fake) shadow. *IEEE Computer Graphics and Applications*, 8 (01):82–86, January 1988. ISSN 1558-1756. doi: 10.1109/MCG.1988.10001.

R. Boukezzoula, L. Jaulin, B. Desrochers, and L. Foulloy. Thick gradual sets and their computations: Application for determining the uncertain zone explored by an underwater robot. *Eng. Appl. Artif. Intel.*, 102:104287, 2021.

L. Briñón-Arranz, A. Seuret, and A. Pascoal. Circular formation control for cooperative target tracking with limited information. *Journal of the Franklin Institute*, 356(4):1771–1788, 2019. ISSN 0016-0032. doi: 10.1016/j.jfranklin.2018.12.011.

D. J. Bucci and P. K. Varshney. Decentralized multi-target tracking in urban environments: Overview and challenges. In *Proc. IEEE FUSION*, pages 1–8, 2019.

E. F. Camacho and C. B. Alba. *Model Predictive Control*. Springer science & business media, 2013.

X. Cao, H. Sun, and G. E. Jan. Multi-AUV cooperative target search and tracking in unknown underwater environment. *Ocean Eng.*, 150:1–11, 2018. ISSN 0029-8018. doi: 10.1016/j.oceaneng.2017.12.037.

S. J. Chung, A. A. Paranjape, P. Dames, S. Shen, and V. Kumar. A survey on aerial swarm robotics. *IEEE Transactions on Robotics*, 34(4):837–855, 2018.

T. H. Chung, M. R. Clement, M. A. Day, K. D. Jones, D. Davis, and M. Jones. Live-fly, large-scale field experimentation for large numbers of fixed-wing UAVs. In *Proc. IEEE ICRA*, pages 1255–1262, 2016.

V. Cichella, I. Kaminer, V. Dobrokhodov, and N. Hovakimyan. Coordinated vision-based tracking for multiple UAVs. In *Proc. IEEE/RSJ IROS*, pages 656–661, 2015.

J. Cortes, S. Martinez, T. Karatas, and F. Bullo. Coverage control for mobile sensing networks. *IEEE Trans. Robotics and Autom.*, 20(2):243–255, 2004.

J. Czyzyk, M. P. Mesnier, and J. J. Moré. The NEOS Server. *IEEE Journal on Computational Science and Engineering*, 5(3):68–75, 1998.

P. Dames, P. Tokekar, and V. Kumar. Detecting, localizing, and tracking an unknown number of moving targets using a team of mobile robots. *The International Journal of Robotics Research*, 36(13-14):1540–1553, 2017.

P. M. Dames. Distributed multi-target search and tracking using the PHD filter. *Autonomous robots*, 44(3):673–689, 2020.

B. Desrochers and L. Jaulin. Computing a guaranteed approximation of the zone explored by a robot. *IEEE Trans. on Automat. Contr.*, 62(1):425–430, 2016.

V. Drevelle and P. Bonnifait. Robust positioning using relaxed constraint-propagation. In *Proc. IEEE IROS*, pages 4843–4848. IEEE, 2010.

V. Drevelle and P. Bonnifait. Localization confidence domains via set inversion on short-term trajectory. *IEEE Transactions on Robotics*, 29(5):1244–1256, 2013.

V. Drevelle, L. Jaulin, and B. Zerr. Guaranteed characterization of the explored space of a mobile robot by using subpavings. *IFAC Proceedings Volumes*, 46(23): 44–49, 2013.

J. W. Durham, A. Franchi, and F. Bullo. Distributed pursuit-evasion without mapping or global localization via local frontiers. *Autonomous Robots*, 32(1):81–95, 2012.

N. Farmani, L. Sun, and D. Pack. Tracking multiple mobile targets using cooperative unmanned aerial vehicles. In *Proc. IEEE ICUAS*, pages 395–400, 2015.

M. Flint, E. Fernandez, and M. Polycarpou. Efficient Bayesian methods for updating and storing uncertain search information for UAVs. In *Proc. IEEE CDC*, pages 1093–1098 Vol.1, Nassau, Bahamas, 2004. ISBN 978-0-7803-8682-2. doi: 10.1109/CDC.2004.1428838.

J. Foraker, J. O. Royset, and I. Kaminer. Search-trajectory optimization: Part I, formulation and theory. *J. Optim. Theor. Appl.*, 169(2):530–549, 2016a.

J. Foraker, J. O. Royset, and I. Kaminer. Search-trajectory optimization: Part II, algorithms and computations. *J. Optim. Theor. Appl.*, 169(2):550–567, 2016b.

E. W. Frew and J. Elston. Target assignment for integrated search and tracking by active robot networks. In *Proc. IEEE ICRA*, pages 2354–2359, Pasadena, USA, May 2008. ISBN 978-1-4244-1646-2. doi: 10.1109/ROBOT.2008.4543565.

T. Furukawa, F. Bourgault, B. Lavis, and H. F. Durrant-Whyte. Recursive Bayesian search-and-tracking using coordinated uavs for lost targets. In *Proc. IEEE ICRA*, pages 2521–2526, 2006. doi: 10.1109/ROBOT.2006.1642081.

F. Gu, Y. He, and J. Han. Active persistent localization of a three-dimensional moving target under set-membership uncertainty description through cooperation of multiple mobile robots. *IEEE Trans. Ind. Electron.*, 62(8):4958–4971, 2015.

A. Guerra, N. Sparnacci, D. Dardari, and P. M. Djurić. Collaborative target-localization and information-based control in networks of UAVs. In *Proc. IEEE SPAWC*, pages 1–5, Kalamata, Greece, 2018.

A. Guerra, D. Dardari, and P. M. Djuric. Non-Centralized Navigation for Source Localization by Cooperative UAVs. In *Proc. IEEE EUSIPCO*, pages 1–5, A Coruna, Spain, September 2019. ISBN 978-90-827970-3-9. doi: 10.23919/EUSIPCO.2019.8902944.

C.-Y. Han, M. Kieffer, and A. Lambert. Guaranteed confidence region characterization for source localization using RSS measurements. *Signal Processing*, 152:104–117, 2018. ISSN 0165-1684. doi: 10.1016/j.sigpro.2018.03.018.

Sh. He, H.-S. Shin, and A. Tsourdos. Constrained Multiple Model Bayesian Filtering for Target Tracking in Cluttered Environment. *IFAC-PapersOnLine*, 50(1):425–430, July 2017. ISSN 24058963. doi: 10.1016/j.ifacol.2017.08.192.

J. P. Hespanha, H. J. Kim, and S. Sastry. Multiple-agent probabilistic pursuit-evasion games. In *Proc. IEEE CDC*, volume 3, pages 2432–2437. IEEE, 1999.

J. Hou, J. Li, Y. Ni, and W. Dong. Unmanned aerial vehicle's state estimation with multiple unmanned ground vehicles cooperative observation based on set-

membership filter. In *Proc. IEEE RCAR*, pages 411–416, 2021. doi: 10.1109/RCAR52367.2021.9517572.

J. P. How, C. Fraser, K. C. Kulling, L. F. Bertuccelli, O. Toupet, Luc Brunet, Abe Bachrach, and Nicholas Roy. Increasing autonomy of UAVs. *IEEE Robot. Autom. Mag.*, 16(2):43–51, 2009.

J. Hu, L. Xie, K. Y. Lum, and J. Xu. Multiagent information fusion and cooperative control in target search. *IEEE Transactions on Control Systems Technology*, 21 (4):1223–1235, 2012.

J. Hu, L. Xie, J. Xu, and Z. Xu. Multi-agent cooperative target search. *Sensors*, 14 (6):9408–9428, 2014.

X. Hu, Y. Liu, and G. Wang. Optimal search for moving targets with sensing capabilities using multiple UAVs. *Journal of Systems Engineering and Electronics*, 28(3):526–535, 2017.

J. Ibenthal, L. Meyer, M. Kieffer, and H. Piet-Lahanier. Bounded-error target localization and tracking in presence of decoys using a fleet of UAVs. In *Proc. IFAC-PapersOnLine*, volume 53, pages 9521–9528, 2020a. doi: 10.1016/j.ifacol.2020.12.2429.

J. Ibenthal, L. Meyer, H. Piet-Lahanier, and M. Kieffer. Target search and tracking using a fleet of UAVs in presence of decoys and obstacles. In *Proc. IEEE CDC*, pages 188–194, 2020b. doi: 10.1109/CDC42340.2020.9303943.

J. Ibenthal, M. Kieffer, L. Meyer, H. Piet-Lahanier, and S. Reynaud. Bounded-error target localization and tracking using a fleet of UAVs. *Automatica*, 132:109809, 2021a.

J. Ibenthal, L. Meyer, H. Piet-Lahanier, and M. Kieffer. Localization of partially hidden targets using a fleet of UAVs via robust bounded-error estimation. In *Proc. IEEE CDC*, 2021b.

L. Jaulin. Robust set-membership state estimation; application to underwater robotics. *Automatica*, 45(1):202–206, 2009.

L. Jaulin. Range-only slam with occupancy maps: A set-membership approach. *IEEE Transactions on Robotics*, 27(5):1004–1010, 2011a.

L. Jaulin. Set-membership localization with probabilistic errors. *Robotics and Autonomous Systems*, 59(6):489–495, 2011b.

L. Jaulin and E. Walter. Set inversion via interval analysis for nonlinear bounded-error estimation. *Automatica*, 29(4):1053–1064, 1993.

J. Johnson. Analysis of Image Forming Systems. In *Proc. Image Intensifier Symposium*, Fort Belvoir, Fairfax County, Virginia, 1958.

A. Khan, E. Yanmaz, and B. Rinner. Information exchange and decision making in micro aerial vehicle networks for cooperative search. *IEEE Trans. Control Netw. Syst.*, 2(4):335–347, 2015.

A. Khan, B. Rinner, and A. Cavallaro. Cooperative robots to observe moving targets. *IEEE Trans. Cybern.*, 48(1):187–198, 2016.

R. Khodayi-mehr, Y. Kantaros, and M. M. Zavlanos. Distributed state estimation using intermittently connected robot networks. *IEEE Trans. Robot.*, 35(3):709–724, 2019.

M. Kieffer, L. Jaulin, and E. Walter. Guaranteed recursive non-linear state bounding using interval analysis. *Int. J. Adapt. Control Signal Process.*, 16(3):193–218, 2002.

P. Kim, J. Chen, and Y. K. Cho. SLAM-driven robotic mapping and registration of 3D point clouds. *Automation in Construction*, 89:38–48, 2018.

L. Klodt, D. Haumann, and V. Willert. Revisiting coverage control in nonconvex environments using visibility sets. In *Proc. IEEE ICRA*, pages 82–89, 2014. doi: 10.1109/ICRA.2014.6906593.

L. Klodt, S. Khodaverdian, and V. Willert. Motion control for UAV-UGV cooperation with visibility constraint. In *Proc. IEEE CCA*, pages 1379–1385, 2015. doi: 10.1109/CCA.2015.7320804.

A. Kolling and S. Carpin. Multirobot cooperation for surveillance of multiple moving targets - a new behavioral approach. In *Proc. IEEE ICRA*, pages 1311–1316, Orlando, USA, 2006. IEEE.

B. O. Koopman. The theory of search. I. Kinematic bases. *Operations research*, 4 (3):324–346, 1956.

M. J. Kuhlman, M.W. Otte, D. Sofge, and S. K. Gupta. Multipass target search in natural environments. *Sensors*, 17(11):2514, 2017.

J. Kuhn, C. Reinl, and O. Von Stryk. Predictive control for multi-robot observation of multiple moving targets based on discrete-continuous linear models. In *Proc. 18th IFAC World Congress*, pages 257–262, Milano, Italy, 2011.

H. M. La and W. Sheng. Dynamic target tracking and observing in a mobile sensor network. *Robotics and Autonomous Systems*, 60(7):996–1009, 2012.

M. Langerwisch and B. Wagner. Guaranteed mobile robot tracking using robust interval constraint propagation. In *Proc. IEEE ICRA*, pages 354–365, 2012.

M. Lhommeau, L. Jaulin, and L. Hardouin. Inner and outer approximation of capture basins using interval analysis. In *4th International Conference on Informatics in Control, Automation and Robotics (ICINCO)*, 2007.

P. Li and H. Duan. A potential game approach to multiple UAV cooperative search and surveillance. *Aerosp. Sci. Technol.*, 68:403–415, 2017.

Y. Liu and R. Bucknall. A survey of formation control and motion planning of multiple unmanned vehicles. *Robotica*, 36(7):1019–1047, 2018.

Y. Liu and Y. Zhao. Ellipsoidal set filter combined set-membership and statistics uncertainties for bearing-only maneuvering target tracking. In *Proc IEEE/ION*

Position, Location and Navigation Symposium - PLANS, pages 753–759, 2014. doi: 10.1109/PLANS.2014.6851441.

X. Lu, H. Zhang, W. Wang, and K.-L. Teo. Kalman filtering for multiple time-delay systems. *Automatica*, 41(8):1455–1461, 2005.

Y. Lyu, Q. Pan, and J. Lv. Unscented transformation-based multi-robot collaborative self-localization and distributed target tracking. *Applied Sciences*, 9(5), 2019. ISSN 2076-3417. doi: 10.3390/app9050903.

L. Ma and N. Hovakimyan. Vision-based cyclic pursuit for cooperative target tracking. *J. Guid. Control. Dyn.*, 36(2):617–622, 2013.

R. J. Meinhold and N. D. Singpurwalla. Understanding the kalman filter. *The American Statistician*, 37(2):123–127, 1983.

F. Meyer, H. Wymeersch, M. Fröhle, and F. Hlawatsch. Distributed estimation with information-seeking control in agent networks. *IEEE J. Sel. Areas Commun.*, 33 (11):2439–2456, 2015.

R. Moore. Parameter sets for bounded-error data. *Mathematics and Computers in Simulation*, 34(2):113–119, 1992. ISSN 0378-4754. doi: 10.1016/0378-4754(92) 90048-L.

M. Morari and J. H. Lee. Model predictive control: Past, present and future. *Comput. Chem. Eng.*, 23(4-5):667–682, 1999.

F. Morbidi and G. L. Mariottini. Active target tracking and cooperative localization for teams of aerial vehicles. *IEEE Trans. Control Syst. Technol.*, 21(5):1694–1707, 2012.

D. J. Pack, P. DeLima, G. J. Toussaint, and G. York. Cooperative control of UAVs for localization of intermittently emitting mobile targets. *IEEE Transactions on Systems, Man, and Cybernetics, Part B (Cybernetics)*, 39(4):959–970, 2009.

Y. Pan, S. Li, X. Zhang, J. Liu, Z. Huang, and T. Zhu. Directional Monitoring of Multiple Moving Targets by Multiple Unmanned Aerial Vehicles. In *Proc. IEEE GLOBECOM*, pages 1–6, Singapore, December 2017. ISBN 978-1-5090-5019-2. doi: 10.1109/GLOCOM.2017.8253969.

L. E. Parker. Cooperative robotics for multi-target observation. *Intelligent Automation & Soft Computing*, 5(1):5–19, 1999.

L. E. Parker. Distributed algorithms for multi-robot observation of multiple moving targets. *Auton. Robot.*, 12(3):231–255, 2002.

L.E. Parker and B.A. Emmons. Cooperative multi-robot observation of multiple moving targets. In *Proc. IEEE ICRA*, volume 3, pages 2082–2089, Albuquerque, USA, 1997. ISBN 978-0-7803-3612-4. doi: 10.1109/ROBOT.1997.619270.

H. Piet-Lahanier and E. Walter. Exact description of feasible parameter sets and minimax estimation. *International journal of adaptive control and signal processing*, 8(1):5–14, 1994.

R. R. Pitre, X. R. Li, and R. Delbalzo. UAV route planning for joint search and track missions—An information-value approach. *IEEE Trans. Aerosp. Electron. Syst.*, 48(3):2551–2565, 2012.

M. Quigley, K. Conley, B. Gerkey, J. Faust, T. Foote, J. Leibs, R. Wheeler, A. Y. Ng, et al. ROS: An open-source robot operating system. In *ICRA Workshop on Open Source Software*, volume 3, page 5, 2009.

M. Raap, M. Preuß, and S. Meyer-Nieberg. Moving target search optimization – A literature review. *Computers & Operations Research*, 105:132–140, 2019. ISSN 0305-0548. doi: 10.1016/j.cor.2019.01.004.

L. Reboul, M. Kieffer, H. Piet-Lahanier, and S. Reynaud. Cooperative guidance of a fleet of UAVs for multi-target discovery and tracking in presence of obstacles using a set membership approach. In *Proc. IFAC-PapersOnLine*, volume 52, pages 340–345, 2019.

K. Ren, X. Zhang, Y. Han, and Y. Hou. Robust night target tracking via infrared and visible video fusion. In *Proc. Applications of Digital Image Processing XLI*, volume 10752, page 1075206, 2018.

S. Reynaud, M. Kieffer, H. Piet-Lahanier, and L. Reboul. A set-membership approach to find and track multiple targets using a fleet of UAVs. In *Proc. IEEE CDC*, pages 484–489, Miami Beach, USA, 2018. ISBN 978-1-5386-1395-5. doi: 10.1109/CDC.2018.8619672.

C. Robin and S. Lacroix. Multi-robot target detection and tracking: Taxonomy and survey. *Auton. Robot.*, 40(4):729–760, 2016.

Y. Rochefort, H. Piet-Lahanier, S. Bertrand, D. Beauvois, and D. Dumur. Model predictive control of cooperative vehicles using systematic search approach. *Control. Eng. Pract.*, 32:204–217, 2014.

F. Schweppe. Recursive state estimation: Unknown but bounded errors and system inputs. *IEEE Transactions on Automatic Control*, 13(1):22–28, 1968. doi: 10.1109/TAC.1968.1098790.

S. Shah, D. Dey, C. Lovett, and A. Kapoor. AirSim: High-fidelity visual and physical simulation for autonomous vehicles. In *Proc. Field and Service Robotics*, 2017.

L. Shi, N. J H. Marcano, and R. H. Jacobsen. A review on communication protocols for autonomous unmanned aerial vehicles for inspection application. *Microprocessors and Microsystems*, 86:104340, 2021.

O. Shorinwa, J. Yu, T. Halsted, A. Koufos, and M. Schwager. Distributed Multi-Target Tracking for Autonomous Vehicle Fleets. *arXiv preprint arXiv:2004.05965*, 2020.

T. L. Song, D. Musicki, and K. Da Sol. Target tracking with target state dependent detection. *IEEE Trans. on Signal Proces.*, 59(3):1063–1074, 2010.

L. Sun, S. Baek, and D. Pack. Distributed probabilistic search and tracking of agile mobile ground targets using a network of unmanned aerial vehicles. In *Human Behavior Understanding in Networked Sensing*, pages 301–319. Springer, 2014.

Z. Sun, Q. Liu, C. Yu, and B. D. O. Anderson. Generalized controllers for rigid formation stabilization with application to event-based controller design. In *Proc. IEEE ECC*, pages 217–222, 2015. doi: 10.1109/ECC.2015.7330548.

Q. Tang, F. Yu, Z. Xu, and P. Eberhard. Swarm robots search for multiple targets. *IEEE access : practical innovations, open solutions*, 8:92814–92826, 2020. doi: 10.1109/ACCESS.2020.2994151.

H. G. Tanner and D. K. Christodoulakis. Cooperation between aerial and ground vehicle groups for reconnaissance missions. In *Proc. IEEE CDC*, pages 5918–5923, 2006.

D. Tian, J. Zhou, and Z. Sheng. An adaptive fusion strategy for distributed information estimation over cooperative multi-agent networks. *IEEE Transactions on Information Theory*, 63(5):3076–3091, 2017.

P. Tokekar, V. Isler, and A. Franchi. Multi-target visual tracking with aerial robots. In *Proc. IEEE/RSJ IROS*, pages 3067–3072, 2014.

M. Ulmke and W. Koch. Road-map assisted ground moving target tracking. *IEEE Trans. on Aero. Elec. Sys.*, 42(4):1264–1274, 2006.

A. Ur-Rehman, S. M. Naqvi, L. Mihaylova, and J. A. Chambers. Multi-target tracking and occlusion handling with learned variational Bayesian clusters and a social force model. *IEEE Trans. on Signal Proces.*, 64(5):1320–1335, 2015.

K. Vencatasamy, L. Jaulin, and B. Zerr. Secure the zone from intruders with a group robots. In *Marine Robotics and Applications*, pages 101–116. Springer, 2018. ISBN 978-3-319-70724-2.

R. Vidal, S. Rashid, C. Sharp, O. Shakernia, J. Kim, and S. Sastry. Pursuit-evasion games with unmanned ground and aerial vehicles. In *Proc. IEEE ICRA*, volume 3, pages 2948–2955. IEEE, 2001.

R. Vidal, O. Shakernia, H. J. Kim, D. H. Shim, and S. Sastry. Probabilistic pursuit-evasion games: Theory, implementation, and experimental evaluation. *IEEE transactions on robotics and automation*, 18(5):662–669, 2002.

C. Viel, S. Bertrand, M. Kieffer, and H. Piet-Lahanier. Distributed event-triggered control strategies for multi-agent formation stabilization and tracking. *Automatica*, 106:110–116, 2019.

É. Walter. *Numerical Methods and Optimization*. Springer, 2014.

É. Walter and L. Pronzato. *Identification de Modèles Paramétriques à Partir de Données Expérimentales*. Masson, 1994.

C. L. Walton, Qi Gong, I. Kaminer, and J. O. Royset. Optimal motion planning for searching for uncertain targets. *IFAC Proceedings Volumes*, 47(3):8977–8982, 2014.

J. Wang and E. Olson. AprilTag 2: Efficient and robust fiducial detection. In *Proc. IEEE/RSJ IROS*, pages 4193–4198, 2016.

N. Xia, F. Yang, and Q.-L. Han. Distributed networked set-membership filtering with ellipsoidal state estimations. *Information Sciences*, 432:52–62, 2018. ISSN 0020-0255. doi: 10.1016/j.ins.2017.12.010.

X. Xu, L. Yang, W. Meng, Q. Cai, and M. Fu. Multi-agent coverage search in unknown environments with obstacles: A survey. In *Proc. IEEE CCC*, pages 2317–2322, 2019. doi: 10.23919/ChiCC.2019.8865126.

Y. Yang, A. A. Minai, and M. M. Polycarpou. Decentralized cooperative search by networked UAVs in an uncertain environment. In *Proc. American Contr. Conf.*, volume 6, pages 5558–5563. IEEE, 2004.

Y. Yang, M. M Polycarpou, and A. A. Minai. Multi-UAV cooperative search using an opportunistic learning method. *J. Dyn. Sys., Meas., Control.*, pages 716–728, 2007.

P. Yao, H. Wang, and H. Ji. Multi-UAVs tracking target in urban environment by model predictive control and Improved Grey Wolf Optimizer. *Aerosp. Sci. Technol.*, 55:131–143, 2016.

H. Yu, K. Meier, M. Argyle, and R. W. Beard. Cooperative path planning for target tracking in urban environments using unmanned air and ground vehicles. *IEEE ASME Trans. Mechatron.*, 20(2):541–552, 2014.

M. Zhang, J. Song, L. Huang, and C. Zhang. Distributed cooperative search with collision avoidance for a team of unmanned aerial vehicles using gradient optimization. *J. Aero- Eng.*, 30(1):04016064, 2017.

Z. Zhen, Y. Chen, L. Wen, and B. Han. An intelligent cooperative mission planning scheme of UAV swarm in uncertain dynamic environment. *Aerospace Science and Technology*, 100:105826, 2020.

Y. Zhong, P. Yao, Y. Sun, and J. Yang. Method of multi-UAVs cooperative search for Markov moving targets. In *Proc. Chinese Control and Decision Conference*, pages 6783–6789, 2017.